# Characterisation of ADAMTS-L2 and ADAMTS-L4

**A thesis submitted to the University of Manchester for the degree of Master of Philosophy in the Faculty of Biology, Medicine and Health**

**2016**

**Mukti Singh**

**School of Biological Sciences**

**Table of Contents**

**Final word count: 42,892 words**

**List of Figures**

**List of Tables**

**Abbreviations**

| | |
|---|---|
| Å | Angstrom |
| AD | Acromicric dysplasia |
| ADAMTS | A disintegrin and metalloprotease with thrombospondin type 1 repeats |
| ADAMTS-L | ADAMTS-Like |
| ARPE-19 | Adult retinal pigmented epithelial cells |
| Ampr | Ampicillin resistance |
| BCA | Bicinchoninic acid |
| BCM | Barycentric mean fluorescence |
| BFP | Blue fluorescent protein |
| BL | Bacterial lysis |
| β-ME | Beta-mercaptoethanol |
| bp | Base pair |
| BSA | Bovine serum albumin |
| CAD | Coronary artery disease |
| cbEGF | Calcium-binding epidermal growth factor |
| CCD | Charge coupled device |
| cDNA | Complementary deoxyribonucleic acid |
| $CO_2$ | Carbon dioxide |
| COS | CV-1 in Origin, and carrying the SV40 genetic material cells |
| Cryo-EM | Cryo-electron microscopy |
| CS | Craniosynostosis |
| CT | C-terminal |
| CTF | Contrast transfer function |
| DAPI | 4',6-diamidino-2-phenylindole |

| | |
|---|---|
| DDD | Direct detection device |
| $ddH_2O$ | Double-distilled water |
| DTT | Dithiothreitol |
| DMEM | Dulbecco's modified eagle medium |
| DMSO | Dimethyl sulfoxide |
| DNA | Deoxyribonucleic acid |
| DNAse | Deoxyribonuclease |
| dNTP | Deoxynucleotide |
| DSF | Differential scanning fluorimetry |
| $e^-$ | Electron |
| ECM | Extracellular matrix |
| EDC | 1-ethyl-3- (3-dimethylaminopropyl) carbodiimide |
| EDS | Ehlers Danols Syndrome |
| EDTA | Ethylenediaminetetracetic acid |
| EGF | Epidermal growth factor |
| ELP | Ectopia lentis *et pupillae* |
| EL | Ectopia lentis |
| EM | Electron microscopy |
| ER | Endoplasmic reticulum |
| FACS | Fluorescence-activated cell sorting |
| FBN1 | Fibrillin-1 |
| FEG | Field emission gun |
| FL | Full length |
| FSC | Fourier shell correlation |
| FSG | Fish skin gelatin |

| | |
|---|---|
| GAG | Glycosaminoglycan |
| GD | Geleophysic dysplasia |
| GFP | Green fluorescent protein |
| HBS | HEPES buffered saline |
| HDF | Human dermal fibroblast |
| HEK | Human embryonic kidney |
| HS | Heparan sulphate |
| IEL | Isolated ectopia lentis |
| IMAC | Immobilised metal ion affinity chromatography |
| ITC | Isothermal titration calorimetry |
| kb | Kilobase |
| kD | Equilibrium dissociation constant |
| kDa | Kilo Daltons |
| LAP | Latency associated peptide |
| LB | Luria broth |
| LLC | Large latent complex |
| LOX | Lysyl oxidase |
| LSGS | Low serum growth supplement |
| LTBP | Latent transforming growth factor-β binding protein |
| mA | Milli Amps |
| MCS | Multiple cloning site |
| MFS | Marfan syndrome |
| MLS | Musladin-Lueke syndrome |
| MMP | Matrix metalloproteinase |
| MST | Microscale thermophoresis |

| | |
|---|---|
| NaCl | Sodium chloride |
| $NaHCO_3$ | Sodium bicarbonate |
| NHS | N-hydroxysuccinimide |
| NMR | Nuclear magnetic resonance |
| NT | N-terminal |
| OA | Osteoarthritis |
| PACE | Paired basic amino acid cleaving enzyme |
| PBS | Phosphate buffered saline |
| PCR | Polymerase chain reaction |
| PEI | Polyethylenimine |
| PF | Protein fragment |
| PFA | Paraformaldehyde |
| PG | Proteoglycan |
| PIC | Protease inhibitor cocktail |
| PLAC domain | Protease and lacunin domain |
| pmol | Picomoles |
| PNGase F | Peptide: N-Glycoside F |
| RGD | Arg-Gly-Asp peptide |
| RIPA | Radio-immunoprecipitation assay |
| RNA | Ribonucleic acid |
| RNAse | Ribonuclease |
| RPE | Retinal pigmented epithelium |
| SAXS | Small-angle x-ray scattering |
| SEC | Size exclusion chromatography |
| SDS-PAGE | Sodium dodecyl sulphate polyacrylamide gel electrophoresis |

| | |
|---|---|
| SOC | Super optimal broth with catabolite repression |
| SLC | Small latent complex |
| SLS | Static light scattering |
| SMC | Smooth muscle cell |
| SPR | Surface plasmon resonance |
| TAE | Tris-acetate |
| TB domain | TGFβ-binding-like 8-cysteine domain |
| TBS | Tris buffered saline |
| TBS-T | Tris-buffered saline & Tween 20 |
| TEM | Transmission electron microscopy |
| TG | Thioglycerol |
| TGFβ | Transforming growth factor β |
| $T_{agg}$ | Aggregation temperature |
| $T_m$ | Melting temperature |
| TSP-1 | Thrombospondin-1 |
| TSR | Thrombospondin type 1 repeat |
| UA | Uranyl acetate |
| UPR | Unfolded protein response |
| V | Volts |
| vWF | von Willebrand factor |
| WMS | Weill-Marchesani syndrome |
| WPRE | Woodchuck Hepatitis Virus post-transcriptional regulatory element |
| WT | Wild-type |

## Abstract


**University of Manchester**

**Mukti Singh**

**Degree title: Master of Philosophy (MPhil)**

**Thesis title: Characterisation of ADAMTS-L2 and ADAMTS-L4**

**October 2016**

ADAMTS-Ls (A Disintegrin and Metalloprotease with Thrombospondin type 1 motifs-like proteins) have been identified as having important roles in the extracellular matrix (ECM) and in fibrillinopathies. Mutations in *ADAMTSL2* and *ADAMTSL4* have been associated with geleophysic dysplasia (GD) and ectopia lentis (EL) respectively. Despite their involvement in GD and EL, very little is known about the structure, function and interactions of ADAMTS-L2 and ADAMTS-L4. Characterisation of these molecules will therefore enable greater understanding of these molecules and how they may function in the ECM.

The generation of recombinant ADAMTS-L2 and ADAMTS-L4 in mammalian cell lines was established using lentiviral and episomal expression systems. Of these two systems, the lentiviral expression system exhibited long-lasting stable expression of ADAMTS-L2 and ADAMTS-L4 as well as providing greater yields of protein. Biophysical characterisation of ADAMTS-L2 using OPTIM analysis defined optimal buffer conditions required for protein stability. Biochemical analysis confirmed that both ADAMTS-L2 and ADAMTS-L4 have N-linked glycosylation and that under native conditions ADAMTS-L2 exists in monomeric form. Negative stain TEM allowed for structural modelling of ADAMTS-L2 and ADAMTS-L4. 3D modelling generated a 43.4 Å asymmetric lobular structure of ADAMTS-L2. Domain arrangement of ADAMTS-L2 suggests that the C-terminal thrombospondin type 1 repeats (TSRs) may be flexible. Structural analysis of ADAMTS-L4 revealed that it adopted several conformations owing to the highly flexible nature of the C-terminal TSRs. Due to this flexibility, 3D reconstruction of ADAMTS-L4 was not possible, however 2D analysis determined the average length was 40.6 nm. Interactions of ADAMTS-L2 with fibrillin-1 and latent transforming growth factor β-1 (LTBP-1), and co-localisation of ADAMTS-L4 to fibrillin-1 microfibrils have already been reported. Here, with the use of surface plasmon resonance (SPR), ADAMTS-L2 interactions were confirmed with fibrillin-1 fragment PF17 and a novel interaction with fibronectin fragment FN7-14 was found. Immunofluorescence microscopy of ADAMTS-L2 with fibrillin-1, LTBP-1 and fibronectin in cultured human dermal fibroblasts (HDFs) corroborated the interactions observed in this study with SPR. Complete co-localisation of ADAMTS-L4 with fibrillin-1 and partial co-localisation with LTBP-1 and fibronectin was observed.

This investigation reports novel information regarding the structure and biomolecular interactions of ADAMTS-L2 and ADAMTS-L4, contributing towards the characterisation of both molecules and towards a better understanding of their function.

## Declaration

No portion of the work referred to in the thesis has been submitted in support of an application for another degree or qualification of this or any other university or other institute of learning.

## Copyright Statement

## Acknowledgements

First and foremost, I would like to thank my supervisors, Professor Cay Kielty and Professor Clair Baldock, for the help, support and guidance they have provided me throughout the project. Both Cay and Clair have shown tremendous faith in me, for which I will always be grateful.

I would next like to thank all past and present members of the Kielty and Baldock labs. I am indebted to Dr Stuart Cain for guiding me throughout the project, for answering all my questions and for letting me learn from him. I would like to say a special thanks to Dr Ewa Mularczyk, Dr Rana Dajani and all the other members of the lab for believing in me and for lifting my spirits on days which were unfruitful and disheartening. The encouragement and motivation was a blessing!

I would like to extend my gratitude to all staff in the support facilities, especially Mr. Michael Jackson, Ms. Diana Ruiz and Dr Richard Collins for helping me with experiments and for providing me with their expert knowledge.

Thank you to all my friends for being there in times of need, for being my sounding board and supporting me through tough times, but also for celebrating with me when experiments had worked!

Last but never the least, I would like to thank my mum, dad and brother for the love, support and encouragement they have given me every step of the way. I hope I have made you proud.

# Chapter 1 - Introduction

# 1. Introduction

## 1.1 The extracellular matrix

The extracellular matrix (ECM) is a complex network of non-cellular constituents that plays a vital role in supporting cells both structurally and biochemically. It is composed of various secreted molecules, mainly proteins, glycoproteins and proteoglycans (Bateman et al. 2009), which form diverse structures which vary considerably from one tissue to another. It is this structural variation which determines tissue specificity and function (Mouw et al, 2014). In a review by Cromar et al. (2012), as many as 350 proteins were identified as the core components of the human ECM along with over 520 genes which determine their functional roles and interplay within their microenvironment. The ECM is an important support-system for cells which not only provides architectural integrity, strengthen, support and aid cell adhesion, but also acts as a platform through which cell-matrix and cell-cell signalling interactions take place (Naba et al, 2012). These interactions trigger intricate signalling pathways which enable regulation of growth factors and gene expression (Cromar et al, 2102). The ECM is a dynamic microenvironment which is being constantly remodelled by its inhabitant cells in response to physical stresses such as stretch or injury (Mouw et al, 2014), as well as chemical signals in order to maintain homeostasis. Over the years, research has identified that the ECM of elastic tissues plays a vital role in biological processes such as angiogenesis, cell migration, inflammation, apoptosis, morphogenesis, proliferation and tissue regeneration (Bateman et al, 2009; Hubmacher & Apte, 2013; Bonnans et al, 2014). It is now also known that structural disruption of the ECM, variation of its relative abundance or dysregulation of its biological processes results in many severe connective tissue disorders (Hubmacher & Apte, 2013).

## 1.2 Components of Elastic Fibres

The ECM comprises various macromolecules that are inter-dependent with each other to form supramolecular structures of several tissues. These macromolecules share an intra-dependent relationship in which they work together to fulfil tissue-specific functions. For example, elastic tissues require elastic fibres composed of elastin and fibrillin microfibrils for structural support and for bioregulation. Aberrations in elastic fibres caused by mutations disrupt the overall function of tissues and result in diseases. A wide spectrum of such diseases has been discovered of which fibrillinopathies are a part of. Fibrillinopathies encompass a range of diseases which usually affect fibrillin microfibrils. However in recent years, mutations in other matrix molecules have been discovered giving rise to the same phenotype seen in fibrillinopathies such as members of A Disintegrin And Metalloprotease with Thrombospondin type 1 repeats-like (ADAMTS-L) proteins. Reverse genetics has identified genetic mutations in ADAMTS-L2 and ADAMTS-L4 to result in fibrillinopathies. Although these genetic diseases have been discovered, there still is a need for greater understanding of their underlying mechanisms.

Elastin is an insoluble polymer of tropoelastin monomers (60kDa) and is a major constituent of elastic tissues such as skin, lungs, ligaments, articular cartilage and vascular tissues (Kielty, 2006; Muiznieks et al, 2010). Once tropoelastin monomers have been secreted by fibroblasts, they self-assemble into fibres which are then cross-linked with several other elastin-associated molecules by a family of enzymes called lysyl oxidase (LOX) to form cable-like structures (Keeley et al, 2002; Lucero & Kagan, 2006). In addition to having a mechanical role in various tissues, elastic fibres are also thought to serve as chemotactic agents, support cell differentiation and migration, and act as cell signalling molecules (Karnik et al, 2003; Kielty, 2006; Muiznieks et al, 2010).

Latent transforming growth factor-β binding proteins (LTBPs) are large multi-domain ECM proteins with domain structural similarities to fibrillins (Zilberberg et al, 2012). Each member of the superfamily of 4 LTBPs consists of repeating calcium-binding epidermal growth factor (cbEGF)–like domains and 8 cysteine motifs (TB domains), and covalently binds TGFβ (Handford et al, 2000). TGFβ is a key growth factor involved in processes such as proliferation, angiogenesis, migration, development and homeostasis (Le Goff et al, 2008). Intracellular small latent complexes (SLCs) of disulphide bonded TGFβ dimers covalently bind to LTBPs via the latency associated peptide (LAP) and the 3$^{rd}$ TB domain of LTBPs to form a large latent complex (LLC) (Saharinen & Keski-Oja, 2000). This complex is secreted into the ECM where it binds to other ECM molecules such as fibrillin and fibronectin (Taiplae et al, 1994; Isogai et al, 2003). Activation of TGFβ requires the release of the LLC from the ECM via cell surface integrins, followed by further proteolysis of LAP, ultimately leading to the release of active TGFβ (Chaudhry et al, 2007). Active TGFβ then interacts with its cell surface receptors (TGFBR1 and 2) to activate the Smad2/4 intracellular signalling pathway during which phosphorylated Smad2/4 complexes translocate to the nucleus and transcriptionally regulate target gene expression (Rahimi & Leof, 2007). The ECM regulates the bioavailability of TGFβ by sequestering it on ECM molecules.

Fibrillins are considered to be the predominant glycoprotein core of matrices of dynamic tissues. In humans, 3 different isoforms of this 350kDa protein have been identified, fibrillin-1, -2 and -3 (Piha-Gossak et al, 2012). Expression of all three isoforms varies considerably; fibrillin-2 and -3 dominate in most embryonic tissues (Corson et al, 2004; Cain et al, 2006), whereas fibrillin-1 expression has been reported to a lesser degree in embryonic tissue but predominantly in many adult tissues (Charbonneau et al, 2003; Cain et al, 2006). Fibrillins have several important roles in the ECM which they accomplish directly, and by associating with other ECM structures. For example fibrillin-1 interacts with ADAMTS-L2 (Sengle et al, 2012) and ADAMTS-L4 (Gabriel et al, 2012) in the matrix to provide structural and molecular support to a range of tissues.

### 1.3 Fibrillin in the ECM

As previously mentioned, fibrillin-1 is a key ECM component of many adult tissues. It is a 2871 amino acid glycoprotein encoded by the fibrillin-1 (*FBN1)* gene which in humans is located on

chromosome 15q21.1 (Charbonneau et al, 2003, Baldwin et al, 2013). Structurally, a single fibrillin-1 molecule has multiple domains, of which some are is crucial for its purpose in the ECM.

*Epidermal growth factor (EGF)–like domains*

The primary structure of fibrillin-1 is dominated by 47 EGF-like repeating modules of which 43 are calcium-binding (cbEGF-like) (Handford et al, 1991; Kielty et al, 2005). Characteristic 6 cysteine residues form 3 intra-domain disulphide bridges (Downing et al, 1996) endowing this assembly with structural rigidity and integrity. Downing et al (1996) described using nuclear magnetic resonance (NMR) spectroscopy studies that, in the presence of calcium, the cbEGF-like domains form rod-like structures forming inter-domain disulphide interactions and Reinhardt et al (1997) confirmed this by showing that the absence of calcium made the fibrillin-1 molecule shorter.

*TB domains*

A total of 7 TB domains, also known as 8-cysteine motifs, are scattered through the fibrillin-1 molecule. These disulphide-linked domains bear homology to modules that bind transforming growth factor-β (TGF-β) in LTBPs and have been shown to bind the TGFβ as well (Kielty et al, 2005). As well as this function, it is believed that interaction of TB motifs with their neighbouring EGF-like/cb-EGF-like domains endows flexibility to fibrillin-1 (Yuan et al, 1997).

*Hybrid domains*

There are 2 hybrid domains in fibrillin-1, both bestowed with C-terminal features from TB motifs and N-terminal features from EGF-like domains (Pereira et al, 1993; Jensen et al, 2009). Like TB domains, these contain 8 or 9 cysteine residues, and it was once speculated that one of these was critical in stabilising higher-order fibrillin-1 structure via intermolecular disulphide bonds (Reinhardt et al, 2000). However, later a mutant mouse model, H1Δ demonstrated that deletion of the hybrid domain did not alter microfibril assembly (Charbonneau et al, 2010). It is these domains, along with TB and EGF-like domains that confer some homology between fibrillin-1, -2, -3 and the LTBPs (Hubmacher & Reinhardt 2009; Jensen et al, 2009). Mellody et al (2006) has shown that mutations affecting these domains affect their structure and folding. The study also showed that despite structural changes, the binding of tropoelastin to the mutant fibrillin-1 fragments was unaffected (Mellody et al, 2006). El-Hallous et al (2007) demonstrated that hybrid domains are implicated in the engagement of fibrillin-1 microfibrils with other ECM macromolecules.

*Proline-rich domain*

Fibrillin-1 contains a proline-rich domain, whereas fibrillin-2 has a glycine-rich domain and fibrillin-3 has a proline-rich domain (Kielty et al, 2005). Unique to fibrillin-1, this 58 amino acid domain has a proline content of 42% and is free from the presence of cysteine residues (Baldock et al, 2001; Kielty et al, 2005). This region is believed to facilitate folding of the protein by acting as a ‘hinge’ (Ashworth et al, 1999; Kielty et al, 2005; Piha-Gossack et al, 2012). It was once postulated that the

proline-rich region was involved in interacting with tropoelastin (Baldock et al, 2001). Later on it was revealed that tropoelastin bound to different regions of fibrillin-1 with different affinities (Rock et al, 2004) and that the proline-rich region showed moderate binding affinity for tropoelastin (Clarke et al, 2005).

*N- and C-terminal domains*

Fibrillin-1 monomers are secreted from dermal fibroblasts as propeptides called pro-fibrillin-1 (Lonnqvist et al, 1998). Once in the ECM, they have to be processed at the N- and C-termini in order to participate in microfibril formation. Processing of both termini is carried out by the calcium-dependent endoprotease furin (Baldwin et al, 2013). Several researchers over the years have identified and characterised furin cleavage sites in both termini (Lonnqvist et al, 1998; Raghunath et al, 1999; Reinhardt et al, 2000). Marson et al (2005) described that the N- and C-termini of fibrillin-1 monomers align in a head-to-tail fashion. In 2000, Ritty et al proposed that the heparin-binding site is involved in this interaction, and more recently, Yadin et al (2013) presented a model of fibrillin-1 microfibril assembly which denotes that their interactions involve EGF-domains in the N-terminus and a heparan sulphate (HS)interaction site in the C-terminus.

Understanding the assembly of fibrillin-1 monomers into microfibrils is vital for defining their structural properties and functions in the ECM. Upon secretion from fibroblasts and smooth muscle cells, pro-fibrillin-1 undergoes enzymatic processing by furin/PACE (paired basic amino acid cleaving enzyme) convertases to allow the processed fibrillin-1 monomers to interact with each other in a linear manner (Marson et al, 2005; Yadin et al, 2013). Microfibrils are thought to self-assemble, however microscopy findings suggest a role for cells in this process. It is thought that a tripeptide, Arg-Gly-Asp (RGD) in the fourth TB motif of fibrillin-1 binds to specific integrins on cell surfaces (Bax et al, 2003; Jovanovic et al, 2007) and aids microfibril arrangement. A number of cell surface HS syndecans may also play a role in microfibril assembly (Tiedemann et al, 2001). Fibrillin-1 monomers interact laterally to form a stronger lattice arrangement of 8 fibrillin-1 molecules, and align linearly, giving rise to fibrillin-1 microfibrils. In tissues, these 10-12nm diameter microfibrils can be interlinked via transglutaminase (Qian & Glanville, 1997). The resulting microfibrils, when observed structurally, showed a distinct ‘beads on a string’ organisation (Keene et al, 1991; Baldock et al, 2001).

Widely expressed fibrillin-1 is found not only in elastic tissues such as skin, lungs, aorta and other blood vessels, but also in non-elastic tissues such as bone and the ciliary zonule of the eye (Ashworth et al, 2000; Kitahama et al, 2000; Kielty et al, 2002). In elastic tissues, fibrillin-1 orchestrates biogenesis of elastic fibres by serving as a scaffold upon which polymerised elastin globules deposit, ultimately forming a structure that has a cross-linked elastin core within an encasement of fibrillin microfibrils (Kielty et al, 2002; Baldwin et al, 2013). It is this arrangement of elastic fibres in elastic tissues that endows them with the ability to stretch or recoil in response to mechanical stimuli over long periods of time (Baldwin et al, 2013).

Fibrillin-1 microfibrils also occur in non-elastic tissues. For example, in the eye, fibrillin-1 microfibrils have been located in the iris, cornea and corneal stroma, scleral stroma, ciliary zonule, ciliary processes and stroma as well as the vitreous (Wheatley et al, 1995; Ashworth et al, 2000). The microfibrils provide scaffolding and strength to these connective tissues. The ciliary zonule itself is composed of aligned bundles of microfibrils which are anchored to the ciliary body and lengthen to the lens capsule, where they attach and assist in lens accommodation (Mayne et al, 1997). Recently it was shown in a mouse model that the microfibril composition of the ocular zonule can vary depending on the levels of fibrillin isoforms -1 and -2 (Charbonneau et al, 2003). The researchers analysed ciliary zonules of *FBN1*-deficient mice and found that despite the absence of fibrillin-1 the mice still had intact and functional zonules composed of fibrillin-2 microfibrils. It could thus be that in humans and mice, *FBN2* expression dominates in developing tissues and a switch to *FBN1* occurs in adult tissues. In *FBN1* deficient mice, this switch does not occur and so the zonule is formed only of fibrillin-2 microfibrils (Beene et al, 2013). The authors of this article also showed that microfibrils can be heterogeneous in composition consisting of a mix of fibrillin-1 and fibrillin-2 (Beene et al, 2013).

Fibrilin-1 microfibrils interact with fibronectin which provide a mechanical and tensile structure to the ECM. However, fibrillin-1 microfibrils also have a regulatory role in which they bind LTBPs and sequester growth factors such as TGFβ (Hubmacher et al, 2014). Isogai et al (2003) and Ono et al (2009) first demonstrated that the C-terminal of LTBP1 interacts within 4 N-terminal domains of fibrillin-1 (EGF-like 2, 3, hybrid domain 1 and cbEGF-like 1). Specifically it was shown that LTBP-1 and LTBP-4 binding sites were located in the hybrid domain 1 of fibrillin-1, and that mutations affecting the neighbouring EGF-like domain 3 either diminished or abolished fibrillin-1 binding to LTBP-1 and LTBP-4 respectively (Ono et al, 2009).Later, Massam-Wu et al, (2010) showed that whereas C-terminal fragments of LTBP1 bind strongly to the N-terminus of fibrillin-1, full-length LTBP1 has a much weaker interaction, suggesting that the fibrillin-1 binding site on full-length LTBP1 is impeded. Massam-Wu et al (2010) showed that C-terminus of LTBP1 binds to fibrillin-1 hybrid domain 1 and the next cbEGF-like domain, and that this interaction is influenced by the EGF-like 3 domain situated before the hybrid domain. Based on these findings it can be said that fibrillin-1 not only has a major architectural role and strengthens the matrix of different tissues, but is also is a key player in bioregulation of the matrix. A review by Sengle & Sakai (2015) focusses on this property of fibrillin-1 and comments on its mechano-sensory attributes. The review comments on the direct and indirect interaction fibrillin-1 has with many growth factors, and questions whether this dynamic relationship is crucial to understanding the mechanisms underlying growth factor signalling in healthy and diseased tissues (Sengle & Sakai, 2015). The review highlights a need for further research to learn more about the contributions of fibrillin-1 mechano-sensation.

Novel discoveries regarding the composition of the elastic and non-elastic tissue extracellular matrices are continuously enhancing our knowledge of how their various components self-

assemble and function. Identification of molecular structures, binding sites, proteases and signalling mechanisms have all contributed to understanding the dynamic nature of the ECM (Mouw et al, 2014).

The ECM is affected by several genetic diseases which disrupt its proper functioning and structure. Mutations occurring in different components of the matrix can lead to conditions which range in severity from mild to life-threatening. Subsets of such diseases are called fibrillinopathies.

### 1.4 Fibrillinopathies – Fibrillin-1 microfibrils in disease

Mutations in the *FBN1* gene lead to heritable connective tissues disorders, named fibrillinopathies. They encompass various conditions some of which share similar clinical features, but at the same time, have distinct phenotypes. (Figure 1.1)

### 1.5 Marfan syndrome (MFS)

MFS is the most commonly occurring fibrillinopathy, having an incidence of 3 in 10,000 people (Pyeritz, 2000). Despite being inherited as an autosomal dominant trait, surprisingly 25% of MFS cases are sporadic and are caused by a new mutation (Robinson, et al, 2006). To date, many more than 1000 mutations in the *FBN1* gene have been discovered that are responsible for several MFS clinical manifestations; particularly in the cardiovascular, ocular and skeletal systems (Loeys et al, 2003). Patients can either present with isolated features or have a combination of MFS manifestations. MFS sufferers are usually tall in stature and have disproportionately longer extremities with arachnodactyly (Ammash et al, 2008). Cardiovascular defects including dilation and dissection of the aorta are classed as severe and life-threatening and result in high rates of early mortality (Loeys et al, 2003). Ocular abnormalities include severe myopia, ectopia lentis (EL), glaucoma and in some cases, retinal detachment (Robinson et al, 2006; Ammash et al, 2008). A proportion of MFS-causing mutations in *FBN1* are missense mutations (Kirschner et al, 2011) i.e. the mutation causes a single nucleotide change resulting in a different amino acid. Consequently mutations in the gene may interfere with fibrillin-1 interactions or structural folding, render the protein non-functional or result in a truncated molecule.

### 1.6 Weill-Marchesani syndrome (WMS)

WMS is a connective tissue disorder phenotypically characterised by short stature, brachydactyly, joint stiffness and a range of ocular abnormalities (Figure 1.1). Microspherophakia, in which the lens of the eye is much smaller and more spherical than usual, results in myopia that worsens over time (Kochhar et al, 2013). Ectopia lentis (EL), also one of the main manifestations of WMS, is a condition in which the lens is abnormally positioned or dislocated. This condition can present on its own where the sufferer does not have any other symptoms of WMS or MFS. When caused by mutations in *FBN1,* EL represents an autosomal dominant trait and the condition is referred to as isolated EL (IEL) (Chandra et al, 2014). Glaucoma wherein internal ocular pressure can increase, resulting in blindness (Faivre et al, 2003).

Mutations in *FBN1* cause an autosomal dominant trait of inheritance in patients. There have been many studies in which several generations of a family have the same mutations in the *FBN1* gene, leading to their clinical presentations (Gorlin et al, 1974; Wirtz et al, 1996; Everekliogl u et al, 1999). So far, 3 mutations have been identified in *FBN1* that cause WMS.

Faivre et al (2003) identified a 24-nucleotide (8-amino acid) deletion in the *FBN1* gene (Figure 1.2). The researchers reported this deletion occurs in the 5$^{th}$ TB motif (TB5) and that it deletes one of the cysteine residues within the domain. This mutation ultimately results in an unstable domain which then interferes with microfibril assembly and function. Furthermore, Cain et al (2012) went on to study the effect of this 8-amino acid deletion by investigating the binding of WMS mutant and wild-type TB5 fibrillin-1 protein fragments (PF17) to HS. Their findings showed that wild-type PF17 monomers had the greatest affinity for HS. However, monomeric PF17 WMS did not bind HS and the dimeric form of the mutant fragment, created by disulphide-bonding of the unpaired cysteine residues, showed some heparin binding. These data suggest that intact TB5 domain containing 8 disulphide-bonded cysteine residues may be vital for HS binding. Although PF17 WMS dimers showed some HS binding, in a physiological context, their diminished ability to bind HS would be likely to significantly affect their interactions with other ECM molecules.

Another large deletion in the *FBN1* gene causing WMS was reported by Sengle et al (2012). They identified a heterozygous 7895-nucleotide deletion spanning from exon 8 to 11, resulting in the loss of the TB1 domain, the proline-rich region and EGF-like domain 4 (Figure 1.2). The group then went on to replicate this mutation in a mouse model which mirrored the human WMS phenotype. The mutant mice were short in stature with reduced growth of the long bones with thickened skin. Histological analysis of patient and mutant mouse skin depicted very similar skin fibrosis in which, there was a widened dermal layer, less hypodermal fat and an increased, dense deposition of collagen fibres (Sengle et al, 2012). Further examination of microfibril ultrastructure using electron microscopy revealed large aggregates of microfibrils with reduced periodicity and elastic fibres which appeared ‘moth-eaten’ in both patient and mutant mouse (Sengle et al, 2012). Overall, Sengle et al (2012) presented a mouse model which is genotypically and phenotypically identical to human WMS patients. This implies that both models share a common pathogenic mechanism.

The most recent *FBN1* mutation causing WMS was described by Wang et al (2014) and is the missense mutation C1748Y affecting the TB5 domain. Further research implicating this mutation has not been published yet.

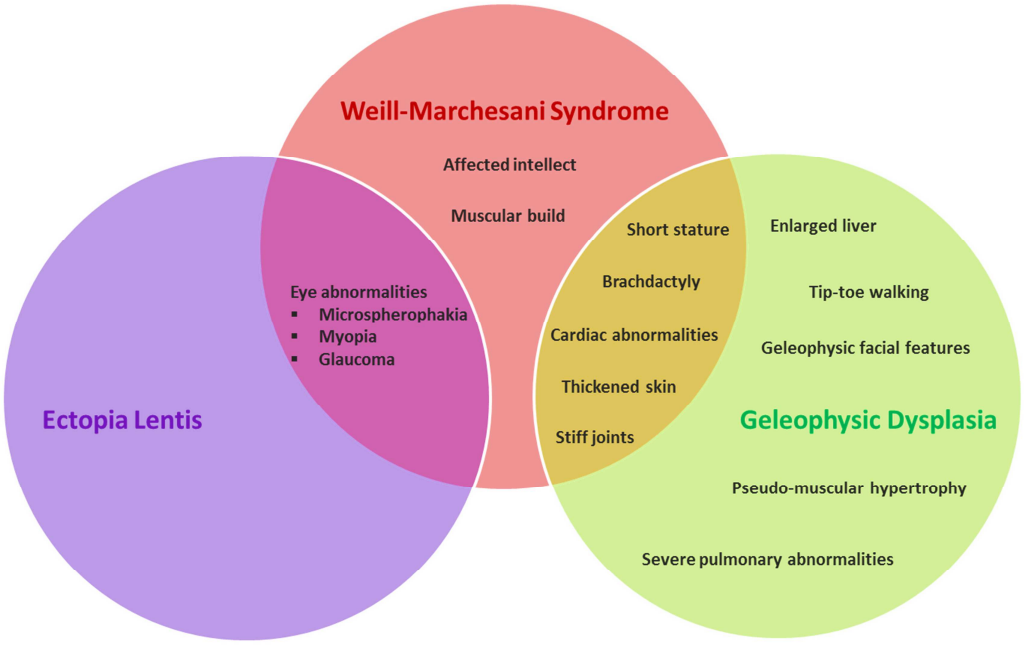


**Figure 1.1:** Phenotypes of different fibrillinopathies. There is distinct overlap of clinical manifestations between Weill-Marchesani Syndrome (WMS) and Geleophysic Dysplasia, as well as WMS and Ectopia Lentis.

### 1.7 Geleophysic dysplasia (GD) and Acromicric dysplasia (AD)

Mutations in the *FBN1* gene that cause GD carry an autosomal dominant trait of inheritance, whereas AD causing mutations are autosomal recessive (Le Goff et al, 2011). GD shares many clinical manifestations with WMS such as short stature, stiff joints and brachydactyly, however it has some features which are unique, for instance the sufferers have 'happy' faces with distinct features and some develop pulmonary difficulties (Figure 1.1). Due to similar phenotypes, GD and WMS are easily mistaken for one another (Kochhar et al, 2013; Pimienta et al, 2013), however like WMS, GD patients do not present with eye abnormalities. Several autosomal dominant *FBN1* mutations have been reported that cause GD (Figure 1.2).

As seen in Figure 1.2, the majority of mutations causing WMS, GD and AD are located in the TB5 domain. Some of the mutations cause defective domain folding by affecting the number of cysteine residues and disulphide bonds within the domain. These structural changes in turn interfere with fibrillin-1 function as a whole. Furthermore, Cain et al (2012) investigated other mutations and their effect on HS binding. Their findings confirmed that a wild-type fragment of fibrillin-1 containing the TB5 domain (PF17) has a high affinity for HS. They also discovered that the PF17 fragments containing WMS, GD and AD-causing mutations (8 amino acid deletion 1692-1699 [WMS], Y1696C [GD], Y1699C [GD/AD], M1714R [AD], G1726V [AD], A1728T [GD/AD] and S1750R [AD]) showed disrupted binding to HS.

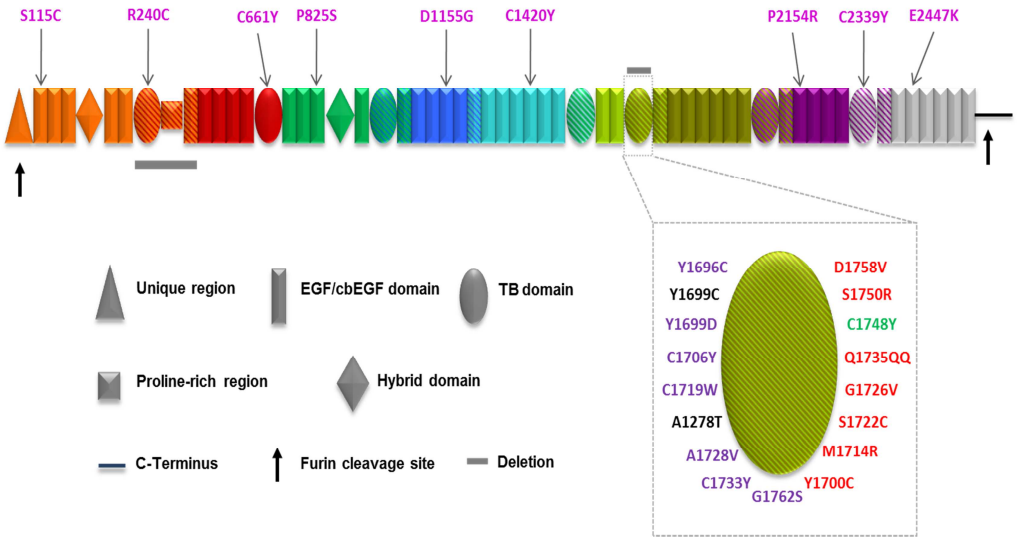


**Figure 1.2:** Domain structure of Fibrillin-1 and mutations causing fibrillinopathies. TB5 enlarged to show large number of mutations. Mutations: Purple cause GD; Red cause AD; Black cause AD and GD; Pink cause EL; Green causes WMS, grey bars represent deletions. Figure complied using: Kainulainen et al, (1993); Lonngvist et al, (1993); Loeys et al, (2000); Katze et al, (2001); Koerkkoe et al, (2001); Faivre et al, (2003); Biggin et al, (2003); Hubmacher & Apte, (2011); Le Goff et al, (2011); Chandra et al, (2012); Sengle et al, (2012).

Two novel mutations have been discovered by Wang et al (2014). Both are missense mutations affecting the TB5 domain of fibrillin-1. The first of these mutations, N1730I presented with pulmonary difficulties and hepatomegaly confirming that the patient had GD (Wang et al, 2014). The second mutation C1733F, resulted in the patient presenting with short stature and limbs, facial dysmorphyism and stiff joints however, the patient did not have cardiac or ocular abnormalities, consistent with the AD phenotype (Wang et al, 2014).

The fibrillinopathies described above, namely WMS, GD and EL/IEL, are not always caused by mutations in *FBN1*. Mutations in other ECM glycoproteins can also give rise to the same phenotype in patients and the discovery of several genotypic variants shows that these fibrilliopathies are heterogeneous in nature. The molecules, apart from fibrillin-1, that can cause these fibrillinopathies are a family of matrix metalloproteases termed A Disintegrin And Metalloprotease with Thrombospondin type 1 repeats (ADAMTS) and ADAMTS-like (ADAMTS-L) proteins.

## 1.8 The ADAMTS family

The mammalian ADAMTS family are multi-domain zinc metalloproteases. Since their discovery about 2 decades ago, extensive research has revealed the complex structure, nature and function of each member.

Structurally, all ADAMTS proteases are distinct; however they share a similar arrangement containing multiple domains, motifs and modules, all of which are important to their specific functions.

*Propeptide domain*

Located in the N-terminal part following the signal peptide, the propeptide domain prevents ADAMTS protease activity by binding to the catalytic domain, thereby keeping the molecule in a latent state (Jones & Riley, 2005; Tortorella et al, 2009). The domain itself varies in size and contains a furin cleavage site at is C-terminal end (Tang, 2001).

*Catalytic domain*

The catalytic domain contains the reprolysin-type (snake venom-type) zinc-binding site in which histidine residues hold the water-bound zinc firmly associated to the protein (Tortorella et al, 2009). Within the domain exists a methionine residue which is characteristic of zinc-binding metalloproteases and is required to maintain the structure of the active site (Porter et al, 2005). Functionally it is this domain that is responsible for ADAMTS enzyme activity.

*Disintegrin-like module*

The disintegrin-like domain is partly homologous to disintegrin modules that are known to bind cell surface integrins during cell adhesion (White, 2003). However, as the name suggests, these modules are disintegrin-like and thus far have not been reported to show disintegrin activity (Tang, 2001; Jones & Riley, 2005; Tortorella et al, 2009).

*Thrombospondin type 1 repeat (TSR)*

All ADAMTS molecules contain a single central TSR, whilst the C-termini contain a varying number of these repeats (Tang, 2001). It has been suggested that the central module has the potential to bind to various glycosaminoglycans (GAGs) owing to the presence of a specific sequence of amino acids (Tortorella et al, 2000). TSRs are found in many matrix-binding proteins (de Fraipont et al, 2001), therefore it can be suggested that these TSR domains may also serve in ADAMTS anchorage.

*Cysteine-rich and spacer domains*

Each ADAMTS member contains a cysteine-rich region which contains 10 conserved cysteine residues (Tang, 2001). The spacer domain follows the cysteine-rich domain and is said to be the

least homologous in all the ADAMTSs (Tang et al, 2001). The spacer domain itself varies in length in different ADAMTSs and contains several hydrophobic residues (Jones & Riley, 2005). Together with the cysteine-rich region, the spacer module may play a vital role in substrate specificity, as removal of these modules leads to the ADAMTS in question binding to more substrates (Kashiwagi et al, 2004; Tortorella et al, 2009).

*Protease and Lacunin (PLAC) domain*

Most ADAMTS members contain a PLAC domain at their C-terminus. It consists of 6 conserved cysteine residues, and is homologous to most proprotein convertases that are required for ADAMTS activation (Zhou et al, 1999; Tortorella et al, 2000). Despite being part of several ADAMTSs, the function of the PLAC domain remains unknown.

Together, the propeptide, catalytic, disintegrin-like units and the central TSR modules of ADAMTSs are referred to as the protease domain, while the remaining parts of the molecule form the ancillary domain (Figure 1.3). The ancillary domain in each ADAMTS endows unique properties on each individual member of the family, and is considered to be essential for substrate recognition and anchorage (Apte, 2004). ADAMTS molecules are secreted as inactive zymogens which require post-translational modification. Activation of these proteases is achieved by excision of the propeptide domain by furin, a proprotein convertase (Apte, 2004; Dubail & Apte, 2015). Some ADAMTS molecules undergo additional proteolysis at the C-terminal end (Hubmacher & Apte, 2011) which may alter the function of the full-length protease or create smaller fragments displaying novel biological activities. Further modifications such as disulphide bonding, N-glycosylation and O-glycosylation also take place post-translationally (Dubail & Apte, 2015). Once secreted and activated, the ADAMTS proteases bind to cell surfaces or to other ECM macromolecules.

ADAMTS involvement has been seen in many biological processes, for example angiogenesis, cancer, arthritis, coagulation, development, morphogenesis, inflammation and tissue organisation (Porter et al, 2005). All 19 members of the ADAMTS family have distinct biological roles, however they have been divided into clades, which groups together members with similar sequences and biochemical functions (Apte, 2004). ADAMTS1, 4, 5, 8, 9, 11 and 15 are grouped together and are proteoglycanases as they have been shown to cleave the proteoglycans aggrecan and versican (Porter et al, 2005; Zeng et al, 2006); ADAMTS2, 3 and 14 have been termed the procollagen amino peptidases (Colige et al, 1997; Wang et al, 2003); ADAMTS7 and 12 make up the mucin proteoglycan clade (Apte, 2009); ADAMTS13 is the von Willebrand factor-cleaving protease (Levy et al, 2001). The functions of the remaining ADAMTSs (6, 10, 16, 17, 18 and 19) are yet to be discovered, however it is unclear whether ADAMTS 10 is enzymatically active in the ECM (Somerville et al, 2004). It must also be recognised that mutations in genes encoding ADAMTS10 and ADAMTS17 are linked to fibrillinopathies such as WMS (Le Goff & Daire, 2011)

## 1.9 ADAMTS10

Several members of the ADAMTS family are implicated in diseases which arise from mutations; ADAMTS10 is associated with the fibrillinopathy WMS (Apte, 2009).

The *ADAMTS10* gene is located on chromosome 19p13 and encodes the glycoprotein ADAMTS10. Expression studies have revealed that *ADAMTS10* is ubiquitously expressed in embryonic and adult tissues including the heart, lung, liver, kidneys, brain, pancreas and placenta (Porter et al, 2005).

The protease itself has the classic ADAMTS molecular organisation, however, upon closer analysis several differences have been observed in ADAMTS10 subdomains in comparison to other members of the family. Structurally, ADAMTS10 has comparable domain structure to that of ADAMTS17 (Apte, 2004) and is known to be very similar to ADAMTS6 due to the presence of 4 TSRs in the ancillary domain (Somerville et al, 2004) (Figure 1.3). Present in the ADAMTS10 catalytic domain, like in all other ADAMTS proteases, is the zinc-binding site (Somerville et al, 2004). All 4 TSRs located in the ancillary domain contain 6 cysteine residues each (Somerville et al, 2004). In most other ADAMTSs, the propeptide domain contains multiple proprotein convertase recognition sites to ensure efficient cleavage for protease activation (Somerville et al, 2003; Somerville et al, 2004; Wang et al, 2003; Wang et al, 2004). However, in ADAMTS10 there exists only one such recognition site for furin; other potential furin sites in ADAMTS10 are incompatible with furin cleavage due to amino acid sequence variations (Somerville et al, 2004). The lack of furin-compatible cleavage sites accounts for the reported inefficient activation of secreted ADAMTS10 as the propeptide domain is not completely excised from the ADAMTS10 protease (Kutz et al, 2011).

Once activated by experimental mutations, Kutz et al (2011) showed that ADAMTS10 was able to bind fibrillin-1 more efficiently. ADAMTS10 binds to two different sites on fibrillin-1 with high affinity, one of them in the N-terminus and the other in the C-terminal region (Kutz et al, 2011). To further validate this result, Sengle et al (2012) showed ADAMTS10 C-terminal binding to fibrillin-1 C-terminus. Binding studies also showed that ADAMTS10 did not bind other ECM molecules such as fibronectin or LTBP-1 (Kutz et al, 2011). Addition of exogenous ADAMTS10 to cultured bovine nuchal ligament cells enhanced deposition of fibrillin-1 matrix. Furthermore, fibroblasts from a WMS sufferer with ADAMTS10 mutations deposited very few fibrillin-1 fibres in comparison to wild-type controls (Kutz et al, 2011). These data suggest that ADAMTS10 is more involved in microfibril biogenesis than ECM turnover.

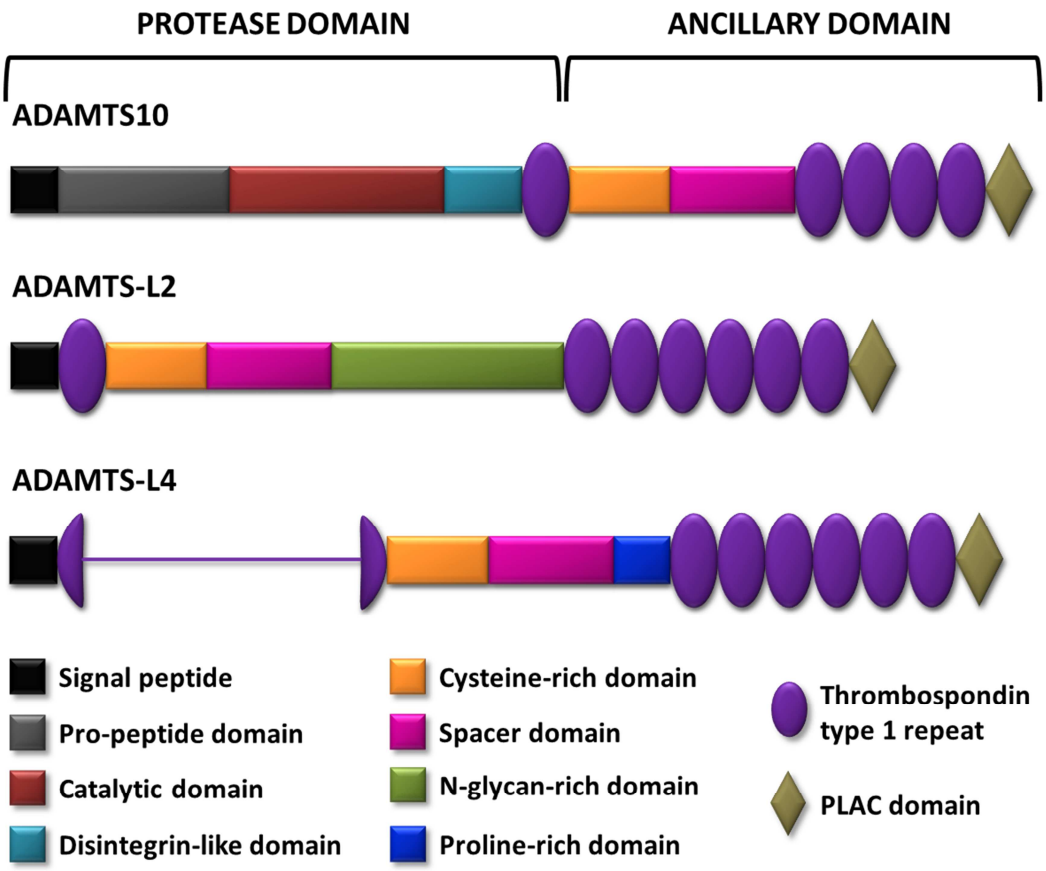


**Figure 1.3:** Domain structures of ADAMTS10, ADAMTS-L2 and ADAMTS-L4. The protease and ancillary domains are also shown. Figure adapted from Le Goff & Cormier-Daire (2011) and www.uniprot.org (unique entry identifiers: ADAMTS10 – Q9H324; ADAMTS-L2 – Q86TH1; ADAMTS-L4 – Q6UY14)

### 1.10 ADAMTS10 in WMS

Mutations in *ADAMTS10* cause autosomal recessive WMS which is phenotypically indistinguishable to autosomal dominant WMS caused by *FBN1* mutations (Apte, 2004). Furthermore, *FBN1* mutations that cause WMS can lead to TGFβ dysregulation (Apte, 2009). Binding studies conducted by Sengle et al (2012) showed that the ancillary C-termini of ADAMTS10 binds to the N-terminal region of fibrillin-1. Knowing that ADAMTS10 can bind fibrillin-1, it can be postulated that complexes of ADAMTS10 and fibrillin-1 could play a major role in TGFβ regulation. Using confocal and immuno-electron microscopy, ADAMTS10 was seen to co-localise with fibrillin-1 in the ciliary zonules of the eye, which are disrupted in WMS sufferers causing EL. This further supports a role for ADAMTS10 in assembly or maintenance of the microfibrillar structure rather than degradation (Kutz et al, 2011). In 2004, Dagoneau et al. first identified three ADAMTS10 mutations in WMS sufferers which include two splice variants and one nonsense mutation. The nonsense mutation, R237X results in a truncated protein which terminates in the

catalytic domain. Two splice variants that were identified in the catalytic domain were reported as 810+1G>A which results in a frameshift and a stop codon 20 codons downstream, and 1190+1G>A which again causes a frameshift and a downstream stop codon (Dagoneau et al, 2004). Kutz et al, (2008) reported the mutation A25T in the signal peptidase cleavage site of ADAMTS10. This mutation prevents secretion of full-length ADAMTS10. However, a fragment containing signal peptide, propeptide and catalytic domains is secreted (no ancillary domain), which also undergoes furin processing, suggesting that the ancillary domain and its folding must play a vital role in the WMS pathway. The same researchers also identified a nonsense mutation Q318X which was shown to mediate mRNA decay (Kutz et al, 2008). Morales et al (2009) described three new mutations in *ADAMTS10* that phenotypically exhibited WMS. The research group identified two missense mutations, G518A in the disintegrin-like domain and G700C located in the cysteine-rich module of patients exhibiting classical WMS manifestations. More recently Li et al (2014) discovered a novel compound heterozygous mutation affecting two alleles: c.1586G>A and c.2485T>A which results in the amino acid changes G529E in the disintegrin-like domain and W829R in the second ancillary TSR domain respectively (Li et al, 2014). Furthermore, another recessive WMS-causing missense mutation (L14Q) was described in 2014 by Steinkelner et al. This mutation in the signal peptide leads to diminished secretion of the mutated fragment; however this effect is coupled with intracellular mis-targeting and increased cytoplasmic concentrations of un-glycosylated ADAMTS10 (Steinkelner et al, 2014).

An ADAMTS10 mutation in dogs causes open-angle glaucoma (Kutchey et al, 2011). Molecular modelling of an *ADAMTS10* variant (G661R) demonstrated disrupted folding of the cysteine-rich module and biochemical analysis showed increased instability of the mutant in comparison to the wild-type.

### 1.11 ADAMTS17

Mutations in *ADAMTS17* cause WMS-like syndrome, with symptoms including ocular abnormalities and short stature. However, brachydactyly, joint stiffness and cardiovascular problems are absent (Morales et al, 2009). Morales et al confirmed this phenotype by reporting 3 mutations: a single base pair insertion in exon 18 leading to a truncation in the protein, a splice mutation in intron 12 that produced 3 truncated fragments and a nonsense mutation in exon 4. The insertion and splice variants are predicted to produce truncated fragments consisting of the catalytic domain of ADAMTS17, but none of the TSRs. However, the nonsense mutation product would lack the catalytic domain and all TSRs (Morales et al, 2009). All of these domains are critical for ADAMTS binding and function. An ADAMTS17 splice variant mutation, which was identified as frame-shift occurred due to the skipping of exon 10, was seen to cause IEL in terriers. This mutation resulted in progressive degradation of the ocular zonule over time, with increased hypertrophy in the underlying ciliary epithelium which, together with elevated intra-ocular pressure, resulted in lens dislocation (Farais et al, 2010).

## 1.12 ADAMTS-Ls

ADAMTS-L proteins have been implicated in several biological processes such as angiogenesis, coagulation and cell migration (Chandra et al, 2013). Thus far, their specific functional roles are unknown; however their structural and ECM binding properties resemble that of ADAMTS proteases, which could suggest a role in ADAMTS regulation as well as a structural and organisational role in the ECM. A recent review by Hubmacher & Apte (2015) suggests that ADAMTS-Ls have a major role in microfibril assembly, matrix anchorage and stability as mutations in certain ADAMTS-Ls result in structural disruption of the matrix. ADAMTSs and ADAMTS-Ls may act somewhat like linkers that stabilise microfibrillar assembly in the supramolecular matrix, especially in tissues in which architectural integrity is vital for function (Hubmacher & Apte 2015).

## 1.13 Structure of ADAMTS-Ls

ADAMTS-Ls are ECM glycoproteins that are products of distinct genes (Apte, 2009). They have a similar molecular backbone organisation to that of ADAMTS proteases in that they share homology with the ancillary domain. The difference lies in the N-terminal region as ADAMTS-Ls lack the pro-peptide and catalytic domains (Le Goff & Cormier-Daire, 2011), which means they do not possess any catalytic abilities. Having said that ADAMTS-Ls share several similarities with ADAMTSs, the domains that are homologous may have similar functions. ADAMTSs and ADAMTS-Ls, as seen in Figure 1.3, both contain cysteine-rich and spacer domains. Although the role of these domains in ADAMTS-Ls is yet to be deciphered, in ADAMTSs they have been investigated. For example, in ADAMTS13, a von Willebrand factor (vWF) cleaving protease involved in thrombosis (Sandler, 2002), the cysteine rich and spacer domains are essential for cleaving vWF (Soejima et al, 2003). Soejima et al (2003) found that mutant ADAMTS13, where the cysteine-rich and spacer domains had been truncated, was unable to cleave vWF efficiently. Cysteines are involved in disulphide bond formation which inevitably contribute towards the tertiary structure and correct folding of a protein. In turn, this helps the protein to interact with other proteins and fulfil its function. From this it can be deduced that the cysteine-rich domain, and possibly spacer domain, in ADAMTS-Ls might be vital for their function.

All ADAMTSs and ADAMTS-Ls contain chains of TSRs which are ubiquitously found in several matrix proteins (Adams & Tucker 2000). Each TSR is 60 amino acids in length and is encoded on a separate exon, which means each TSR is an independently folded structure (Adams & tucker, 2000). Structural studies on TSRs have been conducted on thrombospondin-1 (TSP-1) which consists of 3 TSRs in its C-terminus, and properdin which is formed of a chain of 7 TSRs (Kouser et al, 2013; Tan et al, 2002). Tan et al first published the crystal structure of 2 of the 3 TSRs that are part of TSP-1 (Figure 1.4A). Their model shows that each TSR is a long, thin spiralling unit which is composed of 3 beta strands folded. Figure 1.4A also shows disulphide bonds (yellow) which can be seen linking one TSR to the second as well as bridging the cysteine residues at the bottom of

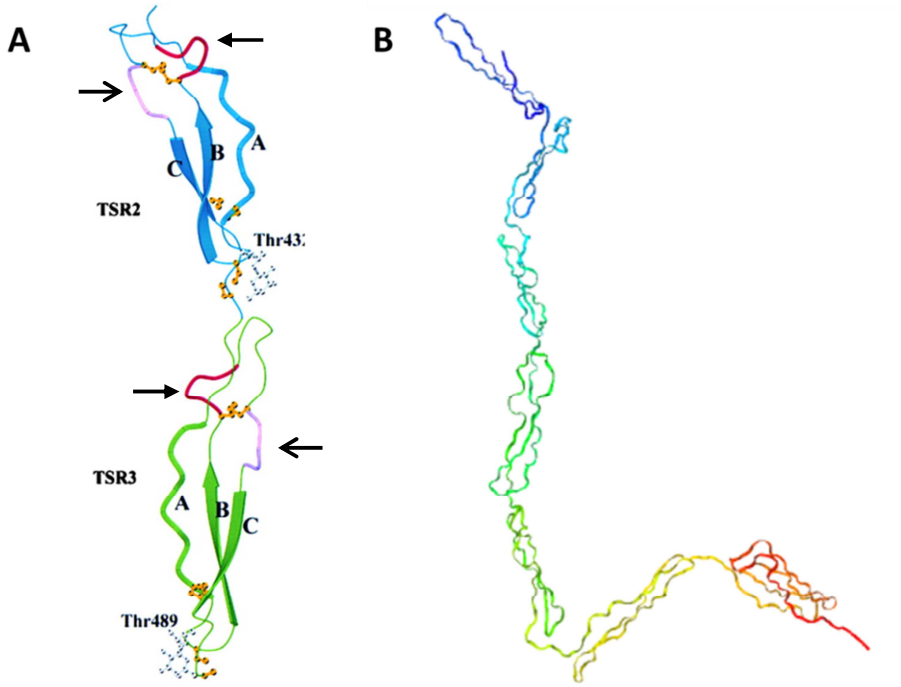


**Figure 1.4:** Structure of individual TSRs from TSP-1 and properdin. (A) Ribbon diagram of human TSR2 (blue) and 3 (green) of TSP-1; disulphide bonds are shown in yellow, loop region C-terminal to beta sheet B is red (block arrows) and top of beta sheet C is purple (open arrows). (B) Ribbon diagram of properdin consisting of 7 consecutive TSR domains each represented by a different colour (PDB file 1W0S). Figure A adapted from: Tan et al (2002). Figure B image from the RCSB (www.rcsb.org) of PDB 1W0S.

beta sheet B (red handle indicated by block arrows) and the top of beta sheet C (purple handle indicated by open arrows).

Properdin is formed of 7 TSRs and is described as a 26 nm flexible rod-like structure (Higgins et al, 1995). Figure 1.4B illustrates this arrangement with each individual TSR in the structure shown as a different colour. The C-terminal region of ADAMTS-Ls are also comprised of chains of TSR repeats. Given the structural similarities between ADAMTS-Ls and properdin, and also due to the lack of structural information for ADAMTS-Ls in literature, it may be assumed that the former exhibits flexibilities and conformation similar to that of the latter. In the literature, properdin has been shown to bind to GAGs such as heparan sulphate and chondroitin sulphate (Yu et al, 2005). Therefore, it can be assumed that in ADAMTS-Ls the C-terminal chain of TSRs will also interact with GAGs and possibly other matrix proteins.

Like fibrillin-1 and ADAMTS10, mutations in some members of the ADAMTS-L subfamily are responsible for microfibril related fibrillinopathies. Phenotypically, mutations in ADAMTS-Ls resemble mutations that occur in the *FBN1* gene. Gene analysis studies in such patients have

determined the involvement of ADAMTS-L2 in GD and ADAMTS-L4 in EL (Le Goff & Cormier-Daire, 2011).

### 1.14 ADAMTS-L2

ADAMTS-L2 is a secreted ~110 kDa glycoprotein encoded by the *ADAMTSL2* gene located on the chromosome 9q34.2 in humans (Koo et al, 2007). Although all ADAMTS-Ls share their basic ancillary domain structure with ADAMTS proteases they have some differences in domain structure. In the case of ADAMTS-L2, the modular backbone lacks the propeptide, catalytic and disintegrin-like domains, but contains a longer spacer region with an N-glycan rich module and 6 TSRs in the ancillary domain (Koo et al, 2007) (Figure 1.3). Functional studies carried out by Koo et al in 2007 support the suggestion that the N-glycan domain in the spacer region may prevent proteolysis of the molecule, aid inter-domain interactions and provide greater separation between the first 2 TSRs. Koo et al (2007) show in their investigation that ADAMTS-L2 is approximately a 140 kDa glycoprotein, however treatment with Peptide: N-Glycoside F (PNGase F) resulted in the protein mass reducing to 110 kDa, indicating that ADAMTS-L2 is N-glycosylated.

Gene expression of ADAMTS-L2 is widely distributed: in the mouse, expression was seen in the kidneys, lungs, heart, brain, placenta, brain and skeletal muscle but the highest level was observed in the liver (Koo et al, 2007; Hubmacher et al, 2015). In humans, *ADAMTSL2* mRNA was strongly detected in the skin epidermis, the tracheal wall, blood vessels, pulmonary arteries and developing bronchioles and also in cardiac myocytes (Le Goff et al, 2008). This expression pattern is consistent with clinical manifestations observed in GD. More recently, Hubmacher et al (2015) presented an *ADAMTS-L2* deficient mouse as a model of GD. They showed relative expression of *ADAMTSL2* dominates in embryonic tissues such as smooth muscle in lung bronchioles and the liver which consistent with previous findings.

Le Goff et al (2011) and Sengle et al (2012) demonstrated the binding of ADAMTS-L2 specifically to the N-terminal region of fibrillin-1 and not to the C-terminus. The ADAMTS-L2 binding site on fibrillin-1 is within the region encompassing TB1, the proline-rich domain and EGF-like 4 domain as mutant fibrillin-1 fragments missing these domains (also a WMS mutation) did not bind ADAMTS-L2. Interactions of ADAMTS-L2 with both N- and C-termini of fibrillin-1 were shown recently by Hubmacher et al (2015).

Le Goff et al (2008) showed that ADAMTS-L2 interacted with the central region of LTBP-1 however; Sengle and colleagues opposed these findings showing that ADAMTS-L2 binds to the C-terminal region of LTBP-1, not the central region (Sengle et al, 2012). Taking both sets of data into consideration, it can be suggested that ADAMTS-L2 plays a TGFβ-regulatory role.

ADAMTS-L2 deposition has previously been investigated in CV-1 in origin and carrying the SV40 genetic material (COS) cells which had been transfected with ADAMTS-L2 and embryonic mouse tissue (Koo et al, 2007). This study reported that in cultured COS cells ADAMTS-L2 was secreted

and localised to at the cell surface (Koo et al, 2007). This group also looked at immunolocalisation of ADAMTS-L2 in mouse tissue from 16.5 and 17.5 day old embyros. ADAMTS-L2 was detected in several organs and it was noted that its expression was stronger in some tissues compared to others. For example, ADAMTS-L2 was strongly detected in smooth muscle cells (SMCs) found surrounding the vasculature in the liver, heart and lungs (Koo et al, 2007). Strong immunolocalisation was also described in skeletal muscle, skin epidermis and the ECM of developing cartilage of the spinal cord. However weaker expression was reported in lung bronchioles and skin dermis (Koo et al, 2007). More recently the same research group described immunohistochemical observations they recorded in a knock-out mouse model they created. Hubmacher et al (2015) found that knocking down the expression of ADAMTS-L2 led to an increase in expression of fibrillin-2 in bronchial SMCs of ADAMTS-L2 deficient mice compared to WT littermates at birth; however no differences in fibrillin-2 expression were observed in embryonic tissue. They also looked at the expression of fibrillin-1 and found that during embryonic stages fibrillin-1 staining in bronchial SMCs was weak as expected. At birth this expression increased, however there was no statistical difference between the ADAMTS-L2 and WT tissues, implying that ADAMTS-L2 does not affect levels of fibrillin-1 expression (Hubmacher et al, 2015). Co-staining of fibrillin-1 and -2 in WT lung tissue at birth showed that fibrillin-1 expression was dominant in both bronchial epithelium and in the SMCs surrounding the bronchi and very little fibrillin-2 was detected (Hubmacher et al, 2015). Whereas in ADAMTS-L2 null tissue, fibrillin-2 expression was seen in the bronchial epithelium partially co-localising with fibrillin-1, but was absent from SMCs surrounding blood vessels (Hubmacher et al, 2015). These data suggest that the absence of ADAMTS-L2 in lung tissue does not affect the expression and localisation of fibrillin-1; however it does enhance the fibrillin-2 expression in some areas. This group also went on to investigate the effect of knocking down ADAMTS-L2 on other matrix proteins such as fibronectin, LTBP-1 and MAGP-1. Fibronectin staining appeared to be reduced in ADAMTS-L2 deficient lung tissue, but quantification revealed that this was not significant in comparison to WT tissue. LTBP-1 staining was enhanced in the bronchial epithelium and MAGP-1 staining was increased in bronchial SMCs and these differences were statistically significant in comparison to WT mouse lung tissue (Hubmacher et al, 2015).

### 1.15 ADAMTS-L2 and GD

Over the past decade screening of several patients consistently presenting with tip-toe walking, pulmonary difficulties and facial dysmorphisms, which are discriminating phenotypic features of GD have allowed the discovery of mutations in the *ADAMTSL2* gene (Table 1.1).

Disrupted and disorganised microfibrils coupled with increased TGFβ signalling are distinct pathological features observed in tissues of patients with GD. Interestingly, upon birth, a large proportion of *ADAMTSL2* deficient mice in a study conducted by Hubmacher et al, (2015), were reported to die due to breathing difficulties owing to severe bronchial epithelial dysplasia. However

the surviving mice lived 1-2 weeks displaying typical characteristics of GD, short stature, reduced skin elasticity and stiff joints.

Recessive *ADAMTSL2* mutations exhibit a more severe phenotype with higher incidence of intracellular inclusions as seen in GD patient liver biopsy electron microscopy, which suggests a storage disorder element to the phenotype (Spranger et al, 1984). Liver sections from the *ADAMTSL2* deficient mouse model had the same characteristic inclusions, confirming via immunostaining that these inclusions stained strongly for glycogen, implying that GD is at least in part, a glycogen storage disorder (Hubmacher et al, 2015).

Le Goff et al (2008) pinpointed GD-causing *ADAMTSL2* mutations throughout the gene. They discovered 4 missense mutations R113H, P147L and E114K in the cysteine-rich module and G811R in the TSR6 domain. A nonsense mutation, W862X, was also revealed in the TSR6 domain Le Goff et al, 2008). The consequences of some of these mutations (R113H, P147L and G811R), in comparison to wild-type ADAMTS-L2, were investigated and it was shown that in culture, mutant ADAMTS-L2 was not secreted into the media (Le Goff et al, 2008). This finding suggests that these mutations in the *ADAMTSL2* gene produce a misfolded protein which hinders its secretion from fibroblasts. Active TGFβ was enhanced ten-fold in cultured medium, levels of phosphorylated Smad2 were elevated in cell lysates and localised with the nuclei of fibroblasts from GD patients in comparison to wild-type (Le Goff et al, 2008). Increased TGFβ signalling and Smad2 phosphorylation, coupled with profound epithelial dysplasia and glycogen-containing inclusions were also detected in bronchial epithelium of *ADAMTSL2* deficient embryonic mice (Hubmacher et al, 2015). The researchers also reported that administration of TGFβ-neutralising antibody decreased levels of active TGFβ in the bronchial tissue of the mice, however it was unable to reverse the dysplasia or inclusions, suggesting that structural irregularity of the ECM observed in GD may not be caused by TGF-β dysregulation, but by another underlying anomaly.

Porayette et al (2014) described a GD causing mutation in exon 13 of *ADAMTSL2*, R645H. The patient presented with classical GD symptoms, however the authors also reported that the patient also presented with hydrocephalus. Thus far, this symptom has not been associated with GD or ADAMTS-L2 and may only be a coincidental occurrence.

ADAMTS-L2 causes GD in humans and Musladin-Lueke syndrome (MLS) in beagles. The MLS dogs are smaller in size, with thickened skin and joint contractures (Bader et al, 2011). MLS in beagles is caused by the mutation R221C in ADAMTS-L2 which leads to a less severe phenotype than GD in humans. The MLS-causing mutation inserts a cysteine into the ADAMTS-L2 spacer region which causes ADAMTS-L2 to form dimers held together by disulphide bonds, overall reducing its ability to bind LTBP-1 leading to over-activation of the TGFβ signalling pathway (Bader et al, 2011).

More recently there have been reports of *ADAMTSL2* being involved in different diseases. For example, Snelling et al (2014) showed in a gene expression study that in osteoarthritis (OA) there was an upregulation of *ADAMTSL2* in the damaged cartilage. With *ADAMTSL2* being an antagonist of TGFβ, it can be postulated that upregulation of the *ADAMTSL2* gene may be acting as a negative feedback mechanism in order to reduce TGFβ signalling, which is increased in OA. Desai et al (2016) published their discovery of an *ADAMTS-L2* mutation causing Ehlers Danols Syndrome (EDS). EDS is characterised by disruptive collagen synthesis and fibril formation in the matrix which results in articular hypermobility, fragile skin, tissues and blood vessels, and lax joints (Desai et al, 2016). The authors document that after not having found mutations in any of the genes involved in collagen synthesis, a genome-wide screen revealed the Q421S mutation in *ADAMTS-L2*. Therefore this suggests that ADAMTS-L2 is interacting with collagens as well as fibrillin-1 in the matrix. Studies reporting the discovery of mutations arising in *ADAMTS-L2* that are resulting in multiple matrix diseases, are putting focus on the importance of ADAMTS-L2 and its function in the matrix.

It can be speculated that many of these mutations may produce misfolded ADAMTS-L2 proteins which in turn are not secreted by the cells, but instead may be targeted for intracellular degradation processes (Ali et al, 2007). A noteworthy observation is that many GD causing mutations occurring in the *ADAMTSL2* gene can be placed in cysteine rich regions of the sequence. Despite not knowing the exact mechanism of how ADAMTS-L2 functions in the matrix, it can be deduced that the correct folding and tertiary structure is highly important for its role in healthy tissues.

| Mutation | Nucleotide change | Type of mutation | Domain/Location | Reference |
|---|---|---|---|---|
| R113H | 338G>A | Missense | Cysteine-rich | Le Goff et al, 2008 |
| P147L | 440C>T | | | |
| E114K | 340G>A | | | |
| G811R | 2431G>A | | TSR6 | |
| W862X | 2586G>A | Nonsense | TSR6 | |
| W50C | 150G>T | Missense | TSR1 | Allali et al, 2011 |
| R72Q | 215G>A | | TSR1 | |
| R159W | 475C>T | | Cysteine-rich | |
| A165T | 493G>A | | Cysteine-rich | |
| C171R | 511T>C | | Cysteine-rich | |
| R221C | 661C>T | | Spacer | |
| A239T | 715G>A | | Spacer | |
| R593C | 1777C>T | | TSR2 | |
| S635L | 1904C>T | | TSR3 | |
| P906L | 2717C>T | | PLAC | |
| R425X | 1273C>T | Nonsense | N-glycan-rich | |
| C407C | 1219C>T | Splice | N-glycan-rich | |
| - | 1148_1177del | Deletion/Frameshift | N-glycan-rich | |
| D167N | 499G>A | Missense | Cysteine-rich | Ben-Salem et al, 2013 |
| M313T | 938T>C | | Spacer | |
| R645H | 1934G>A | Missense | TSR3 | Porayette et al, 2014 |
| - | IVS8-2A>G | Splice | Intron 8 | Kocchar et al, 2013 |
| - | IVS14-7G>A | Splice | Intron 14 | |
| - | 12471–12479del | Deletion/Frameshift | Intron 4 | Garcia-Ortiz et al, 2015 |
| E845X | 2533G>T | Nonsense | - | Mackenroth et al, 2016 |
| G267S | 799G>A | Missense | - | |
| Q421S | 1261G > A | Missense | N-glycan-rich | Desai et al, 2016 |

**Table 1.1** Published mutations in *ADAMTSL2* causing Geleophysic dysplasia.

### 1.16 ADAMTS-L4

The gene of human ADAMTS-L4 is located on chromosome 1q21.2, and encodes a ~117 kDa glycoprotein. Like other ADAMTS-Ls, it has a similar modular organisation to ADAMTS proteases, but lacks the whole pro-domain. Its unique features include a single TSR towards the N-terminus which is split by an insertion, and 6 TSRs in the ancillary domain (Figure 1.3). Another distinct feature of ADAMTS-L4 is the proline-rich domain located near the C-terminal TSRs. A proline-rich domain is also found in fibrillin-1 and this proline-rich domain may act as a "hinge-like region" granting the molecule flexibility (Baldock et al, 2001). Bearing this in mind it can be suggested that in ADAMTS-L4 the proline-rich domain may have a similar purpose and allow it to serve a flexible structure in the matrix.

Upon secretion from fibroblasts in culture, ADAMTS-L4 is seen to exist in the media as a extracellular protein and immunohistochemical analysis also found that ADAMTS-L4 co-localised with fibrillin-1 microfibrils which enhanced their deposition in the ECM of cultured fibroblast (Gabriel et al (2012).

ADAMTS-L4 is expressed in tissues such as the brain, eye, kidneys, liver, lungs colon, heart, pancreas and spleen (Chandra et al, 2011). Gabriel et al (2012) had previously established expression of ADAMTS-L4 in the retina; however Chandra et al (2013) showed ADAMTSL4 mRNA and ADAMTS-L4 protein expression in different parts of the eye, revealing a high level of expression in the choroid but little or no expression in the retina. On the basis of these data, Chandra, et al (2013) argue that ADAMTS-L4 is absent in the retina. Gabriel et al (2012) showed ADAMTS-L4 co-localisation to fibrillin-1 microfibrils in anterior chamber of the eye (ciliary body, trabecular meshwork, iris stroma, lens, cornea and retina). But it was also observed in posterior parts of the eye such as the choroid and retinal pigment epithelium (Chandra et al, 2013), but the exact functions of ADAMTS-L4 are unknown.

### 1.17 ADAMTS-L4 and Isolated ectopia lentis (IEL)

EL, if not caused by trauma, is usually a symptom associated with other genetic disorders such as WMS or MFS, however the disease can manifest on its own and in those cases it is referred to as IEL. Ciliary zonules are composed of highly organised fibrillin microfibrils that function to accommodate the ocular lens. In patients with EL/IEL significant disruption of ciliary zonules has been observed on a molecular level. *ADAMTSL4* mutations cause autosomal recessive EL which presents itself as partial or complete dislocation of the lens. *ADAMTSL4* mutations also cause ectopia lentis *et pupillae* (ELP) which is displacement of the pupil, suggesting a prominent role for ADAMTS-L4 in the eye. Many mutations in *ADAMTSL4* causing EL/IEL/ELP have been reported in literature (Table 1.2).

Ahram et al (2009) described the nonsense mutation Y595X in *ADAMTSL4* in exon11 which encodes the spacer domain. The authors suggest that the mutation would either result in a shorter, truncated protein lacking TSRs 6 and 7, or the mutant mRNA would be degraded.

Aragon-Martin et al (2010) were the next to report the discovery of new *ADAMTSL4* mutations. Their clinical study screened patients with EL whom did not present with other typical clinical manifestations of MFS. The authors described 2 heterozygous compound deletions: [767_786del] and [826_836del] resulting in 29 base pair and 11 base pair deletions in exon 6 respectively. They also reported that both mutations encode a premature stop codon further along the sequence. The study then described a homozygous compound deletion of 20 base pairs at position [767_786del] which is unrelated to the heterozygous deletion described above, however does result in a truncated protein (Aragon-Martin et al, 2010). This deleterious mutation (later also described as the European founder mutation), was also described by Christensen et al (2010) to cause ELP, whereas, Neuhann et al (2011) associated it with EL. Furthermore, 5 missense and nonsense mutations spanning the *ADAMTSL4* gene were pinpointed: P654S and R670X in exon 12, Y1051X and Y1054C present in exon 19 and R309Q in exon 6 (Aragon-Martin et al, 2010). The authors speculated that mutations in exons 6 and 12 would encode truncated proteins lacking TSRs required for ADAMTS-L4 binding to the ECM. Exon 19 encodes the PLAC domain in ADAMTS-L4; the described mutations in this exon are predicted to either eliminate the domain from the protein, or insert an extra cysteine residue which would interfere with ADAMTS-L4's ECM interactions (Aragon-Martin et al, 2010).

Four novel *ADAMTSL4* mutations were identified in a cohort study comparing IEL caused by mutations in the *FBN1* gene and the *ADAMTSL4* gene by Chandra et al (2012). The first and most commonly occurring mutation in the pool of patients was a 20 base pair deletion [767_786del20] in exon 6 which causes a frameshift and a truncated protein after 38 codons. This mutation deletes a portion of TSR 2 in ADAMTS-L4 and has been linked to craniosynostosis (CS) in which the sufferer is born with or develops an abnormal shaped skull (Chandra et al, 2013). Their study highlights that having both EL and CS is a very rare occurrence, as only a few sporadic cases have been reported where all other possible genes associated with CS have not presented with mutations. This evidence of two overlapping syndromes caused by a nonsense mutation in *ADAMTSL4* is suggestive of ADAMTS-L4 having a prominent role in microfibril biogenesis.

Four nonsense mutations, all of which result in a truncated protein have also been reported which cause ELP (Chandra et al, 2012). This particular study compared the phenotype of patients with IEL/ELP caused by *FBN1* or *ADAMTSL4,* and found that mutations in the *ADAMTSL4* gene were responsible for a more severe ocular phenotype as patients developing eye abnormalities were significantly younger than those whose symptoms were due to *FBN1* mutations (Chandra et al, 2012). Notably, patients who suffered from *ADAMTSL4* mutations have a lower risk of developing cardiac abnormalities than those suffering from mutations in the *FBN1* gene (Chandra et al, 2012).

Therefore, distinct phenotypic manifestations can help to distinguish the exact genotype of a heterogeneous disorder.

A further 2 new mutations causing ELP were described in a clinical study by Sharifi et al (2013). A homozygous nonsense mutation Q752X and a compound heterozygous pair Q752X and Q758fs. Both mutations affect TSR1 of the ancillary domain, where the nonsense mutation would result in a truncated protein product and the second mutation results in a frameshift. More recently, Reinstein et al (2016) published a newly discovered homozygous mutation R888H in a cohort of patients sharing a common gene pool. The paper also reported that this mutation has a high allele frequency as within the cohort, 1 in 48 patients screened was a carrier of the mutation. IEL is not a life threatening condition, as the affected patients live a normal life span without the complications associated with WMS, however, they do stress that early onset of IEL does alter quality of life (Reinstein et al, 2016).

Thus far, in the timeline of *ADAMTSL4* mutational discoveries, mutations causing IEL have been most prevalent in European and Caucasian communities (Ahram et al, 2009; Greene et al, 2010; Aragon-Martin et al, 2010; Neuhann et al, 2011; Chandra et al, 2012; Sharifi et al, 2013). However in 2015, Zhou et al published the first occurrence of IEL in an Asian family caused by two heterozygous mutations in *ADAMTSL4*. One mutation in exon 11 which causes a frameshift resulting in downstream truncation of the translated protein and the other mutation in exon 16 in which an arginine is substituted for a histidine, R865H.

A mutant *ADAMTSL4*$^{tvrm267}$ mouse model, bearing a nonsense mutation (Q609X) in the *ADAMTSL4* gene, phenotypically mimics human EL (Collin et al, 2015). The mutant mice lack zonular attachment and subsequently present with lens dislocation. These observations were not seen in new born mutant mice, but juvenile mice developed the phenotype within 3 weeks which sustained till adulthood. They also observed that ciliary zonules lacked the presence of ordered fibrillin-1 microfibrils in the mutant, which again indicates the role ADAMTS-L4 has in microfibril deposition. Mutant mice also suffered from myopia (increased axial length) which is also an attribute of human EL. Cells in the retinal pigment epithelium (RPE) dedifferentiated as there was significant downregulation of RPE specific gene expression; they were of deformed morphology and had reduced pigmentation. The authors also reported a severe thinning of the monolayer RPE lining with the cells appearing flatter in some regions, as well as a loss in function in comparison to wild-type (WT) mice. Such RPE defects have not yet been seen in human EL.

Recently new mutations in *ADAMTSL4* were reported (Neuhann et al, 2015). Two mutations where a frameshift results in the generation of downstream a stop codon and mutations are substitutions (R746H and G592S). The patients in the cohort were described of being young of age, presenting with IEL and not having any systemic complications.

Genome sequencing for genetic risk factors contributing to coronary artery disease (CAD), found that the *ADAMTSL4* gene in individuals who were highly likely to develop CAD having being exposed to several risk factors, still presented with healthy arteries harboured splice variants which were not found in CAD affected patients (Abramowitz et al, 2016). This study suggests that specific gene variants of *ADAMTSL4* could be contributing towards protecting high risk individuals from developing CAD.

Several mutations in *ADAMTSL4* have been reported to date; however the mechanism of ADAMTS-L4 and its involvement in the ECM are still yet to be discovered.

| Mutation | Nucleotide change | Type of mutation | Domain/Location | Reference |
|---|---|---|---|---|
| Y595X | 1785T>G | Nonsense | Spacer | Ahram et al 2009 |
| | IVS4-1G>A | Splice | Intron 4 | Greene et al, 2010 |
| Q256_P*fs*X38 | 767_786del | Deletion/Frameshift | Exon 6 | Aragon-Martin et al, 2010 |
| R276S*fs*X21 | 826_836del | Deletion/Frameshift | Exon 6 | |
| P654S | 1960C>T | Missense | TRS 2 | |
| R670X | 2008C>T | Nonsense | TSR 2 | |
| Y1051X | 3153C>A | Nonsense | PLAC | |
| Y1054C | 3161A>G | Missense | PLAC | |
| R309Q | 926G>A | Missense | Exon 6 | |
| G99A*fs*X34 | 293delG | Deletion/Frameshift | Exon 5 | Chandra et al, 2012 |
| - | 237delC | Deletion | Exon 5 | |
| R309X | 925C>T | Missense | Exon 6 | |
| G758W*fs*X59 | 2270dupG | Duplication/Frameshift | TSR 3 | |
| Q752X | 2254C>T | Nonsense | TSR 3 | Sharifi et al, 2013 |
| Q752X/Q758fs | - | Deletion/Frameshift | TSR 3 | |
| R888H | 2663G > A | Missense | Exon 16 | Reinstein et al, 2016 |
| R865H | 2594G>A | Missense | Exon 16 | Zhou et al, 2015 |
| - | 1783dupT | Duplication/Frameshift | Exon 11 | |
| R746H | 2237G>A | Missense | TSR 3 | Neuhann et al, 2015 |
| G592S | 1774G>A | Missense | Spacer | |
| L249T*fs*X21 | 745delC | Deletion/Frameshift | Exon 6 | |
| A388G*fs*X8 | 1162dupG | Duplication/Frameshift | - | |

**Table 1.2** Published mutations in *ADAMTSL4* causing Ectopia lentis.

### 1.18 Conclusions

Extensive literature surrounding the functions and mechanisms of the ADAMTS and ADAMTS-L superfamily has shown that there are many members of this family that are strongly associated with fibrillin-1 related disorders. Symptoms of WMS, GD and EL overlap as do molecules involved in these pathologies, especially ADAMTS-Ls and fibrillin-1. The involvement of ADAMTS-L2 and ADAMTS-L4 in fibrillinopathies suggests that these ECM proteins may modulate fibrillin-1 function. However, the expression and regulation of the genes encoding these proteins determines their involvement and function in specific tissues. Several disruptive mutations identified in these genes change the way the resulting proteins function and interact in the ECM, giving rise to disease states.

ADAMTS-L2 has been shown to bind to a specific N-terminal region of fibrillin-1. This region, consisting of the TB1 domain, proline-rich region and the EGF-like4 domain, has been recognised as a WMS causing deletion. Therefore, loss of this ADAMTS-L2 binding region suggests that ADAMTS-L2 may play a vital role in stabilising fibrillin-1 microfibril arrangements. As well as binding to fibrillin-1, ADAMTS-L2 also binds LTBP-1. Both LTBP-1 and fibrillin microfibrils regulate TGBβ bioavailability; hence ADAMTS-L2 may participate in this as well. Another point that should be taken into account is that the ADAMTS-L2 binding site on fibrillin-1 is in close proximity to the LTBP-1 binding site. This further indicates the possibility of ADAMTS-L2, fibrillin-1 and LTBP-1 forming an intra-dependent 'complex' which functions to sequester TGFβ.

Mutations in ADAMTS-L2 hinder its secretion from cells. Consequently ADAMTS-L2s inability to bind LTBP-1 may contribute to enhanced TGFβ activity. It must also be noted that regulating levels of TGFβ in ADAMTS-L2 deficient mice had no effect on the dysplasia and ECM disruption, suggesting that TGFβ regulation is not necessary for maintenance of the ECM structure. This, however indicates a dual role for ADAMTS-L2 where it is needed to regulate TGFβ in the ECM as well as being required to maintain structural integrity of connective tissues.

A potential role for ADAMTS10 has not been identified in GD, but mutations in ADAMTS10 cause WMS which shares some phenotypic homology with GD. The very similar structural organisation of ADAMTSs and ADAMTSLs proposes that both have related functions in the ECM and may be either inhibitory or complementary towards each other. ADAMTS10 and ADAMTS-L2 do not interact, however both bind LTBP-1 and fibrillin-1. As a unit, fibrillin-1, ADAMTS10, ADAMTS-L2 and LTBP-1 could have an interdisciplinary role in ECM biogenesis and maintenance where fibrillin-1 and ADAMTS10 work together to build and stabilise the matrix, and fibrillin-1, LTBP-1 and ADAMTS-L2 function together to regulate growth factors.

Fibrillins are the main constituent of ciliary zonules and as shown in literature *FBN1* mutations most commonly cause EL. Mutations in ADAMTS10, 17 and ADAMTS-L4 also cause EL as part of WMS or as an isolated manifestation. ADAMTS10 binds fibrillin-1 and ADAMTS-L4 co-localises

with fibrillin-1; both of these interactions have been shown to enhance microfibril biogenesis. So far, binding of other ADAMTS-Ls to ADAMTS10 have been studied, however interactions between ADAMTS10 and ADAMTS-L4 remain unknown. Therefore it can be hypothesised that fibrillin-1, ADAMTS10 and ADAMTS-L4 may form a ternary complex which builds and maintains the ciliary zonule. Like ADAMTS-L2, ADAMTS-L4 may have the potential to play a role in regulation of growth factors and important signalling pathways, which when perturbed would result in EL, IEL or ELP. We now know of several mutations that occur throughout the *ADAMTSL4* gene and we know of the phenotypic consequences they bring. However, the effect of these mutations on the fate of ADAMTS-L4 is still unknown. Hence, further research is required to investigate the folding, secretion and binding of wild-type and mutant ADAMTSL4.

Unfortunately very little is known about the structure of ADAMTSL-2 and ADAMTSL-4 and how their structure aids their function in the matrix. As the literature describes, there have been structural studies on domains in other proteins that are homologous to ADAMTSL-2 and ADAMTS-L4. However these data can only allow us to predict the structure of ADAMTS-Ls and speculate how each domain is linked to their functions. It is therefore crucial for us to learn more about ADAMTS-L2 and ADAMTS-L4 to progress towards understanding their contributions structurally, biophysically and biochemically in healthy and diseased matrix.

### 1.19 Project aims

ADAMTS-L2 and ADAMTS-L4 have been recognised as having important roles in the ECM, as genetic mutations affecting their genes result in GD and EL respectively. Thus far literature lacks comprehensive understanding of the structure, function and interactions of these molecules in the ECM. The aim of this project is to characterise ADAMTS-L2 and ADAMTS-L4 to define their structures and interactions.

The first aim of the project is to establish an efficient system to produce recombinant human ADAMTSL-L2 and ADAMTS-L4 by engineering mammalian cell line using lentiviral and episomal expression systems. Secondly, to purify ADAMTS-L2 and ADAMTS-L4 under optimal buffer conditions and characterise their physical and chemical properties with the use of protein analytical techniques.

The structures of ADAMTS-L2 and ADAMTS-L4 are as yet unresolved therefore the third aim is to solve the structures of ADAMTS-L2 and ADAMTS-L4 using negative stain TEM and analyse domain arrangement with the use of molecular modelling.

ADAMTS-L2 is known to bind to the N-terminal region of fibrillin-1 and to the C-terminal of LTBP-1, whereas ADAMTS-L4 has been co-localised to fibrillin-1 microfibrils in the matrix. These interactions, in some ways, propose a mechanism for ADAMTS-L2 and ADAMTS-L4 in healthy and diseased matrix. However, little is known whether ADAMTS-L2 and ADAMTS-L4 interact with other ECM molecules. Therefore the final aim of this project will be to gain further insight into interactions of ADAMTS-L2 and ADAMTS-L4 with other matrix molecules using SPR and immunofluorescence staining.

# Chapter 2 - Materials and Methods

## 2. Materials and Methods

General chemicals used in the project were sourced from Fisher Scientific *(Loughborough, UK)*, Thermofisher Scientific *(Paisley, UK)* or Sigma-Aldrich *(Gillingham, UK)* unless otherwise stated.

All culture flasks, dishes and plates used in the study were sourced from Corning Incorporated (*New York, USA*).

Ultrapure MilliQ water of 18.2 Ω cm quality was used to make up reagents and buffers, unless otherwise stated. Nuclease-free water used in all reactions was sourced from Promega (*Wisconsin, USA)*.

### 2.1 Molecular cloning

Oligonucleotide primers were designed using the Primer Design tool for In-Fusion HD Cloning (*http://www.clontech.com*) and were sourced from Eurofins Genomics (*MWG Operon, Edersberg, Germany*).

The pCDH lentiviral cloning vector (*System Biosciences, California, USA*) containing an EF1α promoter, a T2A peptide and the cop-green fluorescent protein (GFP) tag was a gift from K. Brennan (*Brennan Lab*, *Faculty of Biology, Medicine and Health, University of Manchester UK*). This vector backbone was modified by Dr Michael Leverentz to incorporate a C-terminal V5-tag, a polyhistidine tag (6xHis-tag) and the tagBFP (blue fluorescent protein) epitope. The episomal pCEP expression vectors were also engineered to exhibit puromycin resistance as well as contain a C-terminal V5-tag, 6xHis tag and a tag-BFP epitope.

Polymerase chain reaction (PCR) and complementary DNA (cDNA) synthesis reactions were carried out in a GeneAmp 2700 thermocycler *(Applied Biosystems, California, USA)* or gradient PCR was performed in a G-Storm thermocycler *(Uckfield, UK)*.

All samples of RNA (ribonucleic acid) and DNA (deoxyribonucleic acid) were quantified at an absorbance of 260/280nm using a Nanodrop 1000 spectrophotometer (*Thermo Scientific, Loughborough, UK*).

### 2.2 Molecular cloning of ADAMTS-L2 and ADAMTS-L4

Reference mRNA sequence of full length human ADAMTS-L2 (Accession number: NM_014694.3) and ADAMTS-L4 (Accession number: NM_019032) were obtained from GenBank (www.ncbi.nlm.nih.gov/genbank). GeneArt Strings or gene synthesis of ADAMTS-L2 and ADAMTS-L4 (Appendix Figure A1, A2 and A3) were designed and sourced from GeneArt Gene Synthesis Service Thermo Fisher Scientific (*Paisley, UK*). Both DNA inserts were cloned into the pCDH lentiviral (Figure 2.1) and pCEP episomal vectors (Figure 2.2) using various molecular cloning strategies.

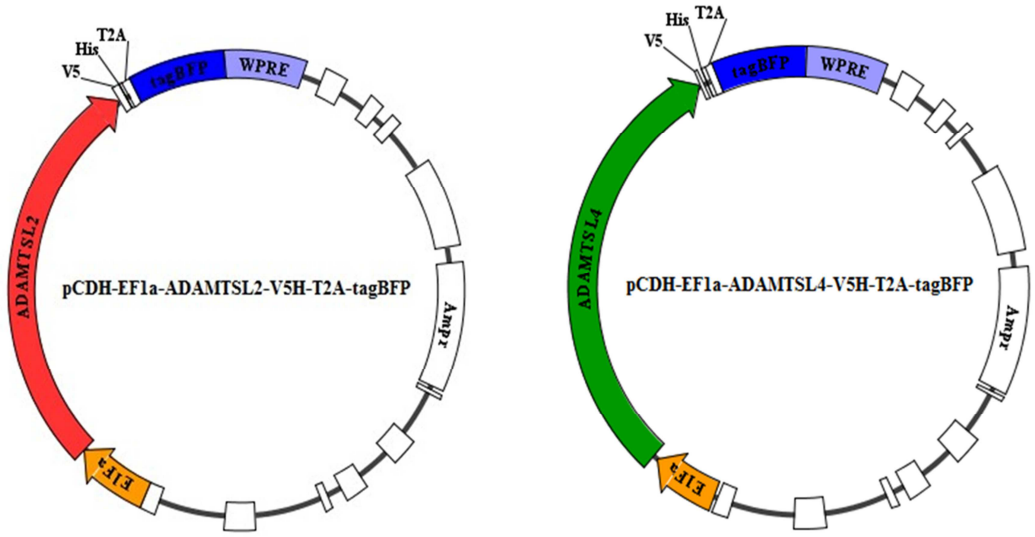


**Figure 2.1 Lentiviral pCDH vector maps for ADAMTS-L2 and ADAMTS-L4**

Vector maps of pCDH lentiviral vectors engineered for the cloning of ADAMTS-L2 (red) and ADAMTS-L4 (green). The construct contains an EF1α promoter (orange), C-terminal V5 and His tags, a T2A peptide and tagBFP marker (dark blue). The constructs also contain the Woodchuck Hepatitis Virus post-transcriptional regulatory element (WPRE) (pale blue) to enhance expression of the DNA insert, and exhibit ampicillin antibiotic resistance (Ampr).

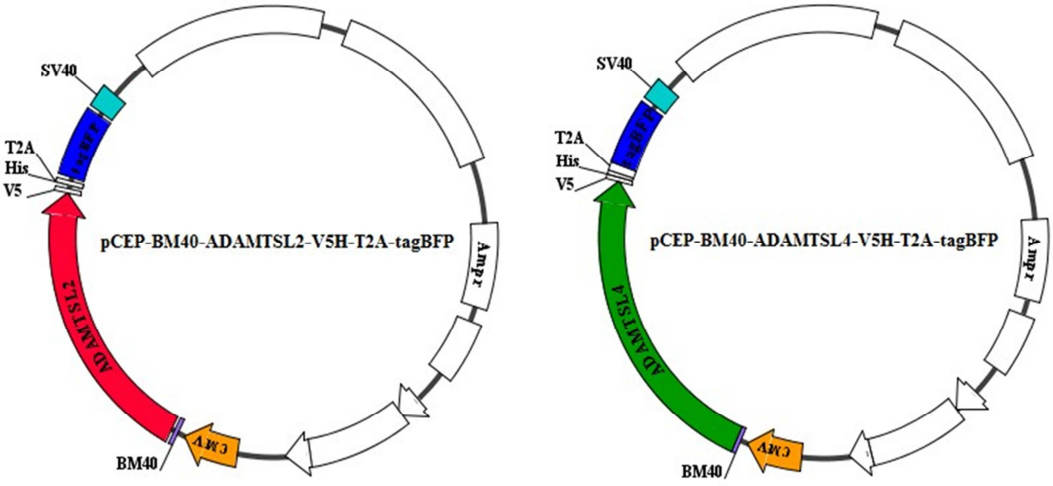


**Figure 2.2 Episomal pCEP vector maps for ADAMTS-L2 and ADAMTS-L4**

Vector maps of pCEP episomal vectors engineered for the cloning of ADAMTS-L2 (red) and ADAMTS-L4 (green). The construct contains a CMV promoter (orange), a BM40 signal peptide, C-terminal V5 and His tags, a T2A peptide and tagBFP marker (dark blue). The constructs also contain the SV40 promoter (light blue) to enhance expression of the DNA insert, and exhibit ampicillin antibiotic resistance (Ampr).

## 2.3 RNA Isolation

RNA was isolated using the ReliaPrep RNA Cell Miniprep System kit (*Promega, Wisconsin, USA*) in accordance to manufacturer's instructions. Human ARPE -19 (adult retinal pigmented epithelial) cells (*ATCC, Middlesex, UK*) were cultured in 75 $cm^2$ (T75) culture flasks until ~80% confluent. Whilst kept on ice culture medium was removed from the cells and they were washed twice with 5 ml of ice cold 1X PBS (phosphate buffered saline) (*Sigma-Aldrich*, *Gillingham, UK)* to remove residual medium. To lyse the cells, 2 ml BL (bacterial lysis) buffer with added TG (thioglycerol) was added to the flask and swirled to cover the cells. The lysis buffer was incubated for 2 minutes, after which the cells were scraped from the flask with a sterile cell scraper. The lysate was collected into DNA/RNA LoBind microcentrifuge tubes (*Eppendorf, Stevenage, UK*) and pulsed for 5 sets of 3 seconds pulses using a Q55 QSonica sonicator (*QSonica Sonicators LLC, Connecticut, USA*) at 30% amplitude. At this stage, the lysate was either used to isolate RNA immediately, or was stored at -80ºC for future use. To isolate total RNA, 80 µl of 100% isopropanol (*Fisher Scientific, Loughborough, UK)* was added to 250 µl of cell lysate. RNA was then purified from this suspension according to the miniprep protocol, in which impurities and genomic DNA was removed with the use of DNAses (deoxyribonuclease), spin columns and buffers supplied with the kit. Concentration of total RNA was determined and RNA samples were stored at -80ºC.

## 2.4 cDNA synthesis

cDNA was synthesised from isolated RNA using the Tetro cDNA synthesis kit (*Bioline, London, UK)* according to the manufacturer's recommended protocol. The synthesis reaction was carried out in a GeneAmp 2700 thermocycler. Equal concentrations of purified RNA were prepared up to a total volume of 8 µl with nuclease-free water on ice. To each sample, 1 µl of 10 mM dNTPs (deoxynucleotides), 0.5 µl of oligo dT at a concentration of 0.5 µM, and 0.5 µl of random hexamer at a concentration of 2 µM were added and mixed thoroughly. Samples were briefly centrifuged and incubated together for 10 minutes at 65 ºC and then chilled to 4 ºC. Following this, 4 µl of reaction buffer, 1 µl of RNase (ribonuclease) inhibitor, 0.25 µl of reverse transcriptase at 200 units/µl and 4.75 µl of nuclease-free water, were added to each sample. The samples were mixed, briefly centrifuged and incubated as per the following conditions: 10 minutes at 30 ºC, 90 minutes at 42 ºC and 10 minutes at 70 ºC. After the reaction was complete, cDNA samples were held at 4 ºC. For storage, the cDNA was diluted with nuclease free water and stored at -20 ºC.

## 2.5 PCR reactions

PCR was used to amplify DNA fragments with the aid of Phusion High-Fidelity DNA polymerase or Q5 High-Fidelity DNA polymerase (*New England Biolabs Inc., Massachusetts, USA*), in accordance to manufacturer's instructions. Freshly synthesised cDNA or template DNA, primers at a concentration of 100 pmol/µl and DNA polymerase were used to set up PCR reactions as follows: 5 µl 5X reaction buffer, 1 µl each of forward and reverse primers (10 µM) (Table 2.1), 0.5 µl 10 mM dNTPs, 5-10 µg of cDNA or template DNA, 0.75 µl DMSO (dimethyl sulfoxide) or GC enhancer

buffer, 0.25 µl DNA polymerase at 20 units/ml, and nuclease-free water to reach a final reaction volume of 25 µl. Gradient PCR was performed to determine an optimal annealing temperature with the following cycle conditions: 1 cycle of 30 seconds at 98 °C, 35 cycles of 10 seconds at 98 °C, 30 seconds at 55 °C to 75 °C, 1 cycle of 3 minutes at 72 °C, 1 cycle of 7 minutes at 72 °C and a hold at 4 °C. Standard PCR was run using the same cycle parameters, but at a single fixed annealing temperature.

| Primer | Forward (5'-3') | Reverse (3'-5') |
|---|---|---|
| **ADAMTS-L2** | CTACTCTAGAGCTAGCCCTAG GATGGATGGCAGA | TAGGCTTACCGGATCCGGA GTGGGGGGGCCTGCA |
| **ADAMTS-L4 (cop-GFP*)** | CTACTCTAGAGCTAGCGAGCG ATGGAGAACTGGA | TAGGCTTACCGGATCCGGA GGGATCCTGGGGAGA |
| **ADAMTS-L4 (tBFP**)** | CTACTCTAGAGCTAGCGGAGC GATGGAGAACTGG | TAGGCTTACCGGATCCGGA GGGATCCTGGGGAGA |
| **ADAMTS-L4 mid** | TGGGCTGTGGATCCCCCTGGG TCCT | CCTGTAGGACCCAGGGGGA TCCACAGCCCA |
| **ADAMTS-L4 F EX (tBFP)** | CTACTCTAGAGCTAGCGGAGC GATGGAGAACTGGACTGGC | - |
| **ADAMTS-L4 mid F EX (tBFP)** | TGGGCTGTGGATCCCCCTGGG TCCTACAGGGCTGGCGGCACC GTG | - |
| **ADAMTS-L4 1** | TCAAGCCAGGAATGTTCG | CGAACATTCCTGGCTTGA |
| **ADAMTS-L4 2** | GTGAACAGCTAAGAGCCT | AGGCTCTTAGCTGTTCAC |
| **ADAMTS-L4 3** | GACAAGCTCTTGGAGCGA | ATGTTGGGTCTGGGCAGAT G |

**Table 2.1** Primers used for cloning ADAMTS-L2 and ADAMTS-L4. *green fluorescent protein cloned from copepod Pontellina plumata. **tag blue fluorescent protein.

### 2.6 Agarose gel electrophoresis and DNA gel extraction

All PCR reactions of amplified DNA were resolved using a 1% w/v agarose gel (*Bioline, London, UK*) prepared using 1X tris-acetate (TAE) buffer (40 mM Tris-acetate, 1 mM ethylenediaminetetracetic acid (EDTA)). Red Safe (*Chembio, London, UK*) was added at a 1:10000 dilution to stain the agarose gels. Gels were resolved in 1X TAE buffer at 100 volts (V) and were visualised using a BioDoc-It UV transilluminator imaging system (*UVP, California, USA*).

DNA bands excised from agarose gels were purified using the QIAEX II gel extraction kits (*Qiagen, Crawley, UK*), in accordance to the manufacturers protocol. Extracted bands were dissolved in high salt buffer (provided with the kit) and QIAEX II resin at 50 ºC. DNA bound to the resin was centrifuged at 10,000 x g, washed with several low salt buffers (provided with the kit) and

centrifugation cycles. Finally DNA was eluted in nuclease-free water. The concentration of DNA was determined and all DNA samples were stored at -20 ºC.

### 2.7 Restriction digestion

All restriction enzymes used in the study (Table 2.2) were purchased from New England BioLabs Inc. (*Massachusetts, USA*). Such reactions were used to linearise cloning vectors, to cut inserts out of existing vectors or to check if inserts were present in plasmid preparations before sequencing. Reactions were set up according to manufacturer's instructions and typically performed for 2 hours at the recommended temperature.

| Restriction enzyme | Recognition sequence (5'-3') |
|---|---|
| NheI | G/CTAGC |
| BamHI | G/GATCC |
| SalI | G/TCGAC |
| XhoI | C/TCGAG |
| NotI | GC/GGCCGC |
| ClaI | AT/CGAT |
| AvrII | C/CTAGG |
| SfiI | GGCCNNNN/NGGCC |

**Table 2.2** Restriction enzymes used in restriction digestion reactions. The table also depicts the enzyme recognition sequence sourced from www.neb.com. All enzymes were purchased from New England BioLabs Inc.

### 2.8 DNA ligation reaction

T4 Quick Ligation kit (*New England BioLabs Inc. Massachusetts, USA*) was used to ligate DNA inserts into pCEP-V5-His-tagBFP vectors in accordance to the protocol outlined by the manufacturer.

Linearized pCEP-V5-His-tagBFP vectors and DNA fragments were purified by agarose gel electrophoresis and gel extraction as described previously. The following reaction was set up: 50 ng linearized vector, 3-fold molar excess of insert than vector, nuclease-free water to adjust reaction volume to 10 µl, 10 µl 2X Quick Ligation buffer (66 mM tris-HCl, 10 mM $MgCl_2$, 1 mM dithiothreitol, 1 mM ATP, 7.5% polyethylene glycol (PEG6000), pH 7.6) and 1 µl T4 DNA Ligase at a concentration of 2000 units/ml). Ligation reaction was mixed thoroughly, centrifuged briefly and

incubated at 25 ºC for 5 minutes. The ligation was chilled on ice, after which it was transformed into bacterial cells or stored at -20 ºC.

### 2.9 In-Fusion cloning

In-Fusion HD Cloning kit (*Clonetech Laboratories*, *Takara Bio USA Inc. California, USA*) was used to clone DNA inserts into the lentiviral pCDH vectors as per the manufacturers recommended protocol.

DNA fragments and linearized vectors were resolved using agarose gel electrophoresis and purified using gel extraction as described previously. The following reaction was prepared: 2 µl 5X In-Fusion HD enzyme pre-mix, 10-200 ng of each DNA fragment, 50-200 ng linearized vector and nuclease-free water to achieve a final reaction volume of 10 µl. Alongside this a negative reaction without the DNA inserts was also prepared with vector and nuclease-free water. The reactions were adequately mixed and incubated at 50 ºC for 15 minutes, after which they were cooled on ice. The ligation mixes could now be stored at -20 ºC or transformed into XL10 Gold bacterial cells.

### 2.10 Bacterial transformation

Bacterial transformations of plasmid DNA constructs or ligation reactions was carried out using XL-1 Blue competent cells or XL-10 Gold ultracompetent cells (*Agilent Technologies, Cheshire, UK*) as per manufacturers protocol. Aliquots of competent cells were thawed on ice, of which 100 µl of cells were used for each transformation. To increase transformation efficiency, beta-mercaptoethanol (β-ME), supplied with the cells was added to the cells: 1.7 µl to XL-1 Blue cells and 4 µl to XL-10 Gold cells respectively. The suspension was gently mixed and incubated on ice for 10 minutes before 1-2 µl of plasmid DNA or 5-10 µl of ligation mixture was added, gently mixed and incubated for a further 30 minutes on ice. After incubation, the cell suspension was heat-shocked at 42 ºC for 45 seconds and then immediately placed on ice for a further 2 minutes. Next, 400 µl of SOC (Super optimal broth with catabolite repression) medium (*Thermofisher Scientific, Paisley,* UK) was added to the reaction under aseptic conditions. The cell suspension was incubated at 37 ºC for 60 minutes. Following incubation, 50-100 µl of the bacterial cultures were plated out onto freshly prepared and autoclaved LB (Luria broth) agar (*Merck Chemicals Ltd, Nottingham, UK*) plates containing 0.05 mg/ml carbenicillin (*Melford Laboratories Ltd, Ipswich, UK*) under aseptic conditions. The plates were incubated at 37 ºC to allow the transformed bacteria to propagate overnight.

### 2.11 Colony PCR

Colony PCR was performed to identify bacterial colonies which had been transformed with the desired plasmid. Primer combination used for PCR reactions at 10 µM were the EF1α forward primer (Table 2.3) and reverse primer of the insert (Table 2.1).

After overnight propagation, LB plates with bacterial colonies were removed from the incubator. For each single colony to be tested, the following PCR mastermix was prepared: 7.5 µl MyTaq Red mix (*Bioline, London, UK*), 0.75 µl forward primer, 0.75 µl reverse primer and 6 µl nuclease-free water. The prepared mastermix was pipetted into wells of a 96-well PCR multi-plate (*Bio-rad, California, USA*). Under aseptic conditions half of a single bacterial colony was picked using a pipette tip and placed in a well containing the PCR mastermix. This step was repeated for all single colonies to be tested. The bacteria were mixed with the PCR reaction in each well by pipetting up and down several times. Once all wells had been prepared, the plate was sealed using flat PCR cap strips (*Bio-rad, California, USA*) and centrifuged briefly. The plate was placed in a GeneAmp 2700 thermocycler and the following PCR program was run: 94 ºC for 3 minutes, 25 cycles at 94 ºC for 30 seconds, 55 ºC for 30 seconds, 72 ºC for 2 minutes, a final extension at 72 ºC for 7 minutes and a final hold at 4 ºC.

The PCR reactions were resolved and visualised using agarose electrophoresis as described previously.

### 2.12 Plasmid preparation

DNA plasmids were grown from successful bacterial transformations following aseptic inoculation of single bacterial colonies into 5 ml or 100 ml of autoclaved LB broth containing 0.05 mg/ml carbenicillin, in a shaking incubator set at 37 ºC overnight for mini- and maxi-preps respectively.

Mini-preps were performed according to the manufacturer's instructions using the QIAprep Spin Miniprep Kit (*Qiagen, Crawley, UK*). Bacterial mini-prep cultures were centrifuged at 2370 x g for 5 minutes to obtain cell pellets. The cell pellets were re-suspended and lysed using buffers supplied with the kit. The reaction was then neutralised and centrifuged at 10,000 x g for 10 minutes. Supernatant from the centrifugation was then subjected to several washes and purification steps using buffers and spin columns provided with the kit. Plasmid DNA was eluted from the spin column filter with nuclease-free water and the concentration was determined. All DNA plasmids were stored at -20 ºC.

Plasmid DNA from maxi-prep cultures was purified using the NucleoBond Xtra Maxiprep kits (*Macherey Nagel GmbH & Co., Düren, Germany*) as per the protocol provided by the supplier. Cell pellets of bacterial cells containing plasmid DNA were obtained by centrifugation of maxi-prep cultures at 2370 x g for 10 minutes. The pellets were re-suspended, lysed, neutralised and then added to NucleoBond Xtra columns together with an inserted column filter which had been equilibrated with the appropriate buffers. The lysate was allowed to empty slowly by gravity flow through the filter and onto the column itself. The column and filter were washed with low salt buffer and allowed to empty with gravity flow. The filter column was removed and discarded from the column. The column was then washed with low salt buffer in order to remove impurities. Plasmid DNA was eluted into a 50 ml falcon tube (*Corning Incorporated, New York, USA*) with elution buffer

which had been heated to 50 ºC. The eluent was precipitated by adding 0.7 volumes of isopropanol and vortexing for 2 minutes. To elute and concentrate the precipitated plasmid DNA NucleoBond Finalizers syringe filters were used. The eluent was pressed though the finalizer with a 50 ml syringe at a very slow rate. The flow-through was discarded. The finalizer was then washed slowly using 70% ethanol and thoroughly dried by pressing air through it repeatedly until no more liquid could be extracted from the finalizer. The plasmid DNA was eluted by passing 1 ml nuclease-free water through the finalizer. This step was repeated to increase the yield of DNA using the same 1 ml of nuclease-free water. Concentration of plasmid DNA was quantified and all samples were then stored at -20 ºC.

Plasmid preparations were also restriction digested with appropriate enzymes to verify the presence of the insert before sequencing.

### 2.13 NEBuilder HiFi DNA assembly

The NEBuilder HiFi DNA assembly kit (*New England BioLabs Inc. Massachusetts, USA*) was used to assemble and polymerise DNA fragments with a 20 base pair (bp) overlap together or into a linearized vector as per manufacturer's instructions. The assembly reaction required 0.03 – 0.5 pmols of each DNA fragment, 10 µl NEBuilder HiFi DNA assembly master mix and sufficient nuclease-free water for a final reaction volume of 20 µl. The reaction was incubated at 15 ºC for 15 – 60 minutes depending on the number of DNA fragments being assembled, after which it was cooled on ice. The reaction was then either transformed into bacterial cells, as described previously, or stored at -20 ºC.

### 2.14 pMiniT cloning

Cloning of DNA fragments into the pMiniT cloning vector was performed using the PCR Cloning Kit (*New England BioLabs Inc. Massachusetts, USA*) in accordance to manufacturer's instructions. It was recommended that the ligation reaction contain a 3:1 insert to vector ratio. The ligation reaction was assembled as follows: 1 µl linearized pMiniT vector (25 µg/ml), 1-4 µl insert, 4 µl Cloning Mix 1, 1 µl Cloning Mix 2 and nuclease-free water to reach a final reaction volume of 10 µl. The reaction was mixed gently and incubated at 25 ºC for 15 minutes and then on ice for a further 2 minutes. The ligation reaction was either immediately transformed into bacterial cells or stored at -20 ºC.

### 2.15 DNA sequencing

DNA sequence analysis of all plasmids and PCR products was outsourced to GATC Biotech (*Cologne, Germany*). Sequencing reactions were prepared in separate eppendorfs as follows: 80-100 ng/ µl of plasmid DNA or 20-80 ng/ µl of purified PCR product, 5 µl of sequencing primer (Table 2.3) at a concentration of 5 pmol/ µl, and nuclease-free water to reach a final reaction volume of 10 µl. DNADynamo software (*Blue Tractor Software Ltd, North Wales, UK*) was used to align sequencing results to designed vector maps.

| Primer | Sequence (5'-3') |
|---|---|
| **EF1α Fwd** | CTCCACGCTTTGCCTGACCCT |
| **BM40 Fwd** | ACTGAGGGTTCCCAGCACCATG |
| **ADAMTS-L2 Seq 1** | CAAGTGCGGCATCTGTCA |
| **ADAMTS-L2 Seq 2** | CCTGTGAAGGACCTCCTA |
| **ADAMTS-L2 Seq 3** | GACAAGCTCTTGGAGCGA |
| **ADAMTS-L2 Seq 4** | AGATCCGGACCTGAGTGT |
| **ADAMTS-L4 Seq 1** | ATGTTCGGCTACGGCAGA |
| **ADAMTS-L4 Seq 2** | CAGAGCAGCCTGATCCTA |
| **ADAMTS-L4 Seq 3** | CTACCAGTACGTGATCAG |
| **ADAMTS-L4 Seq 4** | AGTGCTCCGTCAGATGTG |
| **ADAMTS-L4 Seq 5** | CATCATCTGCGTGTCCAA |

**Table 2.3** Sequencing primers used to sequence all vectors

### 2.16 Cells and cell culture techniques

Human ARPE-19 cells (*ATCC, Middlesex, UK*), adult human dermal fibroblasts (HDFs) and human embryonic kidney (HEK) 293-EBNA cells (*Thermofisher Scientific, Paisley, UK*) were cultured in Dulbecco's modified eagle medium (DMEM) with 4.5 g/L glucose and L-Glutamine (*Lonza, Walkersville, USA*). The media was supplemented with 10% (v/v) foetal calf serum (*Gibco by Thermofisher Scientific, Paisley, UK*) and 100 units/ml penicillin and 100 µg/ml streptomycin (*Sigma-Aldrich, Gillingham, UK*). Culture medium for ARPE-19 cells and HDFs was also supplemented with low serum growth supplement (LSGS) (*Gibco by Thermofisher Scientific, Paisley, UK*), whereas culture medium for HEK 293-EBNA cells contained 0.6% (v/v) of 500 µg/ml G418/geneticin solution *(Sigma-Aldrich, Gillingham, UK)*. HEK 293T cells were kindly gifted from K. Brennan (Brennan Lab, *Faculty of Biology, Medicine and Health (FBMH), University of Manchester, UK*). These cells were also cultured in DMEM with 4.5 g/L glucose and L-Glutamine with the addition of 10% (v/v) foetal calf serum, and 100 units/ml penicillin and 100 µg/ml streptomycin.

All cell lines were cultured in sterile 75 $cm^2$ (T75), 162 $cm^2$ (T162) or 225 $cm^2$ (T225) vented-lid cell culture flasks and maintained in a humidified incubator at 37 °C with 5% $CO_2$. All media was warmed to 37 °C prior to being used in cell culture techniques.

For cell maintenance, cells were passaged upon reaching confluence. To do so, culture medium was removed from the cells and they were washed twice with pre-warmed 1X PBS to remove residual medium. Cells were dissociated (trypsinised) from the culture flask by incubating them at 37 °C in 5% $CO_2$ with 5 ml (T75) or 10 ml (T162 and T225) of 1X trypsin-EDTA *(Sigma-Aldrich, Gillingham, UK*). Once trypsinised equal volumes of culture medium containing serum was added to neutralise the trypsin. This cell suspension was then transferred to a sterile falcon tube (*Corning Incorporated, New York, USA*), and centrifuged at 210 x g for 4 minutes. The supernatant was discarded and the cell pellet was re-suspended in the required volume of serum-containing culture medium. The cell suspension was then seeded in to sterile culture flasks and incubated. Culture media was changed on all cell lines every 2-3 days.

Cell lines were also banked following trypsinisation and centrifugation by re-suspending in Recovery cell culture freezing medium *(Gibco by Thermofisher Scientific, Paisley, UK)*, and stored at -80 °C.

When it was required, cells were counted using a haemocytometer cell counter, CASY counter (*Schärfe Systems, Roche Diagnostics, Hertfordshire, UK*).

### 2.17 Lentivirus production in HEK 293T cells

For the effective introduction of lentiviral vectors into mammalian cell lines, the pCDH vectors were packaged into virus particles using two packaging vectors, psPAX2 (packaging plasmid) and pMD2.G (envelope plasmid) (*Addgene, Cambridge, UK*), and 293T cells. Polyethylenimine (PEI) (*Sigma-Aldrich, Gillingham, UK*) was used as the transfection reagent, for which 100X PEI (100 mg/ml) was diluted to a concentration of 1X (1 mg/ml) using 150 mM Nanofectin diluent NaCl solution (*PAA Laboratories GmbH, Pasching, Austria*).

For each pCDH lentiviral plasmid to be infected, HEK 293T cells were cultured to 70-80% confluence. Alongside this, target cells (ARPE-19 cells, HDFs and HEK 293-EBNA cells) were also maintained ready for transduction. After the HEK 293T cells were at the required confluence, the following transfection mix was prepared for each flask of cells (Table 2.4) in Optimem (*Gibco by Thermofisher Scientific, Paisley, UK*):

| Tube A | Tube B |
|---|---|
| 6 µg pCDH lentiviral vector | 27 µl 1X PEI |
| 4.5 µg psPAX2 | |
| 3 µg pMD2.G | 250 µl Optimem |
| 250 µl Optimem | |

**Table 2.4** Reaction mix for lentiviral transfection of HEK 293T cells. Components of each tube represents amount of each vector and volume of each reagent required to transfect 1X T75 flask of HEK 293 T cells

After the above reaction mixes detailed in Table 2.4 were prepared, Tube B was incubated for 2 minutes at room temperature. Following the incubation, contents of Tube B was added to Tube A, and mixed by gentle pipetting. Existing culture medium on HEK 293T cells was removed and replenished with 6 ml of fresh serum-medium. The combined transfection mix was added to each flask and the cells were incubated overnight at 37 °C in 5% $CO_2$. The following day, existing medium in each flask of HEK 293T was replaced with 6 ml of fresh serum-medium containing 60 µl of 10 mM sodium butyrate (histone deacetylase (HDAC) inhibitor) (*Millipore UK Ltd, Hertfordshire, UK*). After culturing the HEK 293T cells for a further 4-8 hours, the medium was again replaced with serum containing target cell medium and the cells were incubated overnight. The next day, virus-containing media from the flasks was collected and filtered using 0.45 µm syringe filters (*Millipore UK Ltd, Hertfordshire, UK*). At this point, if the target cells were not at 70-80% confluence, the virus medium was stored at 4 °C in falcon tubes sealed with parafilm in a contained box.

### 2.18 Lentiviral transduction of target cells

Once target cells were 70-80% confluent, 6 ml of virus medium, 4 ml of fresh target cell culture medium and 10 µl of 5 mg/ml protamine sulphate (*Sigma-Aldrich, Gillingham, UK*) were added to each flask. The cells were then incubated for 24 hours at 37 °C in 5% $CO_2$. After 24 hours, medium on the target cells was replenished. Target cells were cultured for a further 3-4 days before being sorted by flow cytometry.

### 2.19 Fluorescence-activated cell sorting

All generated pCDH plasmids contain a tag-BFP epitope; therefore, targets cells (ARPE-19, HDFs and HEK 293-EBNA) which had been successfully transduced with the pCDH vector containing lentivirus could be selected using fluorescence-activated cell sorting (FACS).

After culturing virus-transduced target cells for 3-4 days, the adherent cells were washed twice with warmed PBS to remove all traces of serum-containing medium, and dissociated using trypsin,

EDTA. Once all the cells had dissociated from the flask, equal volume of serum- containing medium was added to neutralise the reaction. The cell suspension was collected and centrifuged at 210 x g for 4 minutes to obtain a cell pellet and the supernatant was discarded. The cell pellet was re-suspended in 1 ml of serum-free DMEM containing 1% penicillin/streptomycin and filtered using a sterile 50 µm cup filcon (*BD Biosciences, Oxford, UK*) into a sterile 5 ml round-bottom polypropylene tube (*BD Biosciences, Oxford, UK*). Cell samples were kept at room temperature prior to FACS analysis which was carried out at the Flow Cytometry Facility (*Faculty of Biology, Medicine and Health, University of Manchester, UK*). FACS-selected target cells were centrifuged and re-suspended in serum-containing medium. The cells were seeded in appropriate culture flasks at optimal density and cultured until confluent. Several batches of virally transduced, selected stable cells were expanded and frozen down in order to create a cell bank.

### 2.20 Episomal transfection of HEK 293-EBNA cells

Xfect transfection reagent (*Takara Bio USA Inc. California, USA*) was used to introduce episomal pCEP expression vectors containing ADAMTS-L2 or ADAMTS-L4 into HEK 293-EBNA cells in accordance to manufacturer's instructions.

HEK 293-EBNA cells were cultured in serum-containing medium until 60-70% confluent. The following reaction was assembled at room temperature in an eppendorf: 20 µg of pCEP vector and 400 µl of Xfect reaction buffer (supplied with the kit). The mixture was vortexed thoroughly for 5-10 seconds. 7 µl of Xfect polymer, which had been vortexed prior to use, was added to the mixture and the reaction was incubated for 10 minutes at room temperature. Spent medium on the HEK 293-EBNA cells was replenished with fresh, pre-warmed serum media. After the transfection reaction had been incubated it was added to the HEK 293-EBNA cells. The cells were incubated overnight at 37 °C in 5% $CO_2$, after which their culture medium was replaced with fresh serum-medium. The cells were further incubated for 24 hours, after which serum-medium containing 5 µg/ml puromycin (*Sigma-Aldrich, Gillingham, UK*) was applied. Puromycin selection was continued for subsequent days, during which the transfected cells were subjected to several passages. This was done to remove cells which had not been successfully transfected, hence did not confer resistance to puromycin. Once selection of HEK 293-EBNA cells had been determined, the concentration of puromycin in the culture medium was reduced to 0.5-1 µg/ml.

As the pCEP vectors used to transfect the HEK 293-EBNA cells with ADAMTS-L2 or ADAMTS-L4 contained the tag-BFP epitope, the puromycin-selected cells were further selected using FACS analysis. FACS analysis was carried out as previously described. Selected cells were expanded and banked for future use.

### 2.21 Expression of recombinant proteins

HEK 293-EBNA cell lines transfected with the pCEP vectors or transduced with the pCDH lentivirus were created for recombinant expression of ADAMTS-L2 and ADAMTS-L4. Such cell lines were revived in serum containing culture medium and were expanded into T225 culture flasks. Once the cells were 80-90% confluent, each cell line was trypsinised and re-suspended into 560 ml of serum-containing culture medium. This cell suspension was seeded into a 1720 $cm^2$ HYPERFlask multi-layer culture vessel and incubated at 37 °C in 5% $CO_2$ for 48 hours, or until cells in first few layers were 80% confluent. Once confluent, serum-containing medium was removed and the cells were gently rinsed with pre-warmed 1X PBS to remove traces of serum-medium. The cells in the HYPERFlask were then incubated with 560 ml DMEM/F12 + Glutamax expression medium (*Lonza, Walkersville, USA*) containing 100 units/ml penicillin and 100 µg/ml streptomycin and cultured at 37 °C in 5% $CO_2$. Expression medium was collected from the HYPERFlasks every 4 days and replaced with fresh DMEM/F12 expression medium. Medium was collected from the cells for a maximum of 20 days. Collected medium was centrifuged at 2370 x g for 5 minutes to remove any cell debris. The medium was then and stored at -20 °C until purified.

### 2.22 Purification of recombinant proteins

Expression media containing recombinant proteins were subjected to two stages of purification by immobilised metal ion affinity chromatography (IMAC) and then size exclusion chromatography (SEC). All buffers and MilliQ water used were filtered using 0.45 µm filter paper (*Millipore UK Ltd, Hertfordshire, UK*) and de-gassed.

### 2.23 His-tagged purification of recombinant protein using IMAC

HisTrap Excel columns (*GE Healthcare, Buckinghamshire, UK*), pre-packed with nickel sepharose were used to purify his-tagged proteins from collected expression medium using nickel affinity chromatography. IMAC purifications were performed using the AKTA Prime instrument (*GE Healthcare Life Sciences, Upssala, Sweden*).

The following buffers were prepared for purification of recombinant proteins using IMAC: Wash buffer: 20 mM tris 400 mM NaCl, 10 mM imidazole, pH 8.0; Elution buffer: 20 mM tris 400 mM NaCl, 240 mM imidazole, pH 8.0.

A 1 ml HisTrap excel column was washed with 10 ml MilliQ water and then equilibrated with 10 ml wash buffer. The filtered expression medium was loaded onto a 1 ml HisTrap excel column at a slow flow rate using a peristaltic pump overnight at 4 °C. The flow-through was retained. The loaded column was then attached to the AKTA Prime and washed with 10 column volumes of wash buffer, this wash was collected. His-tagged protein was eluted from the column with elution buffer over a step gradient into protein LoBind eppendorfs (*Eppendorf, Stevenage, UK*). Elution fractions along with samples of flow-through and column wash were analysed by SDS-PAGE as described in section 2.4.

### 2.24 Recombinant protein purification using size exclusion chromatography (SEC)

SEC was performed using an AKTA Purifier (*GE Healthcare Life Sciences, Upssala, Sweden*) and proteins were separated using a Superdex 200 (S200) 10/300 GL column or a S200 Increase 10/300 GL column, both having a column volume of 24 ml and an internal diameter of 10 mm (*GE Healthcare, Buckinghamshire, UK*). Proteins (ADAMTS-L2 and ADAMTS-L4) were both eluted in 10mM phosphate, 500 mM NaCl 2.7 mM KCl pH 7.4 (SEC buffer).

The S200 column was washed with 50 ml MilliQ water and then equilibrated with 50 ml SEC buffer. The peak fractions (500 µl – 1 ml) from IMAC His-purification were injected onto the equilibrated S200 column and the protein was eluted with SEC buffer. Fractions were collected in protein LoBind eppendorfs. Fractions corresponding to the elution peak were analysed by SDS-PAGE and western blotting as described in section 2.26 and 2.27.

### 2.25 Protein analysis techniques

### 2.26 Sodium dodecyl sulphate polyacrylamide gel electrophoresis

All sodium dodecyl sulphate polyacrylamide gel electrophoresis (SDS-PAGE) gels were run using the Novex NuPAGE SDS-PAGE gel system (*Thermofisher Scientific, Paisley, UK*).

All protein samples were prepared with NuPAGE 4 × lithium dodecyl sulphate (LDS) sample buffer (*Thermofisher Scientific, Paisley, UK*) either with or without NuPAGE 10 × Sample reducing agent (*Thermofisher Scientific, Paisley, UK*). Once thoroughly mixed, samples were heated at 95 °C for 5 minutes, after which they were cooled and briefly centrifuged. Gel tanks were assembled with pre-cast NuPAGE 4-12% Bis-Tris gels (*Thermofisher Scientific, Paisley, UK*) and filled with either NuPAGE MES running buffer or NuPAGE MOPS running buffer (*Thermofisher Scientific, Paisley, UK*). Prepared protein samples were loaded on to the pre-cast gel along with Precision Plus protein all blue pre-stained protein marker *(Bio-rad, California, USA),* ranging from 10 to 250 kDa. Electrophoresis was performed at 200 V for 60 minutes.

Following electrophoresis, gels were stained with InstantBlue protein stain (*Expedeon, Cambridge, UK*) overnight, and de-stained the next day with MilliQ water. For enhanced staining of protein bands, gels were stained overnight with Coomassie brilliant blue G stain (*Sigma-Aldrich, Gillingham, UK*). Gels were de-stained by immersing into 10% acetic acid in 25% (v/v) methanol (de-staining solution) for 30 minutes, rinsing with 25% methanol and finally de-staining with 25% methanol until protein bands were visibly clear. Gels were then stored in MilliQ water for scanning.

### 2.27 Western blotting

Western blotting was carried out using the XCell SureLock Mini-Cell and XCell II Blot Module (*Thermofisher Scientific, Paisley, UK*). Tris-glycine (transfer) buffer (96 mM tris, 780 mM lycine and 0.075% (v/v) SDS) was prepared with 10% (v/v) methanol. Following SDS-PAGE gels were transferred on to nitrocellulose membrane (*Whatman, GE Healthcare, Denmark*) Resolved SDS-

PAGE protein gels were assembled in accordance to manufacturer's instruction as part of a gel-membrane sandwich, and packed into the blot module with filter paper and foam pads. The transfer tank was filled with transfer buffer and ran at 35 V for 90 minutes.

After the transfer was complete, nitrocellulose membranes were placed in opaque Li-Cor western blot boxes (*Li-Cor, Nebraska, USA*) and blocked for 1 hour at room temperature with 5% bovine. serum albumin (BSA) (*Sigma-Aldrich, Gillingham, UK*), prepared in TBS-T (tris-buffered saline (50 mM Tris, 150 mM NaCl pH 7.4), 0.05% (v/v) Tween 20 *(Sigma-Aldrich, Gillingham, UK)*) on a bench-top shaker. Once blocked, membranes were incubated overnight with primary antibody (Table 2.7) diluted in 5% BSA in TBS-T at 4 °C. Following incubation with primary antibody, 3 x 10 minute washes were performed using TBS-T. Membranes were then incubated on a shaker with Li-Cor secondary antibody (IRDye 680RD Donkey anti-Mouse IgG (*Li-Cor, Nebraska, USA*)) diluted in TBS-T, for 1 hour at room temperature. Finally, 3 x 10 minute TBS-T washes were performed to wash away excess antibody. All blots were scanned using Odyssey CLx Imaging system (*LI-COR Biosciences, Ltd., UK*) and analysed using Image Studio Lite software version 5.0 (*LI-COR Biosciences, Ltd., UK*).

### 2.28 Preparation of cell lysates

Cells were lysed and stored in radio-immunoprecipitation assay (RIPA) buffer (*Sigma-Aldrich, Gillingham, UK*) with added protease inhibitor cocktail (PIC), 1mM sodium orthovanadate and 1mM sodium fluoride (*Sigma-Aldrich, Gillingham, UK)*. This lysis buffer was prepared and kept on ice.

Cells cultured in 6-well culture dishes were placed on ice and washed twice with ice cold PBS to remove residual culture medium. After removing excess PBS, 200 µl of lysis buffer was. A cell scraper was used to ensure the adherent cells were removed from the culture plastic. Lysates were collected into eppendorfs and sonicated as described in section 2.1.2. Lysates were stored at -80 °C until required.

### 2.29 Bicinchoninic acid (BCA) protein assay

BCA protein assay was performed to determine total protein concentration of protein samples in comparison to known BSA standards. The BCA protein assay kit (*Pierce, Thermo Scientific, Essex, UK*) was used in accordance to the manufacturer's protocol.

Serial dilutions of 2 mg/ml BSA (provided with the kit), with nuclease-free water were used to generate a set of standards of known concentrations, ranging from 25 µg/ml to 2 mg/ml of BSA. In a 96-well micro-plate BSA standard was pipetted in increasing concentration in duplicate and 25 µl protein cell lysate was added. BCA working reagent was made up using solutions A and B (supplied with the kit), in the appropriate ratios. 200 µl of BCA reagent was added to each well of the micro-plate containing BSA standards or cell lysate. The micro-plate was incubated at 37 °C for 30 minutes under dark conditions, after which it was cooled to room temperature. Absorbance of

the BSA standards and protein samples at 570 nm was measured using the Infinite F50 plate reader (*Tecan, Switerland*). Total protein concentration of each sample was estimated in comparison to the concentration of the BSA standards.

### 2.30 Determining the stability of purified recombinant proteins – OPTIM analysis

The Optim 1000 instrument (*Avacta, Isogen Life Sciences, Netherlands*) housed in the Biomolecular Analysis Facility (*FBMH, University of Manchester, UK*) was utilised to determine the conformational and colloidal resistance to thermal degradation of purified recombinant proteins under different buffer conditions.

Purified protein sample was diluted into the following buffers: 50 mM sodium acetate, 500 mM NaCl, pH 5.5; tris buffer (50 mM Tris, 500 mM NaCl, pH 7.4); HEPES buffer (50 mM HEPES, 500 mM NaCl, pH 7.4); Phosphate buffer (50 mM sodium phosphate, 50 mM NaCl, pH 7.4), briefly centrifuged and loaded into the cuvette capillaries, sealed and inserted into the Optim 1000 instrument.

The samples were run according to the following cycle: start temperature: 21 °C, end temperature: 90 °C; an increase of 0.5 °C per step with a ±0.1 °C temperature tolerance, each step was held for 15 seconds. The melting temperature ($T_m$) of the protein sample was determined by measuring the intrinsic fluorescence of the tryptophan and tyrosine residues in the sample. Aggregation temperature ($T_{agg}$) was determined at 266 nm and 473 nm by static light scattering (SLS). Data collected were analysed using the Optim Analysis software version 2.0 (*Avacta, Isogen Life Sciences, Netherlands*).

### 2.31 Native-PAGE

The NativePAGE Novex Bis-Tris Gel system (*Thermofisher Scientific, Paisley, UK*) was used to assess the state of the protein under non-denaturing conditions. Buffers used for electrophoresis were prepared as follows: 1 × Anode buffer: 50 ml 20 × NativePAGE Running buffer and 950 ml MilliQ water; 1 × Cathode buffer (dark blue): 10 ml 20 × NativePAGE Running buffer, 10 ml 20 × NativePage Cathode additive and 180 ml MilliQ water; 1 × Cathode buffer (light blue): 10 ml 20 × NativePAGE Running buffer, 1 ml 20 × NativePage Cathode additive and 189 ml MilliQ water.

7.5 µl protein sample was combined with 2.5 µl 4 × NativePAGE sample buffer. The electrophoresis tank fitted with the XCell Surelock Mini-cell was equipped with a 3-12% NativePAGE Novex BisTris gel (*Thermofisher Scientific, Paisley, UK*). The wells of the gel were then filled with cathode buffer (dark blue) to displace all air from the wells. The protein sample was loaded onto the gel along with NativeMark unstained protein marker (*Thermofisher Scientific, Paisley, UK*) ranging from 20 kDa to 1200 kDa. The inner chamber of the electrophoresis tank was filled with 200 ml cathode buffer (dark blue) and the outer chamber was filled with approximately 600 ml anode buffer. The gel was run at 150 V for 25 minutes, after which the dark blue cathode

buffer was aspirated out of the inner chamber and replaced with cathode buffer (light blue). The gel was run for an additional 65 minutes. The protein was visualised using coomassie staining.

### 2.32 Mass spectrometry

Protein identification was carried out at the Biological Mass Spectrometry Facility (*FBMH, University of Manchester, UK*). Protein samples were resolved using SDS-PAGE as described in section 2.26 and stained with Coomassie brilliant blue G stain (*Sigma-Aldrich, Gillingham, UK*). Visible gel bands were excised and subjected to reduction with dithiothreitol (DTT), alkylation in iodoacetamide and then a tryptic digest. Samples were analysed on a Q-TOF Micro with Waters CapLC chromatography system (*Waters, Hertfordshire, UK*) and the results were interpreted using Mascot species-specific database (*Matrix Science, London, UK*) followed by validation and distribution using Scaffold version 4.0 (*Proteome Software, Oregon, USA*).

### 2.33 PNGase F assay

The PNGase F assay was used to determine N-glycosylation states of ADAMTS-L2 and ADAMTS-L4 (*New England BioLabs Inc. Massachusetts, USA*) under denaturing conditions in accordance with the manufacturers' protocol.

A 10 µl reaction containing 20 µg of purified protein and 1 µl 10X glycoprotein denaturing buffer was incubated at 100 °C for 10 minutes. The reaction was chilled on ice and centrifuged briefly. Then 2 µl 10X glycobuffer 2, 2 µl10% Nonidet-40 (NP-40), 1 µl PNGase F enzyme and 6 µl nuclease-free water was added to the reaction. The reaction was gently mixed, briefly centrifuged and incubated for 1 hour at 37 °C. Deglycosylation was analysed by SDS-PAGE and western blotting.

### 2.34 Single Particle Transmission Electron Microscopy (TEM)

### 2.35 Preparation of negative stain EM carbon-coated grids

CF400-Cu carbon-coated grids (*Electron Microscopy Sciences, Pennsylvania, USA*) glow discharged in a K100X Glow Discharger (*EMITECH,* France) at a 25 mA current for 30 seconds. 5 µl of protein sample was applied to the carbon-coated surface of the grids for 60 seconds, then washed with 60 µl 2% uranyl acetate (UA). The 2% UA was allowed to stain the grid for 30 seconds. The grids were blotted on filter paper to remove excess UA.

For ADAMTS-L2 grids were made using approximately 25 µg/ml of protein sample which was either put on to the grids neat or at a 1:2 dilution. For ADAMTS-L4 a protein sample at approximately 15 µg/ml was used undiluted or at a 1:2 dilution.

### 2.36 TEM of negative stain protein grids

Images were recorded by Dr Richard Collins on a FEI Tecnai G2 Polara Transmission Electron Microscope housed in the Electron Microscopy Facility (*FBMH, University of Manchester, UK*). The

FEI Tecnai G2 Polara Transmission Electron Microscope is equipped with a 300 kV field emission gun (FEG) and the images were recorded using a 2048 x 2048 pixel charge coupled device (CCD) 4K Ultrascan (Gatan) camera. The images were recorded at a dose of 30-40 electrons ($e^-$) per Angstrom (Å) and at a specimen level of 3.05 Å $pix^{-1}$ with a defocus range of -0.5 µm to -4.0 µm.

### 2.37 Single particle analysis and generation of a 3D model

Single particle analysis was carried out using the EMAN 2.1 image processing suite (Tang et al, 2007). Particles were manually selected and centred using *eboxer.py*. For ADAMTS-L2, a box size of 128 pixels was used to pick 12,892 particles, whereas for ADAMTS-L4 a box size of 150 pixels was used to select 7054 particles. Once all the particles had been selected, the *e2ctf.py* utility in in EMAN 2.1 was used to estimate and subsequently correct contrast transfer function (CTF). Several iterations of multi-reference alignment classified the particle data set into 100 2D class averages using the function *e2classaverage.py*. The command *e2refine_easy.py* allowed for single particle reconstruction and iterative refinement to generate an initial 3D model from a set of class-averaged particles. Resolution of the final 3D model was determined by Fourier shell correlation (FSC) at a spatial frequency criterion of 0.5.

### 2.38 3D modelling of ADAMTS-L2

The 3D model generated by EMAN2 was visualised using UCSF Chimera (Pettersen et al, 2004). SWISS-MODEL (Biasini et al, 2014) was used to generate a structural model of the cysteine-rich, spacer and N-glycan-rich domains of ADAMTS-L2 as well as TSR domain pairs. A monomer of properdin (*Accession number: P27918*) shares homology with the ancillary domain of ADAMTS-L2, therefore models of properdin generated by small-angle x-ray scattering (SAXS) (PDB: 1W0S or 1W0R) were used as a template to model a chain of TSRs. These templates were then manually fitted using UCSF Chimera into the generated 3D structure of ADAMTS-L2, to predict structural alignment.

### 2.39 2D structural analysis of ADAMTS-L4

Particles of ADAMTS-L4 imaged by negative stain EM appeared to be highly flexible and therefore, a 3D model of the protein could not be generated by EMAN2. Using ImageJ the length of 100 particles from refined particle data sets were measured and used to determine average particle length of ADAMTS-L4.

### 2.40 Surface Plasmon Resonance (SPR)

To investigate binding of ADAMTS-L2 to matrix proteins SPR was carried out using the BIAcore T200 (*GE Healthcare, Little Chalfont, UK*) housed in the Biomolecular Analysis Facility (*FBMH, University of Manchester, UK*). All recombinant protein fragments used in the binding study were

kindly provided by members on the Baldock lab and Kimber lab (*FBMH, University of Manchester, UK*). Buffers used in the study were filtered with 0.45 µm filter paper and de-gassed.

Purified ADAMTS-L2 was immobilised in 50 mM sodium acetate, pH 4 by amine-coupling with an 1-ethyl-3- (3-dimethylaminopropyl) carbodiimide (EDC) and N-hydroxysuccinimide (NHS) linker on to a Series S CM5 sensor chip (*GE Healthcare, Little Chalfont, UK*). Immobilisation of a 0.2 µM solution of ADAMTS-L2 resulted in a binding response of ~1640 response units (RU).

Analytes were (Table 2.5), were prepared at 200-400 nM in 10 mM HEPES, 150 mM NaCl with 0.05% (v/v) Tween-20 (HBS-T) buffer, pH 7.4 (Running buffer). Proteins were injected over immobilised ADAMTS-L2 at: flow rate 30 µl/minute, contact time of 3 minutes and dissociation time of 60 seconds. The chip was regenerated with 2 injections of regeneration buffer (10 mM HEPES, 800 mM NaCl, pH 7.4) at: flow rate 30 µl/minute, contact time of 30 seconds and a stabilisation time of 2 minutes.

After potential binding candidates had been identified, a kinetics analysis was performed. Analytes were prepared in running buffer at concentrations ranging from 0 – 600 nM. The analytes were injected over the immobilised ADAMTS-L2 with a flow rate of 30 µl/minute, contact time of 3 minutes and dissociation time of 5 minutes.

Data collected was analysed using the BIAcore T200 Evaluation software (*GE Healthcare, Little Chalfont, UK*).

| Recombinant protein | Reference |
|---|---|
| Fibrillin-1 PF1 | Rock et al, 2004 |
| Fibrillin-1 PF2 | Rock et al, 2004 |
| Fibrillin-1 PF3 WT | Rock et al, 2004 |
| Fibrillin-1 PF3 WMS | Cain et al, 2012 |
| Fibrillin-1 PF5 | Rock et al, 2004 |
| Fibrillin-1 PF7 | Rock et al, 2004 |
| Fibrillin-1 PF10 | Bax et al, 2003 |
| Fibrillin-1 PF12 | Rock et al, 2004 |
| Fibrillin-1 PF13 | Rock et al, 2004 |
| Fibrillin-1 PF17 | Cain et al, 2012 |
| Fibrillin-1 Ex 1-11 | Rock et al, 2004 |
| Fibrillin-1 FL | *Unpublished* |
| MAGP-1 | Rock et al, 2004 |
| Fibronectin 7-14 | *Unpublished* |
| Fibronectin FL | *Unpublished* |
| LTBP-1 NT | Troilo et al, 2016 |
| LTBP-1 CT | Chaudhry et al, 2007 |
| LTBP-1 FL | Chaudhry et al, 2007 |
| Syndecan 4 ectodomain | *Unpublished* |

**Table 2.5** Protein fragments used in SPR.

### 2.41 Immunofluorescence staining and microscopy

Adult HDF cells were seeded into 24-well culture dishes onto sterilised 13mm glass coverslips at density of 30,000 cells per well or 50,000 cells per well respectively. The cells were cultured in growth medium at 3 time-points: 5 days, 7 days or 10 days with the medium being replenished every 2 days.

At the end of each time-point, culture medium from the cells was removed and the cells were fixed with 4% paraformaldehyde (PFA) for 20 minutes at room temperature. The PFA was removed and the cells were washed 3 times with PBS. The cells were then incubated with 500 µl 0.2 M glycine, 0.5% Triton X100 in PBS for a further 20 minutes at room temperature. The cells were then subjected to 3 PBS washes. To block the cells, 500 µl 2% (w/v) fish skin gelatin (FSG) (*Sigma-Aldrich, Gillingham, UK*) prepared in PBS was added to the cells and incubated for 1 hour at room temperature. Following the incubation, the block was removed and the cells were washed thrice with PBS. 30 µl drops of primary antibodies (Table 2.6) prepared in 2% FSG were pipetted onto parafilm; the washed coverslips were inverted onto these drops and incubated for 1 hour at room temperature. The coverslips were then washed 3 times in PBS. Species- and isotope-specific secondary antibodies (Table 2.7) were prepared in 2% FSG and coverslips were incubated similarly for 1 hour at room temperature under darkened conditions. Coverslips were washed 3 times in PBS and then finally in MilliQ water. They were left to dry for 20 minutes under darkened conditions before being mounted onto glass slides using a drop of Prolong Gold Anti-fade reagent plus DAPI (4',6-diamidino-2-phenylindole) (*Thermofisher Scientific, Paisley, UK*). Mounted coverslips were proved overnight at room temperature under darkened conditions before being imaged.

Images were collected on an *Olympus BX51* upright microscope using a *x40* objective and captured using a *Coolsnap ES camera (Photometrics)* through *MetaVue Software (Molecular Devices)*. Specific band pass filter sets for *DAPI, FITC and Texas red* were used to prevent bleed through from one channel to the next. Images were then processed and analysed using ImageJ (http://rsb.info.nih.gov/ij).

| Primary Antibody | Species | Dilution | Company/Catalogue number |
|---|---|---|---|
| Anti-V5 | Mouse Monoclonal | 1:200 – IF<br>1:500 - WB | Bio-rad - MCA1360GA |
| | Rabbit Polyclonal | 1:200 | Millipore – AB3792 |
| Fibrillin-1 | Mouse Monoclonal - clone 11C1.3 | 1:200 | Millipore – MAB1919 |
| | Rabbit Polyclonal | 1:200 | Sigma Aldrich – HPA021057 |
| Fibronectin | Rabbit Polyclonal | 1:200 | Sigma Aldrich – F3648 |
| LTBP-1 | Mouse Monoclonal | 1:200 | R&D Systems - MAB388 |

**Table 2.6** Primary antibodies used for immunofluorescence (IF) staining and western blotting (WB). Table indicates dilutions used. Suppliers and catalogue number are provided.

| Secondary Antibody | Species | Dilution | Company/Catalogue number |
|---|---|---|---|
| Alexa-Fluor® 488 | Donkey anti-mouse | 1:400 | Thermo Fisher Scientific - A21202 |
| Alexa-Fluor® 488 | Donkey anti-rabbit | 1:400 | Thermo Fisher Scientific - A21206 |
| Alexa-Fluor® 555 | Donkey anti-mouse | 1:400 | Thermo Fisher Scientific - A31570 |
| Alexa-Fluor® 555 | Donkey anti-rabbit | 1:400 | Thermo Fisher Scientific - A31572 |

**Table 2.7** Secondary antibodies used for immunofluorescence staining. Table indicates dilutions used. Suppliers and catalogue number are provided.

# Chapter 3 - Results

# 3. Results

## 3.1 Molecular cloning, expression and purification of ADAMTS-L2 and ADAMTS-L4

Dysregulation of the matrix leads to chronic and sometimes life-threatening diseases. Mutations affecting ADAMTS-L2 and ADAMTS-L4 have been found to cause specific diseases of the matrix which affect both its structural integrity and functionality. The literature surrounding these proteins provides very little understanding of how ADAMTS-L2 and ADAMTS-L4 interact and function in the matrix. Therefore it is imperative to further study the properties ADAMTS-L2 and ADAMTS-L4 possess and how they contribute to the matrix.

In order to study and characterise human ADAMTS-L2 and ADAMTS-L4, DNA sequences encoding these proteins were cloned into episomal and lentiviral expression systems. Human mammalian cell lines were then transfected with these expression systems to allow for the expression and secretion of recombinant ADAMTS-L2 and ADAMTS-L4. The recombinant proteins were then purified for further experimentation.

## 3.2 Molecular cloning of recombinant human ADAMTS-L2 and ADAMTSL-L4

In order to express recombinant ADAMTS-L2 (2856 bp) and ADAMTS-L4 (3225 bp) in mammalian cells, the genes encoding both proteins were cloned into the lentiviral pCDH and episomal pCEP expression vectors. RNA from ARPE-19 cells was used to synthesis cDNA after RNA sequencing data (not shown) obtained by Dr Stuart Cain in the lab showed that in comparison to mesenchymal cells types (HDFs and MSCs), these epithelial cells had a higher expression of ADAMTSs and ADAMTS-Ls.

### 3.2.1.1 Molecular cloning of recombinant ADAMTS-L2 into the lentiviral pCDH vector

In order to clone ADAMTS-L2 into the pCDH lentiviral vector, 2 strategies were employed (Figure.3.1.1). The first strategy attempted to amplify ADAMTS-L2 from cDNA which had been synthesised from RNA extracted from ARPE-19 cells. Amplified DNA was cloned into the pCDH vector using In-Fusion ® Cloning Kit cloning, however several attempts failed to generate the clone. Several attempts of amplifying ADAMTS-L2 were made and each attempt involved optimising the protocol, however all were unsuccessful. Due to these failures, a second strategy where a GeneArt String (*Thermofisher Scientific, Paisley, UK*) encoding ADAMTS-L2 was employed. The GeneArt String was amplified using the appropriate primers, gel extracted and cloned into the pCDH expression vector. Sequences of the generated clones were verified.

At first ADAMTS-L2 was cloned into a pCDH vector containing the copGFP fluorescent tag. However, the intense green fluorescence emitted by the copGFP tag was interfering with immunofluorescence investigations. Therefore, ADAMTS-L2 was cloned into a pCDH lentiviral vector containing a blue fluorescent tag (tagBFP) (Figure 3.1.2). Figure 3.1.2 outlines the protocol

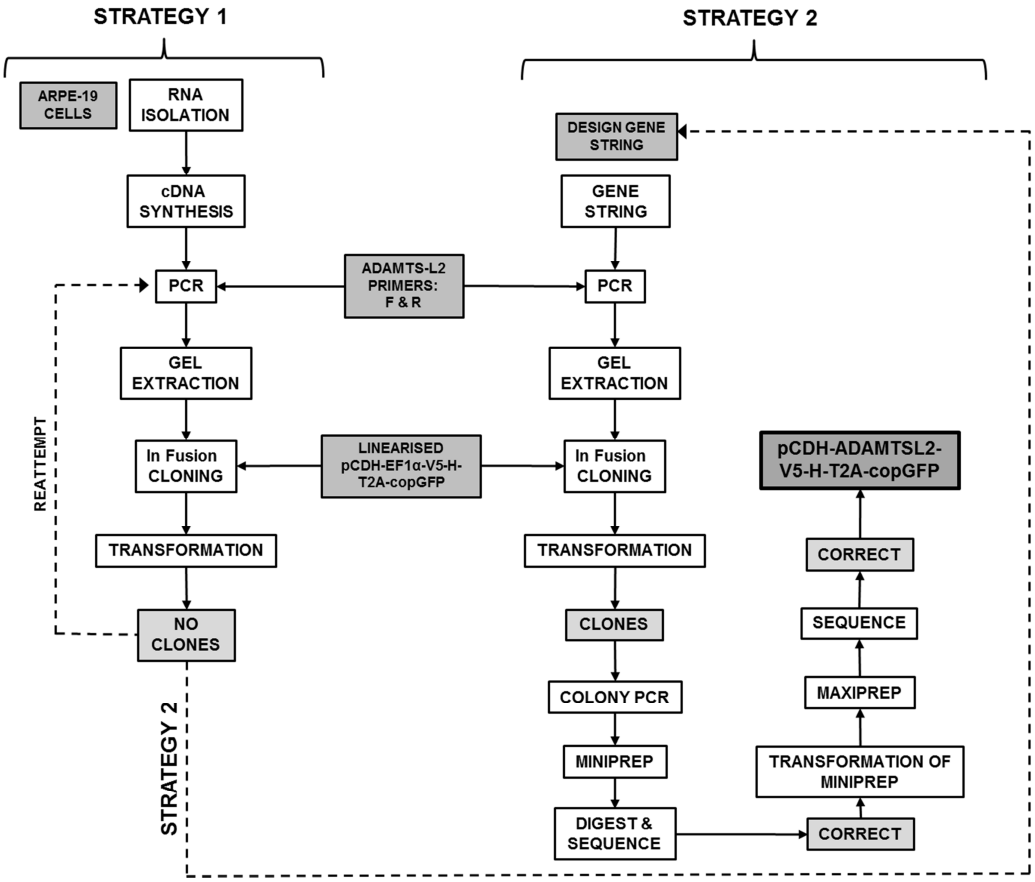


**Figure 3.1.1 Molecular cloning of recombinant ADAMTS-L2 into the lentiviral copGFP vector using In Fusion cloning**

Recombinant ADAMTS-L2 was cloned into the pCDH lentiviral vector with a green fluorescent tag (copGFP). White boxes represent methods employed in the cloning process; light grey boxes denote outcomes; dark grey boxes denote cells, oligomers or DNA fragments used. Solid arrows depict the methodology followed to achieve results and dashed arrows represent changes in strategy. F denotes forward and R denotes reverse. Two strategies were employed to clone ADAMT-L2 in to the pCDH vector. Strategy 1 involved amplifying the gene from cDNA synthesised from RNA isolated from ARPE-19 cells. Reattempts encompass several optimisations to the protocol. Strategy 2 involved the cloning of a gene string encoding ADAMTS-L2 into the lentiviral vector. The pCDH-tagBFP vector was linearised with NheI and BamHI.

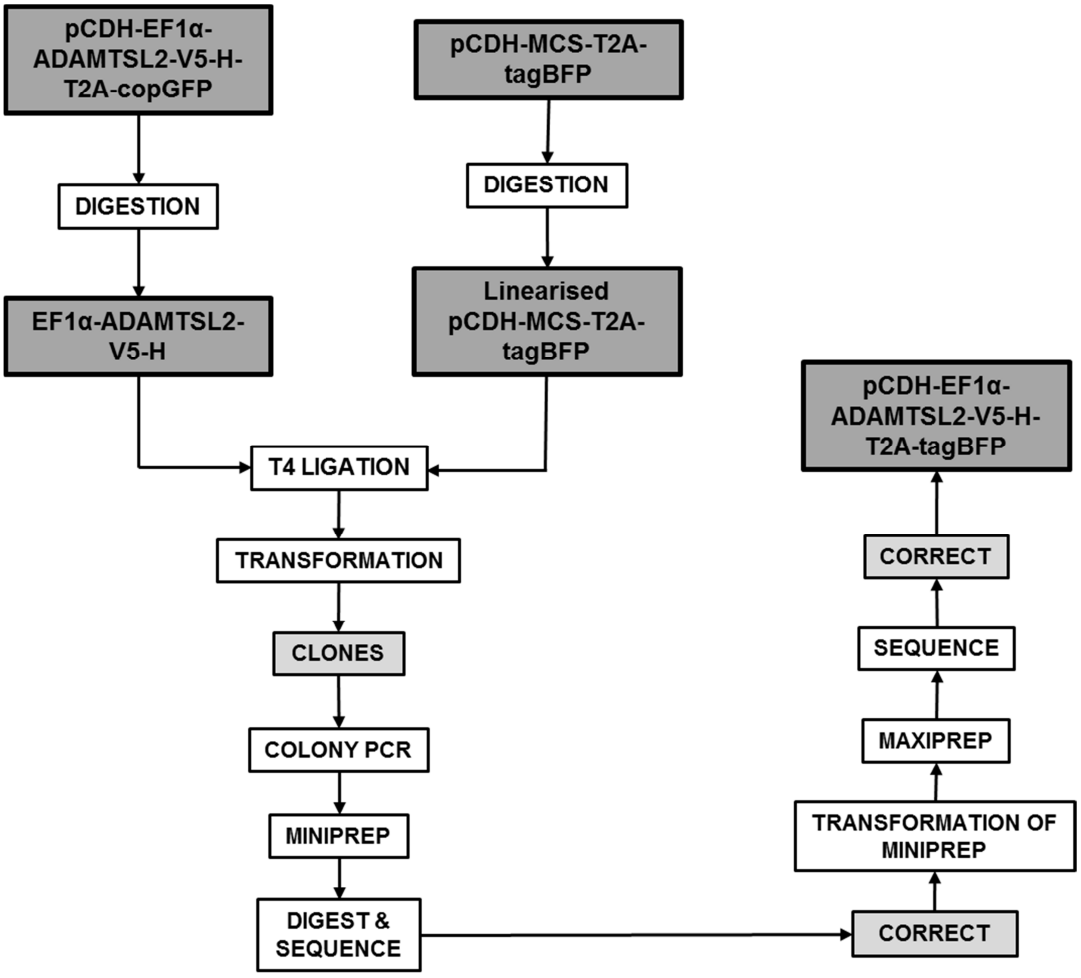


**Figure 3.1.2 Molecular cloning of recombinant ADAMTS-L2 into the lentiviral tagBFP vector**
Recombinant ADAMTS-L2 was cloned into the pCDH lentiviral vector with a blue fluorescent tag (tagBFP). White boxes represent methods employed in the cloning process; light grey boxes denote outcomes; dark grey boxes denote DNA fragments used. Solid arrows depict the methodology followed to achieve results and dashed arrows represent changes in strategy. A section of the pCDH-copGFP lentiviral vector encoding the EF1α promoter, ADAMTS-L2gene and the V5 and His-tag was cut from the vector using NotI and ClaI enzymes. The empty pCDH-tagBFP vector was digested with the same enzymes to create complementary ends, after which the ADAMTS-L2 insert and linearised vector were ligated using T4 ligase.

used in which the DNA fragment encoding the EF1α promoter, ADAMTS-L2 and the V5 and His tag were digested from the pCDH-cop-GFP vector using NotI and ClaI enzymes.

An empty pCDH-tagBFP lentiviral vector was also linearised with the same enzymes, after which the linearised vector and digested insert were ligated using T4 ligase. Generated clones were sequenced for verification of cloning.

#### 3.2.1.2 Molecular cloning of recombinant ADAMTS-L4 into the lentiviral pCDH vector

ADAMTS-L4 was cloned into the pCDH-tagBFP lentiviral vector. To do so, several strategies were employed (Figure 3.1.3A). Firstly, amplification of ADAMTS-L4 from cDNA was attempted several times; however due to inadequate amounts of DNA being extracted and numerous modifications made to the protocol, sufficient amounts of DNA was not obtained from this approach.

Strategy 2 was employed to aid amplification of ADAMTS-L4 from cDNA, by dividing the DNA sequence encoding the gene into 3 parts (Appendix Figure A4). For each part a set of primers were designed which overlapped the adjacent part to help with joining them together at a later stage. Despite having a sufficient yield of DNA from the PCR reactions, In-Fusion ® Cloning Kit cloning of all the sections with the linearised pCDH-tagBFP vector was not successful. Multiple attempts with changes to the protocol were made, however none were successful. The final strategy highlighted in Figure 3.1.3A was to design GeneArt Strings of ADAMTS-L4. Due to manufacturing restrictions and ADAMTS-L4 being larger than 3kb, a single GeneArt String encoding FL ADAMTS-L4 could not be created. Therefore, the ADAMTS-L4 sequence was divided into 2 fragments, the N-terminal Start and the C-terminal End, which had a 30 bp overlap in the centre (Figure 3.1.3B). Owing to the N-terminal half having a higher G-C content, attempts at creating a GeneArt Gene String failed, therefore this fragment was synthesised into a cloning vector (Appendix Figure A5). Primer pairs to allow for the amplification of these fragments, to facilitate in their fusion and insertion into the pCDH-tagBFP vector were also created, placement of which has been illustrated in Figure 3.1.3B. An overview of the final cloning process is depicted in Figure 3.1.4. The N-terminal start fragment was digested out of the cloning vector using the SfiI enzyme and amplified using a longer forward primer and a reverse middle primer. The C-terminal End GeneArt String was amplified with an extended middle forward primer and the appropriate reverse primer. The products of these reactions were cloned in to the linearised pCDH-tagBFP vector using In-Fusion ® Cloning Kit cloning and sequenced to verify successful incorporation. The cloning process for ADAMTS-L4 proved to be a lengthy and extensive process involving several trouble-shooting steps and optimisation. For details of these processes please refer to Appendix Figures A6 and A7.

Following successful cloning and bacterial transformations, colony PCR was conducted on bacterial clones of ADAMTS-L2 and ADAMTS-L4 which had been cloned into the lentiviral pCDH vectors. A forward EF1α primer and a reverse primer specific to the inserts were used. Agarose gel electrophoresis was performed and bands depicting the correct sizes of ADAMTS-L2 and ADAMTS-L4 were observed (Figure 3.1.6).

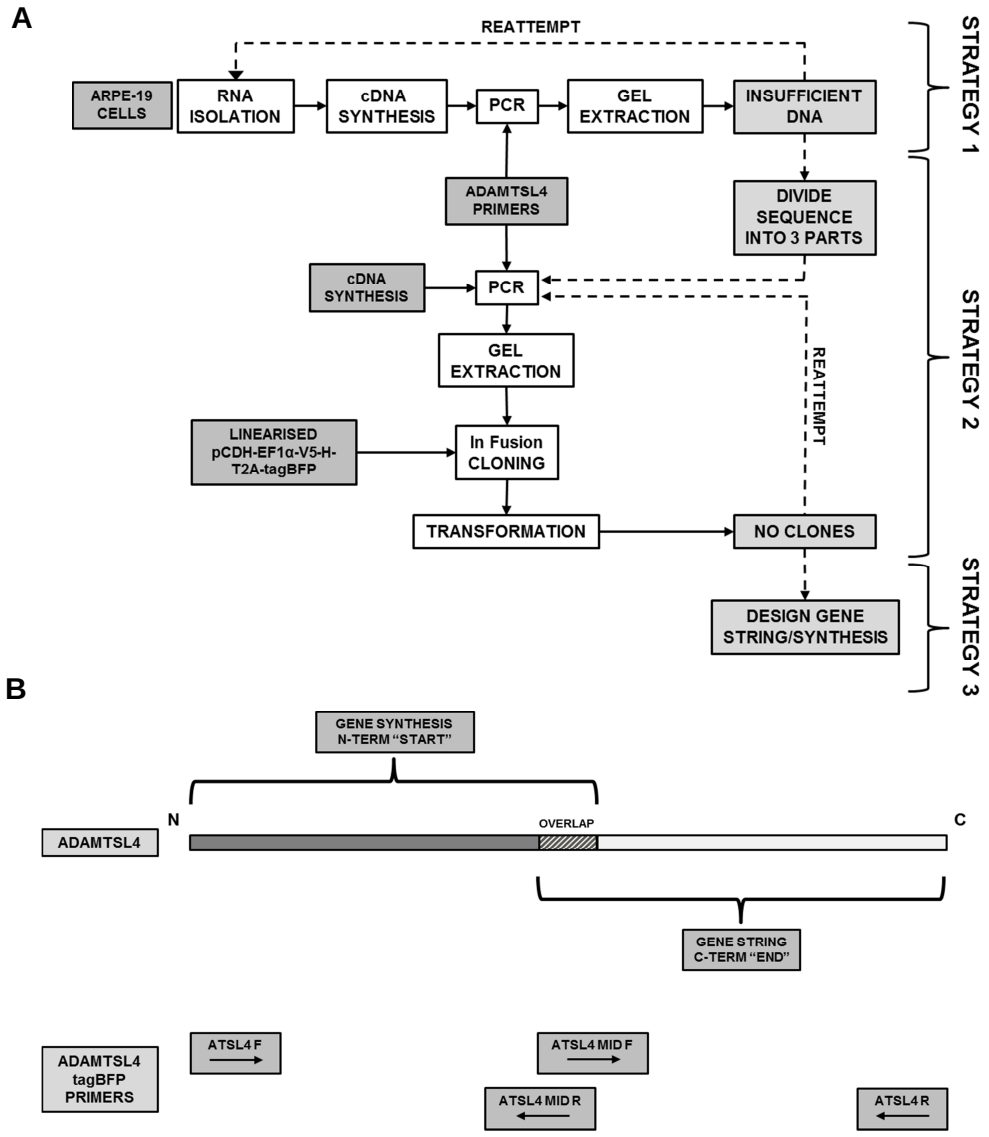


**Figure 3.1.3 Molecular cloning of recombinant ADAMTS-L4 into a lentiviral expression system**

(**A**) Recombinant ADAMTS-L4 was cloned into the pCDH lentiviral vector with a blue fluorescent tag (tagBFP). White boxes represent methods employed in the cloning process; light grey boxes denote outcomes; dark grey boxes denote cells, oligomers or DNA fragments used. Solid arrows depict the methodology followed to achieve results and dashed arrows represent changes in strategy. F denotes forward and R denotes reverse. Three strategies were employed to clone ADAMT-L4 in to the pCDH vector. Strategy 1 involved amplifying the gene from cDNA synthesised from RNA isolated from ARPE-19 cells. Strategy 2 involved dividing the ADAMTS-L4 gene sequence into 3 parts (Appendix Figure A4) and amplifying the sequences from cDNA. Strategy 3 was the designing of gene strings for the gene synthesis. The pCDH-tagBFP vector was linearised with NheI and BamHI. Reattempts encompass several optimisations to the protocol. (**B**) Schematic depicting the overlapping division of ADAMTS-L4 sequence into N-terminal gene synthesis vector and a C-terminal gene string. Position of primer pairs is also shown.

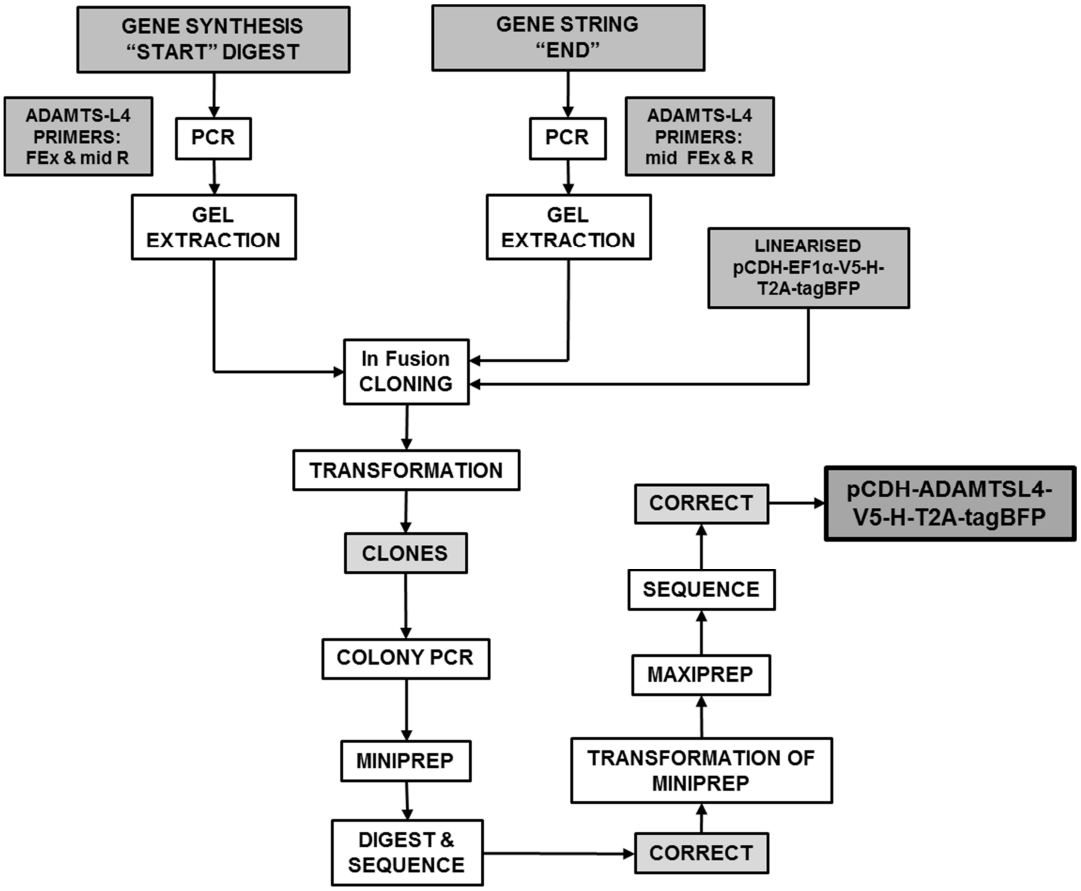


**Figure 3.1.4 Molecular cloning of recombinant ADAMTS-L4 into a lentiviral expression system using gene synthesis and a gene string using In Fusion cloning**
Final overview of the protocol employed to clone recombinant ADAMTS-L4 into the pCDH lentiviral vector with a blue fluorescent tag (tagBFP). White boxes represent methods employed in the cloning process; light grey boxes denote outcomes; dark grey boxes denote primers and DNA fragments used. Solid arrows depict the methodology followed to achieve results. F denotes forward and R denotes reverse. The N-terminal Start gene synthesis fragment was digested out of the cloning vector using SfiI. The 2 halves encoding ADAMTS-L4 were amplified using primers and then cloned into the pCDH-tagBFP vector using In Fusion cloning. The pCDH-tagBFP vector was linearised with NheI and BamHI.

#### 3.2.1.3 Cloning of ADAMTS-L2 and ADAMTS-L4 into the episomal expression system

With the aim of comparing expression levels of ADAMTS-L2 and ADAMTS-L4 using different expression systems, both inserts were cloned into the episomal pCEP-BM40 expression vector (Figure 3.1.5). NheI and XhoI endopeptidases were used to cut out the sequences encoding ADAMTS-L2/ADAMTS-L4 and the V5, His and tagBFP tags. The tagBFP epitope was incorporated into the pCEP-BM40 expression vector to allow for downstream cell sorting using FACS analysis. The pCEP-BM40 vector was linearised with SalI and AvrII enzymes. The inserts and linearised vector were ligated using T4 ligase and transformed. Success of cloning was verified with sequence analysis.

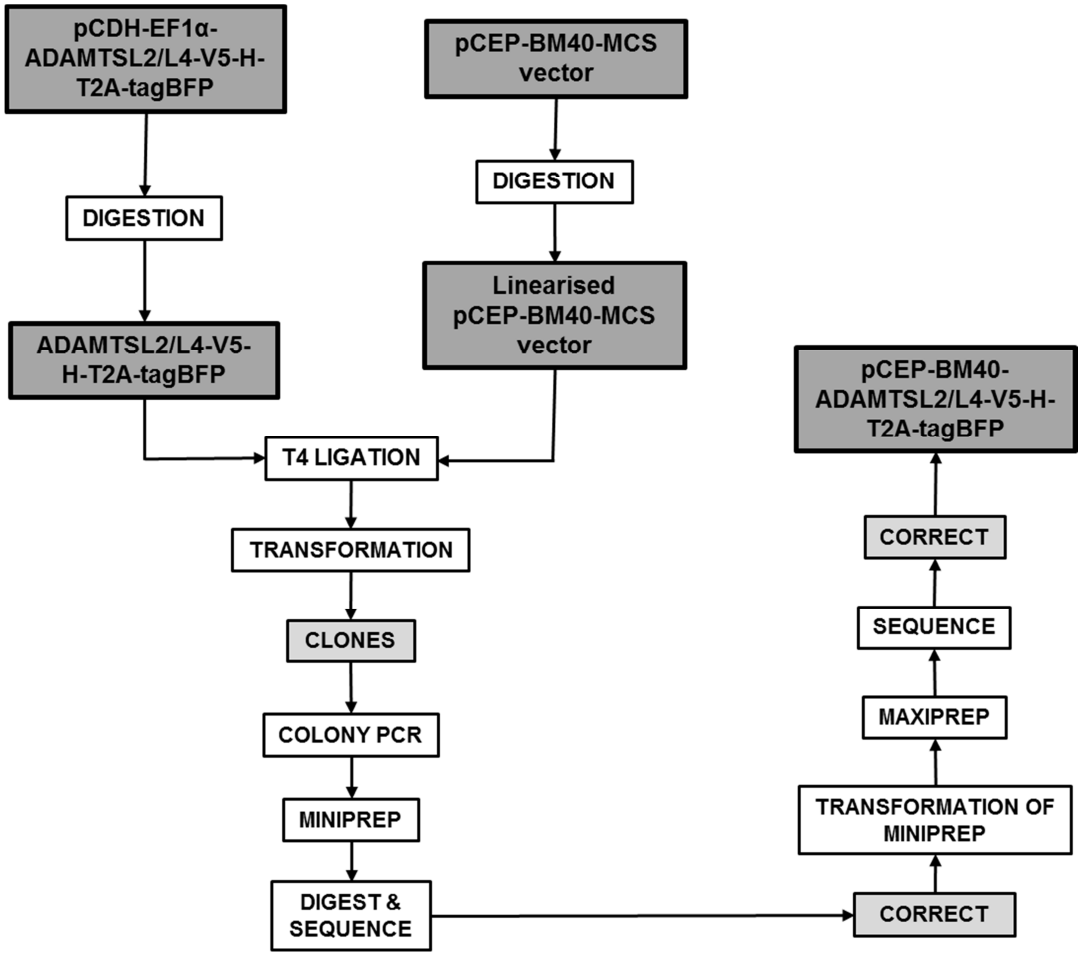


**Figure 3.1.5 Molecular cloning of recombinant ADAMTS-L2 and ADAMTS-L4 into the episomal pCEP expression system**

Recombinant ADAMTS-L2 and ADAMTS-L4 were cloned into the episomal pCEP vector. White boxes represent methods employed in the cloning process; light grey boxes denote outcomes; dark grey boxes denote DNA fragments used. Solid arrows depict the methodology followed to achieve results. A section of the pCDH-tagBFP lentiviral vector encoding the gene of interest and the V5, His and tagBFP tags were cut from the vector using NheI and XhoI enzymes. The empty pCEP-BM40 vector was digested with AvrII and SalI enzymes to create complementary ends, after which the inserts and linearised vector s were ligated using T4 ligase.

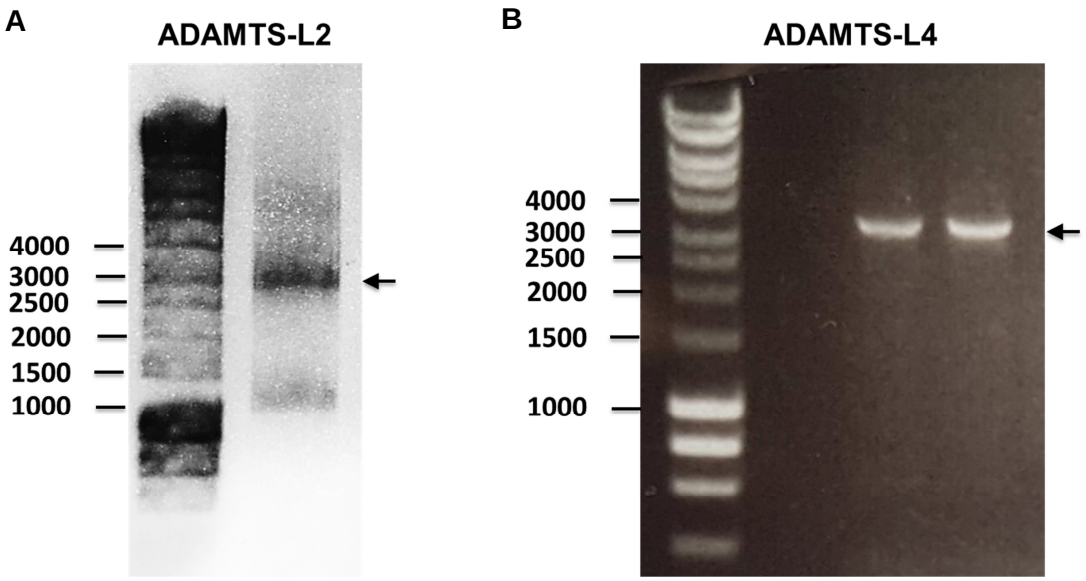


**Figure 3.1.6 Agarose gel depicting colony PCR products of FL ADAMTS-L2 and ADAMTS-L4.** Recombinant ADAMTS-L2 and ADAMTS-L4 were cloned into the pCDH lentiviral vector with a blue fluorescent tag (tagBFP). Colony PCR was conducted using colonies from bacterial transformations. Primer combinations used: EF1α Forward primer and ADAMTS-L2/4 (tBFP) Reverse. (**A**) ADAMTS-L2 (2856 bp) band depicted by arrow. (**B**) ADAMTS-L4 (3225 bp) band depicted by arrow. Hyperladder 1 band sizes in bp.

#### 3.2.1.4 Transfection and selection of recombinant ADAMTS-L2 and ADAMTS-L4 in mammalian cell lines

Both lentiviral pCDH and episomal pCEP expression vectors containing ADAMTS-L2 or ADAMTS-L4 were introduced in to different mammalian cells lines. The lentiviral and episomal expression vectors were engineered to carry the tagBFP epitope downstream of the insert. The episomal vectors also conferred antibiotic resistance to puromycin.

A lentiviral transduction mechanism was used to introduce the ADAMTS-L2 or ADAMTS-L4 containing lentiviral pCDH constructs into target HEK 293 EBNA, ARPE-19 and HDF cells. The viral construct was packaged into virus particles with the aid of 2 packaging vectors and HEK 293T cells. The harvested virus particles were applied to target cells in order to transduce the pCDH vectors into the target cells. Following transduction, the targets cells were sorted using FACS to select for cells expressing the tagBFP epitope. The presence of the tagBFP epitope confirmed that the target cell had taken up the pCDH vector and was expressing the desired insert.

Episomal pCEP vectors containing ADAMTS-L2 or ADAMTS-L4 were introduced into HEK 293 EBNA cells using the Xfect transfection method. Transfected cells were then selected using puromycin. Once antibiotic selection had been established, the cells were then sorted using FACS and the cells were further selected using tagBFP fluorescence.

#### 3.2.1.5 FACS analysis of recombinant ADAMTS-L2 expressing cells

Figure 3.1.7 Ai depicts the lentiviral pCDH vector map containing ADAMTS-L2 introduced into all target cells. FACS analysis of transduced HEK 293 EBNA (Figure 3.1.7Aii), ARPE-19 (Figure 3.1.7Aiii) and HDF (Figure 3.1.7Aiv) shows that 13%, 44% and 43% of the total cell population were expressing the ADAMTS-L2 construct respectively. HEK 293 EBNA cells were also transfected with the pCEP vector (Figure 3.1.7Bi) and then selected with puromycin. FACS analysis of these cells confirmed that 7% of the total cell population were expressing ADAMTS-L2 (Figure 3.1.7Bii).

#### 3.2.1.6 Transfection and selection of recombinant ADAMTS-L4

The pCDH vector containing ADAMTS-L4 (Figure 3.1.8Ai) was transduced into HEK 293 EBNA, ARPE-19 and HDF cell lines. Upon FACS analysis of these cells it was found that out of the total population of cells, 15% of HEK 293 EBNA cells (Figure 3.1.8Aii), 19% of ARPE-19 cells (Figure 3.1.8Aiii) and 3% of HDFs (Figure 3.1.8Aiv) were expressing ADAMTS-L4. Following transfection of the ADAMTS-L4 containing pCEP vector (Figure 3.1.8Bi) into HEK 293 EBNA cells and puromycin selection it was found using FACS analysis that only 4% of the total cell population were positive for ADAMTS-L4 (Figure 3.1.8Bii).

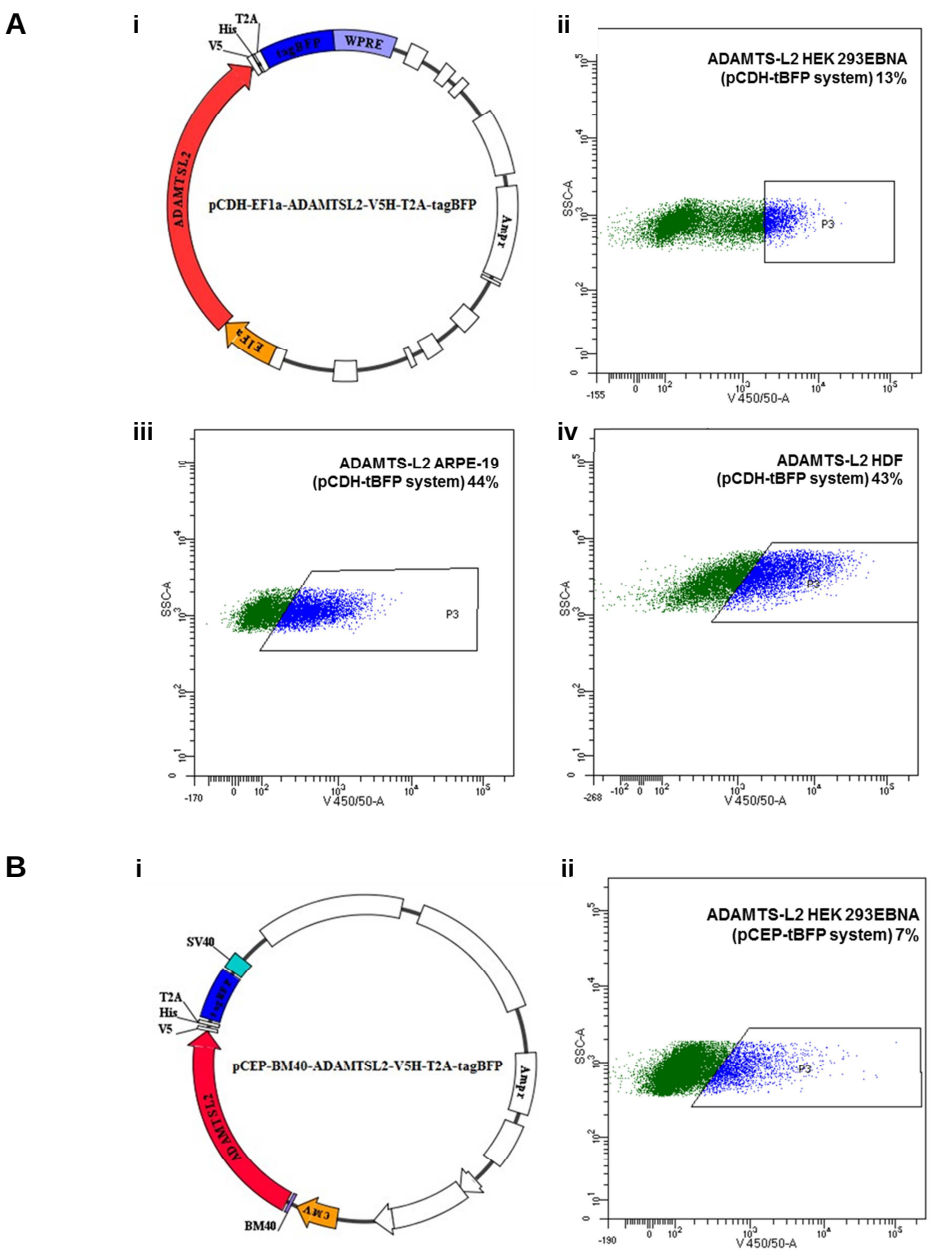


**Figure 3.1.7 FACS analysis of cell lines expressing ADAMTS-L2.**

**(A)** (**i**) Map of pCDH lentiviral vector engineered with the ADAMTS-L2 gene (red) and tagBFP marker (blue). (**ii**) HEK 293 EBNA, (**iii**) ARPE-19 and (**iv**) HDF cells were infected with virus particles containing ADAMTS-L2 containing lentiviral vector. FACS analysis was used to select the population of cells expressing tagBFP marker (blue); percentage of cells obtained shown. **(B)** (**i**) Map of pCEP episomal vector engineered with the ADAMTS-L2 gene (red) and tagBFP marker (blue). (**ii**) HEK 293 EBNA cells were transfected with ADAMTS-L2 containing episomal vector. FACS analysis was used to select the population of cells expressing tagBFP marker (blue); percentage of cells obtained shown. n=1

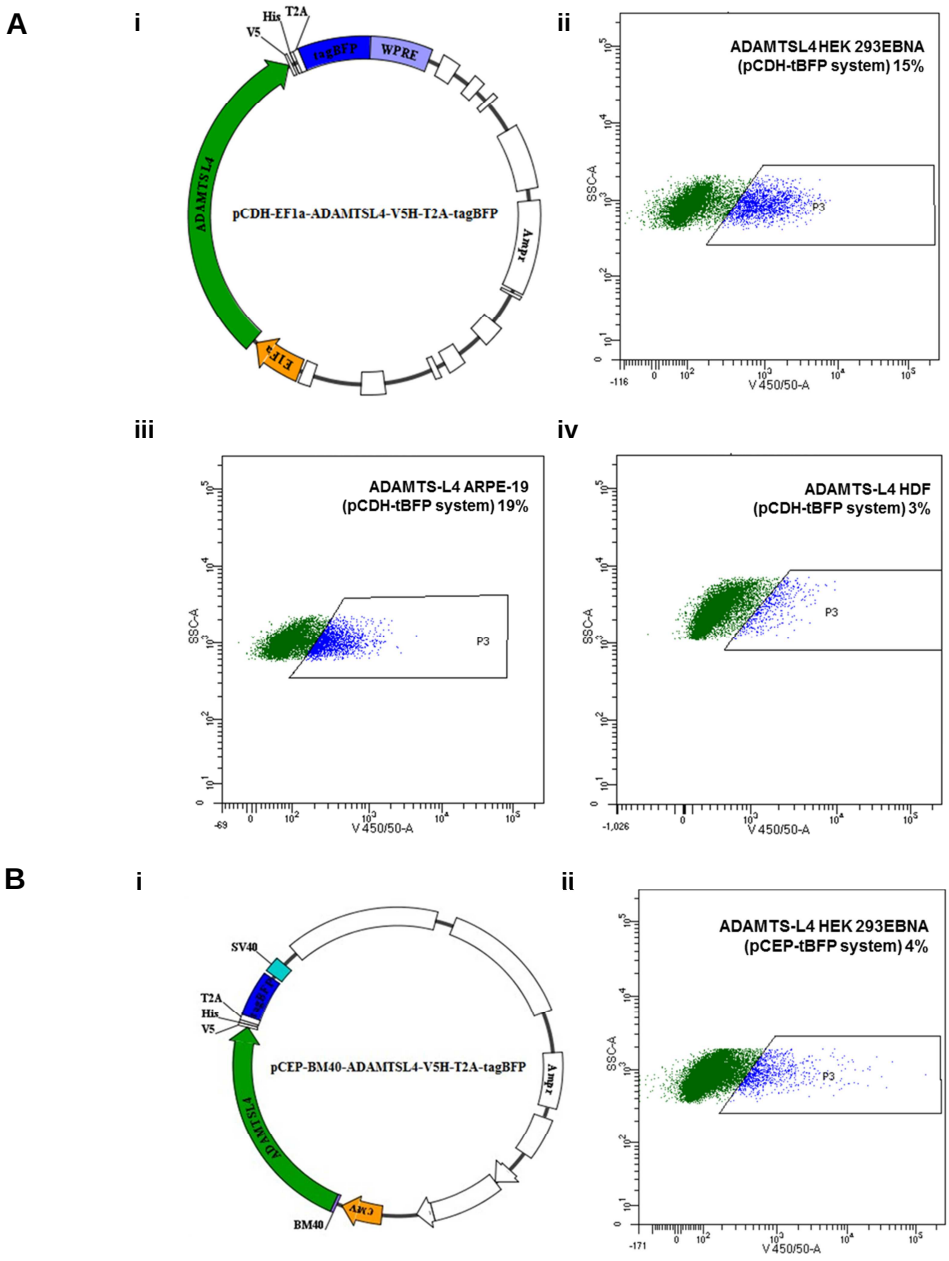


**Figure 3.1.8 FACS analysis of cell lines expressing ADAMTS-L4.**

**(A)** (**i**) Map of pCDH lentiviral vector engineered with the ADAMTS-L4 gene (green) and tagBFP marker (blue). (**ii**) HEK 293 EBNA, (**iii**) ARPE-19 and (**iv**) HDF cells were infected with virus particles containing ADAMTS-L4 containing lentiviral vector. FACS analysis was used to select the population of cells expressing tagBFP marker (blue); percentage of cells obtained shown. **(B)** (**i**) Map of pCEP episomal vector engineered with the ADAMTS-L4 gene (green) and tagBFP marker (blue). (**ii**) HEK 293 EBNA cells were transfected with ADAMTS-L4 containing episomal vector. FACS analysis was used to select the population of cells expressing tagBFP marker (blue); percentage of cells obtained shown. n=1

## 3.3 Expression analysis of recombinant ADAMTS-L2 and ADAMTS-L4 using different expression systems and cell lines

To determine which expression system and cell line expressed the most protein, HEK 293 EBNA cells were transfected with pCEP vectors, and HEK 293 EBNA, ARPE-19 and HDF cells transduced with pCDH lentiviral expression systems, for both ADAMTS-L2 and ADAMTS-L4.

Following recent transfection or transduction, and selection (puromycin only, puromycin and FACS or FACS only), HEK 293 EBNA cells expressing ADAMTS-L2 or ADAMTS-L4 were cultured and expression medium was applied to them. After 4 days, media from all different cell lines was collected and the cells were lysed for protein extraction. The collected media was incubated with Strataclean resin for 1 hour. Following incubation the Strataclean resin and 20 µg of protein lysate from each cell line were resolved using SDS-PAGE and transferred onto nitrocellulose. ADAMTS-L2 and ADAMTS-L4 were detected using anti-V5 antibody.

This experiment was repeated after all cell lines expressing ADAMTS-L2 and ADAMTS-L4 had been subjected to several passages. Unlike the previous expression analysis, transduced ARPE-19 and HDF cells were also included in the experiment. Alternatively, crude expression media rather than Strataclean resin which had been saturated with ADAMTS-L2 or ADAMTS-L4 was resolved using SDS-PAGE to determine a more accurate representation of the levels of the proteins being secreted by the cell lines.

Culture media and cell lysates from non-transfected cell lines (WT) were included in the experiments to serve as negative controls.

#### 3.3.1.1 Expression of recombinant ADAMTS-L2

Expression analysis of ADAMTS-L2 (approximately 140 kDa) indicated very little protein was being secreted into the culture medium by HEK 293 EBNA cells following transient transfection with the pCEP vector and puromycin selection only (Figure 3.1.9A). Interestingly, ADAMTS-L2 could not be detected in pCEP transfected cells which had been subjected to puromycin selection followed by FACS sorting. In contrast to these findings, ADAMTS-L2 expression induced via lentiviral transduction in HEK 293 EBNA cells was strong with plentiful amounts of the protein being secreted into the culture medium (Figure 3.1.9A). Questionably ADAMTS-L2 was not detected in cell lysates from any of the cell lines tested. An explanation for this could be that expression of ADAMTS-L2 could still be very low and that sufficient protein lysate was not loaded onto the SDS-PAGE gel, hence it was not detected via western blot (Figure 3.1.9A).

Repetition of the experiment in cells that had been subjected to several passages revealed that following transduction with the lentiviral pCDH vector, HEK 293 EBNA cells continued to express ADAMTS-L2 (Figure 3.1.9C) and secrete it (Figure 3.1.9B). Similarly, ARPE-19 and HDF cells were also seen to express and secrete ADAMTS-L2 at a comparable level to that seen in lentiviral

transduced HEK 293 EBNA cells. However, it was seen that ADAMTS-L2 secreted form HDFs was of a lower molecular weight, in comparison to ADAMTS-L2 observed in the corresponding cell lysate and other cell types. A species of ADAMTS-L2 of approximately 280 kDa was also detected in the culture media collected from ARPE-19 cells and HDFs. This species may be a dimer of ADAMTS-L2. In both experiments ADAMTS-L2 could not be detected in WT cell lines.

#### 3.3.1.2 Expression of recombinant ADAMTS-L4

It was found that in HEK 293 EBNA cells which had been newly transfected with the pCEP vector and selected using puromycin and FACS analysis did not express ADAMTS-L4 as it could not be detected in the medium (Figure 3.1.10A). Conversely small amounts of full length ADAMTS-L4 (approximately 125 kDa) were detected in the conditioned medium collected from HEK 293 EBNA cells which had been transduced with the lentiviral vector (Figure 3.1.10A). A smaller ADAMTS-L4 cleavage product of approximately 55 kDa was also detected. Although it must be recognised that Strataclean resin was used to capture and detect this level of ADAMTS-L4 in the culture medium. Interestingly, ADAMTS-L4 was not detected in the cell lysates of both HEK 293 EBNA cell lines (Figure 3.1.10A). As speculated before, this result could be due to inadequate amounts of protein being expressed in the cells and that insufficient amounts of protein lysate were analysed.

After having undergone several passages, all cells lines expressing ADAMTS-L4 were screened to compare the expression levels of the protein. As seen from the previous expression analysis (Figure 3.1.10A), pCEP transfected HEK 293 EBNA cells did not express any ADAMTS-L4 both in the conditioned medium (Figure 3.1.10B) and in the cell lysate (Figure 3.1.10C). Interestingly, in all cell lines transduced with the lentiviral vector, ADAMTS-L4 expression was only observed in the cell lysates (Figure 3.1.10C). Previous expression analysis performed in newly transduced HDFs and ARPE-19 cell lines expressing ADAMTS-L4 has shown that the protein has been secreted into the culture media (data not shown). However it was observed that over time as the cells matured, ADAMTS-L4 was still expressed in the cells but was not being secreted into the culture media (Figure 3.1.10B). In addition to full length ADAMTS-L4 a larger oligomeric species at approximately 250 kDa was observed; this could result from the dimerisation of monomeric ADAMTS-L4. A smaller cleavage product of approximately 55 kDa which was earlier visualised in the culture medium was also detected in the cell lysates of all lentiviral transduced cell lines (Figure 3.1.10C). This indicates that ADAMTS-L4 may be undergoing intracellular degradation and these degradation products were being secreted in to the culture medium. ADAMTS-L4 was not detected in any of the non-transfected cell line samples of conditioned media or cell lysates.

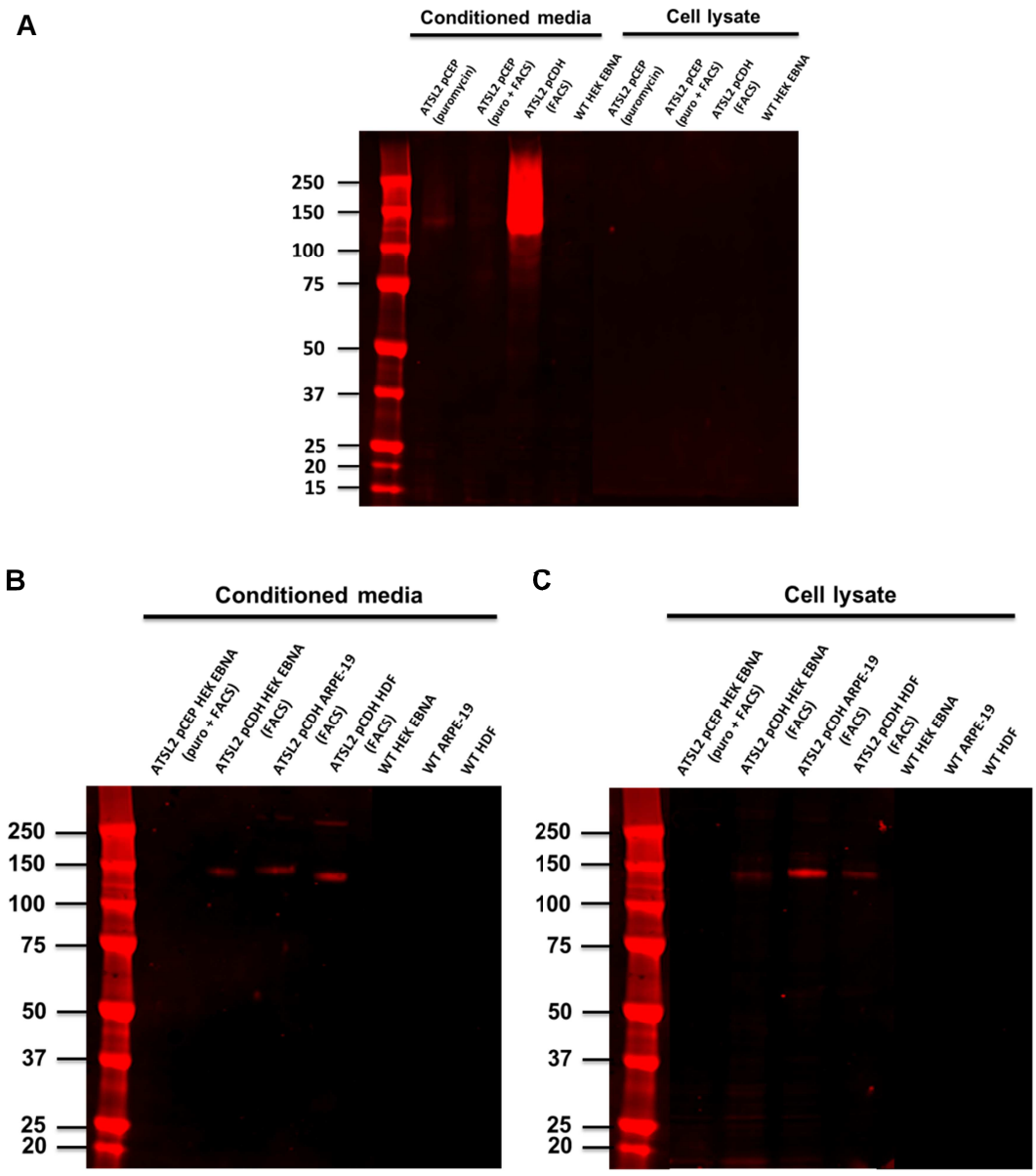


**Figure 3.1.9 Expression analysis of ADAMTS-L2.**

Western blot of non-reduced conditioned media (**A**) and (**B**), and cell lysates (**A**) and (**C**) comparing the expression of ADAMTS-L2 in HEK 293 EBNA, ARPE-19 and HDF cells. (**A**) HEK 293 EBNA cells newly transfected with lentiviral or episomal vectors and selected using antibiotic selection, FACS analysis or both were cultured for 4 days. Conditioned media was collected and incubated with Strataclean resin (*Agilent Technologies, USA*) for 1 hour and the cells were lysed. The incubated Strataclean beads and cell lysates from all conditions were resolved using SDS-PAGE on a 4-12% Bis-Tris gel and then transferred on to nitrocellulose membrane. HEK 293 EBNA, ARPE-19 and HDF cell lines after several passages expressing ADAMTS-L2 were cultured for 4 days; conditioned media was collected from all cell lines and cells were lysed. SDS-PAGE using 4-12% Bis-Tris gels and western blotting of conditioned media (**B**) and cell lysates (**C**) was performed. ADAMTS-L2 was detected using anti-V5 primary antibody and Li-cor secondary antibody. WT cell lines were also blotted as controls. ADAMTSL2 (ATSL2); wild type (WT); puromycin (puro).

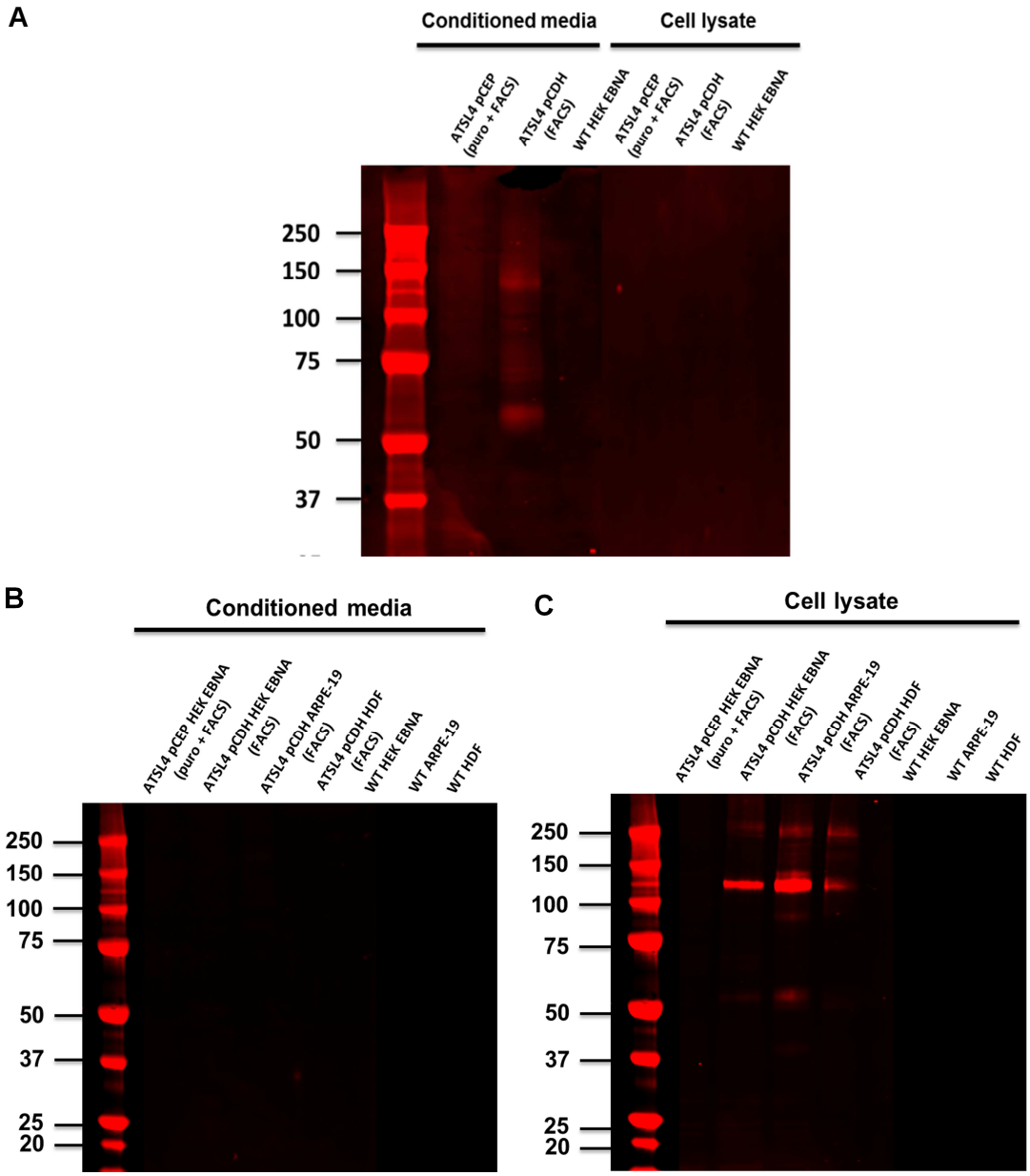


**Figure 3.1.10 Expression analysis of ADAMTS-L4.**
Western blot of non-reduced conditioned media (**A**) and (**B**) and cell lysates (**A**) and (**C**) comparing the expression of ADAMTS-L4 in HEK 293 EBNA, ARPE-19 and HDF cells. (**A**) HEK 293 EBNA cells newly transfected with lentiviral or episomal vectors and selected using antibiotic selection, FACS analysis or both both were cultured for 4 days. Conditioned media was collected and incubated with Strataclean resin (*Agilent Technologies, USA*) for 1 hour and the cells were lysed. The incubated Strataclean beads and cell lysates from all conditions were resolved using SDS-PAGE on a 4-12% Bis-Tris gel and then transferred on to nitrocellulose membrane. HEK 293 EBNA, ARPE-19 and HDF cell lines after several passages expressing ADAMTS-L4 were cultured for 4 days; conditioned media was collected from all cell lines and cells were lysed. SDS-PAGE using 4-12% Bis-Tris gels and western blotting of conditioned media (**B**) and cell lysates (**C**) was performed. ADAMTS-L4 was detected using anti-V5 primary antibody and Li-cor secondary antibody. WT cell lines were also blotted as controls. ADAMTS-L4 (ATSL4).

## 3.4 Purification of recombinant ADAMTS-L2 and ADAMTS-L4

For characterisation and further investigations of human ADAMTS-L2 and ADAMTS-L4, each of the proteins were expressed in mammalian cell lines. Both proteins were recombinantly expressed in stable HEK 293 EBNA cells generated using a lentiviral expression system. This expression system was selected based on results obtained from expression analysis studies (Section 3.1.3) having shown that it yielded the greatest amount of protein.

Recombinant ADAMTS-L2 or ADAMTS-L4 was purified using a 2-step purification protocol from collected expression media. Firstly, immobilised metal ion chromatography (IMAC) was used to extract the recombinant proteins from the expression medium using the His-tag which had been engineered onto the C-terminal end of the protein. Both ADAMTS-L2 and ADAMTS-L4 were eluted in Tris elution buffer (20 mM Tris, 400 mM NaCl, 240 mM imidazole, pH 8.0) and the absorbance was measured at 280 nm. Finally crude protein fractions obtained from IMAC were purified using size exclusion chromatography (SEC) in order to remove contaminants and isolate monomeric and pure protein samples.

Fractions collected from each stage of purification were resolved using SDS-PAGE and western blotting (only for samples obtained from SEC) to verify the presence and purification of ADAMTS-L2 and ADAMTS-L4.

### 3.4.1.1 Purification of recombinant ADAMTS-L2

Figure 3.1.11A illustrates the chromatogram obtained from IMAC of His-tagged recombinant ADAMTS-L2. The trace indicates that the elution of ADAMTS-L2 occurred at approximately 7 ml, diminished around 12 ml, and peaked between 8-9 ml. The eluted protein was collected in fractions samples of which were resolved non-reduced and reduced using SDS-PAGE (Figure 3.1.11B). The gel revealed a band in each fraction running at approximately 140 kDa, intensity of which increased corresponding to the peak fractions. A band approximately 280 kDa was also visualised in all non-reduced fractions, however this band disappeared following reduction of the protein sample (Figure 3.1.11B). This infers that ADAMTS-L2 may be forming a small proportion of disulphide linked dimers which dissociate upon reduction. Reduction of ADAMTS-L2 also showed an apparent increase in the size of the protein, i.e. bands representing ADAMTS-L2 were observed running at approximately 150 kDa (Figure 3.1.11B). This suggests that ADAMTS-L2 may be a globular protein consisting of internal disulphide bonds and that disruption of these linearises the protein. This subsequently slows down migration of the protein through the gel resulting in the visualisation of a higher molecular weight band.

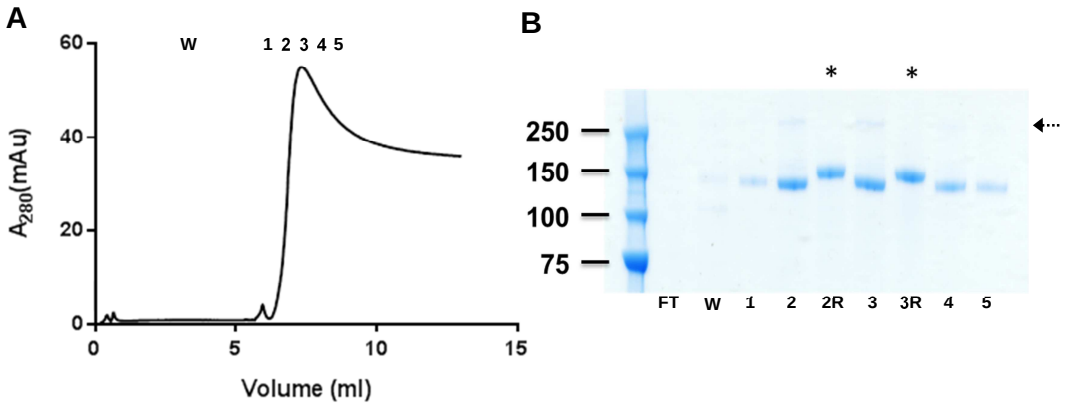


**Figure 3.1.11 His-tagged purification of recombinant ADAMTS-L2 using IMAC.**

(**A**) Chromatogram obtained from His-tagged IMAC purification of recombinant ADAMTS-L2 using a HisTrap Excel column. 500 ml of expression medium collected from HEK 293 EBNA cells expressing ADAMTS-L2 was loaded onto a HisTrap Excel column. Volume (ml) of Tris Elution buffer (20 mM tris 400 mM NaCl, 240 mM imidazole, pH 8.0) applied to the column to elute the protein was plotted against absorbance measured at 280 nm (mAU).(**B**) Fractions of eluted protein were resolved non-reduced and reduced (asterisks) on 4-12% Bis-Tris gels using SDS-PAGE and stained with InstantBlue. FT is flow through; W is wash, numbers represent fractions with R depicting the addition of reducing agent.

Peak fractions from the his-tagged purification of ADAMTS-L2 were pooled and 1 ml of the eluent was injected onto a S200 column for SEC. Figure 3.1.12A represents a purification chromatogram obtained when ADAMTS-L2 was eluted in HBS (10 mM HEPES, 150 mM NaCl, pH 7.4). The absorbance trace obtained demonstrated that with the use of HBS as an eluent, a large proportion of the injected ADAMTS-L2 sample was aggregating and eluting in the void volume (8ml). The remaining sample eluted as a monomer at approximately 11 ml. After subsequent buffer screens (data not shown) SEC of ADAMTS-L2 was repeated employing phosphate buffer as an eluent (10 mM phosphate, 500 mM NaCl, 2.7 mM KCl, pH 7.4). The SEC chromatogram attained demonstrated that in phosphate buffer, ADAMTS-L2 did not form aggregates and that the sample eluted at 11 ml in monomeric form (Figure 3.1.12B). SDS-PAGE (Figure 3.1.12C) and western blotting (Figure 3.1.12D) of non-reduced and reduced fractions collected from SEC displayed a band of the correct molecular size (approximately 140 kDa in non-reduced and 150 kDa in reduced) in each fraction. Western blotting also depicted the previously detected higher molecular weight band at approximately 280 kDa which disappeared following reduction (Figure 3.1.11D). Smaller bands in the peak fractions running at approximately 100 kDa (which ran higher once reduced) were also detected (Figure 3.1.12D). These fragments may represent cleavage products.

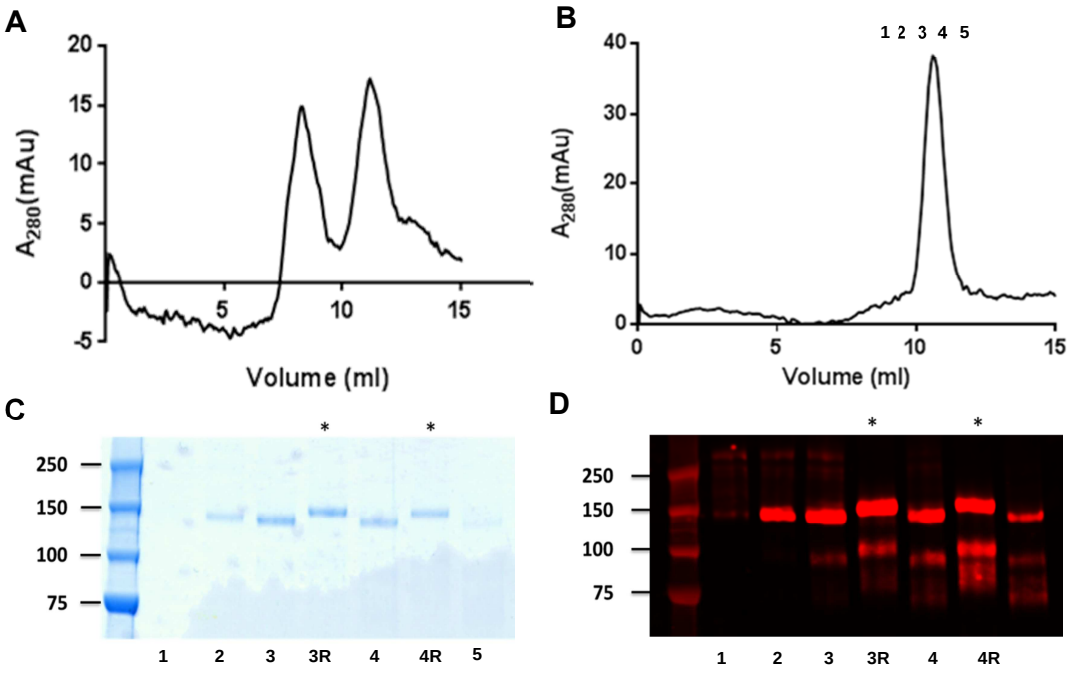


**Figure 3.1.12 Purification of recombinant ADAMTS-L2 using SEC.**

(**A**) Chromatogram obtained from SEC of recombinant ADAMTS-L2 using a S200 column in HBS (10 mM HEPES 150 mM NaCl, pH 7.4). Fractions obtained from IMAC purification of ADAMTS-L2 were injected into a S200 column. Volume (ml) of buffer applied to the column to elute the protein was plotted against absorbance measured at 280 nm (mAU). (**B**) Chromatogram obtained from SEC of recombinant ADAMTS-L2 using a S200 Increase column in phosphate buffer (10 mM phosphate 500 mM NaCl, 2.7 mM KCl, pH 7.4). IMAC purified fractions of ADAMTS-L2 were injected into a S200 Increase column. Absorbance measured at 280 nm (mAU) was plotted against volume (ml) of buffer applied to the column to elute the protein. (**C**) Eluted fractions from SEC were run non-reduced and reduced (asterisks) on a 4-12% Bis-Tris gel using SDS-PAGE and stained using coomassie blue stain. (**D**) Fractions resolved with SDS-PAGE were also transferred on to nitrocellulose membrane. ADAMTS-L2 was detected using primary anti-V5 antibody and Li-cor secondary antibody. Numbers represent fractions with R depicting the addition of reducing agent.

### 3.4.1.2 Purification of recombinant ADAMTS-L4

IMAC purification was performed to extract secreted recombinant ADAMTS-L4 from culture medium collected from HEK 293 EBNA cells. Figure 3.1.13A shows the chromatogram obtained showing protein elution in tris elution buffer. Protein samples containing ADAMTS-L4 were eluted at between 21 ml and 25 ml with the trace peaking at approximately 22 ml. Fractions collected were analysed using SDS-PAGE (Figure 3.1.13B). Several bands were stained in all fractions, indicating the presence of several contaminants. However, distinct bands were observed at approximately 150 kDa and 55 kDa in each fraction. A band at 250 kDa was also visualised in non-reduced fractions which upon reduction was not present. As previously suggested, ADAMTS-L4 may be forming disulphide-linked dimers. Similar to the observations recorded in ADAMTS-L2, reduction of ADAMTS-L4 resulted in an upward shift of fragments (Figure 3.1.13B) indicating the presence of disulphide bonds within the protein.

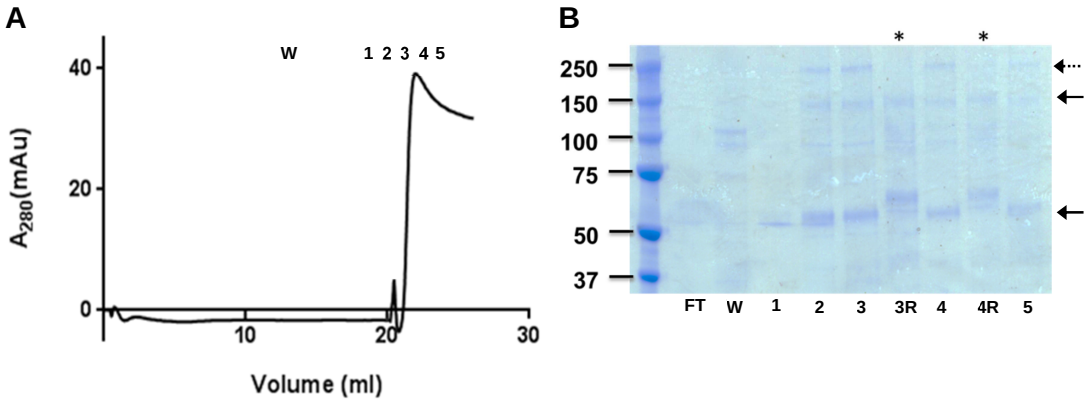


**Figure 3.1.13 His-tagged purification of recombinant ADAMTS-L4 using IMAC.**
(**A**) Chromatogram obtained from His-tagged IMAC purification of recombinant ADAMTS-L4 using a HisTrap Excel column. 500 ml of expression medium collected from HEK 293 EBNA cells expressing ADAMTS-L4 was loaded onto a HisTrap Excel column. Volume (ml) of Tris Elution buffer (20 mM tris 400 mM NaCl, 240 mM imidazole, pH 8.0) applied to the column to elute the protein was plotted against absorbance measured at 280 nm (mAU). (**B**) Fractions of eluted protein were resolved non-reduced and reduced (asterisks) on 4-12% Bis-Tris gels using SDS-PAGE and stained with InstantBlue. Solid arrows indicate prominent bands observed in all fractions and dashed arrow indicates disulphide-linked dimerisation product of ADAMTS-L4. . FT is flow through; W is wash; numbers represent fractions with R depicting the addition of reducing agent.

SEC of peak fractions obtained from IMAC purification of ADAMTS-L4 was performed using an S200 column. The protein sample was injected onto the column and eluted in phosphate buffer. Figure 3.1.14A illustrates the chromatogram obtained displaying the trace depicting ADAMTS-L4 elution. It can be observed that ADAMTS-L4 did not elute in a single peak, rather a higher molecular weight fragment was eluted at 9 ml and a lower molecular weight fragment at 14 ml. The peak observed at 11.5 ml was expected to be monomeric full length ADAMTS-L4. Fractions immediately surrounding this peak were analysed non-reduced and reduced using SDS-PAGE (Figure 3.1.14B) and western blot (Figure 3.1.14C). A band at approximately 125 kDa was observed representing full length ADAMTS-L4. In addition a cleavage fragment at approximately 55 kDa was also detected. Reduction of the protein sample resulted in the slower migration of ADAMTS-L4; however the band representing this was only visible by SDS-PAGE analysis (Figure 3.1.14B) and not by western blot (Figure 3.1.14C).

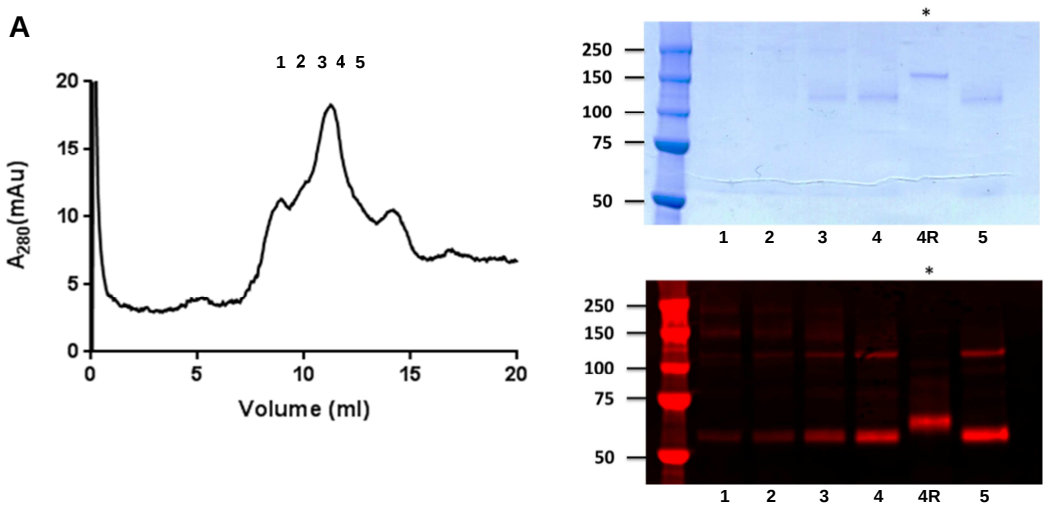


**Figure 3.1.14 Purification of recombinant ADAMTS-L4 using SEC.**
(**A**) Chromatogram obtained from SEC of recombinant ADAMTS-L4 using a S200 Increase column in phosphate buffer (10 mM phosphate 500 mM NaCl, 2.7 mM KCl, pH 7.4). IMAC purified fractions of ADAMTS-L4 were injected into a S200 Increase column. Absorbance measured at 280 nm (mAU) was plotted against volume (ml) of buffer applied to the column to elute the protein. (**B**) Eluted fractions from SEC were run non-reduced and reduced (asterisks) on a 4-12% Bis-Tris gel using SDS-PAGE and stained using coomassie blue stain. (**C**) Fractions resolved with SDS-PAGE were also transferred on to nitrocellulose membrane. ADAMTS-L4 was detected using primary anti-V5 antibody and Li-cor secondary antibody. Numbers represent fractions with R depicting the addition of reducing agent.

## Summary

To investigate ADAMTS-L2 and ADAMTS-L4, both genes were cloned into lentiviral and episomal expression systems. Cloning of both ADAMTS-L2 and especially ADAMTS-L4 was an arduous and extensive process which was achieved through the employment of several molecular cloning techniques. The addition of a fluorescent reporter to the cloning vectors allowed for selection of targeted cells which proved to be a faster process in comparison to the more traditional antibiotic selection.

In comparing transfection efficiencies of ADAMTS-L2 with that of ADAMTS-L4 it was found that ADAMTS-L2 containing expression vectors (both lentiviral and episomal) transfected different cell types better than ADAMTS-L4 expression vectors. FACS analysis determined a greater number of cells expressing the fluorescent reporter and therefore the insert for ADAMTS-L2 containing expression vectors. The use of two different expression systems allowed for the comparison of the overall yield of total protein obtained from each system. The lentiviral pCDH expression system not only had better transfection rates in all cell types, but the expression of protein in these cells was higher than that observed in cells transfected with the pCEP vector. Cells containing the episomal expression system exhibited poor transfection efficiency with the expression of the desired protein diminishing over time despite both systems possessing promoters that are equally strong for gene expression. From this it can be established that in all respects, the lentiviral expression system is

better, having a faster and efficient protocol yielding a greater turnover of cells which exhibit long-lasting stable protein expression.

ADAMTS-L2 was observed in both the cell lysate and conditioned medium of expression cells. Those transduced with the lentiviral system maintained levels of expression after several passages however, in cells transfected with the episomal vector expression of ADAMTS-L2 reduced over time. Expression analysis of ADAMTS-L4 showed that all cell types expressed and secreted small amounts of protein. However over time, it was found that although expression of ADAMTS-L4 was observed in the cell lysate, secretion of the protein from all cell types ceased. A low molecular weight cleavage product of ADAMTS-L4 was also detected in the conditioned medium and cell lysate indicating intracellular cleavage of the protein.

Purification of ADAMTS-L2 was achieved after buffer optimisation. As shown in the results, purification of ADAMTS-L2 in HEPES buffer resulted in the formation of aggregates which eluted in the void volume and therefore, loss of protein suitable for downstream applications. The presence of ADAMTS-L2 was detected in the fractions collected from the void volume using SDS-PAGE and confirmed with western blot (data not shown). The use of phosphate buffer as an eluent however eradicated this allowing for the isolation of monomeric ADAMTS-L2. Western blot of the purified protein detected lower molecular weight species in the purified fractions; this could be the result of extracellular cleavage of the protein, either during the purification or co-purifying with FL ADAMTS-L2.

Buffer optimisation was not carried out for ADAMTS-L4, however based on buffer optimisation of ADAMTS-L2 phosphate buffer was employed to purify ADAMTS-L4, which also resulted in the separation of monomeric protein. However, two distinct bands, a full length monomer and a lower molecular weight species in the same fraction were observed following SEC. As mentioned before the secondary band could be a C-terminal product resulting from intracellular or extracellular degradation or cleavage of ADAMTS-L4 that may be interacting with the full length molecule, therefore being eluted at the same time.

### 3.5 Biophysical and biochemical characterisation of ADAMTS-L2 and ADAMTS-L4

Since ADAMTS-L2 and ADAMTS-L4 have an important role in ECM maintenance, structure, and function, further knowledge about their biophysical and biochemical characteristics is required. Literature provides very little biophysical and biochemical information about ADAMTS-L2 and ADAMTS-L4. Koo et al (2007) reported that ADAMTS-L2 is an N-linked glycoprotein where approximately 20% of its mass (approximately 30 kDa) constitutes of carbohydrates. The ADAMTS-L2 molecule consists of 10 conserved N-glycan carbohydrate attachment sites, 6 of which are contained within the N-glycan rich domain (Koo et al, 2007). Similarly it was shown that ADAMTS-L4 is also N-glycosylated and O-glycosylated (Gabriel et al 2012). This study identified various high molecular weight species of ADAMTS-L4 secreted from HEK 293F cells which upon treatment with N-linked and O-linked de-glycosides reduced in size (Gabriel et al, 2012).

Biophysical and biochemical characterisation of ADAMTS-L2 and ADAMTS-L4 will help in understanding their behaviour and properties. To characterise both recombinant ADAMTS-L2 and ADAMTS-L4, purified protein samples were analysed using different analytical techniques. Due to small quantities of recombinant ADAMTS-L4 available, it was not possible to apply all the techniques employed for ADAMTS-L2 characterisation.

### 3.6 Analysis of purified ADAMTS-L2 using mass spectrometry

To confirm the purification of recombinant ADAMTS-L2, fractions of purified protein using SEC were resolved using SDS-PAGE, stained with coomassie brilliant blue and analysed using mass spectrometry (Figure 3.2.1A). Sequence coverage obtained from mass spectrometry analysis (Figure 3.2.1B), identified amino acid residues of which coincided with 23% of the protein sequence for human ADAMTS-L2. This verifies that the purified protein used in all experimentation from here after is ADAMTS-L2.

### 3.7 Biophysical analysis of ADAMTS-L2

Temperature induced unfolding and aggregation curves of ADAMTS-L2 were measured using the OPTIM 1000 instrument in several different buffers: sodium acetate buffer (50 mM sodium acetate, 500 mM NaCl, pH 5.5); tris buffer (50 mM Tris, 500 mM NaCl, pH 7.4); HEPES buffer (50 mM HEPES, 500 mM NaCl, pH 7.4) and phosphate buffer (50 mM sodium phosphate, 50 mM NaCl, pH 7.4). Samples containing ADAMTS-L2 diluted in different buffers were heated using a step gradient where 1 °C increments were applied. Intrinsic fluorescence of excited tryptophan residues was measured at a range between 300-400 nm and used to determine the barycentric mean fluorescence (BCM) with the following equation:

$$\boldsymbol{BCM\ \lambda\ (nm)} = \frac{\boldsymbol{\Sigma\ I(\lambda)\ \mathrm{x}\ \lambda}}{\boldsymbol{\Sigma\ I(\lambda)}}$$

**A**

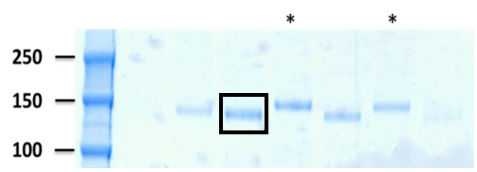


**B**

M L F E V G E G G G A G E E G K G R G R P G R S L C T H A A P A R T A H L A P S A L R S A R P F L W
E D N L L T R S Q G L P D N H D Q L V P D N L E A W A L A G P R G L F P K R T L V I W K R I G A G L
V V T V A L L P R M D G R W Q C S C W A W F L L V L A V V A G D T V S T G S T D N S P T S N S L E G
G T D A T A F W W G E W T K W T A C S R S C G G G V T S Q E R H C L Q Q R R K S V P G P G N R T C T
G T S K R Y Q L C R V Q E C P P D G R S F R E E Q C V S F N S H V Y N G R T H Q W K P L Y P D D Y V
H I S S L P C D L H C T T V D G Q R Q L M V P A R D G T S C K L T D L R G V C V S G K C E P I G C D
G V L F S T H T L D K C G I C Q G D G S S C T H V T G N Y R K G N A H L G Y S L V T H I P A G A R D
I Q I V E R K K S A D V L A L A D E A G Y Y F F N G N T K V D S P K N F N I A G T V V K Y R R P M D
V Y E T G I E Y I V A Q G P T N Q G L N V M V W N G N G K S P S I T F E Y T L L Q P P H E S R P Q P
I Y Y G F S E S A E S Q G L D G A G L M G F V P H N G S L Y G Q A S S E R L G L D N R L F G H P G L
D M E L G P S Q G Q E T N E V C E Q A G G G A C E G P P R G K G F R D R N V T G T P L T G D K D D E
E V D T H F A S Q E F F S A N A I S D Q L L G A G S D L K D F T L N E T V N S I F A Q G A P R S S L
A E S F F V D Y E E N E G A G P Y L L N G S Y L E L S S D R V A N S S S E A P F P N V S T S L L T S
A G N R T H K A R T R P K A R K Q G V S P A D M Y R W K L S S H E P C S A T C T T G V M S A Y A M C
V R Y D G V E V D D S Y C D A L T R P E P V H E F C A G R E C Q P R W E T S S W S E C S R T C G E G
Y Q F R V V R C W K M L S P G F D S S V Y S D L C E A A E A V R P E E R K T C R N P A C G P Q W E M
S E W S E C T A K C G E R S V V T R D I R C S E D E K L C D P N T R P V G E K N C T G P P C D R Q W
T V S D W G P C S G S C G Q G R T I R H V Y C K T S D G R V V P E S Q C Q M E T K P L A I H P C G D
K N C P A H W L A Q D W E R C N T T G C R G V K K R L V L C M E L A N G K P Q T R S G P E C G L A K
K P P E E S T C F E R P C F K W Y T S P W S E C T K T C G V G V R M R D V K C Y Q G T D I V R G C D
P L V K P V G R Q A C D L Q P C P T E P P D D S C Q D Q P G T N C A L A I K V N L C G H W Y Y S K A
C C R S C R P P H S

**Figure 3.2.1 Mass spectrometry of recombinant ADAMTS-L2.** Purified samples of recombinant ADAMTS-L2 were resolved reduced (asterisks) and non-reduced using SDS-PAGE on a 4-12% Bis-Tris gel and stained with coomassie brilliant blue (A). A band (indicated by black box) was excised from the gel for mass spectrometry. (B) Distribution of identified peptide sequences (highlighted) in amino acid sequence of full length ADAMTS-L2.Sequence coverage was obtained from Scaffold 4 programme. Tested sample showed 23% sequence coverage of ADAMTS-L2.

In this equation, *BCM λ* is measured in nanometres (nm), *λ* is the wavelength in nm and *I (λ)* is the fluorescence intensity at the given wavelength. The calculated BCM describes the change in average wavelength of the fluorescence emitted by tryptophan residues as the protein unfolds. The BCM was plotted against temperature for each sample of ADAMTS-L2 (Figure 3.2.2A). The graph plots the BCM of ADAMTS-L2 in HEPES buffer (purple), phosphate buffer (blue), tris buffer (green) and sodium acetate buffer (red). The calculated BCM was then used to determine the melting temperature ($T_m$) of ADAMTS-L2 in different buffers using the following equation:

$$\boldsymbol{Melting\ temperature\ (Tm)(°C) = max\ \frac{dBCM}{dT}\ (T)}$$

In this equation $T_m$ is measured in °C, *max* is the local maximum of the plotted graph, *T* is temperature at any given point and dBCM/*dT* is the first derivative of the BCM as a function of temperature measured in nm/°C. These derivatives were plotted against temperature to allow for

the determination of the $T_m$ of ADAMTS-L2 in different buffers (Figure 3.2.2B). The $T_m$ of ADAMTS-L2 was seen to vary in different buffers, for example in phosphate buffer (blue) the $T_m$ was determined to be 51 °C, in sodium acetate buffer (red) it was 53 °C and in tris buffer (green) it was the highest at 61 °C. A $T_m$ of ADAMTS-L2 in HEPES could not be determined as the BCM did not show any changes, suggesting that in HEPES buffer ADAMTS-L2 immediately aggregates. Interestingly, in the presence of tris buffer ADAMTS-L2 appears to unfold in stages resulting in a shouldered melt peak rather than the sharp peaks noted for phosphate and sodium acetate buffers.

Formation of aggregates of ADAMTS-L2 in each buffer condition with increasing temperature was also recorded by measuring the static light scattering (SLS) at 473 nm (Figure 3.2.2C). The temperature at which ADAMTS-L2 was seen to aggregate ($T_{agg}$) in phosphate buffer was 49 °C and 51 °C in sodium acetate buffer. It was also found that tris buffer granted the best stability to ADAMTS-L2 as aggregates of the protein formed at a higher temperature of 57 °C. Conversely data determining the $T_{agg}$ of ADAMTS-L2 in HEPES buffer was not obtained because the sample had already aggregated.

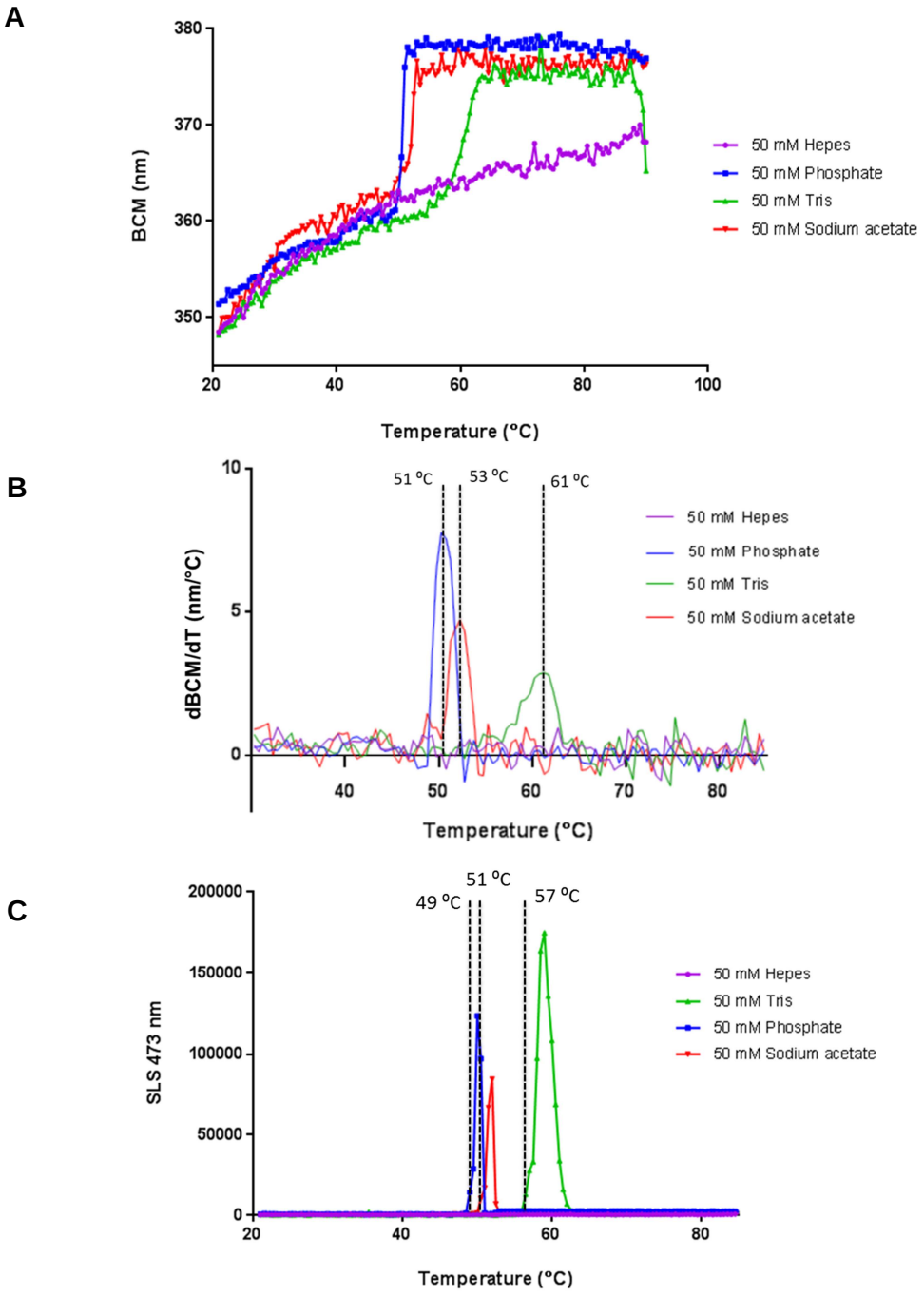


**Figure 3.2.2 Conformational and colloidal resistance to thermal degradation of recombinant ADAMTS-L2.** Melting temperatures and aggregation profiles of ADAMTS-L2 were analysed in different buffers: sodium acetate buffer (50 mM sodium acetate, 500 mM NaCl, pH 5.5) (red); tris buffer (50 mM Tris, 500 mM NaCl, pH 7.4) (green); HEPES buffer (50 mM HEPES, 500 mM NaCl, pH 7.4) (purple); phosphate buffer (50 mM sodium phosphate, 50 mM NaCl, pH 7.4) (blue). The reactions were run on the OPTIM 1000 instrument and analysed using Optim Analysis software 2.0. (**A**) Barycentric mean intrinsic fluorescence (BCM) of tryptophan residues was determined to measure thermal unfolding of ADAMTS-L2. (**B**) First derivative of the BCM was used to calculate the melting temperature of ADAMTS-L2 in different buffers. (**C**) Aggregation temperature was measured using static light scattering (SLS) at 473nm. This experiment was performed once (n=1).

### 3.8 Biochemical analysis of ADAMTS-L2 and ADAMTS-L4

To assess whether ADAMTS-L2 forms self-associated oligomers under native conditions, purified recombinant ADAMTS-L2 was resolved using Native-PAGE and stained with coomassie brilliant blue stain (Figure 3.2.3A). It was found that under non-denaturing conditions, ADAMTS-L2 ran at approximately 150 kDa indicating that it exists in monomeric form.

To confirm N-linked glycosylation of ADAMTS-L2 and ADAMTS-L4, purified recombinant samples of the proteins were incubated with or without PNGase F enzyme under denaturing conditions. The samples were then resolved using SDS-PAGE and transferred on to nitrocellulose. ADAMTS-L2 and ADAMTS-L4 were detected using an anti-V5 antibody.

Analysis of N-linked glycosylation of ADAMTS-L2 (Figure 3.2.3B) revealed a major band at approximately 150 kDa representing full length ADAMTS-L2 in the non-treated sample (closed arrowhead). Following digestion with PNGase F this species had reduced in size to approximately 120 kDa, confirming the previously reported presence of approximately 30 kDa of N-linked glycosylation on the molecule. In addition to this, other cleavage products of ADAMTS-L2 were observed. A species running at approximately 105 kDa in the control sample was seen to have reduced to approximately 75 kDa (closed arrowhead and dashed line), indicating the loss of approximately 30 kDa of N-linked carbohydrates. A smaller band at approximately 85 kDa was further detected in the non-treated sample, which had reduced to approximately 65 kDa following PNGase F digestion (open arrowhead) representing an approximate 20 kDa reduction in size of this ADAMTS-L2 species.

Several species of ADAMTS-L4 were also detected in both the non-treated control sample and PNGase F digested sample of ADAMTS-L4 (Figure 3.2.3C). Two prominent bands in the non-digested sample were visualised at approximately 125 kDa (closed arrowhead), representing full length ADAMTS-L4, and 60 kDa cleavage product (open arrowhead). Following digestion with PNGase F, the band running at approximately 125 kDa had reduced to approximately 100 kDa. Similarly the second prominent band detected at 60 kDa had also shown an approximate 20 kDa reduction in size after PNGase F treatment. Interestingly a double band was identified here at approximately 40 kDa and 45 kDa. The higher band in this case could be the result of incomplete de-glycosylation of the protein sample and the presence of O-linked glycans. A larger species of ADAMTS-L4 was also visualised running at approximately 140 kDa in the non-treated sample (closed arrowhead with a dashed line). After treatment however this band was not detected.

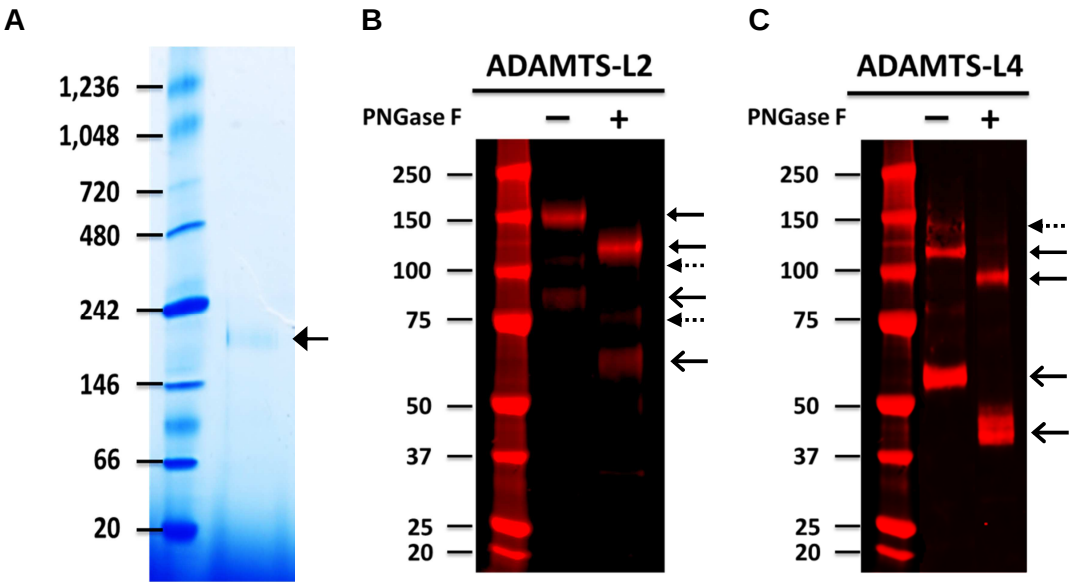


**Figure 3.2.3 Biochemical analysis of ADAMTS-L2 and ADAMTS-L4.** (**A**) Native-PAGE of recombinant ADAMTS-L2. Purified protein sample was mixed with Native-PAGE sample buffer and separated on a 3-12% Native-PAGE Bis-Tris gel. The gel was stained with coomassie blue stain. Arrow indicates ADAMTS-L2 staining at approximately 150 kDa. Western blots of PNGase F assay to determine N-glycosylation states of recombinant ADAMTS-L2 (**B**) and recombinant ADAMTS-L4 (**C**). Purified protein samples were incubated under denaturing conditions with PNGase F enzyme for 1 hour at 37 °C. The reactions were resolved using SDS-PAGE on a 4-12% Bis-Tris gel and then transferred onto nitrocellulose membrane. Protein fragments were detected using an anti-V5 primary antibody and Li-cor secondary antibody. Different species are represented by different arrow types. First arrow of each type represents protein without PNGase F treatment and second arrow represents protein with PNGase F treatment. Experiments performed once (n=1).

**Summary**

Analysis of purified recombinant ADAMTS-L2 using mass spectrometry confirmed that the protein being expressed, purified and utilised in downstream experimentation is human ADAMTS-L2.

The determination of the $T_m$ and $T_{agg}$ of ADAMTS-L2 in different buffers was performed to identify the optimum buffer for protein stabilisation. It was found that HEPES buffer was least favourable for stabilisation of ADAMTS-L2, as $T_m$ and $T_{agg}$ could not be determined suggesting that the protein formed aggregates very rapidly in this buffer. On the other hand, phosphate, sodium acetate and tris buffers stabilised ADAMTS-L2 in solution. In the presence of phosphate and sodium acetate buffers ADAMTS-L2 unfolded at 51 °C and 53 °C respectively. However in tris buffer ADAMTS-L2 unfolded at a higher temperature and gradually. This was represented by the shouldered curve, where the shoulders may be indicative of the different transitions the protein is undergoing at that temperature range. $T_{agg}$ of ADAMTS-L2 in phosphate, sodium acetate and tris buffers were similar to the corresponding $T_m$. A lower $T_{agg}$ in comparison to the $T_m$ may suggest that ADAMTS-L2 is aggregating before the protein is unfolding.

Native-PAGE of purified ADAMTS-L2 revealed that under non-denaturing conditions ADAMTS-L2 does not self-associate to form higher order oligomers.

Data obtained from performing N-linked de-glycosylation of ADAMTS-L2 indicate that full length and the different cleavage products of ADAMTS-L2 are glycosylated, where the full length and larger cleavage product carry 30 kDa and the smaller cleaved fragment has 20 kDa of N-linked carbohydrates bound to them. Similarly, ADAMTS-L4 is an N-glycosylated protein and that both the full length and cleavage products carry approximately 20 kDa of N-linked glycosylation.

### 3.9 Structural studies of ADAMTS-L2 and ADAMTS-L4

ADAMTS-L2 and ADAMTS-L4 are ECM glycoproteins which need to be investigated and characterised in order to gain understanding of how these molecules may function in the matrix. An essential part of this characterisation is to develop a comprehensive understanding of the structural form ADAMTS-L2 and ADAMTS-L4 adopt. So far, literature has yet to explore the structural characteristics of both ADAMTS-L2 and ADAMTS-L4, therefore to address this gap in research TEM and single particle image analysis was performed. To determine the structure of ADAMTS-L2 and ADAMTS-L4, purified recombinant protein was imaged using negative stain TEM. Protein samples were deposited on carbon-coated copper grids, stained with uranyl acetate and imaged.

### 3.10 Single particle analysis and structural modelling of ADAMTS-L2

3D modelling of ADAMTS-L2 was achieved by processing acquired negative stain data using EMAN2 which is a specialised software program used for EM image processing and 3D reconstruction of molecules. Imaged micrographs (Figure 3.3.1A) were used for particle picking. Individual particles were selected manually using a box size of 39 x 39 nm and saved for further processing. The contrast transfer function (CTF) of all selected and aligned particles (Figure 3.3.1B) was determined and corrected to eliminate any aberrations created during image acquisition. The data sets were then subjected to numerous iterations of class averaging to generate 2D classifications of refined particle sets projecting different orientations of ADAMTS-L2 (Figure 3.3.1C).. For further higher resolution refinement of these classifications, several particles were excluded and 2082 particles were submitted to generate an initial 3D model of ADAMTS-L2. The resulting 3D model was then subjected to several iterative refinements to generate a final 3D reconstruction of ADAMTS-L2. UCSF Chimera molecular modelling software was used to visualise the 3D model of ADAMTS-L2 (Figure 3.3.1D, E and F). The resolution of the 3D model was evaluated by splitting the data set into odd and even subsets and generating models from each. The Fourier shell correlation (FSC) was calculated from these odd and even models and used to determine the resolution of the final 3D model at threshold criterion of 0.5 (Figure 3.3.1G). The resolution of the 3D model of ADAMTS-L2 was determined to be 43.4 Å.

Initial analysis of the model reveals that ADAMTS-L2 adopts an asymmetrical lobular conformation. To further interpret this model, it was imported into UCSF Chimera as a reference electron density map to enable three-dimensional molecular modelling. The SWISS MODEL molecular modelling server was used to generate homology models (PDB files) of individual TSR domains and PLAC domain using the protein sequence for ADAMTS-L2 (Appendix Figure A8). A combined homology model of the cysteine-rich, spacer and N-glycan rich domains (C-S-N model) was also generated (Appendix Figure A8).

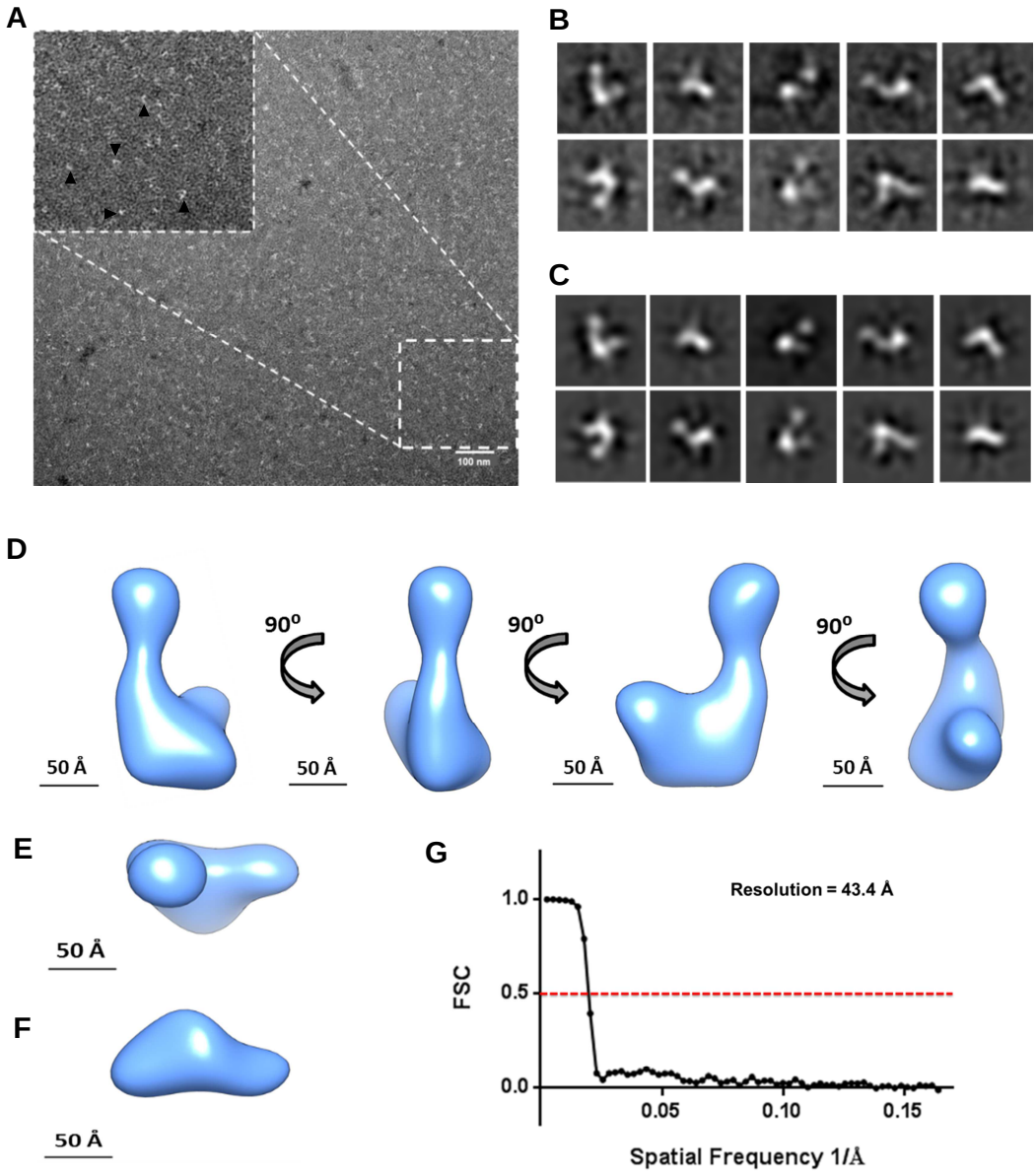


**Figure 3.3.1 Single particle TEM analysis and 3D modelling of ADAMTS-L2.**

(**A**) Negative-stain EM micrograph displaying ADAMTS-L2 particles stained with uranyl acetate. Boxed inset shows magnified region of micrograph. Single particles have been highlighted with black triangles. Scale bar = 100 nm. (**B** Two-dimension selected images of particles selected manually and aligned using EMAN2. Box size = 39 x 39 nm (**C**) Two-dimensional reference free class averages of stacks of aligned particles classified using EMAN2 representing different orientations of ADAMTS-L2. (**D**) Three-dimensional reconstruction of ADAMTS-L2 generated using EMAN2 and visualised using UCSF Chimera. (**E**) and (**F**) Top and bottom view of 3D model of ADAMTS-L2. (**G**) FSC generated for the 3D model of ADAMTS-L2 plotted against spatial resolution to determine the final resolution. Final model resolution = 43.4 Å.

A global search using the UCSF Chimera Fit in Map function (Pettersen et al, 2004) was performed in order to identify potential fitting sites for the C-S-N model in the ADAMTS-L2 reference electron density map. This function aims to optimise the fit of models into an electron density map based on a rotational and translational search. A global search using the C-S-N model generated 2 different potential fits for this model in the reference map. The first fit placed the C-S-N model in the uppermost lobe of the model. The second fit placed the model in the lower region of the map where there was higher density. However due to the structure of ADAMTS-L2 being of low resolution, it was not possible to differentiate between these fits.

Next a sequential fit was employed to fit all the individual homology domains and C-S-N model sequentially as they are in aligned in the molecular domain structure of ADAMTS-L2 into the density map. The sequential fit function fits each domain individually in the specified sequence, subtracting each time the density taken up by that domain. The sequential fitting of all the domain homology models into the ADAMTS-L2 reference density map did not yield a plausible fit. This could be due to the resolution of the map and therefore not providing sufficient features for fitting.

Finally the homology domains were manually fitted to create a hypothetical fit, in order to attempt to illustrate the possible alignment of domains within the model of ADAMTS-L2 (Figure 3.3.2C).The combined C-S-N model was placed in the lower area of the reference map, which also was a fit suggested by the global search due to volume in this region of the map, allowing accommodation of a large domain. Individual TSR domain models and the PLAC domain model were then fitted into the reference map to produce a hypothetical representation of how the domains may be aligned in the 3D structure (Figure 3.3.2C). A schematic representation of this alignment was also drawn (Figure 3.3.2D).

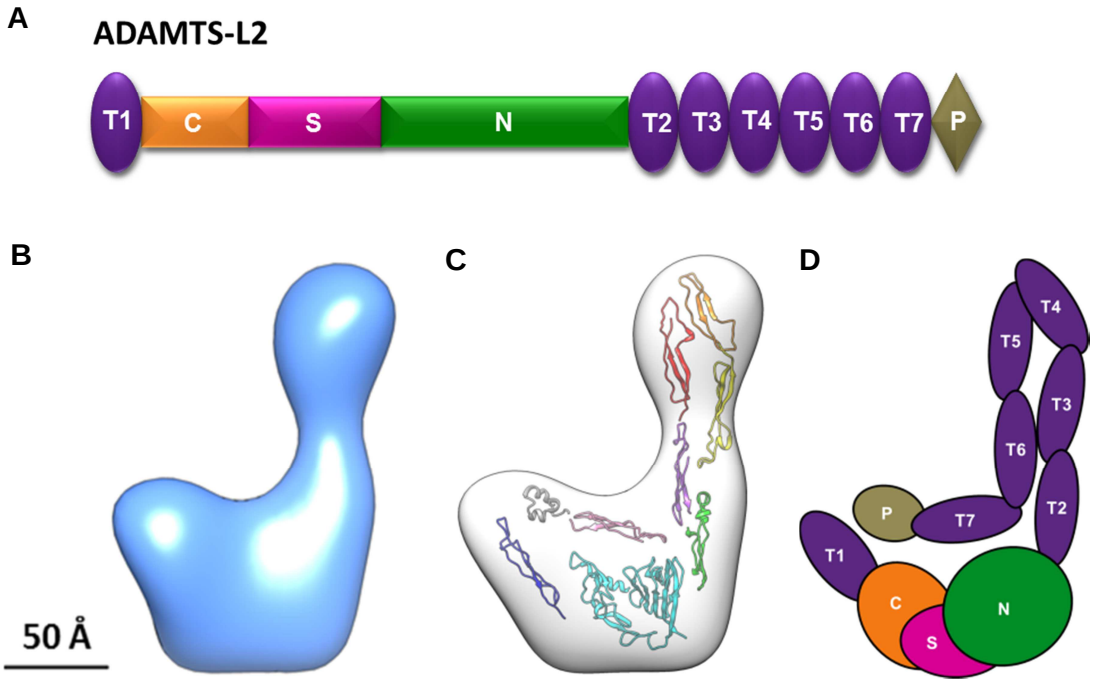


**Figure 3.3.2 Molecular modelling and domain fitting of ADAMTS-L2.**

(**A**) Schematic representation of ADAMTS-L2 with labelled domains: T1-7 = thrombospondin type 1 repeats (TSRs), C = cysteine-rich domain, S = spacer domain, N = N-glycan-rich domain and P = PLAC domain. (**B**) 3D model of ADAMTS-L2 generated using negative stain TEM single particle analysis in EMAN2. (**C**) Representative 3D reference map depicting hypothetical alignment of individual domains of ADAMTS-L2. Homology models of individual domains of ADAMTS-L2 were generated using SWISS MODEL: TSRs depicted as the dark blue, green, yellow, orange, red purple and pink domains, the cysteine-rich, spacer and N-glycan rich (C-S-N) domain are modelled as the light blue domain and the PLAC domain is grey. These domains were manually fitted into the 3D model of ADAMTS-L2 using UCSF Chimera. (**D**) Schematic representation of hypothetical domain alignment of ADAMTS-L2.

### 3.11 Single particle analysis and 2D structural analysis of ADAMTS-L4

EMAN2 was used to process negative stain micrographs of ADAMTS-L4 (Figure 3.3.3A). Individual particles were manually selected from a set of micrographs using a box size of 46 x 46 nm. The CTF was corrected before the particles were subjected to iterative class averaging to align them into similar classes exhibiting different orientations of the molecule (Figure 3.3.3B). At this point in processing it was observed that the ADAMTS-L4 adopted many different conformations, as illustrated in Figure 3.3.3B. The initial 3D model generated from the classifications of ADAMTS-L4 did not yield a structure bearing resemblance to the different particle projections. Therefore, a 3D model of ADAMTS-L4 could not be reconstructed due to the highly flexible nature of the molecule.

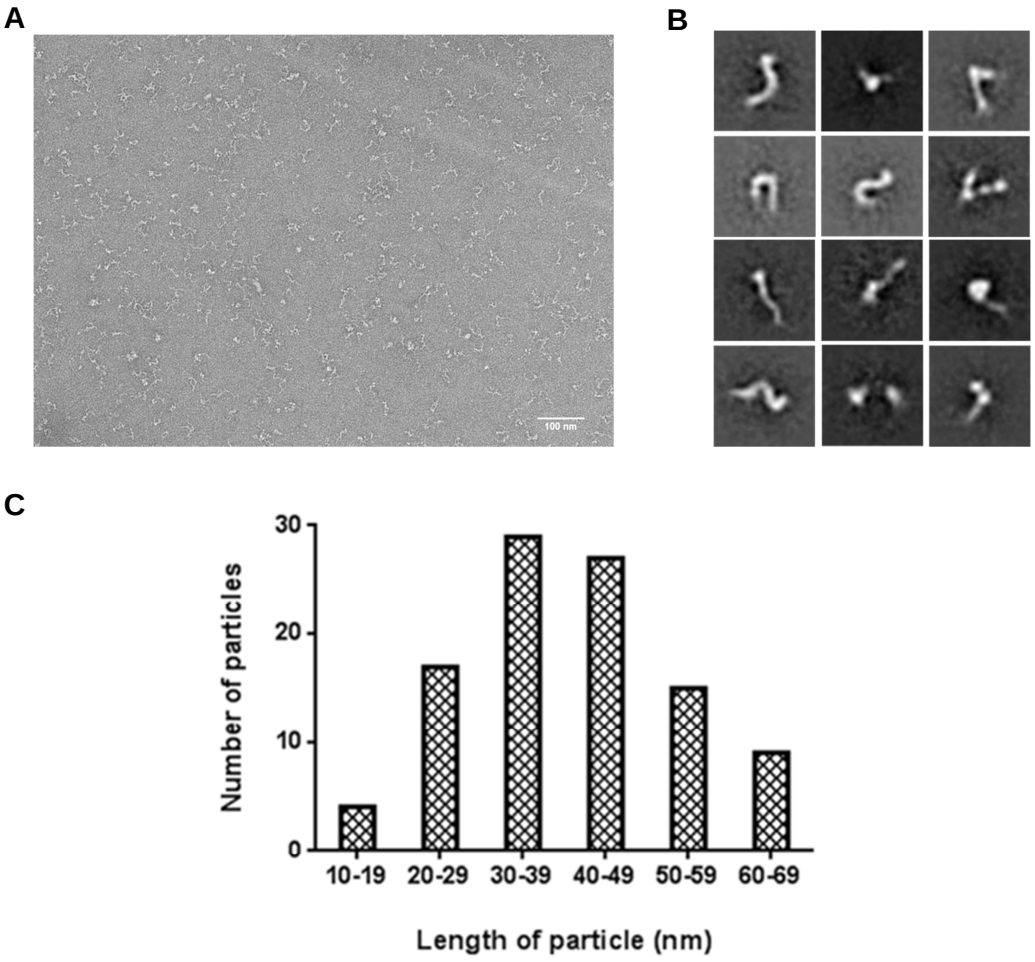


**Figure 3.3.3 Single particle TEM analysis and 2D analysis of ADAMTS-L4.**

(**A**) Negative-stain EM micrograph of ADAMTS-L4 particles stained with uranyl acetate. Scale bar = 100 nm. (**B**) Two-dimensional reference free class averages of stacks of aligned particles classified using EMAN2 representing different orientations of ADAMTS-L4. (**C**) Histogram depicting average length of single particles of ADAMTS-L4 in nm. A particle set of 100 particles selected in EMAN2 were measured in ImageJ and an average length for the data set was calculated. Average length of ADAMTS-L4 was calculated to be approximately 40.6 ± 1.271 nm.

The average length of 100 individual particles of ADAMTS-L4 was measured in the ImageJ software. The length of each molecule was manually measured and plotted in a histogram (Figure 3.3.3C). The histogram showed that the length of ADAMTS-L4 molecules ranged between 10-70 nm and the average length of the molecule was calculated to be approximately 40.6 nm.

As mentioned before, it was determined that ADAMTS-L4 has a highly flexible structure. This flexibility could consequently be due to the chain of TSRs forming the C-terminal part of the molecule. Therefore the 2D ADAMTS-L4 conformations obtained from this structural study were compared to a structurally homologous molecule called properdin (Figure 3.3.4B). Properdin has been described in literature as a flexible, rod-like structure composed of a chain of 7 TSR domains

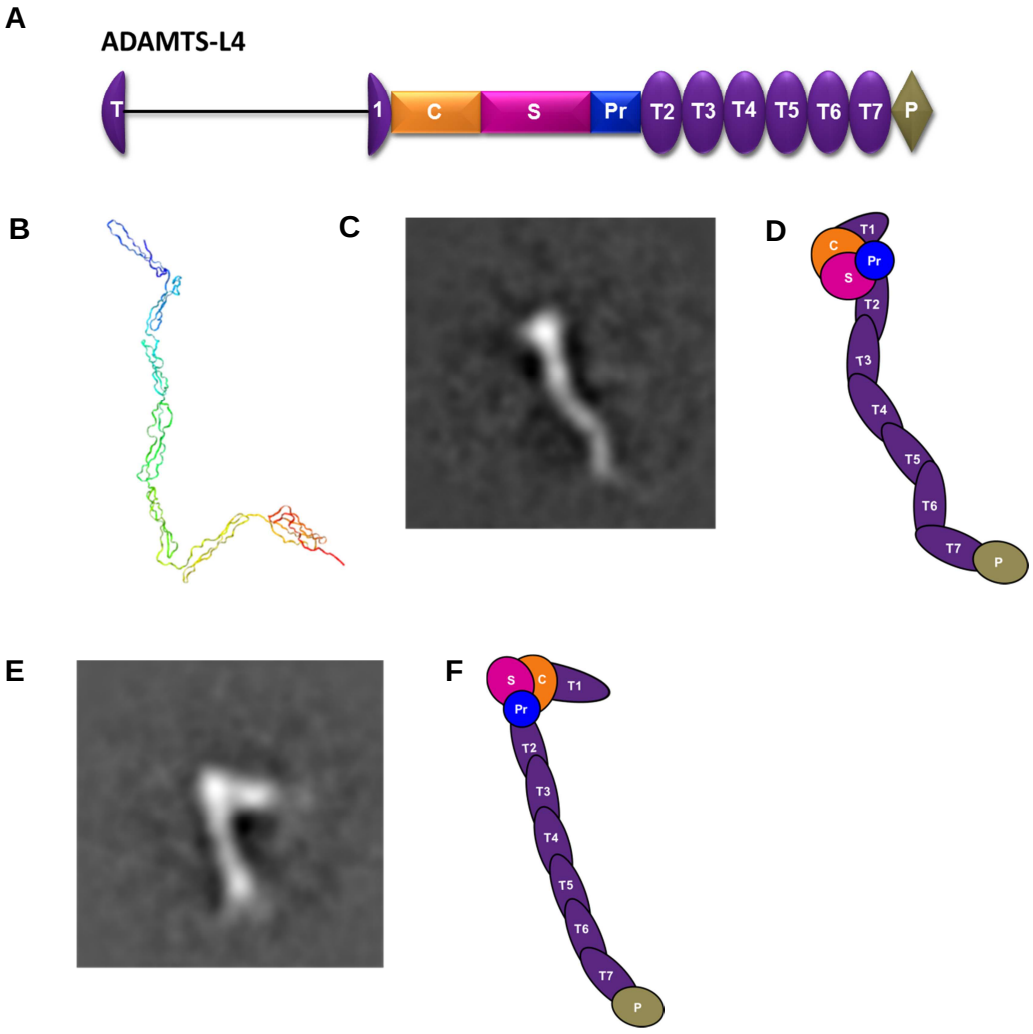


**Figure 3.3.4 Molecular modelling of ADAMTS-L4.**

(**A**) Schematic representation of ADAMTS-L4 with labelled domains: T1-7 = thrombospondin type 1 repeats (TSRs), C = cysteine-rich domain, S = spacer domain, Pr = proline-rich domain and P = PLAC domain. (**B**) Ribbon diagram of properdin consisting of 7 consecutive TSR domains each represented by a different colour (RCSB, www.rcsb.org, PDB file 1W0S) (**C**) Representative 2D image depicting a conformation of a single particle of ADAMTS-L4. (**D**) Schematic representation of hypothetical domain alignment of the ADAMTS-L4 particle shown in (**C**). (**E**) Representative 2D image depicting another conformation of a class of ADAMTS-L4. (**F**) Schematic representation of hypothetical domain alignment of the ADAMTS-L4 particle shown in (**E**).

(Higgins et al, 1995). Due to the C-terminal region of ADAMTS-L4 being structural similar to properdin, it could be that this region of ADAMTS-L4 would also be flexible. To illustrate how the TSRs in ADAMTS-L4 C-terminal region may contributing to the observed flexibility, schematics of 2 representative molecules were drawn (Figure 3.3.4 C and D, and E and F).

**Summary**

Structural analysis using negative stain TEM and single particle analysis of ADAMTS-L2 and ADAMTS-L4 allowed for the visualisation of these molecules. A low resolution 3D model of ADAMTS-L2 was generated to reveal an asymmetric lobular structure. Domains of ADAMTS-L2 were fitted into this 3D model to propose a hypothetical arrangement for the tertiary structure of the protein. 3D reconstruction of ADAMTS-L4 was not possible due to it taking various conformations. However, the average length of ADAMTS-L4 was determined to be approximately 40.6 nm.

### 3.12 Interactions of ADAMTS-L2 with other matrix proteins

Thus far in the literature ADAMTS-L2 has been shown to interact with the N-terminal and C-terminal regions of fibrillin-1 (Le Goff et al, 2011; Sengle et al, 2012; Hubmacher et al, 2015). Interactions of ADAMTS-L2 have also been reported with the central region (Le Goff et al, 2008) and the C-terminal (Sengle et al, 2012) regions of LTBP-1. To verify these interactions and to identify novel binding partners, surface plasmon resonance (SPR) was used by performing an analyte screen of various matrix proteins (Figure 3.4.1). ADAMTS-L2 was immobilised onto a BIAcore sensor chip and protein fragments at 200 and 400 nM concentrations were injected over the immobilised ligand (schematic representations of all protein fragments are shown in Appendix Figure A9. The analyte screen revealed that amongst all fibrillin-1 fragments tested, the protein fragments that bound with the greatest response were full length (FL) fibrillin-1, and fragments PF1 and PF3, which concur with findings of ADAMTS-L2 interacting with the N-terminal regions of fibrillin-1 reported by various research groups (Le Goff et al, 2011; Sengle et al, 2012; Hubmacher et al, 2015). PF17 was also seen to bind ADAMTS-L2 corroborating previously published interactions of ADAMTS-L2 with the C-terminal region of fibrillin-1 (Hubmacher et al, 2015). However other fibrillin-1 protein fragments either bound very weakly, namely the WMS mutant PF3 fragment, or did not show any binding to ADAMTS-L2. The analyte screen also confirmed weak interactions with the N-terminal fragment (NT) of LTBP-1 and full length LTBP-1 which somewhat support the interactions published previously (Le Goff et al, 2008). However in contrast to previous findings reported by Sengle et al, (2012) an interaction was not detected with the LTBP-1 C-terminal (CT) fragment. Syndecan 4 ecto domain (Syn 4 EC) and heparin also interacted very weakly with ADAMTS-L2. Although full length fibronectin did not show any interaction with ADAMTS-L2, the fibronectin 7-14 (Fn 7-14) fragment displayed moderate binding, identifying itself as a novel binding partner which has not yet been described in the literature.

Once ADAMTS-L2 had been immobilised via amine coupling to the chip, a theoretical maximal analyte response was determined using the following equation:

$$R_{max} = \frac{Analyte\ MW}{Ligand\ MW} \times Immobilised\ amount \times stoichiometric\ ratio$$

$R_{max}$ is the maximum theoretical analyte response, MW is the molecular weight of the ligand and analytes in kDa, immobilised amount was 1640 RU and the assumed stoichiometric ratio is 1. These values were calculated for each analyte (Table 2.8) to estimate the response each analyte would generate when interacting with the immobilised ADAMTS-L2. In this investigation, the binding of ADAMTS-L2 to several analytes, some of which have not yet been described in the literature, was studied for the first time. For this, an excessive amount of ADAMTS-L2 was immobilised to determine whether there was an interaction between ADAMTS-L2 and the analyte in question to gather preliminary data. It is known that for kinetic analysis, immobilisation of excessive ligand may lead to the binding response between the analyte and ligand to be disturbed

by factors such as mass transfer and steric hindrance. However, as the interaction studies carried out as part of this project were preliminary experiments, further optimisation of the protocol is required where less ADAMTS-L2 would be immobilised to generate a better binding response, The analyte screen was indicative of several potential binding partners for ADAMTS-L2, however many of these binding partners were ruled out for further investigation. This was due to the absence of a strong or even a moderate interaction with ADAMTS-L2. Some analytes were not considered for further experimentation due to the corresponding sensorgrams indicating bulk shift, which is just the transition between the running buffer and the analyte, rather than definite interactions. It was also found that greater bulk shifts were reported in larger protein fragments such as fibrillin-1 FL and PF3. Based on these analyses, the fibrillin-1 fragment PF17 and fibronectin fragment Fn 7-14 were selected for further kinetic experimentation.

Steady state analysis of fibrillin-1 PF17 binding to ADAMTS-L2 was performed by injecting increasing concentrations (0-600 nM) of PF17 over immobilised ADAMTS-L2 (Figure 3.4.2). The data generated from this interaction experiment showed a moderate interaction of PF17 with ADAMTS-L2 (Figure 3.4.2B). It was also noted that with increasing concentrations of PF17, there was an increase in binding response with ADAMTS-L2. It was also observed that higher concentrations of PF17 had slower dissociation rates once the injection of analyte was stopped.

| Recombinant protein | Molecular weight (kDa) | $R_{max}$ (RU) |
|---|---|---|
| Fibrillin-1 PF1 | 50 | 586 |
| Fibrillin-1 PF2 | 50 | 586 |
| Fibrillin-1 PF3 WT | 75 | 879 |
| Fibrillin-1 PF3 WMS | 60 | 703 |
| Fibrillin-1 PF5 | 50 | 586 |
| Fibrillin-1 PF7 | 50 | 586 |
| Fibrillin-1 PF10 | 50 | 586 |
| Fibrillin-1 PF12 | 50 | 586 |
| Fibrillin-1 PF13 | 50 | 586 |
| Fibrillin-1 PF17 | 75 | 879 |
| Fibrillin-1 Ex 1-11 | 50 | 586 |
| Fibrillin-1 FL | 250 | 2929 |
| MAGP-1 | 30 | 351 |
| Fibronectin 7-14 | 100 | 1171 |
| Fibronectin FL | 250 | 2929 |
| LTBP-1 NT | 63 | 738 |
| LTBP-1 CT | 47 | 551 |
| LTBP-1 FL | 170 | 1991 |
| Syndecan 4 ectodomain | 13 | 152 |

**Table 2.8** Calculated theoretical maximum analyte response ($R_{max}$).

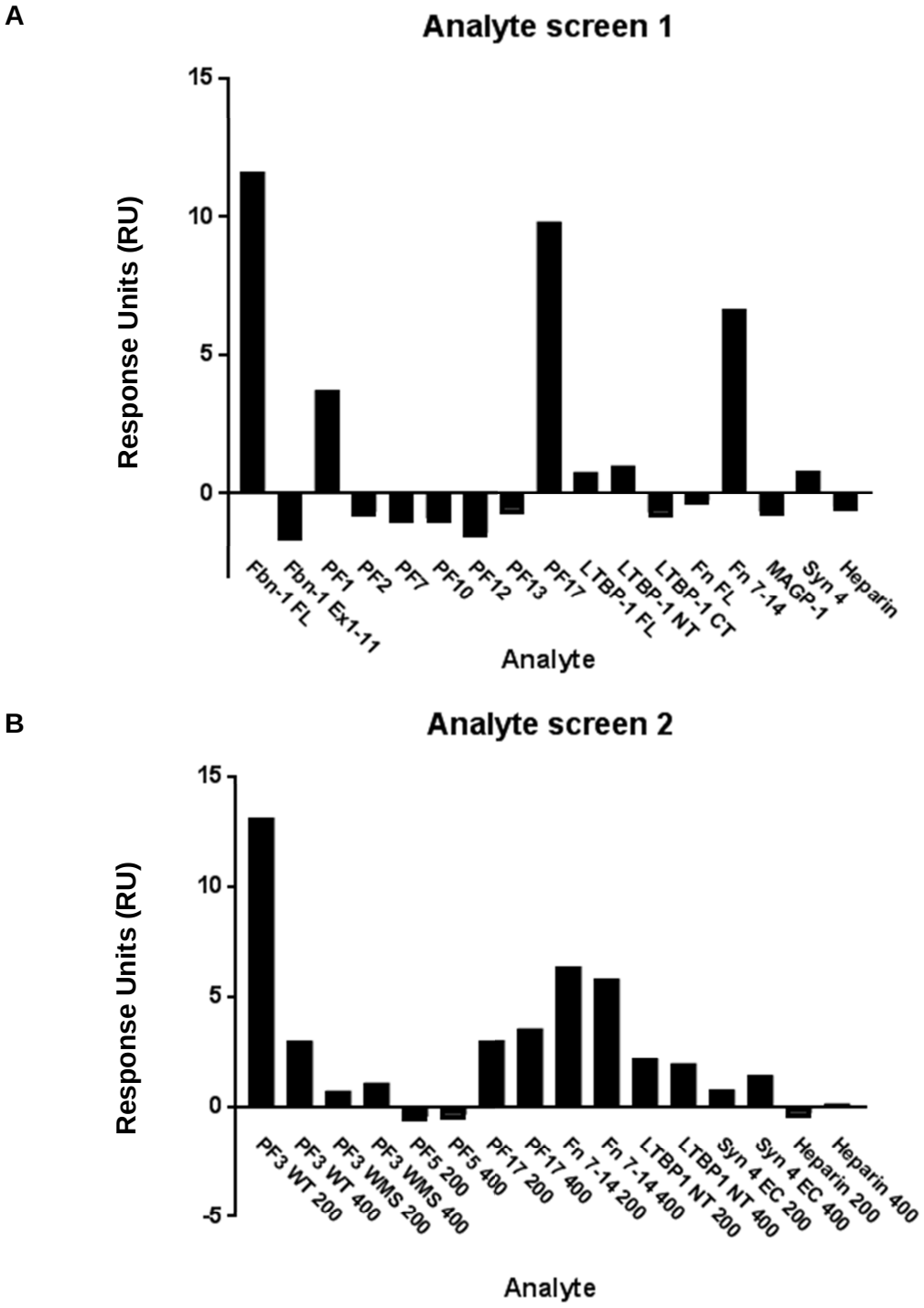


**Figure 3.4.1 Analyte screen to identify potential protein binding partners of ADAMTS-L2.**

ADAMTS-L2 was immobilised onto a BIAcore Series S CM5 sensor chip via amine coupling in 50 mM sodium acetate at pH 4. Protein fragments prepared at a concentration of 200 nM (**A**) and 200 and 400 nM (**B**) in 10 mM HBS-T, pH 7.4 were injected over immobilised ADAMTS-L2. Response units (RU) refers to the difference in response between the experimental and control flow cells on the BIAcore chip. Histograms (**A**) and (**B**) showing preliminary data of the RU obtained from each analyte binding to immobilised ADAMTS-L2. n=1

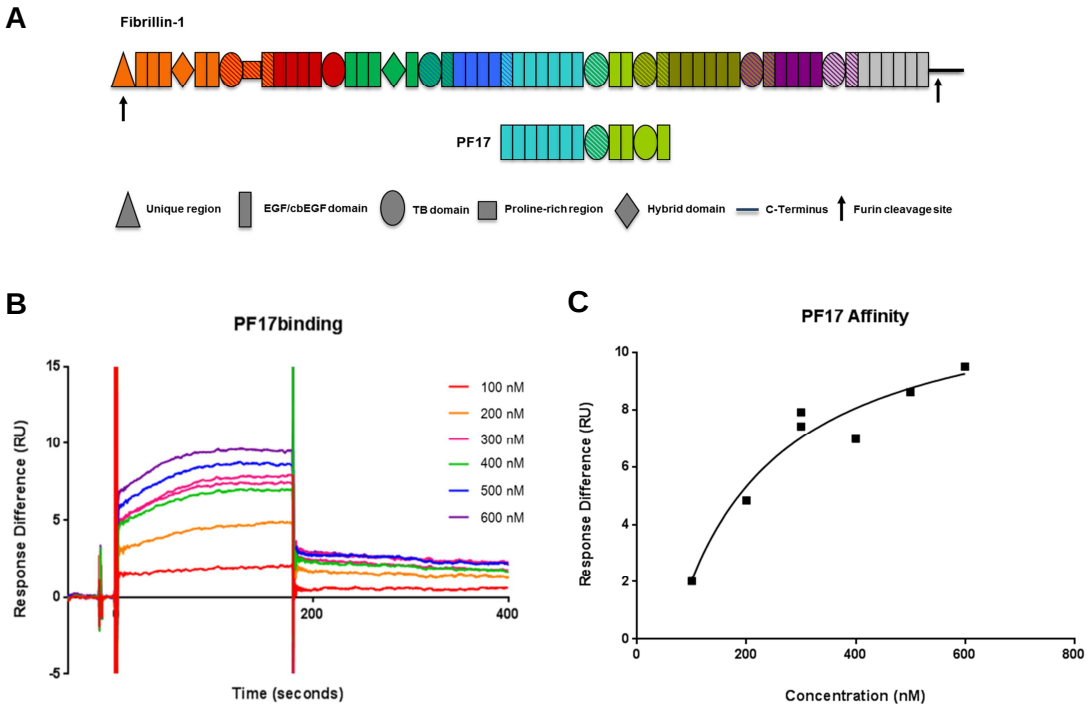


**Figure 3.4.2 Binding of Fibrillin-1 PF17 to ADAMTS-L2.**

(**A**) Schematic of full length fibrillin-1 depicting the PF17 fragment used in the binding experiment. (**B**) Sensorgram showing interaction of the PF17 fragment to immobilised ADAMTS-L2. 0-600 nM of PF17 fragment was injected over immobilised ADAMTS-L2 with 300 nM duplicated in the run. (**C**) Plot of steady state response against concentration depicting the affinity for P17 fragment determined by equilibrium analysis. The experiment was performed once (n=1).

Equilibrium analysis was used to determine the equilibrium dissociation constant ($K_D$) which is a measure of the propensity at which the bound analyte dissociates from the ligand. To determine the $K_D$, the maximum response at equilibrium recorded for each concentration of PF17 was plotted (Figure 3.42C) and a $K_D$ of 117 nM was determined.

Steady state analysis of a second analyte Fn 7-14 to ADAMTS-L2 were also determined. The Fn 7-14 fragment was injected over immobilised ADAMTS-L2 at concentrations varying from 0-600 nM (Figure 3.4.3). The sensorgram generated from these interactions (Figure 3.4.3B) illustrated that with increasing concentrations of Fn 7-14 a greater binding response to ADAMTS-L2 was recorded. Interestingly, the interactions of Fn 7-14 at all concentrations failed to stabilise before injection of the analyte was complete and the fragment appeared to dissociate from ADAMTS-L2. Upon commencement of the dissociation phase, the Fn 7-14 fragment dissociated rapidly from the chip indicating that the interaction between these proteins is very weak.

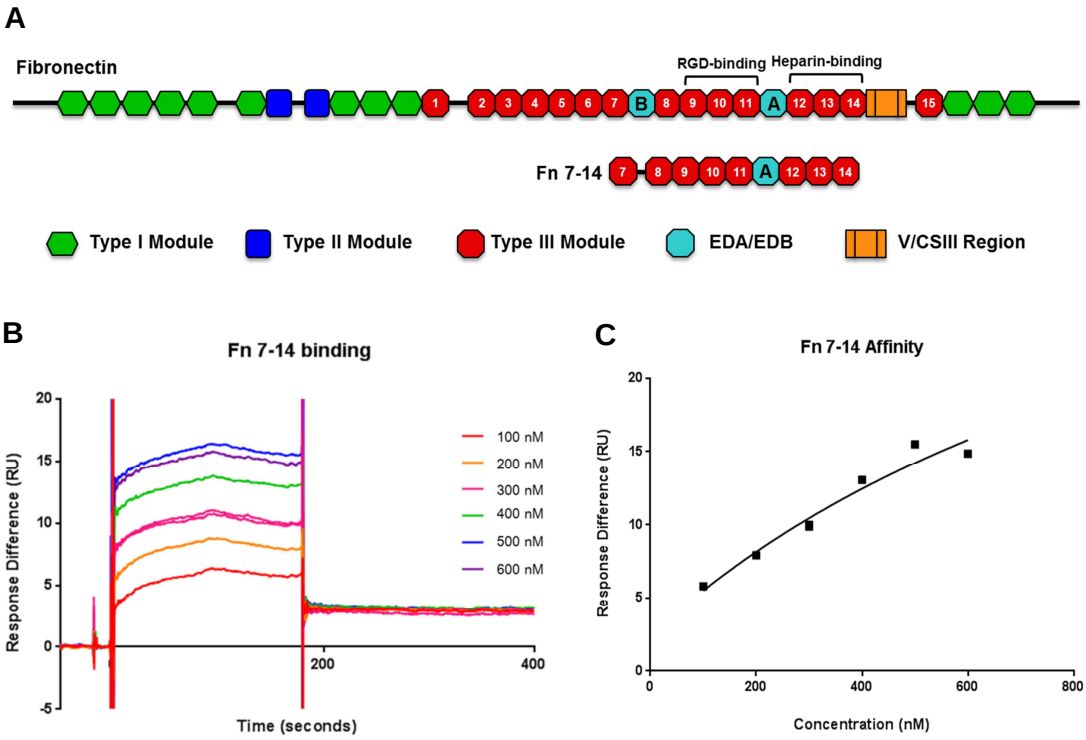


**Figure 3.4.3 Binding of Fibronectin Fn 7-14 fragment to ADAMTS-L2.**
(**A**) Schematic of full length fibronectin depicting the Fn 7-14 fragment used in the binding experiment. RGD and heparin binding sites are also shown. (**B**) Sensorgram showing interaction of Fn 7-14 fragment to immobilised ADAMTS-L2. Increasing concentrations (0-600 nM) of Fn 7-14 fragment were injected over immobilised ADAMTS-L2 with 300 nM duplicated in the run. (**C**) Plot of steady state response against concentration depicting the affinity for Fn 7-14 fragment determined by equilibrium analysis. The experiment was performed once (n=1).

Equilibrium analysis of the binding affinity of Fn 7-14 to ADAMTS-L2 was performed by plotting the maximum response at equilibrium obtained for each concentration of Fn 7-14 (Figure 3.4.3C). The $K_D$ was determined to be 1.2 µM which corroborated the weak interaction and rapid dissociation of FN 7-14 from ADAMTS-L2 observed in Figure 3.4.3B.

**Summary**

Binding of several matrix proteins to ADAMTS-L2 was investigated in order to identify novel binding partners. It was found that many matrix protein fragments tested either displayed moderate or weak interactions or they did not exhibit any affinity for ADAMTS-L2, differing greatly from the calculated theoretical interactions. Fibrillin-1 fragment PF17 and fibronectin fragment Fn 7-14 were further investigated as potential interacting candidates. It was observed that at increasing concentrations, Fn 7-14 exhibited a higher propensity to dissociate from ADAMTS-L2 than PF17. These findings were also reflected in the $K_D$ values obtained for Fn 7-14 (1207 nM) and PF17 (117 nM) demonstrating that PF17 has a greater affinity for ADAMTS-L2 than Fn 7-14.

### 3.13 Immunofluorescence microscopy of ADAMTSL2 and ADAMTS-L4 and co-localisation with other matrix proteins

Immunofluorescence microscopy is used to visualise the deposition of proteins in the matrix and their interactions with cells and other proteins. Immunofluorescence analysis of ADAMTS-L2 and ADAMTS-L4 in the matrix is an area of research which needs to be investigated further. Thus far little data have been published regarding their localisation in the matrix formed by different cell types or in different tissues.

Previously reported findings have provided some insights into expression of ADAMTS-L2 and ADAMTS-L4 in different tissues as well as explore the possible effects of gene knock-down or gene mutation on the deposition of other matrix proteins. However, the literature has not yet addressed the impact of over-expressing these proteins in different cell types and their localisation with other matrix proteins. Therefore to investigate the effects of this, HDFs over-expressing ADAMTS-L2 and ADAMTS-L4 of the same cell densities were cultured for 5 days, 7 days and 10 days on glass coverslips. The expression profiles of ADAMTS-L2 and ADAMTS-L4 vary depending on the cell type, therefore different cell lines (mesenchymal and epithelial) over-expressing both proteins were created. Here data observed in mesenchymal cell type HDFs is shown.The coverslips were then fixed and stained for ADAMTS-L2 and ADAMTS-L4 using an anti-V5 antibody and co-stained with antibodies against fibrillin-1, fibronectin and LTBP-1. For all conditions, ADAMTS-L2 and ADAMTS-L4 were stained green using Alexa Fluor 488 secondary antibody (*Thermofisher Scientific, Paisley, UK*) and fibrillin-1, fibronectin and LTBP-1 were stained red using Alexa Fluor 555 secondary antibody (*Thermofisher Scientific, Paisley, UK*). Non transfected wild type (WT) HDFs was used as controls. These experiments were repeated thrice and the observations made regarding the deposition of both ADAMTS-Ls and their interactions were reproduced in all attempts.

### 3.14 Immunofluorescence visualisation of ADAMTS-L2 with fibrillin-1, fibronectin and LTBP-1.

At all time points, ADAMTS-L2 was visualised with intense green staining at the cell surface of ADAMTS-L2 expressing HDFs. This green staining was absent from the non-transfected WT cells which were used as a negative control. It also appeared that with longer time in culture, more ADAMTS-L2 was expressed in HDFs and the green staining intensified from day 5 to day 10. However to verify this further quantification is required.

Fibrillin-1 staining (Figure 3.5.1A) appeared to be punctate and localised to the cells at day 5 in ADAMTS-L2 expressing HDFs. Whereas in WT HDFs a network of fibrillin-1 fibres was present. Fibrillin-1 staining observed at day 5 in ADAMTS-L2 expressing cells was seen to co-localise with ADAMTS-L2 staining depicted as yellow in the merged image. At day 7 (Figure 3.5.1B) fibrillin-1 fibres were visualised in ADAMTS-L2 expressing cells however, these fibres were sparse and did not form continuous networks unlike the thicker fibrillar network formed by WT HDF cells. After 10

days of culture, a network of fibrillin-1 fibres was formed by ADAMTS-L2 expressing HDFs similar to that seen in WT HDF cells (Figure 3.5.1C). It was observed that deposited fibrillin-1 fibres after 7 and 10 days in culture appeared to form around and in between ADAMTS-L2 expressing and WT HDFs. It was unclear whether the fibrillin-1 fibres co-localised with ADAMTS-L2 as they were seen to interact with the cell surface and display areas of yellow staining, however the fibres which had formed between the HDFs did not show any co-localisation.

At day 5 fibronectin staining was visualised as an intricate framework which had deposited around the ADAMTS-L2 expressing HDFs (Figure 3.5.2A). Fibronectin staining in ADAMTS-L2 expressing HDFs was of similar density and formation to that observed in WT HDFs. Co-localisation of ADAMTS-L2 and fibronectin was observed at the cell surface where the fibronectin fibres interacted with the HDFs (yellow staining). Similar co-localisation of fibronectin and ADAMTS-L2 at the cell surface was seen after 7 days (Figure 3.5.2B) and 10 days (Figure 3.5.2C) in culture and that the fibronectin appeared more aligned than previously seen at 5 days. It was noted that even though the deposition of fibronectin increased at each time point in the ADAMTS-L2 expressing HDFs, it did not appear as dense as the deposition seen in the WT HDFs. To validate this however, quantification is required.

LTBP-1 staining was localised to HDFs after 5 days in culture in both ADAMTS-L2 expressing and WT cells (Figure 3.5.3A). However LTBP-1 staining co-localised with ADAMTS-L2 staining in some areas of ADAMTS-L2 expressing cells. After 7 days in culture, a visible network of LTBP-1 fibres was observed in both ADAMTS-L2 expressing and WT HDFs (Figure 3.5.3B). However, in ADAMTS-L2 cells, LTBP-1 staining was still localised to the cells and only a few thin fibres could be seen. The cellular LTBP-1 was again seen to co-stain with ADAMTS-L2 in some areas. At day 10 however, a network of LTBP-1 fibres was seen in ADAMTS-L2 expressing HDFs, but these fibres did not appear to co-localise with the cell surface ADAMTS-L2 staining (Figure 3.5.3C). Also, co-localisation of LTBP-1 with ADAMTS-L2 was lost after 10 days in culture due to LTBP-1 relocating from the cell surface to microfibrils in the ECM.

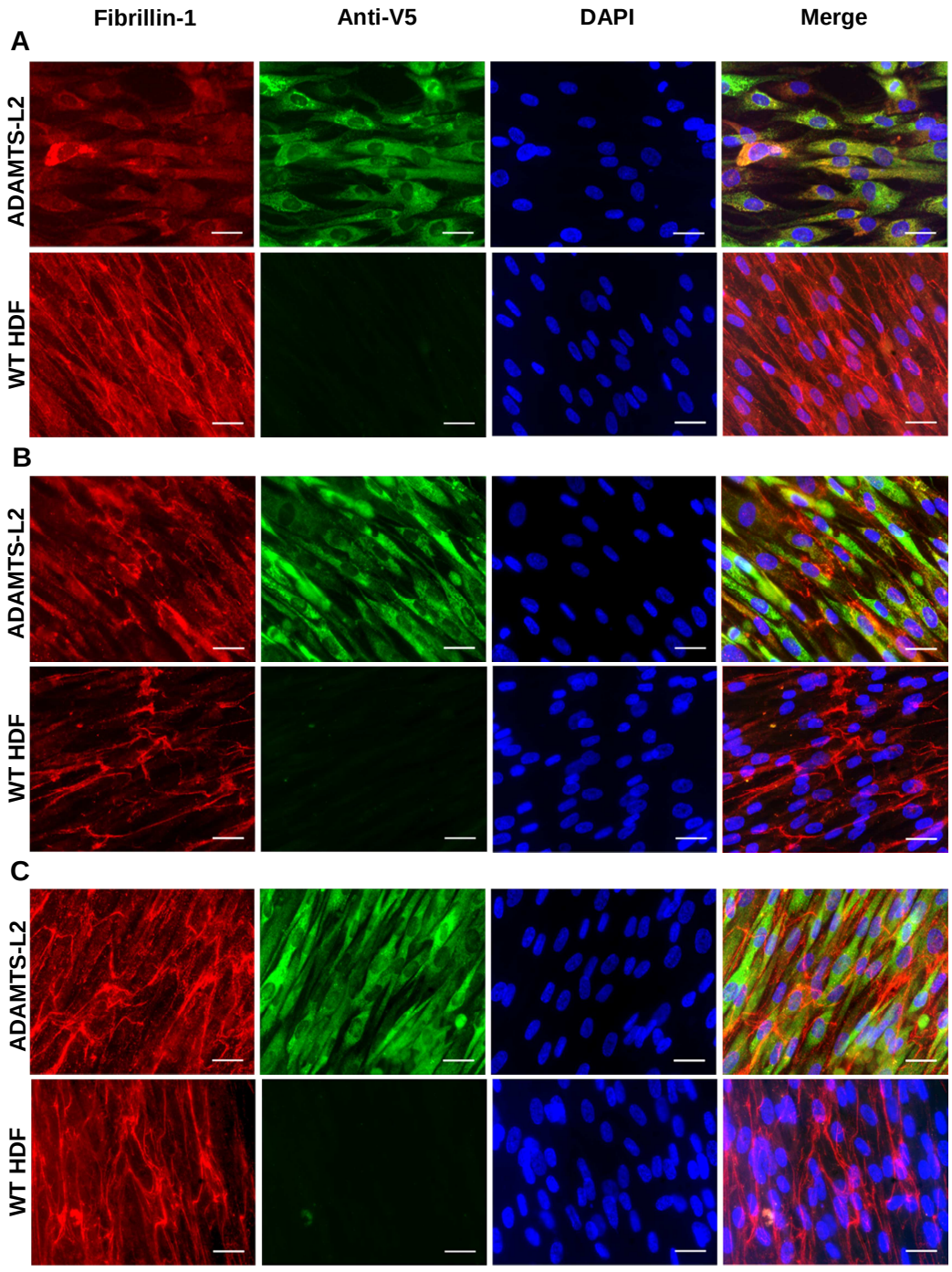


**Figure 3.5.1 Immunofluorescence staining of ADAMTS-L2 with fibrillin-1.**
Immunofluorescence staining of adult human HDFs expressing ADAMTS-L2 (green, Alexa Fluor 488) in comparison to WT HDFs with fibrillin-1 (red, Alexa Fluor 555) after 5 days (**A**), 7 days (**B**) and 10 days (**C**) in culture. ADAMTS-L2 was detected using anti-V5 antibody. Nuclei of HDFs were stained with DAPI (blue). WT HDFs used as negative controls. Images were taken using a x40 objective and merged in Image J. Scale bar = 50 µm. n=3

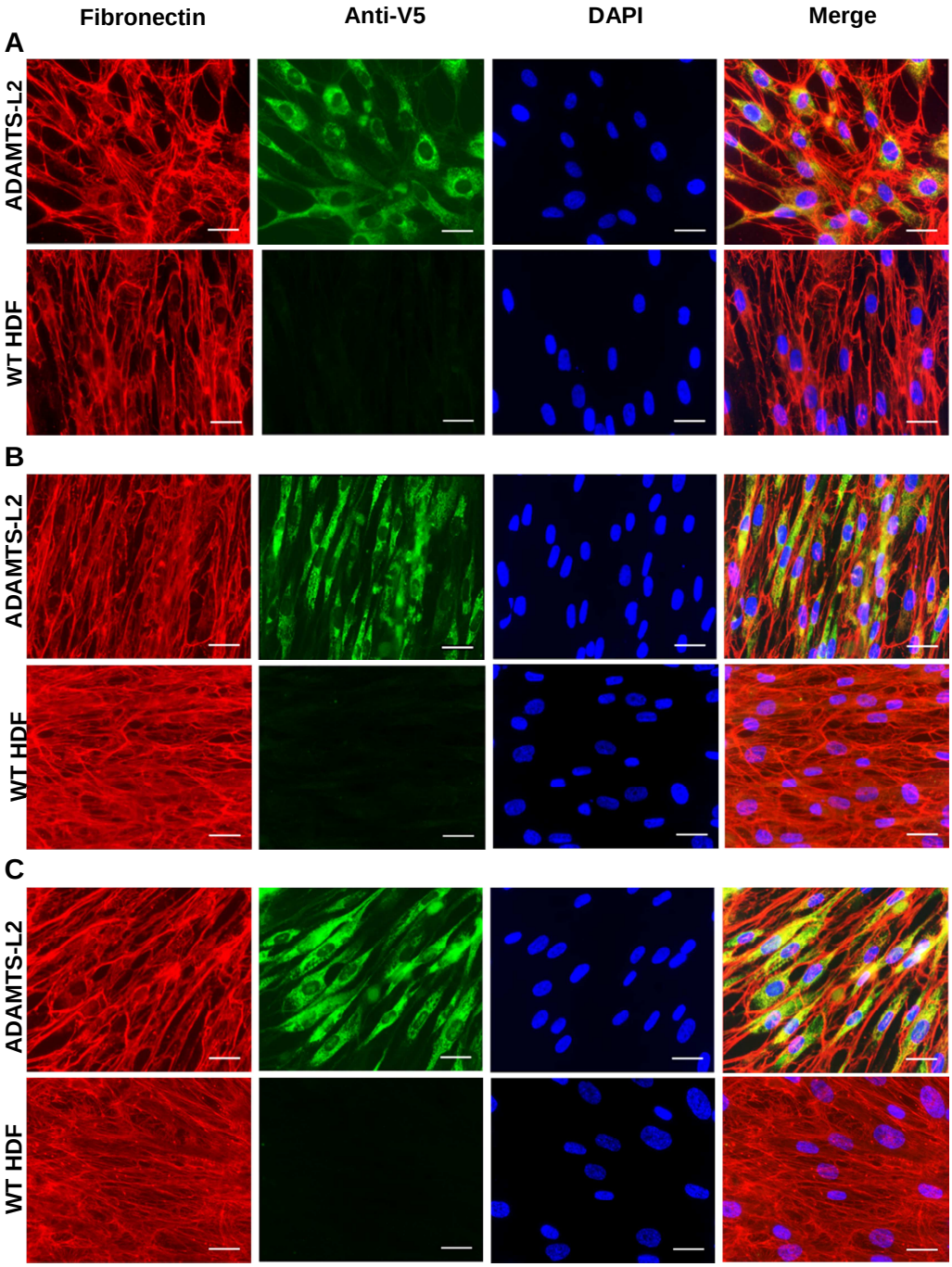


**Figure 3.5.2 Immunofluorescence staining of ADAMTS-L2 with fibronectin.**

Immunofluorescence staining of adult human HDFs expressing ADAMTS-L2 (green, Alexa Fluor 488) in comparison to WT HDFs with fibronectin (red, Alexa Fluor 555) after 5 days (**A**), 7 days (**B**) and 10 days (**C**) in culture. ADAMTS-L2 was detected using anti-V5 antibody. Nuclei of HDFs were stained with DAPI (blue). Images were taken using a x40 objective and merged in Image J. Scale bar = 50 µm. n=3

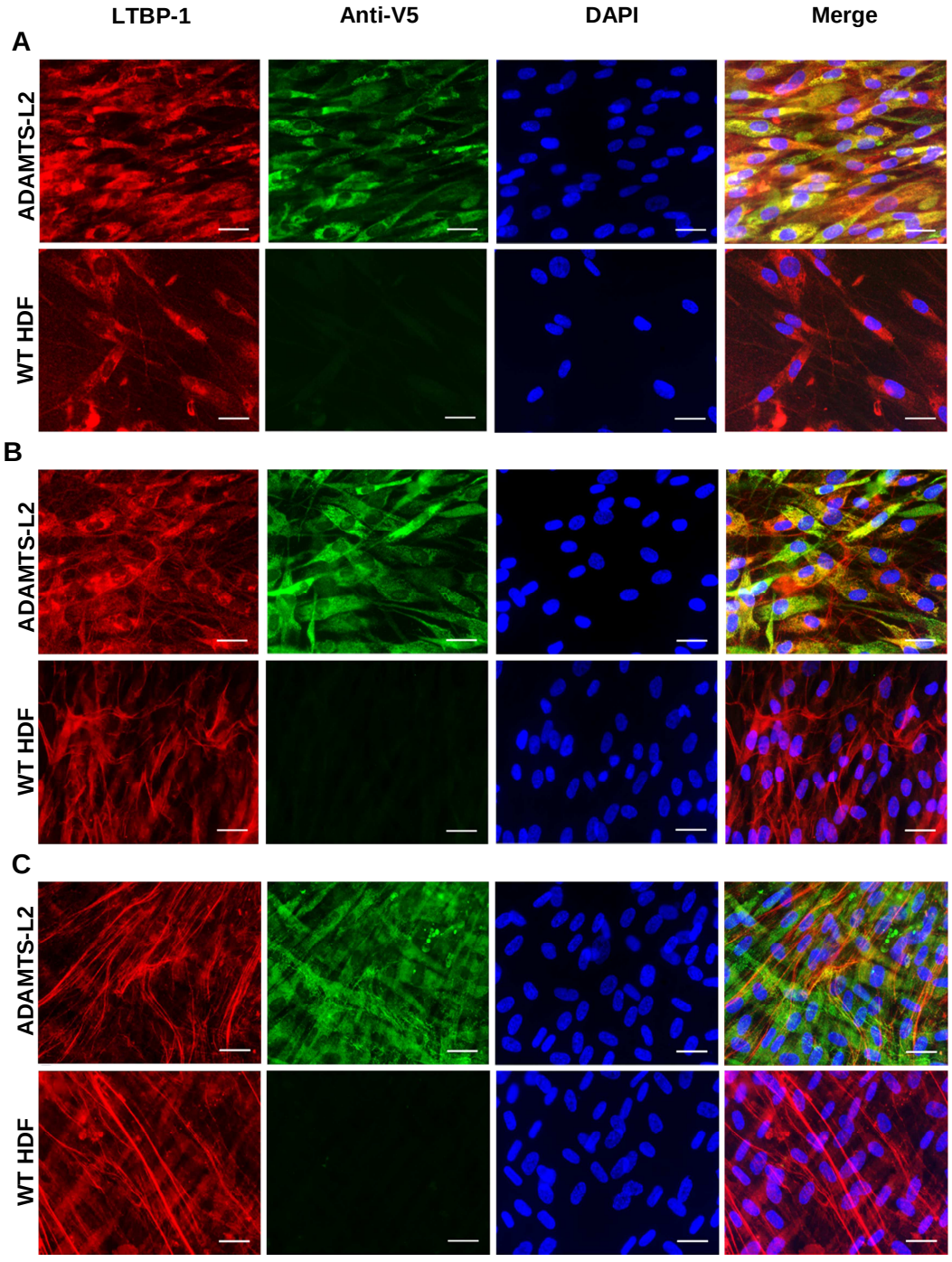


**Figure 3.5.3 Immunofluorescence staining of ADAMTS-L2 with LTBP-1.**

Immunofluorescence staining of adult human HDFs expressing ADAMTS-L2 (green, Alexa Fluor 488) in comparison to WT HDFs with LTBP-1 (red, Alexa Fluor 555) after 5 days (**A**), 7 days (**B**) and 10 days (**C**) in culture. ADAMTS-L2 was detected using anti-V5 antibody. Nuclei of HDFs were stained with DAPI (blue). Images were taken using a x40 objective and merged in Image J. Scale bar = 50 µm. n=3

### 3.15 Immunofluorescence visualisation of ADAMTS-L4 with fibrillin-1, fibronectin and LTBP-1.

After 5 days in culture, both cellular and fibrous ADAMTS-L4 was observed (Figure 3.5.4A). Cellular ADAMTS-L4 staining appeared to be brighter than the extracellular staining indicating that at these earlier stages, ADAMTSL4 was still being deposited in the matrix. Fibrillin-1 staining at this time point in ADAMTS-L4 expressing HDFs and WT HDFs appeared to be mainly extracellular and fibrous. However in comparison to the staining visualised in WT HDFs the fibrillin-1 fibres did not appear as continuous and connected. It was also noted that extracellular ADAMTS-L4 staining completely co-localised with fibrillin-1 staining. A similar pattern of staining for both ADAMTS-L4 and fibrillin-1 was observed after 7 days in culture in ADAMTS-L4 expressing HDFs (Figure 3.5.4B). Again, both cellular and extracellular ADAMTS-L4 staining was detected, however extracellular ADAMTS-L4 was seen to be deposited as thicker continuous fibres. Fibrillin-1 fibres in the ADAMTS-L4 expressing HDFs were less abundant albeit appeared visibly thicker; however they were not continuous like the fibres detected in WT HDFs. Again it was noted that extracellular ADAMTS-L4 fibres completely co-localised with fibrillin-1 staining. Following 10 days in culture, ADAMTS-L4 was depicted as a dense fibrous extracellular network (Figure 3.5.4C) which had formed around the cells. Very little cellular ADAMTS-L4 was visualised in the cells. The fibrillin-1 network in these cells also appeared to be formed of thick continuous fibres much like the fibrillin-1 network observed in the WT HDFs at the same time point. In the ADAMTS-L4 expressing cells the, ADAMTS-L4 network showed greater co-localisation with fibrillin-1 fibres.

Fibronectin formed as a continuous network around the cells after 5 days in culture in both the ADAMTS-L4 and WT HDFs (Figure 3.5.5A). At this time point, ADAMTS-L4 was seen to form into a fibrous network in the matrix as well as present inside the cells. Merging of both stains showed that ADAMTS-L4 co-localised with fibronectin. Interactions of ADAMTS-L4 fibres were observed in distinct regions with the fibronectin network (yellow staining). It was observed that ADAMTS-L4 fibres interacted with parts of fibronectin fibres as both red staining depicting the fibronectin fibres and yellow staining indicating ADAMTS-L4 interactions were visible. This pattern of ADAMTS-L4 and fibronectin deposition was also observed in HDFs expressing ADAMTS-L4 which had been cultured for 7 days (Figure 3.5.5B) and 10 days (Figure 3.5.5C). At these time points fibronectin deposition increased as the network appeared denser in both ADAMTS-L4 expressing and WT HDFs; however the in cells expressing ADAMTS-L4, the fibronectin network was not as dense as seen in the WT controls at the same time points (Figure 3.5.5B and 3.5.5C). Deposition of ADAMTS-L4 did not increased by much over time unlike fibronectin deposition observed in WT cells.

ADAMTS-L4 expressing and WT HDFs were co-stained for ADAMTS-L4 and LTBP-1. After 5 days LTBP-1 was localised to WT HDF cells (Figure 3.5.6A); however in cells expressing ADAMTS-L4, thin LTBP-1 fibres were observed in the ECM as well as localised to cells (Figure 3.5.6A). Intracellular and extracellular ADAMTS-L4 staining was observed in ADAMTS-L4 expressing cells

at this time point, where thin fibres were visualised deposited in the ECM. LTBP-1 and ADAMTS-L4 staining appeared to co-localise partially both at a cellular level and in the ECM. Following 7 days in culture, a network of continuous LTBP-1 fibres was visualised in the ECM of both ADAMTS-L4 expressing and WT HDFs (Figure 3.5.6B). However the fibres forming this network in the ADAMTS-L4 expressing HDFs were thicker than those deposited by WT HDFs. Cellular LTBP-1 was also detected. ADAMTS-L4 at this time point also formed a network of fibres in the ECM which also exhibited complete co-localisation with LTBP-1 fibres (Figure 3.5.6B). However at a cellular level, co-localisation was inconsistent. Finally after 10 days in culture extensive fibrillar networks were detected for both ADAMTS-L4 and LTBP-1, where the fibres for both proteins were thicker (Figure 3.5.6C). Both proteins were also visualised at a cellular level and co-localisation at this level was again inconsistent. The ADAMTS-L4 network was seen to be denser with a mixture of thin and thicker fibres. Co-localisation of ADAMTS-L4 with LTBP-1 was also observed in the ECM, however specific interactions of these fibres was visualised at this time point, where a mixture of red (LTBP-1), green (ADAMTS-L4) and yellow (co-localisation) could be seen in the merged image (Figure 3.5.6C).

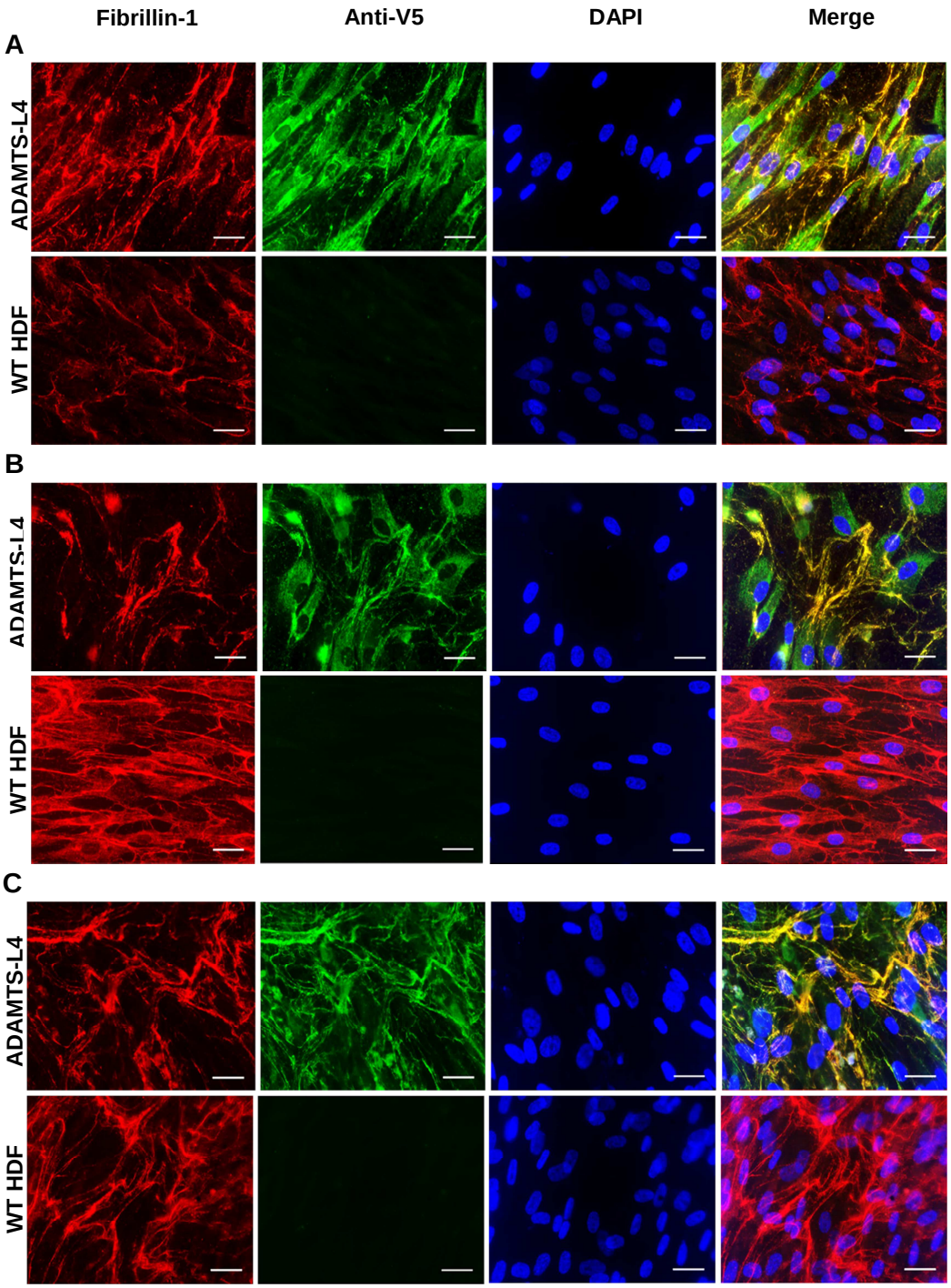


**Figure 3.5.4 Immunofluorescence staining of ADAMTS-L4 with fibrillin-1.**

Immunofluorescence staining of adult human HDFs expressing ADAMTS-L4 (green, Alexa Fluor 488) in comparison to WT HDFs with fibrillin-1 (red, Alexa Fluor 555) after 5 days (**A**), 7 days (**B**) and 10 days (**C**) in culture. ADAMTS-L4 was detected using anti-V5 antibody. Nuclei of HDFs were stained with DAPI (blue). Images were taken using a x40 objective and merged in Image J. Scale bar = 50 µm. n=3

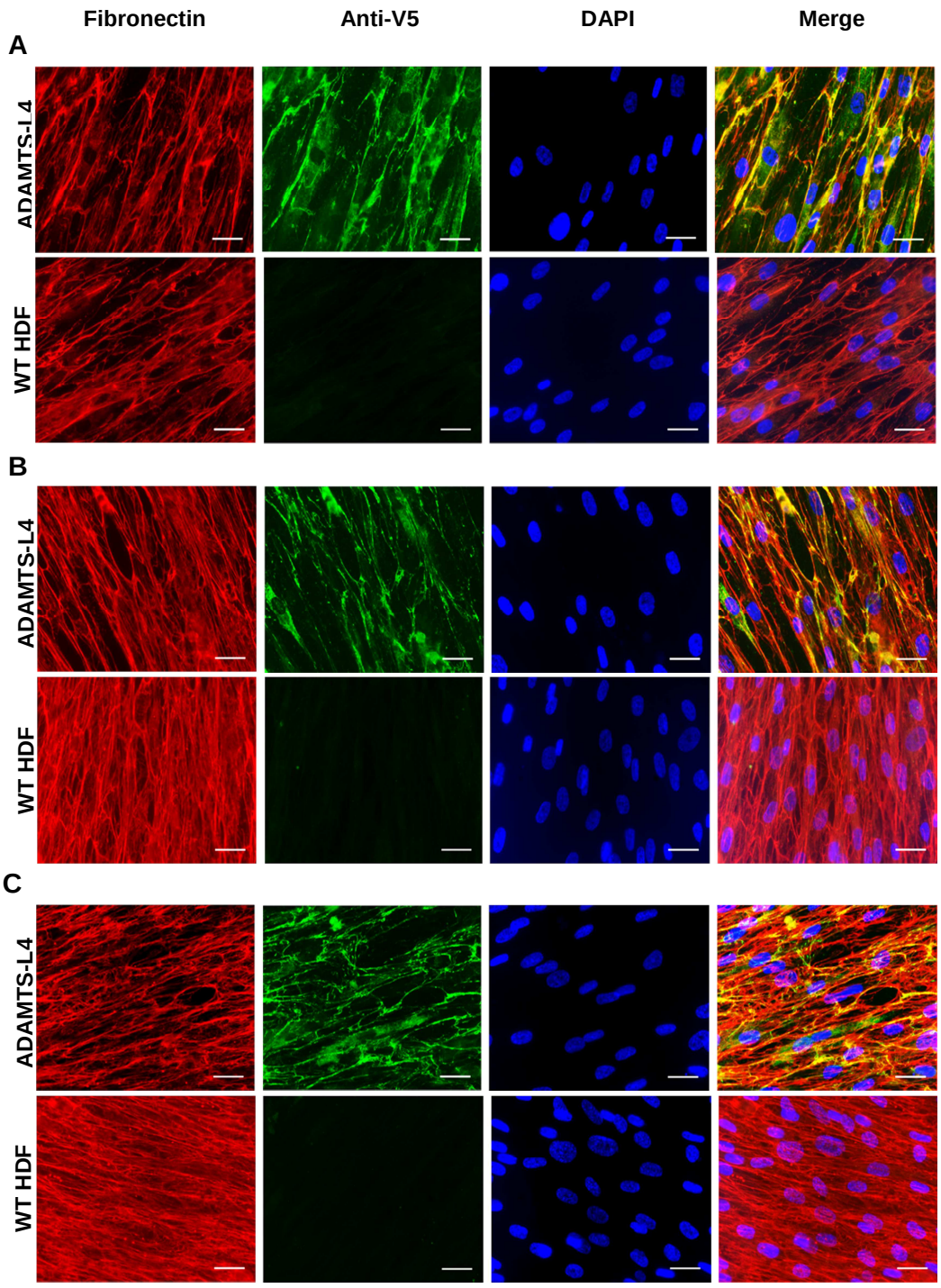


**Figure 3.5.5 Immunofluorescence staining of ADAMTS-L4 with fibronectin.**

Immunofluorescence staining of adult human HDFs expressing ADAMTS-L4 (green, Alexa Fluor 488) in comparison to WT HDFs with fibronectin (red, Alexa Fluor 555) after 5 days (**A**), 7 days (**B**) and 10 days (**C**) in culture. ADAMTS-L4 was detected using anti-V5 antibody. Nuclei of HDFs were stained with DAPI (blue). Images were taken using a x40 objective and merged in Image J. Scale bar = 50 µm. n=3

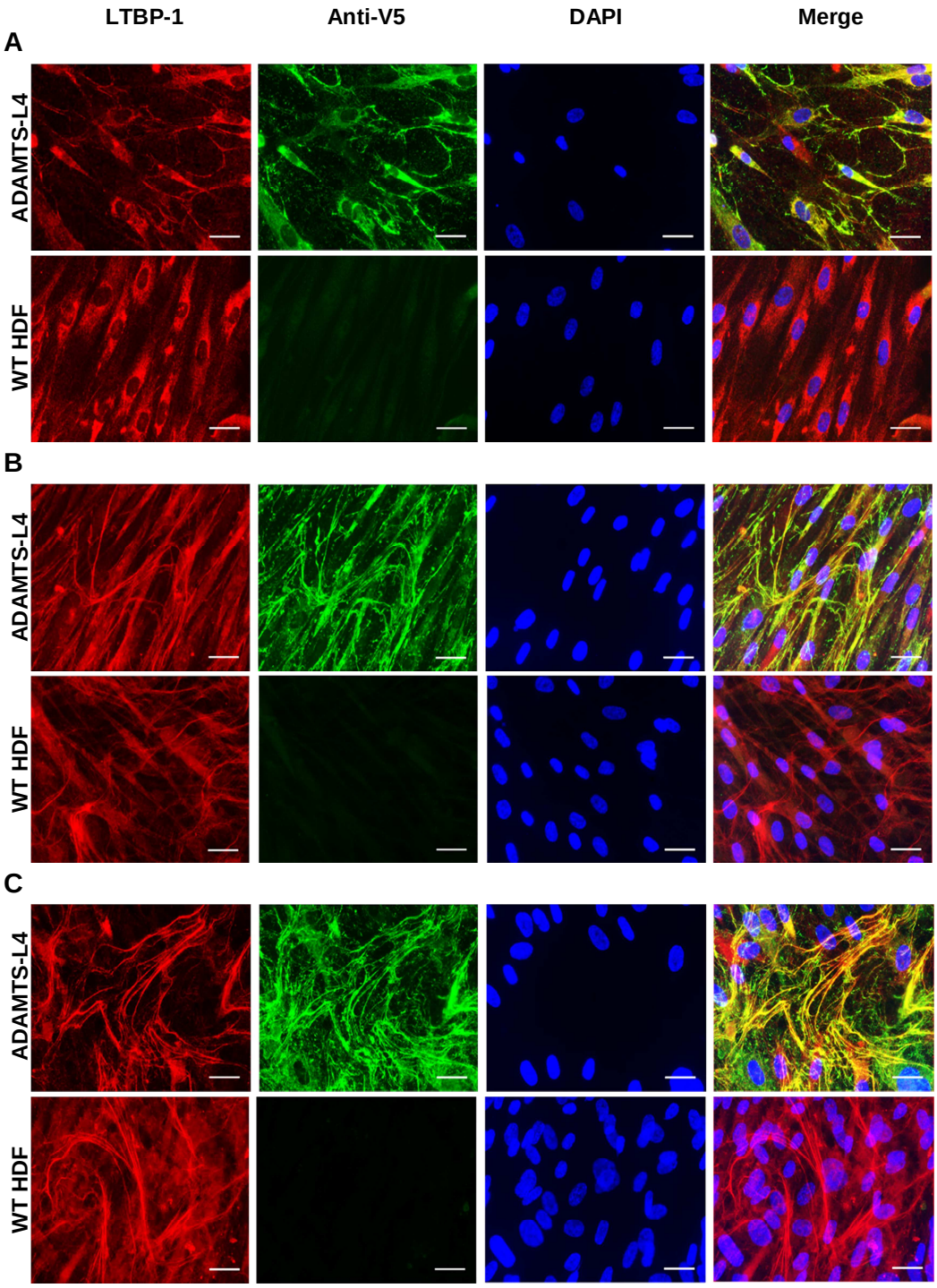


**Figure 3.3.6 Immunofluorescence staining of ADAMTS-L4 with LTBP-1.**

Immunofluorescence staining of adult human HDFs expressing ADAMTS-L4 (green, Alexa Fluor 488) in comparison to WT HDFs with LTBP-1 (red, Alexa Fluor 555) after 5 days (**A**), 7 days (**B**) and 10 days (**C**) in culture. ADAMTS-L4 was detected using anti-V5 antibody. Nuclei of HDFs were stained with DAPI (blue). Images were taken using a x40 objective and merged in Image J. Scale bar = 50 µm. n=3

**Summary**

Immunofluorescence studies confirmed previous reports that ADAMTS-L2 localises to the cell surface after it is secreted from over-expressing cells (Koo et al, 2007). It was also found that accumulation of ADAMTS-L2 at the cell surface increased over time. It was noted that over expression of ADAMTS-L2 in HDFs had a negative effect on the deposition of fibrillin-1, fibronectin and LTBP-1 in the ECM in comparison to deposition of these proteins in WT HDFs. This decrease in rate of deposition was consistently noticed at all time points, where networks of these proteins in ADAMTS-L2 expressing cells were not as abundant and dense as that seen in the corresponding WT controls. ADAMTS-L2 co-localised with fibrillin-1 and LTBP-1 at the cell surface after 5 days in culture; however once they had formed fibrillin-1 microfibrils and LTBP-1 fibres contact was mostly observed at the cell surface, but the staining did not provide confirmation of their co-localisation with ADAMTS-L2. Fibronectin and ADAMTS-L2 co-staining was demonstrated at the cell surface where fibronectin fibres interacted with the HDFs at all time points.

It was established that ADAMTS-L4 localised to both the cell and forms into a network of fibres in the ECM as described previously (Gabriel et al, 2012). As time progressed the accumulation of ADAMTS-L4 increased in the ECM with the presence of denser ADAMTS-L4 networks. At all time points, it was observed that ADAMTS-L4 completely co-localised with fibrillin-1 in the matrix. Fibrillin-1 microfibrils appeared more continuous in WT HDFs, whereas in the ADAMTS-L4 over expressing cells they seem to lack continuity. Co-staining of ADAMTS-L4 with LTBP-1 and fibronectin revealed partial co-localisation of ADAMTS-L4 fibres with the fibronectin network. Interestingly, interactions of ADAMTS-L4 could be traced along both fibres, suggesting that ADAMTS-L4 wraps around the fibronectin and LTBP-1 network to anchor itself in the matrix. It is also likely that because co-localisation of ADAMTS-L4 was seen with parts of the main fibronectin fibres, this pattern of staining is actually co-localising with fibrillin-1. It was also noted that with time fibronectin deposition increased, however the network produced in WT HDFs was consistently denser than that seen in ADAMTS-L4 over expressing cells, indicating that over expression of this protein asserts a negative effect, which has not yet been shown in the literature. This negative effect could be due to over-expression causing greater cell stress, or the insert, ADAMTS-L4 is somewhat toxic to the cells. Conversely it was found that over expressing ADAMTS-L4 in HDFs may help to enhance the deposition of LTBP-1 fibres in the ECM. Partial co-localisation of ADAMTS-L4 with cellular LTBP-1 was noted consistently at all time points.

# Chapter 4 - Discussion

# 4. Discussion

The ECM is a complex system composed of various molecules which provide essential structural and biochemical support to cells. ADAMTS-L2 and ADAMTS-L4 have been identified as part of the ECM having been associated with genetic diseases affecting the matrix and its normal functioning. Literature accounting biophysical, biochemical and structural information about ADAMTS-L2 and ADAMTS-L4 is sparse; therefore characterisation of ADAMTS-L2 and ADAMTS-L4 is essential to understand the role both of these ECM glycoproteins portray in health and disease.

In this project, several molecular and cellular techniques have been employed to investigate the structure, function and interactions of ADAMTS-L2 and ADAMTS-L4 in a bid to further our understanding of them and their role in the ECM.

## 4.1 Expression analysis of ADAMTS-L2 and ADAMTS-L using different expression systems

To investigate ADAMTS-L2 and ADAMTS-L4, it was essential to establish a system which allowed for the production of recombinant protein. For this, expression of both proteins was trialled in mammalian cells. The expression of ADAMTS-L2 and ADAMTS-L4 in two expression systems was compared to determine which yielded greater amounts of protein. Both proteins were cloned into a pCEP episomal system which is commonly employed to express recombinant proteins, and a pCDH lentiviral expression system. In using two very different expression systems, we were able to compare the yields of protein they generated, but also the impact transfection methods had on the target cells. The lentiviral transduction and FACS selection protocol is a much faster method of introducing DNA into cells. The protocol does not require lengthy antibiotic selection used in episomal systems which can have a detrimental effect on the target cells. However the size of the insert can be a limiting factor in that the larger the insert the more difficult it is to package into virus particles, whereas in the episomal system this is not a major concern. It was found that the number of cells expressing the gene of interest, i.e. ADAMTS-L2 or ADAMTS-L4 obtained through lentiviral transduction was greater than that acquired by episomal transfection. However in comparing between ADAMTS-L2 and ADAMTS-L4 it was found that episomal and lentiviral vectors expressing ADAMTS-L2 transfected different cell types better than ADAMTS-L4 expression vectors. Keeping in mind that all other factors influencing transfection efficiency such as cell type and viability, medium and transfection methods (for each system) were constant, the discrepancy in efficiencies could be due to the nature of the insert. ADAMTS-L4 is larger in size (3225 bp) than ADAMTS-L2 (2856 bp) and therefore could be more difficult to package into virus particles or chaperone into the cells. Another factor could be that rather than the protocols being employed or the size of the insert is that the target cells may find the insert difficult to transcribe or translate and are resistant to higher expression. This was also corroborated by low protein expression levels.

The use of two expression systems allowed for the comparison of the overall yield of total protein obtained from each system. Stable and long-term expression of ADAMTS-L2 and ADAMTS-L4 was observed in cells which had been transduced with lentivirus. However, in comparison to this the episomal system exhibited poor transfection efficiency with the expression of the desired protein diminishing over time despite both systems possessing promoters that are equally strong for gene expression. From this it can be established that in all respects, the lentiviral expression system is better, having a faster and more efficient protocol and yielding a greater turnover of cells which exhibit longer-lasting stable protein expression.

Expression analysis of ADAMTS-L4 showed that over time the amount of secreted protein diminished over time but was present in the cell lysate. Several theories can explain the cause for this. Firstly, it could be speculated that the cells have somehow stopped secreting ADAMTS-L4. The reason for this could be that ADAMTS-L4 is not folding correctly inside the cells; therefore instead of being secreted it is being targeted for intracellular degradation. The accumulation of misfolded protein leads to ER stress which consequently activates the unfolded protein response (UPR) pathway. Initiation of the UPR pathway causes the dissociation of an ER chaperone immunoglobulin binding protein (BiP) from three transmembrane proteins: inositol requiring 1(IRE1), protein kinase RNA-like endoplasmic reticulum kinase (PERK), activating transcription factor 6 (ATF6) (Hetz, 2012). This subsequently results in the activation of an adaptive response via three signalling pathways which serve to re-establish homeostasis, up-regulate the process of protein folding and prevent apoptosis (Oslowski & Urano, 2010). Detection of UPR markers will allow the determination of whether ADAMTS-L4 is being misfolded in the cell. However, another reason explaining the lack of ADAMTS-L4 in the culture medium is that very little is actually present. Experiments using Strataclean resin to concentrate protein from the culture medium detected low amounts of ADAMTS-L4, whereas none was observed in western blots probing crude medium. Therefore the expression analysis could be repeated with the matured cell lines but employ the use of Strataclean resin to concentrate the protein in the media. In support to this, immunofluorescence studies conducted as part of this project confirmed the secretion and deposition of ADAMTS-L4 in the ECM. Cell lysates extracted from all culture dishes and used in the experiments included both lysed cells and any deposited matrix, meaning ADAMTS-L4 detected in these lysates could be from both the matrix and cells. Upon secretion, ADAMTS-L4 may quickly deposit to the matrix, or bind to the cell surface leaving very little ‘free’ protein in the medium to be detected from crude medium. To test whether this hypothesis is true, experiments to separate cells and ECM could be used.

The presence of smaller molecular weight species in western blots of ADAMTS-L4 cell lysates suggest that the protein may be undergoing intracellular degradation due to misfolding, for which the detection of UPR as mentioned before, will confirm this hypothesis. However bearing in mind that the cell lysate is a composition of deposited ECM and lysed cells, it can be suggested that full length ADAMTS-L4 may either be undergoing intracellular cleavage and being secreted, or it is

subjected to extracellular cleavage following secretion as a full length molecule. Degradation or cleavage of ADAMTS-L4 has not yet been described in literature. However enhanced detection of the cleavage product in the culture medium and in purified protein fractions suggests that ADAMTS-L4 may most likely be subject to extracellular cleavage. The cleavage product, also detected in the western blots of SEC purifications, is approximately half the size of full length ADAMTS-L4 and represents the C-terminal half of the protein (due to the presence of the V5 tag located on the C-terminus). Knowing that a TSR domain is approximately 60 amino acids (Adams & Tucker, 2000) it may be assumed that the detected cleavage fragment (approximately 55 kDa, including any glycosylation) is comprised of the chain of 7 TSRs located at the C-terminus of ADAMTS-L4, suggesting that the cleavage site is located just prior to the TSRs. Regardless of whether ADAMTS-L4 is cleaved intracellularly or extracellularly, further investigations are required to pinpoint the cleavage site, and decipher which enzymes are targeting the protein and the mechanism by which cleavage is achieved.

It was observed that ADAMTS-L2 produced by HDFs was of a lower molecular weight than that produced by ARPE-19 cells and HEK-293 EBNA cells. A possible explanation could be that in HDFs, proteins may undergo different post-translational modifications than those in other cell systems. In this case, the different host cells could be glycosylating ADAMTS-L2 in a different pattern or with different N-Linked or O-linked sugars (Werner et al, 2007), which could bring about the discrepancy observed in the sizes of ADAMTS-L2 from different host cells.

The cleavage products of ADAMTS-L2 and ADAMTS-L4 were more visible in the western blots of the purified protein than they were using SDS-PAGE. Reasoning behind this observation could be that western blotting with an antibody is a much more sensitive approach of protein detection than staining with Coomassie stain; therefore the cleavage products are more visible. It could also be argued that ADAMTS-L2 and ADAMTS-L4 in their native state could be folded obscuring the V5 epitope. Upon cleavage the epitope could become more exposed allowing the antibody to bind and created a higher signal when detected. To determine whether this is the case, further work and quantification of the western blots are required.

### 4.2 Stability, biophysical and biochemical properties of ADAMTS-L2 and ADAMTS-L4

Ensuring the stability of a protein is paramount to allow for its use in further experimentation. For this it was important to find a stabilising buffer for ADAMTS-L2 and ADAMTS-L4 which prevent their aggregation. Buffer screens are most often used to determine unique compositions of buffers and additives required to keep proteins stable, however many screens require great quantities of protein. With regards to finding optimum buffers for ADAMTS-L2 and ADAMTS-L4 the limitation was the amount of protein obtained from the expression systems. Despite this, OPTIM analysis of ADAMTS-L2 enabled the screening of several buffers commonly used for protein purification. It was found that ADAMTS-L2 was least stable in HEPES buffer as data reporting its colloidal stability and propensity for aggregation did not produce informative data, suggesting that the

protein aggregates very quickly. This evidence validated the aggregation of ADAMTS-L2 observed during SEC purification. The remaining buffers investigated during OPTIM analysis all appeared to stabilise ADAMTS-L2, with tris emerging as the best buffer. It was found that tris buffer prevented the aggregation of ADAMTS-L2 at higher temperatures compared to phosphate and sodium acetate buffers. Colloidal stability of ADAMTS-L2 was better at higher temperatures in tris buffer, with the data illustrating a gradual unfolding of ADAMTS-L2 rather than a sharp transition noted in phosphate and sodium acetate buffers. This also suggests that tris buffer is somehow acting to keep ADAMTS-L2 in its native form at higher temperatures, hence stable for as long as possible. Another noteworthy observation is that the onset of aggregation in each buffer for ADAMTS-L2 was calculated to be before the melting temperature indicating that ADAMTS-L2 begins to aggregate before it denatures. This phenomenon is a well observed biophysical characteristic of proteins that are subjected to thermal degradation. The $T_m$ of a protein is determined when half of the protein molecules have unfolded due to disruption of hydrogen bonds within the protein, whereas aggregation measured by SLS is detected by a change in the angle of light scattered due to a change in the size of a protein. With increasing temperature and as the protein begins to unfold, covalent interactions within the protein are disrupted and hydrophobic regions gradually become exposed. This increase in hydrophobicity of several molecules causes the exposed hydrophobic regions to interact with each other and form aggregates. Hence the onset of aggregation of a protein only requires a few molecules to aggregate, and therefore is observed before the $T_m$ which is only determined when half the molecules have denatured. Based on this it was found that in tris buffer ADAMTS-L2 was able to remain in its native state at higher temperatures in comparison to phosphate and sodium acetate buffers. Overall in terms of colloidal and conformational stability it was found that tris buffer provided the optimal stabilising conditions to prevent denaturisation and aggregation of ADAMTS-L2 at higher temperatures; however it is not ideal for downstream experimental applications. For example, as part of this project the interactions of ADAMTS-L2 with other matrix protein fragments were assessed using SPR. Ideally, tris buffer must not be used for such investigations as it contains free amines, therefore can interfere with amine coupling interactions by competing with amine ligands (GE Healthcare Bio-Sciences AB, 2013). Instead, sodium acetate was used to immobilise ADAMTS-L2 onto the sensor chip which in the OPTIM analysis, was also seen as a favourable and stabilising buffer choice for ADAMTS-L2.

Higher molecular weight species were observed in western blots of both ADAMTS-L2 and ADAMTS-L4 which suggest that the proteins are dimerising. Upon reduction, these dimers were no longer visible, indicating that the dimers are disulphide linked. In molecules such as fibrillin-1, dimerisation occurs due to the presence of a free cysteine (Ashworth et al, 1999). ADAMTS-Ls are comprised of a cysteine rich domain and multiple TSR domains which could be causing dimerisation. However, it must be noted that native-PAGE of ADAMTS-L2 confirmed that ADAMTS-L2 exists as a monomer, therefore dimerisation could be an artefact of over-expression.

Both ADAMTS-L2 and ADAMTS-L4 are glycosylated proteins possessing N-linked sugars. The glycosylation states observed in this investigation of full length ADAMTS-L2 and ADAMTS-L4 have previously been reported in literature (Koo et al, 2007; Gabriel et al, 2012); however in this study glycosylation states of cleavage products were also observed. Although it is not known which domains of ADAMTS-L2 and ADAMTS-L4 comprise the cleavage products, a glycosylation pattern was noted for both proteins. Literature has previously reported that TSRs are N-glycosylated domains (Adams & Tucker, 2000). As both ADAMTS-L2 and ADAMTS-L4 were seen to possess C-terminal glycosylation it can be hypothesised that the observed glycosylation may exist on the chain of TSRs. It is known that PNGase F only cleaves N-linked glycans, however O-linked glycosylation may also exist on both ADAMTS-Ls and it would explain the incomplete deglycosylation observed in this study. To determine if this is true, further work will be required to investigate the presence of O-linked glycans.

### 4.3 Structural analysis of ADAMTS-L2 and ADAMTS-L4

Current literature documenting experimental data regarding ADAMTS-L2 and ADAMTS-L4 does not provide any structural information. As part of this investigation, structural analysis of ADAMTS-L2 and ADAMTS-L4 using negative stain TEM allowed for the visualisation and modelling of both proteins.

After several iterations of image processing, a low resolution 3D structural model was generated for ADAMTS-L2 illustrating the conformation that the protein adopts. The model can be described as possessing an asymmetrical lobular structure, almost resembling a ‘rubber duck’ conformation. Due to the low resolution of the model, domains comprising ADAMTS-L2 had to be fitted manually to produce a hypothetical model of domain organisation. This hypothetical model depicts that the C-terminal TSR chain is folding back onto the N-terminal region of the protein which consists of a large N-glycan rich domain and a cysteine-rich domain. The presence of the heavily glycosylated N-glycan rich domain, deems the protein to be of a ‘sticky’ nature. This attribute of the molecule, and knowing that TSRs bind PGs (Chen et al, 2000; Totorella et al, 2000), may be attracting the TSRs to interact with the GAG chains attached to ADAMTS-L2 by folding towards it. Another interaction which may influence the TSR-containing C-terminal region to fold onto the N-terminal region is the cysteine-rich domain. TSRs are known to contain cysteine residues which facilitate the formation of disulphide bonds (Tan et al, 2002); therefore it may be believed that the cysteine-rich domain located in the N-terminal may be forming disulphide bridges with the TSRs causing the chain to fold back onto the N-terminal region. However, the 6 cysteine residues found in each TSRs are involved in intradomain interactions as shown in the crystal structure of TSRs by Tan et al (2000). Keeping this in mind and due to lacking existence of such high MW species in western blots, it is most likely that ADAMTS-L2 cysteine-rich domain will be interacting with the C-terminal TSR chain. Also, the structure of properdin comprised of 7 TSRs was used as a base to model the TSRs found in the C-terminal region of ADAMTS-L2 and ADAMTS-L4. Published data regarding properdin states that the 26 nm molecule is highly flexible in nature (Higgins et al, 1995).

Therefore, it can be speculated that the TSR chains forming the C-terminal regions of ADAMTS-L2 and ADAMTS-L4 will also possess the same flexibility as properdin. Despite these plausible explanations, it must be kept in mind that the domain organisation of ADAMTS-L2 presented here in this investigation is entirely hypothetical due to the obtained structure being of low resolution. To determine whether the proposed domain organisation is true to the model, further experimentation and efforts to generate a higher resolution structure are necessary.

Negative stain images of ADAMTS-L4 revealed that this protein is highly flexible in nature. Due to the variety of conformations ADAMTS-L4 was seen to adopt, a model depicting the 3D shape of the molecule could not be generated. As mentioned before, the flexibility that the molecule possesses can be due to the C-terminal TSR chain which is homologous to the highly flexible properdin. However, another factor which may contribute to the flexibility of ADAMTS-L4 is the presence of the proline-rich domain towards the C-terminus. Previously published data regarding the proline-rich region in fibrillin-1 molecules dictates that this region grants fibrillin-1 a degree of flexibility by acting like a 'hinge' (Ashworth et al, 1999; Kielty et al, 2005). Hence ADAMTS-L4 may also possess this attribute. With this in mind, some conformations observed of ADAMTS-L4 appeared to be flexed at a single point granting the molecule a 'hinge' like form. The average length of ADAMTS-L4 molecules was calculated to be approximately 40.6 nm, which implies that the length of TSRs in the C-terminus of ADAMTS-L4 may be similar to the stated length of TSRs comprising the 26 nm properdin chain. However this also infers that the C-terminal chain of TSRs in ADAMTS-L4 accounts for more than 50% of the molecule, which is most likely, not the case. Purified samples used for negative stain TEM analysis contained both full length and cleaved C-terminal product of ADAMTS-L4, i.e. the samples were heterogeneous in composition. This may suggest that the lengthy, flexible tail-like extensions visualised as part of the 2D conformations of ADAMTS-L4 may be a complex of the full length and C-terminal cleavage product. The heterogeneous composition of the protein sample was reflected in the varying lengths of ADAMTS-L4. The shorter protein molecules may represent isolated cleaved fragments, and the greater ratio of these may correlate to the increased amount of cleaved ADAMTS-L4 seen in comparison to the FL protein. Although this investigation has provided some insights into the structure of ADAMTS-L4, the flexible nature of the protein and the heterogeneity of the protein sample have limited the amount of information obtained from the techniques employed. However, several other approaches can be employed in the future to overcome these limitations to study the 3D structure of ADAMTS-L4.

### 4.4 Interactions of ADAMTS-L2 and ADAMTS-L4 with other ECM proteins

A noteworthy observation seen in western blots obtained from purifications of both ADAMTS-L2 and ADAMTS-L4 detected C-terminal cleavage products in the same protein fractions as the full length fragment. Ideally, these cleavage fragments should have eluted from the SEC column later based on their size. However due to their presence in the same fractions as the full length protein, it can be suggested that the cleaved fragments may be interacting with the full length molecules.

Considering the cleaved fragments of both ADAMTS-L2 and ADAMTS-L4 consist of the C-terminal TSRs, and that TSRs are capable of interacting with PGs (Chen et al, 2000; Totorella et al, 2000), it can be speculated that it is these TSRs that are interacting with the full-length counterparts of their respective proteins. In FL form both ADAMTS-L2 and ADAMTS-L4 may be folded granting them a certain hydrodynamic radii, however upon cleavage the proteins may unravel and the hydrodynamic radii of the cleaved products may be of a similar size to their FL counterparts. As SEC separates protein based on their size and shape, another explanation for observing the cleavage products of both ADAMTS-L2 and ADAMTS-L4 co-eluting with FL fragments could be due to a larger hydrodynamic radii of the cleaved fragments.

Additionally, localisation and interactions of both ADAMTS-L2 and ADAMTS-L4 with other matrix proteins were investigated. For this the techniques of immunofluorescence microscopy and SPR analysis were employed, however due to the amount of protein obtained from purifications of ADAMTS-L4, and time constraints of the project, interactions of ADAMTS-L4 could not be studied using SPR.

Previously described immunofluorescence studies in the literature have not co-stained ADAMTS-L2 with other matrix proteins. As part of this project the localisation of ADAMTS-L2 in the ECM and localisation with other matrix proteins were investigated. Immunofluorescence staining of ADAMTS-L2 confirmed co-localisation with fibrillin-1, fibronectin and LTBP-1. On the other hand, SPR analysis of ADAMTS-L2 in literature has shown the protein to interact with fibrillin-1 and LTBP-1 (Le Goff et al, 2011; Sengle et al, 2012; Hubmacher et al, 2015). Here we confirmed the binding of ADAMTS-L2 to fibrillin-1, but we also suggest that ADAMTS-L2 may associate with fibronectin. Images obtained from immunofluorescence microscopy of HDFs expressing ADAMTS-L2 confirmed that it is a cell surface associated protein, accumulation of which increased with time. It was also shown that over time, as fibrillin-1 and LTBP-1 became less cellular and formed fibres in the ECM, their co-localisation with ADAMTS-L2 was only observed when the fibres interacted with the cellular interface. Previous SPR analysis reporting ADAMTS-L2 interactions with fibrillin-1 have not narrowed down the binding to specific fragments of fibrillin-1. However, as part of this investigation it was shown that ADAMTS-L2 interacted with the PF17 fibrillin-1 fragment which contains the domains TB4 and TB5. The TB5 domain is a very important domain in that mutations affecting this domain have been associated with WMS, GD and AD (Faivre et al, 2003; Le Goff et al, 2011; Sengle et al, 2012). Mutations in ADAMTS-L2 also cause GD; therefore it can be hypothesised that the interactions of ADAMTS-L2 with this specific fibrillin-1 domain may be compromised in disease. GD is associated with increased levels of TGFβ, therefore implicating LTBP-1. It has previously been suggested that ADAMTS-L2 may play a major role in regulating TGFβ availability in the ECM by interacting with LTBP-1 alongside fibrillin-1. SPR data published by other research groups have confirmed the binding of LTBP-1 to ADAMTS-L2 however; in this study we were not able to study these interactions due to time constraints and ligand availability. so, we report co-localisation of the two proteins observed with immunofluorescence microscopy.

Another reason for not being able to reproduce results published in literature regarding the interactions of LTBP-1 and ADAMTS-L2 (Sengle et al, 2012) could be the difference in experimental approach. Sengle et al, (2012) immobilised LTBP-1 via lysyl crosslinking and utilised ADAMTS-L2 as an analyte. In this study, amine coupling may have disrupted the binding sites on ADAMTS-L2 and resulted in a negative outcome. Although it is known that these proteins interact, specifically which domains of ADAMTS-L2 are involved is not yet known. A similar pattern of cell surface co-localisation of ADAMTS-L2 was noted with fibronectin, with evident co-staining visible where fibronectin fibres anchored to the cell surface. To corroborate this, SPR analysis presented as part of the project pinpointed the interactions of ADAMTS-L2 with a specific fragment of fibronectin. The FN 7-14 fragment which bound to ADAMTS-L2 contains two functional regions, the first being the RGD binding site and the other being a heparin binding site. Interestingly, the TB4 domain of fibrillin-1 also contains an RGD motif, whereas the TB5 domain contains a heparin binding site. There is no evidence in literature regarding fibrillin-1 and fibronectin interaction at these regions. However, a model of their interactions with ADAMTS-L2 can be proposed. The first being that all three of these proteins may form a complex in which ADAMTS-L2 tethers both fibrillin-1 and fibronectin to the cell surface. However further investigations need to be performed in order to prove or disprove this theoretical model.

Overall immunofluorescence analysis suggested that expression of ADAMTS-L2 may have a somewhat negative effect on the deposition of other matrix protein as staining for each protein in WT HDFs was found to be denser than that observed in ADAMTS-L2 cells. To verify this however, quantification of intensity of staining is required, but the reason as to why this phenomenon was observed is unknown. Further experimentation will be required to determine the mechanism of these observations.

A large array of matrix protein fragments were tested using SPR analysis to determine whether they interacted with ADAMTS-L2 however, most fragments that were analysed did not interact or showed very weak interactions with ADAMTS-L2. It is possible that immobilisation of ADAMTS-L2 may affect its binding capability, in that immobilisation may result in masking of the binding site. Therefore it would be desirable to repeat these assays with a solution phase binding assay such as microscale thermophoresis.

In this investigation binding analysis of ADAMTS-L2 with fibrillin-1 fragment PF17 and fibronectin fragment FN 7-14 was carried out using the steady state phase of interaction which calculates when the rate of association between the ligand and analyte equals the rate of dissociation. While these measurements are not affected by mass transport limitations, the drawback of using this method is that lower concentrations of analyte take longer to reach a state of equilibrium and this may lead to inaccuracies in the determining the affinities of the interactions. As these experiments were conducted once, the data shown here must be regarded as preliminary data for which the methodology and analysis requires optimisation. In future experiments the use of the Langmuir

model for 1:1 binding may be beneficial to determine the kinetics of an interaction as it eliminates inaccuracies of mass transport.

As mentioned earlier, protein interaction studies of ADAMTS-L4 with other matrix proteins using SPR were not possible due to limiting amounts of protein obtained from purifications. However, immunofluorescence microscopy allowed for the localisation and co-staining of ADAMTS-L4 in the matrix to be visualised. Over time it was observed that ADAMTS-L4 formed an extensive fibrous network throughout the ECM. It was also found that ADAMTS-L4 fibres exhibited co-localisation with fibrillin-1, LTBP-1 and fibronectin. Out of these matrix fibres, ADAMTS-L4 exhibited completed co-localisation with the fibrillin-1 network, whereas partial co-staining was noted with LTBP-1 and fibronectin. Interestingly, the interacting ADAMTS-L4 fibres could be traced along the fibronectin and LTBP-1 fibres. This suggests that for ADAMTS-L4 deposition, the fibrillin-1 network is the most important as depicted by the level of co-localisation. Despite co-localisation with LTBP-1 and fibronectin it can be suggested that unlike fibrillin-1, these molecules are not important for the deposition of ADAMTS-L4, as these fibres were seen to form independent networks with which ADAMTS-L4 did not co-stain with. The interactions of TSRs studied in literature have shown that in ADAMTSs, C-terminal TSRs are involved in cell anchorage and proteolytic activity (Tortorella et al, 2000). However, due to ADAMTS-Ls lacking catalytic activity, it can be assumed that the TSRs are mainly involved in interactions with cells and other matrix molecules. Investigations of TSR interactions in TSP-1 led to the identification of a specific sequence located between the first and second TSRs which binds to and activates TGFβ (Schultz-Cherry et al, 1995). Although the same sequence is not present in either ADAMTS-L2 or -L4, screening for an interaction to TGFβ would address whether either protein binds TGFβ directly via a different sequence.

### 4.5 Final conclusions

The aim of this project was to contribute towards understanding the biophysical, biochemical and structural characteristics of ADAMTS-L2 and ADAMTS-L4, as well as learn more about their interactions with other ECM molecules.

Comparison of two expression systems enabled the selection of a lentiviral expression system which in turn yielded the greatest amount of recombinant protein for both ADAMTS-L2 and ADAMTS-L4 from mammalian cells. Optimisation of purification conditions and assessment of protein stability identified several buffers which will stabilise both ADAMTS-L2 and ADAMTS-L4. The ideal buffer appeared to be tris as it prevented thermal induced degradation and aggregation of ADAMTS-L2 at higher temperatures however, use of this buffer not appropriate for some downstream experimental applications. Instead, phosphate buffer and sodium acetate buffer, which were equally suitable, were employed for purification purposes and further experimentation.

The 3D structure of ADAMTS-L2 was solved as part of this project revealing that it adopts an asymmetrical lobular conformation. However due to the model being of low resolution (43.4 Å), the domains comprising ADAMTS-L2 had to be manually fitted to generate a hypothetical model

predicting the alignment of the protein. From the fit that was generated, it can be suggested that the chain of C-terminal TSR domains is flexible and is folding back onto the N-terminal region of the protein as well as interacting with certain domains. On the other hand, 3D structural analysis of ADAMTS-L4 was not possible due to the highly flexible nature of the protein. However 2D analysis showed that the molecule is approximately 40.6 nm in length. Also it was speculated that the flexibility of the C-terminal TSR domains and possibly the proline-rich domain located near the C-terminus.

Deposition and interaction studies using immunofluorescence microscopy and SPR confirmed binding of ADAMTS-L2 with fibrillin-1 and LTBP-1. With the use of SPR, a more defined ADAMTS-L2 binding site encompassing the TB5 domain was pinpointed on fibrillin-1. This region of fibrillin-1, especially the TB5 domain is implicated in fibrillinopathies such as WMS, GD and AD (Faivre et al, 2003; Le Goff et al, 2011; Sengle et al, 2012). With mutations in ADAMTS-L2 also resulting in GD, the interactions between ADAMTS-L2 and this region of fibrillin-1 may be central to the mechanisms involved in matrix disruption observed in GD. Experimental data gathered from immunofluorescence studies and SPR also show that ADAMTS-L2 interacts with a fragment of fibronectin which also interacts with a region of fibrillin-1 containing both the TB4 and TB5 domains. Therefore binding of ADAMTS-L2 with fibrillin-1 and fibronectin fragments may provide insights into how ADAMTS-L2 is involved in the structural organisation of the matrix.

Finally immunofluorescence studies of ADAMTS-L4 showed that the protein forms an extensive fibrillar network in the ECM which was also seen to completely co-localise with fibrillin-1. Partial co-localisation of ADAMTS-L4 fibres was observed with fibronectin and LTBP-1. This pattern of staining suggests that ADAMTS-L4 may require the presence of a fibrillin-1 network for deposition, however it is not dependent on fibronectin and LTBP-1 networks as they were seen to form independent fibres in the ECM. These observations have also led to the assumption that ADAMTS-L4 may also be an integral part of microfibril bundles along with fibrillin-1, LTBP-1 and other matrix proteins.

### 4.6 Future directions

Although a major part of this project to establish an optimised expression system for the expression and purification of ADAMTS-L2 and ADAMTS-L4 was achieved, the small quantities of recombinant protein generated are still a cause for concern. Therefore employing techniques to increase expression of ADAMTS-L2 and ADAMTS-L4 will be paramount. Several options to achieve this can be tested; for example, adopting a different cell culture technique by using roller bottles instead of HYPERFlasks may increase the yield of protein. The advantages of using roller bottles over static monolayer flasks are that not only do the bottles provide a larger surface area for the cells to grow, but the continuous gentle agitation of the medium prevents the formation of gradients which may deprive the cells of nutrition. Another advantage is that due to the existence of a single monolayer of cells at one given time, there is a higher rate of efficient gaseous exchange,

keeping the cells healthier. Recently this approach has been adopted in our research lab and a significant increase in protein expression levels has been reported. Alternatively the use of an inducible expression system may also help in boosting expression levels, as with this form of system the level of expression can be modulated as well as controlling the expression in a timely manner. The advantage is that expression of the gene of interest can be controlled and stopped to allow the cells to recuperate, as well as control how much protein is transcribed which in turn puts less stress on the cells. Another advantage of employing an inducible system for protein expression is that if the transcribed protein is toxic to the cells, turning off the expression will help to bypass the toxic effect exerted on to the cells from continuous expression.

As discussed earlier, investigations assessing the secretion of ADAMTS-L4 need to be carried out. Currently, reduced protein levels in the conditioned medium and in purified samples, and its detection in cell lysates suggest that very little ADAMTS-L4 is being secreted. As mentioned earlier in the discussion, several scenarios could be the cause for these observations. To determine whether the protein is being targeted for intracellular degradation, efforts must be made to detect this by determining the presence or up-regulation of UPR markers. However, if ADAMTS-L4 is indeed secreted into the medium and then strongly bound to the matrix, separating deposited ECM from the 'cell lysate' should allow for its localised detection in either the ECM, cell lysate or both.

Future work concerning both ADAMTS-Ls is to determine which ECM or intracellular proteases are cleaving them. For this, the composition of cleavage products must be deciphered to identify cleavage sites, and hence the proteases that act at these sites. It was noted that the cleavage products of ADAMTS-L2 and ADAMTS-L4 are glycosylated as a shift in their molecular weight was observed upon deglycoyslation with PNGase F. However, it is not known if these cleavage products contain the consensus sequences for N-linked glycans, therefore future work will be carried out to determine the location of these sequences in both ADAMTS-L2 and ADAMTS-L4. As part of this investigation, mass spectrometry was employed following a tryptic digest of the protein from a SDS-PAGE gel to determine that the protein obtained from SEC was ADAMTS-L2. This was sufficient for protein identification however; it did not provide information regarding its correct expression. Therefore, to ensure this, intact mass spectrometry by liquid chromatography will be employed for both ADAMTS-L2 and ADAMTS-L4. This technique will also be a useful tool in identifying the specific location of N-linked and O-linked glycosylation sequences.

Thus far, we have only scratched the surface in terms of structural analysis of ADAMTS-L2 and ADAMTS-L4. In this project the extent of structural analysis was limited to the generation of a low resolution 3D structure of ADAMTS-L2 with a hypothetically fitted arrangement of domains and the minimal 2D structural analysis of ADAMTS-L4. However, future endeavours investigating the structural characterisation of ADAMTS-L2 and ADAMTS-L4 must aim to generate higher resolution 3D models of both proteins. Higher resolution modelling of ADAMTS-L2 and ADAMTS-L4 can be achieved through the use of cryo-electron microscopy (cryo-EM) which is a well-established technique utilised for generation of near-atomic resolution structures, which is now possible with

the new generation of detectors and termed a “resolution revolution” (Kuhlbrandt, 2014). Cryo-EM imaging employs the use of a direct detection device (DDD) which has an improved signal to noise ratio meaning structures are seen in more detail (Milazzo et al, 2011). Another advantage of using cryo-EM is that protein molecules are imaged in their native, unstained and hydrated state. Staining samples, as practiced in negative stain TEM, is known to introduce artefacts such as flattening and twisting of the protein, which will be bypassed with the use of cryo-EM. As discussed in this thesis both ADAMTS-L2 but especially ADAMTS-L4 have highly flexible in nature. To overcome the limitations of 3D modelling faced due to the flexibility of the proteins, a sub-modelling approach can be applied. Imaging of sub-domains of ADAMTS-L2 and ADAMTS-L4 with cryo-EM will allow for the generation of higher resolution reconstructions. Alternatively a second approach to stabilise ADAMTS-L2 and ADAMTS-L4 would be to complex them to a known binding partner such as fibrillin-1 to restrict any flexibility that the molecules exhibit. Apart from cryo-EM, another notable technique widely used to study the structure of proteins, small angle X-ray scattering (SAXS) could also be used. This technique analyses the structure of a protein using x-rays in solution, therefore in their native state providing more accurate representation of the protein.

Interactions studies performed as part of this project with ADAMTS-L2 need to be repeated to reproduce the results achieved. The protein fragments used as analytes in this study had been frozen, hence repetitions of the experiment should be carried out using freshly purified analytes to ensure their viability in the experiment. Due to time constraints and limited protein availability, SPR analysis of ADAMTS-L4 could not be performed as part of this thesis. Therefore future experiments concerning ADAMTS-L4 must also include SPR to confirm previously predicted interactions and to identify novel binding partners. A criticism made regarding the use of SPR and ADAMTS-L2 in this study was that potentially this technique may not be the ideal biomolecular interaction technique to assess ADAMTS-L2 interactions. As mentioned previously, immobilising ADAMTS-L2 onto the chip surface may interfere with its functioning and binding capabilities. Based on this assumption, other techniques evaluating biomolecular interactions such as isothermal titration calorimetry (ITC) and microscale thermophoresis (MST) can be applied. ITC is a technique which measures the changes in thermodynamics when two proteins interact (Pierce et al, 1999), whereas MST monitors the motion of proteins along microscopic temperature gradients measuring changes in the hydration shells of proteins due to conformational changes induced by interactions with other proteins (Jerabek-Willemsen et al, 2011). The advantage of using these techniques would be that they are ‘immobilisation-free’ and the proteins are in solution. Similarly, protein-protein interaction analyses such as co-immunoprecipitation assays or crosslinking assays could be used to verify and assess both strong and weak interactions of ADAMTS-L2 and ADAMTS-L4 with other ECM proteins. Fragments encoding different domains, such as the C-terminal TSR chains, of ADAMTS-L2 and ADAMTS-L4 could also be generated and used in biomolecular interaction studies in order to decipher which regions are involved in interactions with other matrix proteins.

Immunofluorescence analysis of ADAMTS-L2 and ADAMTS-L4 was performed in HDF cells; however the data obtained only reflects the deposition and behaviour of the proteins in mesenchymal cell types. A publication from our research group reported that certain epithelial cell types, namely ARPE 19 cells do not require fibronectin networks to deposit fibrillin-1 microfibrils in the ECM (Baldwin et al, 2014), thus function differently to HDFs. Therefore, endothelial and epithelial cell types expressing both ADAMTS-L2 and ADAMTS-L4 should also be analysed for comparisons. In addition to this, co-staining of ADAMTS-L2 and ADAMTS-L4 with several other matrix components will provide greater visual knowledge of the scope of interactions ADAMTS-L2 and ADAMTS-L4 have within in the ECM. Desai et al (2016) published findings of ADAMTS-L2 involvement in EDS, indicating its interactions with collagens. Knowledge that TSRs bind GAGs, investigations looking into HS and syndecans may reveal a novel function for ADAMTS-Ls in the ECM. Immunofluorescence data obtained for ADAMTS-L4 suggested that its deposition in the matrix may be dependent on the fibrillin-1 microfibril network, therefore knock down of fibrillin-1 and other matrix proteins in the future may help in elucidating whether this hypothesis is true.

Finally, all the work carried out in this project involved the investigations and characterisation WT ADAMTS-L2 and ADAMTS-L4. Undoubtedly further work is required to obtain greater knowledge of these proteins; however their physiological involvement and functions in disease are yet to be investigated. Thus far literature has dictated that mutations in these proteins result in fibrillinopathies; however these are yet to be investigated. Therefore, it is vital to generate ADAMTS-L2 and ADAMTS-L4 harbouring disease-causing mutations in order to assess how these mutations affect the structure, function and interactions of these proteins in the ECM. Assessment of changes in biophysical and biochemical properties will allow for the determination of how mutations can affect the stability of the proteins. Structural analysis will be key in defining any conformational changes the mutations have on ADAMTS-L2 and ADAMTS-L4 and how this may affect their functions in the ECM. Lastly, biomolecular interaction analysis will determine changes in the abilities of mutant ADAMTS-L2 and ADAMTS-L4 to bind ECM proteins. These investigations will be crucial to elucidating mechanisms and contributions of mutant ADAMTS-L2 and ADAMTS-L4 in fibrillinopathies.

# References

## 5. References


Abramowitz, Y., Roth, A., Keren, G., Isakov, O., Shomron, N., Laitman, Y., Weissglas-Volkov, D., Arbel, Y., Banai, S., Finkelstein, A. & Friedman, E. (2016) Whole-exome sequencing in individuals with multiple cardiovascular risk factors and normal coronary arteries. *Coronary Artery Disease* 24: 257-66.

Adams, J.C. & Tucker, R.P. (2000) The thrombospondin type 1 repeat (TSR) superfamily: Diverse proteins with related roles in neuronal development. *Developmental Dynamics* 218: 280-99

Ahram, D., Sato, T.S., Kohilan, A., Tayeh, M., Chen, S., Leal, S., Al-Salem, M. & El-Shanti, H. (2009) A homozygous mutation in ADAMTSL4 causes autosomal recessive isolated ectopia lentis. *American journal of Human Genetics* 84: 274-8.

Allali, S., Le Goff, C., Pressac-Diebold, I., Pfennig, G., Mahaut, C., Dagoneau, N., Alanay, Y., Brady, A.F., Crow, Y.J., Devriendt, K., Drouin-Garraud, V., Flori, E., Genevieve, D., Hennekam, R.C., Hurst, J., Krakow, D., Le Merrer, M., Lichtenbelt, K.D., Lynch, S.A., Lyonnet, S., Macdermot, K., Mansour, S., Megarbane, A., Santos, H.G., Splitt, M., Superti-Furga, A., Unger, S., Williams, D., Munnich, A. & Cormier-Daire, V. (2011) Molecular screening of ADAMTSL2 gene in 33 patients reveals the genetic heterogeneity of geleophysic dysplasia. *Journal of Medical Genetics* 48: 427-21.

Ali, B.R., Jeffery, S., Patel, N., Tinworth, L.E., Meguid, N., Patton, M.A. & Afzal, A.R. (2007) Novel Robinow syndrome causing mutations in the proximal region of the frizzeled-like domain of ROR2 are retained in the endoplasmic reticulum. *Human Genetics* 122: 389-95.

Ammash, N.M., Sundt, T.M. & Connolly, H.M. (2008) Marfan syndrome – diagnosis and management. *Current Problems in Cardiology* 33: 7-39.

Apte, S.S. (2004) A disintegrin-like metalloprotease (reprolysin type) with thrombospondin type 1 motifs: the ADAMTS family. *Molecules in Focus* 36: 981-5.

Apte, S.S. (2009) A Disintegrin-like and Metalloprotease (Reprolysin-type) with Thrombospondin Type 1 Motif (ADAMTS) Superfamily: Functions and mechanisms. *Journal of Biological Chemistry* 284: 31493-7.

Aragon-Martin, J.A., Ahnood, D., Charteris, D.G., Saggar, A., Nischal, K.K., Comeglio, P., Chandra, A., Child, A.H. & Arno, A.H. (2010) Role of ADAMTSL4 mutations in *FBN1* mutation-negative ectopia lentis patients. *Human Mutations* 31: E1622-31.

Ashworth, J.L., Kelly, V., Wilson, R., Shuttleworth, C.A. & Kielty, C.M. (1999) Fibrillin assembly: dimer formation mediated by amino-terminal sequences. *Journal of Cell Science* 112: 3549-58.

Ashworth, J.L., Kielty, C.M. & McLeod, D. (2000) Fibrillin and the eye. *British Journal of Ophthalmology* 84:1312-17.

Bader, H.L., Ruhe, A.L., Wang, L.W., Wong, A.K., Walsh, K.F., Packer, R.A., Mitelman, J., Robertson, K.R., O'Brien, D.P., Broman, K.W., Shelton, G.D., Apte, S.S. & Neff, M.W. (2010) An ADAMTSL2 founder mutation causes Musladin–Lueke Syndrome, a heritable disorder of beagle dogs, featuring stiff skin and joint contractures. *PLoS One* 5: E12817.

Baldock, C., Koster, A.J., Ziese, U., Rock, M.J., Sherratt, M.J., Kadler, K.E., Shuttleworth, C.A. & Kielty, C.M. (2001) The supramolecular organisation of fibrillin-rich microfibrils. *Journal of Cell Biology* 153: 1045-56.

Baldwin, A.K., Simpson, A., Steer, R., Cain, S.A. & Kielty, C.M. (2013) Elastic fibres in health and disease. *Expert Reviews in Molecular Medicine* 15: 1-30.

Baldwin, A.K., Cain, S.A., Lennon, R., Godwin, A., Merry, C.L. & Kielty, C.M. (2014) Epithelial-mesenchymal status influences how cells deposit fibrillin microfibrils. *Journal of Cell Science* 127: 158-71.

Bateman, J.F., Boot-Handford, R.P. & Lamandé, S.R. (2009) Genetic disease of connective tissues: cellular and extracellular effects of ECM mutations. *Nature Reviews Genetics* 10: 173-83.

Bax, D.V., Bernard, S.E., Lomas, A., Morgan, A., Shuttleworth, C.A., Humphries, M.J. & Kielty, C.M. (2003) Cell adhesion to fibrillin-1 molecules and microfibrils is mediated by α5β1 and αvβ3 integrins. *Journal of Biological Chemistry* 278: 34605-16.

Beene, L.C., Wang, L.W., Hubmacher, D., Keene, D.R., Reinhardt, D.P., Annis, D.S., Mosher, D.F., Mecham, R,P., Traboulsi, E.I. & Apte, S.S. (2013) Nonselective assembly of fibrillin 1 and fibrillin 2 in the rodent ocular zonule and in cultured cells: Implications for Marfan Syndrome. *Investigative Ophthalmology and Visual Science* 54: 8337-44.

Ben-Salem, S., Hertecant, J., Al-Shamsi, A.M., Ali, B.R. & Al-Gazali, L. (2013) Novel mutations in ADAMTSL2 gene underlying geleophysic dysplasia in families form United Arab Emirates. *Birth Defects Research – Clinical and Molecular Teratology* 97: 764-9. Biasini, M., Bienert, S., Waterhouse, A., Arnold, K., Studer, G., Schmidt, T., Kiefer, F., Cassarino, T.G., Bertoni, M., Bordoli, L. & Schwede, T. (2014) SWISS-MODEL: modelling protein tertiary and quaternary structure using evolutionary information. *Nucleic Acids Research* 42: 252-8.

Biggin, A., Holman, K., Brett, M., Bennetts, B. & Adès, L. (2004) Detection of thirty novel FBN1 mutations in patients with Marfan syndrome or a related fibrillinopathy. *Human Mutation* 23:99.

Bonnans, C., Chou, J. & Werb, Z. (2014) Remodelling the extracellular matrix in development and disease. *Nature Reviews Molecular Cell Biology* 15: 786-801.

Cain, S.A., Morgan, A., Sherratt, M.J., Ball, S.G., Shuttleworth, C.A. & Kielty, C.M. (2006) Proteomic analysis of fibrillin-rich microfibrils. *Proteomics* 6:111-22.

Cain, S.A., McGovern, A., Baldwin, A.K., Baldock, C. & Kielty, C.M. (2012) Fibrillin-1 mutations causing Weill-Marchesani syndrome and acromicric and geleophysic dysplasias disrupt heparan sulphate interactions. *PLoS One* 7: e48634.

Chandra, A., Aragon-Martin, J.A., Hughes, K., Gati, S., Reddy, M.A., Deshpande, C., Cormack, G., Child, A.H., Charteris, D.G. & Arno, G. (2012) A genotype-phenotype comparison of *ADAMTSL4* and *FBN1* in isolated ectopia lentis. *Investigative Ophthalmology and Visual Science* 53: 4889-96.

Chandra, A., D'Cruz, L., Aragon-Martin, J.A., Charteris, D.G., Limb, G.A., Child, A.H. & Arno, G. (2012) Focus on molecules: ADAMTSL4. *Experimental Eye Research* 104: 95-6.

Chandra, A., Aragon-Martin, J.A., Sharif, S., Parulekar, M., Child, A. & Arno, G. (2013) Craniosynostosis with Ectopia Lentis and a homozygous 20-base deletion in ADAMTSL4. *Ophthalmic genetics* 34: 78-82.

Chandra, A., Jones, M., Cottrill, P., Eastlake, K. & Limb, G.A. (2013) Gene expression and protein distribution of ADAMTSL4 in human iris, choroid and retina. *British Journal of Ophthalmology* 97: 1208-12.

Chandra, A., Patel, D., Aragon-Martin, J.A., Pinard, A., Collod-Beroud, G., Comeglio, P., Faivre, L., Charteris, D., Child, A.H. & Arno, G. (2014) The revised Ghent Nosology; Reclassifying Isolated Ectopia Lentis. *Clinical Genetics* 87: 284-7.

Charbonneau, N.L., Dzamba, B.J., Ono, R.N., Keene, D.R., Corson, G.M., Reinhardt, D.P. & Sakai, L.Y. (2003) Fibrillins can co-assemble in fibrils, but fibrillin fibril composition displays cell-specific differences. *Journal of Biological Chemistry* 278: 2740-49.

Charbonneau, N.L., Carlson, E.J., Tufa, S., Sengle, G., Manalo, E.C., Carlberg, V.M., Ramirez, F., Keene, D.R. & Sakai, L.Y. (2010) In vivo studies of mutant fibrillin-1 microfibrils. *Journal of Biological Chemistry* 285: 24943-55.

Chaudhry, S.S., Cain, S.A., Morgan, A., Dallas, S.L., Shuttleworth, C.A. & Kielty, C.M. (2007) Fibrillin-1 regulates the bioavailability of TGFbeta1. *Journal of Cell Biology* 176: 355-67.

Chen, H., Herndon, M.E. & Lawler, J. (2000) The cell biology of thrombospondin-1. *Matrix Biology* 19: 597-614.

Christensen, A.E., Fiskerstrand, T., Knappskog, P.M., Boman, H. & Rodahl, E. (2010) A novel ADAMTSL4 mutation in autosomal recessive ectopia lentis et pupillae. *Investigative Ophthalmology and Visual Science* 51: 6369-73.

Clarke, A.W., Wise, S.G., Cain, S.A., Kielty, C.M. & Weiss, A.S. (2005) Coacervation is promoted by molecular interactions between the PF2 segment of fibrillin-1 and the domain 4 region of tropoelastin. *Biochemistry* 40(30): 10271-81.

Colige, A., Li, S.W., Sieron, A.L., Nusgens, B.V., Prockop, D.J. & Lapiere, C.M. (1997) cDNA cloning and expression of bovine procollagen I N-proteinase: a new member of the superfamily of zinc-metalloproteinases with binding sites for cells and other matrix components. *Proceedings of the National Academy of Sciences (PNAS)* 94: 2374-9.

Collin, G.B., Hubmacher, D., Charette, J.R., Hicks, W.L., Stone, L., Yu, M., Naggert, J.K., Krebs, M.P., Peachey, N.S., Apte, S.S. & Nishina, P.M. (2015) Disruption of murine *ADAMTSL4* results in zonular fibre detachment from the lens and in retinal pigment epithelium dedifferentiation. *Human Molecular Genetics* 24: 6958-74.

Corson, G. M., Charbonneau, N. L., Keene, D. R. & Sakai, L. Y. (2004) Differential expression of fibrillin-3 adds to microfibril variety in human and avian but not rodent connective tissues. *Genomins* 83: 461-72.

Cromar, L.C., Xiong, X., Chautard, E., Ricard-Blum, S. & Parkinson, J. (2012) Toward a systems level view of the ECM and related proteins: A framework for the systematic definition and analysis of biological systems. *Proteins* 80: 1522-44.

Dagoneau, N., Benoist-Lasselin, C., Huber, C., Faivre, L., Megarbane, A., Alswaid, A., Dollfus, H., Alembik, Y., Munnich, A., Legai-Mallet, M. & Cormier-Daire, V. (2004) ADAMTS10 mutation in autosomal recessive Weill-Marchesani syndrome. *American Journal of Human Genetics* 75: 801-6.

De Fraipont, F., Nicholson, A.C., Feige, J.J. & Van Meir, E.G. (2001) Thrombospondins and tumour angiogenesis. *Trends in Molecular Medicine* 9: 401-7.

Desai, A., Connolly, J.J., March, M., Hou, C., Chiavacci, R., Kim, C., Lyon, G., Hadley, D. & Hakonarson, H. (2016) Systemic data-querying of large paediatric biorepository identifies novel Ehlers-Danlos Syndrome variant. *BMC Musculoskeletal Disorders* 17:80.

Downing, A.K., Knott, V., Werner, J.M., Cardy, C.M., Campbell, I.D. & Handford, P.A. (1996) Solution structure of a pair of calcium-binding epidermal growth factor-like domains: Implications for the Marfan syndrome and other genetic disorders. *Cell* 85: 597-605.

Dubail, J. & Apte, S.S. (2015) Insights on ADAMTS proteases and ADAMTS-like proteins from mammalian genetics. *Matrix Biology* 44-46: 24-37.

El-Hallous, E., Sasaki, T., Hubmacher, D., Getie, M., Tiedmann, K., Brinckmann, J., Batge, B., Davis, E.C. & Reinhardt, D.P. (2007) Fibrillin-1 interactions with fibulins depend on the first hybrid domain and provide an adaptor function to tropoelastin. *Journal of Biological Chemistry* 282: 8935-46.

Evereklioglu, C., Hepsen, I.F. & Or, H. (1999) Weill-Marchesani syndrome in three generations. *Eye (London)* 6: 773-7.

Faivre, L., Dollfus, H., Lyonnet, S., Alembik, Y., Megarbane, A., Samples, J., Gorlin, R.J., Alswaid, A., Feingold, J., Le Merrer, M., Munnich, A. & Cormier-Daire, V. (2003) Clinical homogeneity and genetic heterogeneity in Weill-Marchesani syndrome. *American Journal of Medical Genetics* 123A: 204-7.

Faivre, L., Gorlin, R.J., Wirtz, M., Godfrey, M., Dagoneau, N., Samples, J.R., Le Merrer, M., Collod-Beroud, G., Boileau, C., Munnich, A. & Cormier-Daire, V. (2003) In frame fibrillin-1 gene deletion in autosomal dominant Weill-Marchesani syndrome. *Journal of Medical Genetics* 40: 34-6.

Farais, F.H., Johnson, G.S., Taylor, J.F., Giuliano, E., Katz, M.L., Sanders, D.N., Schnabel, R.D., McKay, S.D., Khan, S., Gharahkhani, P., O'Leary, C.A., Pettitt, L., Forman, O.P., Boursnell, M., McLaughlin, B., Ahonen ,S., Lohi, H., Hernandez-Merino, E., Gould, D.J., Sargan, D. & Mellersh, C.S. (2010) An ADAMTS17 splice donor site mutation in dogs with primary lens luxation. *Investigative Ophthalmology and Visual Science* 51:4716–4721.

Gabriel, L.A.R., Wang, L.W., Bader, H., Ho, J.C., Majors, A.K., Hollyfield, J.G., Traboulsi, E.I. & Apte, S.S. (2012) ADAMTSL4, a secreted glycoprotein widely distributed in the eye, binds fibrillin-1

microfibrils and accelerates microfibril biogenesis. *Investigative Ophthalmology and Visual Science* 53: 461-9.

Garcia-Ortiz, L., Gutierrez-Salinas, J., del Carmen Chima Gala, M., Garcia, R.L.R. & de la Concepcion Yerena, M. (2015) Geleophysic Dysplasia: A novel in-frame deletion of a tandem repeat in the *ADAMTSL2* gene. *American Journal of Medical Genetics* 167: 1949-51.

GE Healthcare Bio-Sciences AB (2013) Biacore T200 Handbook. Uppsala, Sweden pp. 21.

Gorlin, R.J., L'Heureux, R.R. & Shapiro, I. (1974) Weill-Marchesani syndrome in two generations: genetic heterogeneity or pseudodominance? *Journal of Paediatric Ophthalmology* 11: 139-44.

Greene, V.B., Stoetzel, C., Pelletier, V., Perdomo-Trujillo, Y., Liebermann, L., Marion, V., De Korvin, H., Boileau, C., Dufier, J.L. & Dollfus, H. (2010) Confirmation of ADAMTSL4 mutations for autosomal recessive isolated bilateral ectopia lentis. *Ophthalmic Genetics* 31: 47-51.

Handford, P.A., Mayhew, M., Baron, M., Winship, P.R., Campbell, I.D.& Brownlee, G.G. (1991) Key residues involved in calcium binding motifs in EGF-like domains. *Nature* 351:164-167.

Handford, P.A., Downing, A.K., Reinhardt, D.P. & Sakai, L.Y. (2000) Fibrillin: from domain structure to supramolecular assembly. *Matrix Biology* 19: 457-70.

Hetz, C. (2012) The unfolded protein response: controlling cell fate decisions under ER stress and beyond. *Nature Reviews Molecular Cell Biology* 13: 89-102.

Higgins, J. M., Wiedemann, H.,Timpl, R., and Reid, K. B. (1995).Characterization of mutant forms of recombinant human properdin lacking single thrombospondin type I repeats. Identification of modules important for function. *Journal of Immunology* 155: 5777–85.

Hubmacher, D. & Reinhardt, D.P. (2009) One more piece in the fibrillin puzzle. *Structure* 17: 635-6.

Hubmacher, D. & Apte, S.S. (2011) Genetic and functional linkage between ADAMTS superfamily proteins and fibrillin-1: a novel mechanism influencing microfibril assembly and function. *Cellular and Molecular Life Sciences* 68: 3137-48.

Hubmacher, D & Apte, S.S. (2013) The biology of the extracellular matrix: novel insights. *Current Opinions in Rheumatology* 25: 65-70.

Hubmacher, D., Bergeron, E., Fagotto-Kaufmann, C., Sakai, L.Y. & Reinhardt, D.P. (2014) Early fibrillin-1 assembly monitored through a modifiable recombinant cell approach. *American Chemical Society* 15: 1456-68.

Hubmacher, D & Apte, S.S. (2015) ADAMTS proteins as modulators of microfibril formation and function. *Matrix Biology* 47: 34-43.

Hubmacher, D., Wang, L.W., Mecham, R.P., Reinhardt, D.P. & Apte, S.S. (2015) *ADAMTSL2* deletion results in bronchial fibrillin microfibril accumulation and bronchial epithelial dysplasia: A novel mouse model providing insights on geleophysic dysplasia. *Disease models and Mechanisms* 8: 487-99.

Isogai, Z., Ono, R.N., Ushiro, S., Keene, DR., Chen, Y., Mazzieri, R., Charbonneau, N.L., Reinhardt, D.P., Rifkin, D.B. & Sakai, L.Y. (2003) Latent transforming growth factor beating-binding protein 1 interact with fibrillin and is a microfibril-associated protein. *Journal of Biological Chemistry* 278: 2750-57.

Jensen, S.A., Iqbal, S., Lowe, E.D., Redfield, C. & Handford, P.A. (2009) Structure and interdomain interactions of a hybrid domain: A disulphide-rich module of the fibrillin/LTBP superfamily of matrix proteins. *Structure* 17: 759-68.

Jerabek-Willemsen, M., Wienken, C.J., Braun, D., Baaske, P. & Duhr, S. (2011) Molecular interaction studies using microscale thermophoresis. *Assay and Drug Development Technologies* 9: 342-53.

Jones, G.C. & Riley, G.P. (2005) ADAMTS proteinases: a multi-domain, multi-functional family with roles in extracellular matrix turnover and arthritis. *Arthritis Research & Therapy* 7: 160-9.

Jovanovic, J., Takagi, J., Choulier, L., Abrescia, N.G., Stuart, D.I., van der Merwe, P.A., Mardon, H.J. & Handford, P.A. (2007) AlphaVbeta6 is a novel receptor for human fibrillin-1. Comparative

studies of molecular determinants underlying integrin-rgd affinity and specificity. *Journal of Biological Chemistry* 282: 6743-51.

Kainulainen, K., Karttunen, L., Puhakka, L., Sakai, L. & Peltonen, L. (1994) Mutations in the fibrillin gene responsible for dominant ectopia lentis and neonatal Marfan syndrome. *Nature Genetics* 6:64-9.

Karnik, S.K., Brooke, B.S., Bayes-Genis, A., Sorensen, L., Wythe, J.D., Schwartz, R.S., Keating, M.T. & Li, D.Y. (2003) A critical role for elastin signalling in vascular morphogenesis and disease. *Development* 130: 411-23.

Kashiwagi, M., Enghild, J.J., Gendron, C., Hughes, C., Caterson, B., Itoh, Y. & Nagase, H. Altered proteolytic activities of ADAMTS4 expressed by C-terminal processing. *Journal of Biological Chemistry* 279: 10109-19.

Katzke, S., Booms, P., Tiecke, F., Palz, M., Pletschacher, A., Türkmen, S., Neumann, L.M., Pregla, R., Leitner, C., Schramm, C., Lorenz, P., Hagemeier, C., Fuchs, J., Skovby, F., Rosenberg, T. & Robinson, P.N. (2002) TGGE screening of the entire FBN1 coding sequence in 126 individuals with Marfan syndrome and related fibrillinopathies. *Human Mutation* 20: 197-208.

Keeley, F.W., Bellingham, C.M. & Woodhouse, K.A. (2002) Elastin as a self-organising biomaterial: use of recombinantly expressed human elastin polypeptides as a model for investigations of structure and self-assembly of elastin. *Philosophical Transactions Royal Society* 357: 185-9.

Keene, D.R., Maddox, B.K., Kuo, H.J., Sakai, L.Y. & Glanville, R.W. (1991) Extraction of beaded structures and their identification as fibrillin-containing matrix microfibrils. *Journal of Histochemistry and Cytochemistry* 39: 441-449.

Kirschner, R., Hubmacher, D., Iyengar, G., Kaur, J., Fagotto-Kaufmann, C., Bromme, D., Bartels, R. & Reinhardt, D.P. (2011) Classical and neonatal Marfan syndrome mutations in fibrillin-1 cause differential protease susceptibilities and protein function. *Journal of Biological Chemistry* 286: 32810-23.

Kielty, C.M., Baldock, C., Lee, D., Rock, M.J., Ashworth, J.L. & Shuttleworth, C.A. (2002) Fibrillin: from microfibril assembly to biomechanical function. *Philosophical Transactions Royal Society* 357:207-17.

Kielty, C.M., Sherratt, M.J., Marson, A. & Baldock, C. (2005) Fibrillin microfibrils. *Advances in Protein Chemistry* 70: 405-35.

Kielty, C.M. (2006) Elastic fibres in health and disease. *Expert Reviews in Molecular Medicine* 8: 1-23.

Kitahama, S., Gibson, M.A., Hatzinikolas, G., Hay, S., Kuliwaba, J.L., Evdokiou, A., Atkins, G.J. & Findlay, D.M. (2000) expression of fibrillins and other microfibril-associated proteins in human bone and osteoblast-like cells. *Bone* 27: 61-7.

Kochhar, A., Kirmani, S., Cetta, F., Younge, B., Hyland, J.C. & Michels, V. (2013) Similarity of Geleophysic dysplasia and Weill-Marchesani syndrome. *American Journal of Medical Genetics* 161A: 3130-2.

Koo, B., Le Goff, C., Jungers, K.A., Vasanji, A., O'Flaherty, J., Weyman, C.M. & Apte, S.S. (2007) ADAMTS-like 2 (ADAMTSL2) is a secreted glycoprotein that is widely expressed during mouse embryogenesis and is regulated during skeletal myogenesis. *Matrix Biology* 26: 431-441.

Körkkö, J., Kaitila, I., Lönnqvist, L., Peltonen, L. & Ala-Kokko, L. (2002) Sensitivity of conformation sensitive gel electrophoresis in detecting mutations in Marfan syndrome and related conditions. *Journal of Medical Genetics* 39: 34-41.

Kouser. L., Abdul-Aziz, M., Nayak, A., Stover, C.M., Sim, R.B. & Kishore, U. (2013) Properdin and factor H: opposing players on the alternative complement pathway "see-saw". *Frontiers in Immunology* 4: 93.

Kuhlbrandt, W. (2014) Cryo-EM enters a new era. *eLife* 3: e03678.

Kutchey, J., Olsen, L.M., Rinkoski, T., Mackay, E.O., Iverson, T.M., Gelatt, K.N., Haines, J.L. & Kutchey, R.W. (2011) Mapping of the disease locus and identification of ADAMTS10 as a candidate gene in a canine model of primary open angle glaucoma. *PLoS Genetics* 7:e1001306.

Kutz, W.E., Wang, L.W., Agoneau, N., Odrcic, K.J., Cormier-Daire, V., Traboulsi, E.I. & Apte, S.S. (2008) Functional analysis of an ADAMTS10 signal peptide mutation in Weill-Marchesani syndrome demonstrates a long-range secretion of the full-length enzyme. *Human Mutations* 29: 1425-34.

Kutz, W.E., Wang, L.W., Bader, H.L., Majors, A.K., Iwata, K., Traboulsi, E.I., Sakai, L.Y., Keene, D.R. & Apte, S.S. (2011) ADAMTS10 protein interacts with fibrillin-1 and promotes its deposition in the extracellular matrix of cultured fibroblasts. *Journal of Biological Chemistry* 286: 17156-67.

Le Goff, C., Morice-Picard, F., Dagoneau, N., Wang, L.W., Perrot, C., Crow, Y.J., Bauer ,F., Flori, E., Prost-Squarcioni, C., Krakow, D., Ge, G., Greenspan, D.S., Bonnet, D., Le Merrer, M., Munnich, A., Apte, S.S. & Cormier-Daire, V. (2008) ADAMTSL2 mutations in geleophysic dysplasia demonstrate a role for ADAMTS-like proteins in TGF-beta bioavailability regulation. *Nature Genetics* 40:1119–1123.

Le Goff, C. & Cormier-Daire, V. (2011) The ADAMTS(L) family and human genetic disorders. *Human Molecular Genetics* 20: 163-7.

Le Goff, C., Mahaut, C., Wang, L.W., Allali, S., Abhyankar, A., Jensen, S., Zylberberg, L., Collod-Beroud, G., Bonnet, D., Alanay, Y., Brady, A.F., Cordier, M.P., Devriendt, K., Genevieve, D., Kiper, P.O.S., Kitoh, H., Krakow, D., Lynch, S.A., Le, Merrer, M., Megarbane, A., Mortier, G., Odent, S., Polak, M., Rohrbach, M., Sillence, D., Stolte-Dijkstra, I., Superti-Furga, A., Rimoin, D.L., Topouchian, V., Unger, S., Zabel, B., Bole-Feysot, C., Nitschke, P., Handford, P., Casanova, J.L., Boileau, C., Apte, S.S., Munnich, A. & Cormier-Daire, V. (2011) Mutations in the TGFβ binding-protein-like domain 5 of *FBN1* are responsible for acromicric and geleophysic dysplasias. *The American Journal of Human Genetics* 89: 7-14.

Le Goff, C. & Cormier-Daire, V. (2012) From tall to short: The role of TGFβ signalling in growth and its disorders. *American Journal of Medical Genetics* 160C: 145-53.

Levy, G.G., Nichols, W.C., Lian, E.C., Foroud, T., McClintick, J.N., McGee, B.M., Yang, A.Y., Siemieniak, D.R., Stark, K.R., Gruppo, R., Sarode, R., Shurin, S.B., Chandrasekaran, V., Stabler, S.P., Sabio, H., Bouhassira, E.E., Upshaw, J.D. Jr, Ginsburg, D., Tsai, H.M. (2001) Mutations in a member of the ADAMTS gene family cause thrombotic thrombocytopenic purpura. *Nature* 413: 488-94.

Li, J., Jia, X., Li, S., Fang, S. & Guo, X (2014) Mutation survey of candidate genes in 40 Chinese patients with congenital ectopia lentis. *Molecular Vision* 20: 1017-24.

Loeys, B.L., Nuytinck, L., Delvaux, I., De Bie, S. & De Paepe, A. (2000) Genotype and phenotype analysis of 171 patients referred for molecular study of the fibrillin-1 gene FBN1 because of suspected Marfan syndrome. *Archives of Internal Medicine* 161: 2447-54.

Loeys, B.L., Matthys, D.M. & De Paepe, A.M. (2003) Genetic fibrillinopathies: new insights in molecular diagnosis and clinical management. *Acta Clinica Belgica* 58: 3-11.

Lonnqvist, L., Child, A., Kainulainen, K., Davidson, R., Puhakka, L. & Peltonen, L. (1993) A novel mutation of the fibrillin gene causing ectopia lentis. *Genomics* 19: 573-6.

Lonnqvist, L., Reinhardt, D., Sakai, L. & Peltonen, L. (1998) Evidence for furin-type activity-mediated C-terminal processing of profibrillin-I and interference in the processing by certain mutations. *Human Molecular Genetics* 7: 2039-44.

Lucero, H.A. & Kagan, H.M. (2006) Lysyl oxidase: an oxidative enzyme and effector of cell function. *Cellular and Molecular Life Sciences* 63: 2304-16.

Mackenroth, L., Rump, A., Lorenz, P., Schröck, E. & Tzschach, A. (2016) Novel *ADAMTSL2* mutations in a patient with geleophysic dysplasia type I. *Clinical Dysmorphology.* 25: 106-9.

Marson, A., Rock, M.J., Cain, S.A., Freeman, L.J., Morgan, A., Mellody, K., Shuttleworth, C.A.& Kielty, C.M. (2005) Homotypic fibrillin-1 interactions in microfibril assembly. *Journal of Biological Chemistry* 280: 5013-21.

Massam-Wu, T., Chiu, M., Choudhury, R., Chaudhry, S.S., Baldwin, A.K., McGovern, A., Baldock, C., Shuttleworth, C.A. & Kielty, C.M. (2010) Assembly of fibrillin microfibrils governs extracellular deposition of latent TGFβ. *Journal of Cell Science* 123: 3006-18.

Mayne, R., Mayne, P.R. & Baker, J.R. (1997) Fibrillin-1 is the major protein present in bovine zonular fibrils. *Investigative Ophthalmology Visual Science* 38: 1399.

Mellody, K.T., Freeman, L.J., Baldock, C., Jowitt, T.A., Siegler, V., Raynal, B.D.E., Cain, S.A., Wess, T.J., Shuttleworth, C.A. & Kielty, C.M. (2006) Marfan syndrome-causing mutations n fibrillin-1 result in gross morphological alterations and highlight the structural importance of the second hybrid domain. *Journal of Biological Chemistry* 281: 31854-62.

Milazzo A,C., Cheng, A., Moeller, A., Lyumkis, D., Jacovetty, E., Polukas, J., Ellisman, M.H., Xuong, N.H., Carragher, B. & Potter, C.S. (2011) Initial evaluation of a direct detection device detector for single particle cryo-electron microscopy. *Journal of Structural Biology* 176: 404-8.

Morales, J., Al-Sharif, L., Khalil, D.S., Shinwari, J.M., Bavi, P., Al-Mahrouqi, R.A., Al-Rajhi, A., Alkuraya, F.S., Meyer, B.F. & Al Tassan, N. (2008) Homozygous mutations in ADAMTS10 and ADAMTS17 cause lenticular myopia, ectopia lentis, glaucoma, spherophakia and short stature. *American Journal of Human Genetics* 85: 558-68.

Mouw, J.K., Ou, G. & Weaver, V.M. (2014) Extracellular matrix assembly: a multiscale deconstruction. *Nature Reviews Molecular Cell Biology* 15: 771-85.

Muiznieks, L.D., Weiss, A.K. & Keeley, F.W. (2010) Structural disorder and dynamics of elastin. *Biochemistry and Cell Biology* 88: 239-50.

Naba, A., Clauser, K.R., Hoersch, S., Liu, H., Carr, S.A. & Hynes, R.O. (2012) The matrisome: *in silico* definition and in vivo characterization by proteomics of normal and tumour extracellular matrices. *Molecular & Cellular Proteomics* 11: M111.014647.

Neuhann, T.M., Artelt, J., Neuhann, T.F, Tinschert, S. & Rump, A. (2011) A homozygous microdeletion within ADAMTSL4 in patients with isolated ectopia lentis: evidence of a founder mutation. *Investigative Ophthalmology and Visual Science* 52: 695-700.

Niesen, F.H., Berglund, H. & Vedadi, M. (2007) The use of differential scanning fluorimetry to detect ligand interactions that promote protein stability. *Nature Protocols* 2: 2212-21.

Ono, R.N., Sengle, G., Charbonneau, N.L., Carlberg, V., Bachinger, H.P., Sasaki, T., Lee-Arteaga, S., Zilberberg, L., Rifkin, D.B., Ramirez, F., Chu, M.L. & Sakai, L.Y. (2009) Latent transforming growth factor beta-binding proteins and fibulins compete for fibrillin-1 and exhibit exquisite specificities in binding sites. *Journal of Biological Chemistry* 284: 16872-81.

Oslowski, C.M. & Urano, F. (2010) The binary switch between life and death of endoplasmic reticulum-stressed beta cells. *Current Opinion in Endocrinology, Diabetes and Obesity* 17: 107-12.

Pereira, L., D'Alessio, M., Ramirez, F., Lynch, J.R., Sykes, B., Pangilinan, T. & Bonadio, J. (1993) Genomic organisation of the sequence coding fibrillin, the defective gene product on Marfan syndrome. *Human Molecular Genetics.*2: 961-8.

Pettersen, E.F., Goddard, T.D., Huang, C.C., Couch, G.S., Greenblatt, D.M., Meng, E.C. & Ferrin, T.E. (2004) UCSF Chimera--a visualization system for exploratory research and analysis. *Journal of Computational Chemistry* 25: 1605-12.

Pierce, M.M., Raman, C.S. & Nall, B.T. (1999) Isothermal titration calorimetry of protein-protein interactions. *Methods* 19: 213-21.

Pimienta, A.L., Wilcox, W.R. & Reinstein, E. (2013) More than meets the eye: The evolving phenotype of Weill-Marchesani syndrome – diagnostic confusion with geleophysic dysplasia. *American Journal of Medical Genetics* 161: 3126-29.

Piha-Gossak, A., Sossin, W. & Reinhardt, D.P. (2012) The evolution of extracellular fibrillins and their functional domains. *PLos One* 7: e33560.

Porayette, P., Fruitman, D., Lauzon, J.L., Le Goff, C., Cormier-Daire, V., Sanders, S.P., Pinto-Rojas, A. & Perez-Atayde, A.R. (2014) Novel mutations in Geleophysic dysplasia type I. *Paediatric and Developmental Pathology* 17: 209-16.

Porter, S., Clark, I.M., Kevorkian, L. & Edwards, D.R. (2005) The ADAMTS metalloproteinases. *Biochemical Journal* 386: 15-27.

Pyeritz, R.E. (2000) The Marfan syndrome. *Annual Review of Medicine* 51: 481-510.

Qian, R.Q. & Glanville, R.W. (1997) Alignment of fibrillin molecules in elastic microfibrils is defined by transglutaminase-derived cross-links. *Biochemistry* 36: 15841-7.

Raghunath, M., Putnam, E.A., Ritty, T., Hamstra, D., Park, E.S., Tschodrich-Rotter, M., Peters, R., Rehemtulla, A. & Milewicz, D.M. (1999) Carboxy-terminal conversion of profibrillin to fibrillin at a basic site by PACE/furin-like activity required for incorporation in the matrix. *Journal of Cell Science* 112: 1093-1100.

Rahimi, R.A. & Leof, E.B. (2007) TGF-beta signaling: a tale of two responses. *Journal of Cellular Biochemistry* 102: 593-608.

Reinhardt, D.P., Mechling, D.E., Boswell, B.A., Keene, D.R., Sakai, L.Y. & Bachinger, H.P. (1997) Calcium determines the shape of fibrillin. *Journal of Biological Chemistry* 272: 7368-73.

Reinhardt, D.P., Gambec, J.E., Ono, R.N., Bachinger, H.P. & Sakai, L.Y. (2000) Initial steps in assembly of microfibrils. Formation of disulphide-cross-linked multimers containing fibrillin-1. *Journal of Biological Chemistry* 275: 2205-10.

Reinstein, E., Smirin-Yosef, P., Lagovsky, I., Davidov, B., Amit, G.P., Neumann, D., Orr-Urtreger, A., Ben-Shachar, S. & Basel-Vanagaite, L. (2016) A founder mutation in *ADAMTSL4* causes early onset bilateral ectopia lentis among Jews of Bukharian origin. *Molecular Genetics and Metabolism* 117: 38-41.

Ritty, T.M., Broekelmann, T.J. & Mecham, R.P. (2000) Fibrillin-1 contains a proteolytically activated heparin-binding site important for extracellular matrix deposition. *Molecular Biology of the Cell* 11: S1377.

Robinson, P.N., Arteaga-Solis, E., Baldock, C., Collod-Beroud, G., Booms, P., De Paepe, A., Guo, G., Handford, P.A., Judge, D.P., Kielty, C.M., Loeys, B., Milewicz, D.M., Ney, A., Ramirez, F., Reinhardt, D.P., Tiedemann, K., Whiteman, P. & Godfrey, M. (2006) The molecular genetics of Marfan syndrome and related disorders. *Journal of Medical Genetics* 43: 769-87.

Rock, M.J., Cain, S.A., Freeman, L.J., Morgan, A., Mellody, K., Marson, A., Shuttleworth, C.A., Weiss, A.S. & Kielty, C.M. (2004) Molecular basis of elastic fibre formation: critical interactions and a tropoeastin-fibrillin-1 cross-link. *Journal of Biological Chemistry* 279: 23748-58.

Sadler, J.E. (2002) A new name in thrombosis, ADAMTS13. *PNAS* 99: 11552-4.

Saharinen, J. & Keski-Oja, J. (2000) Specific sequence motif of 8-Cys repeats of TGF-beta binding proteins, LTBPs, creates a hydrophobic interaction surface for binding of small latent TGF-beta. *Molecular Biology of The Cell* 11: 2691-704.

Sengle, G., Tsutsui, K., Keene, D.R., Tufa, S.F., Carlson, E.J., Charbonneau, N.L., Ono, R.N., Sasaki, T., Wirtz, M.K., Samples, J.R., Fessler, L.I., Fessler, J.H., Sekiguchi, K., Hayflick, S.J. & Sakai, L.Y. (2012) Microenvironmental regulation by fibrillin-1. *PLos Genetics* 8: e1002425.

Sengle, G. & Sakai, L. (2015) The fibrillin microfibril scaffold: A niche for growth factors and mechanosensation? *Matrix Biology* 47: 3-12.

Sharifi, Y., Tjon-Fo-Sang, M.J., Cruysberg, J.R.M. & Maat-Kievit, A.J. (2013) Ectopia lentis et pupillae in four generations caused by novel mutations in the ADAMTSL4 gene. *British Journal of Ophthalmology* 97: 583-7.

Schultz-Cherry, S., Chen, H., Mosher, D.F., Misenheimer, T.M., Krutzsch, H.C., Roberts, D.D. & Murphy-Ullrich, J.E. (1995) Regulation of transforming growth factor-beta activation by discrete sequences of thrombospondin 1. *Journal of Biological Chemistry* 270: 7304-10.

Singh, P., Carraher, C. & Schwarzbauer, J.E. (2010) Assembly of fibronectin extracellular matrix. *Annual Review of Cell and Developmental Biology* 26: 397-419.

Snelling, S., Rout, R., Davidson, R., Clark, I., Carr, A., Hulley, P.A. & Price, A.J. (2014) A gene expression study of normal and damaged cartilage in anteromedial gonarthrosis, a phenotype of osteoarthritis. *Osteoarthritis and Cartilage* 22: 334-43.

Soejima, K., Matsumoto, M., Kokame, K., Yagi, H., Ishizashi, H., Maeda, H., Nozaki, C., Miyata, T., Fujimura, Y. & Nakagaki, T. (2003) ADAMTS-13 cysteine-rich/spacer domains are functionally essential for von Willebrand factor cleavage *Blood* 102: 3232-7.

Somerville, R.P.T., Longpre, J., Jungers, K.A., Engle, J.M., Ross, M., Evanko, S., Wight, T.N., Leduc, R. & Apte, S.S. (2003) Characterisation of ADAMTS-9 and ADAMTS-20 as a distinct ADAMTS subfamily related to *Caenorhabditis elegans* GON-1. *Journal of Biological Chemistry* 278: 9053-13.

Somerville, R.P.T., Jungers, K.A. & Apte, S.S. (2004) ADAMTS10: discovery and characterisation of a novel, widely expressed metalloprotease and its proteolytic activation. *Journal of Biological Chemistry* 279: 51208-17.

Somerville, R.P.T., Longpre, J., Apel, E.D., Lewis, R.M., Wang, L.W., Sanes, J.R., Leudec, R. & Apte, S.S. (2004) ADAMTS7B, the full length product of the *ADAMTS7* gene, is a chondroitin sulphate proteoglycan containing a mucin domain. *Journal of Biological Chemistry* 279: 35159-75.

Spranger, J., Gilbert, E.F., Arya, S., Hoganson, G.M. & Opitz, J.M. (1984) Geleophysic dysplasia. *American Journal of Medical Genetics* 19: 487–499.

Stinkellner, H., Etzler, J., Gogoll, L., Neesen, J., Stifter, E., Brandau, O. & Laccone, F. (2014) Identification and molecular characterisation of a homozygous missense mutation in the *ADAMTS10* gene in a patient with Weill-Marchesani syndrome. *European Journal of Human Genetics* doi: 23:1186-91.

Taipale, J., Miyazono, K., Heldin, C. & Keski-Oja, J. (1994) Latent transforming growth factor-beta 1 associates to fibroblast extracellular matrix via latent TGF-beta binding protein. *The Journal of Cell Biology* 124:171-181.

Tan, K., Duquette, M., Liu, J., Dong, Y., Zhang, R., Joachimiak, A., Lawler, J. & Wang, J. (2002) Crystal structure of TSP-1 type 1 repeats: a novel layered fold and its biological implication. *Journal of Cell Biology* 159: 373-82.

Tang, B.L. (2001) ADAMTS: a novel family of extracellular matrix proteases. *The International Journal of Biochemistry and Cell Biology* 33: 33-44.

Tang, G., Peng, L., Baldwin, P.R., Mann, D.S., Jiang, W., Rees, I. & Ludtke, S.J. (2007) EMAN2: an extensible image processing suite for electron microscopy. *Journal of Structural Biology* 157: 38-46.

Tiedemann, K., Batge, B., Muller, P.K. & Reinhardt, D.P. (2001) Interactions of fibrillin-1 with heparin/heparan sulphate, implications for microfibrillar assembly. *Journal of Biological Chemistry* 276: 36035-42.

Tortorella M., Pratta, M., Liu, R.Q., Abbaszade, I., Ross, H., Burn, T. & Arner, E. (2000) The thrombospondin motif of aggrecanase-1 (ADAMTS-4) is critical for aggrecan substrate recognition and cleavage. *Journal of Biological Chemistry* 275: 25791-7.

Tortorella, M.D., Malfait, F., Barve, R.A., Shieh, H.S. & Malfait, A.M. (2009) A review of the ADAMTS family, pharmaceutical targets in the future. *Current Pharmaceutical Design* 15: 2359-74.

Troilo, H., Steer, R., Collins, R.F., Kielty, C.M. & Baldock, C. (2016) Independent multimerisation of latent TGFβ binding protein-1 stabilised by cross-linking and enhanced heparan sulphate. *Scientific Reports* 6: 34347.

Wang, W.M., Lee, S., Steiglitz, B.M., Scott, I.C., Lebares, C.C., Allen, M.L., Brenner, M.C., Takahara, K. & Greenspan, D.S. (2003) Transforming growth factor-beta induces secretion of activated ADAMTS2. A procollagen III N-proteinase. *Journal of Biological Chemistry* 278: 19549-57.

Wang, P., Tortorella, M., England, K., Malfait, A., Thomas, G., Arner, E.C. & Pei, D. (2004) Proprotein convertase furin interacts with and cleaves pro-ADAMTS4 (aggrecanase-1) in the *trans*-golgi. *Journal of Biological Chemistry* 279: 15434-40.

Wang, Y., Zhang, H., Ye, J., Han, L. & Gu, X. (2014) Three novel mutations of *FBN1* gene in Chinese children with acromelic dysplasia. *Journal of Human Genetics* 59: 563-7.

Werner, R. G., Kopp, K. & Schlueter, M. (2007) Glycosylation of therapeutic proteins in different production systems. *Acta Paediatrica* 96: 17-22.

White, J.M. (2003) ADAMs: modulators of cell-cell and cell-matrix interactions. *Current opinions in Cell Biology* 15: 598-606.

Wheatley, H.M., Traboulsi, E.I., Flowers, B.E., Maumenee, I.H., Azar, D., Pyeritz, R.E. & Whittum-Hudson, J.A. (1995) Immunohistochemical localisation of fibrillin in human ocular tissues. Relevance to Marfan syndrome. *Archives of Ophthalmology* 113: 103-9.

Wirtz, M.K., Samples, J.R., Kramer, P.L., Rust, K., Yount, J., Acott, T.S., Koler, R.D., Cisler, J., Jahed, A., Gorlin, R.J. & Godfrey, M. (1996) Weill-Marchesani syndrome – possible linkage of the autosomal dominant for to 15q21.1. *American Journal of Medical Genetics* 65: 68-75.

Yadin, D.A., Robertson, I.B., McNaught-Davis, J., Evans, P., Stoddart, D., Handford, P.A., Jensen, S.A. & Redfield, C. (2013) Structure of the fibrillin-1 N-terminal domains suggests that heparan sulphate regulates the early stages of microfibril assembly. *Structure* 21: 1743-56.

Yu, H., Munoz, E. M., Edens, R. E. & Linhardt, R. J. (2005) Kinetic studies on the interactions of heparin and complement proteins using surface plasmon resonance. *Biochimica et Biophysica Acta – General Subjects* 1726: 168-76

Yua, X., Downing, A.K., Knott, V. & Handford, P.A. (1997) Solution structure of the transforming growth factor beta-binding protein-like module, a domain associated with matrix fibrils. *European Molecular Biology Organisation Journal* 16: 6659-66. Zeng, W., Corcoran, C., Collins-Racie, L.A., Lavallie, E.R., Morris, E.A. & Flannery, C.R. (2006) Glycosaminoglycan-binding properties and aggrecanase activities of truncated ADAMTS: Comparative analysis with ADAMTS-5, -9, -18 and -18. *Biochimica et Biophysica Acta* 1760: 517-24.

Zhang, H., Apfelroth, S.D., Hu, W., Davis, E.C., Sanguineti, C., Bonadio, J., Mecham, R.P. & Ramirez, F. (1994) Structure and expression of fibrillin-2, a novel microfibrillar component preferentially located in elastic matrices. *Journal of Cell Biology* 124: 855-863.

Zhou, A., Webb, G., Zhu, X. & Steiner, D.F. (1999) Proteolytic processing in the secretory pathway. *Journal of Biological Chemistry* 274: 20745-8.

Zhou, X.M., Wang, Y., Zhao, L., Yu, W.H., Fan, N., Yan, N.H., Su, Q., Liang, Y.Q., Wang, Y., Li, L.P., Cai, S.P., Jonas, J.B. & Liu, X.Y. (2015) Novel compound heterozygous mutations identified in *ADAMTSL4* gene in a Chinese family with isolated ectopia lentis. *Acta Ophthamologica* 93: 91-2.

Zilberberg, L., Todorovic, V., Dabovic, B., Horiguchi, M., Courousse, T, Sakai, L.Y. & Rifkin, D.B. (2012) Specificity of latent TGF-β binding protein (LTBP) incorporation into matrix: Role of fibrillins and fibronectin. *Journal of Cellular Physiology* 227: 3828-36.

# Appendix

# 6. Appendix

## 6.1 Appendix – Figure A1

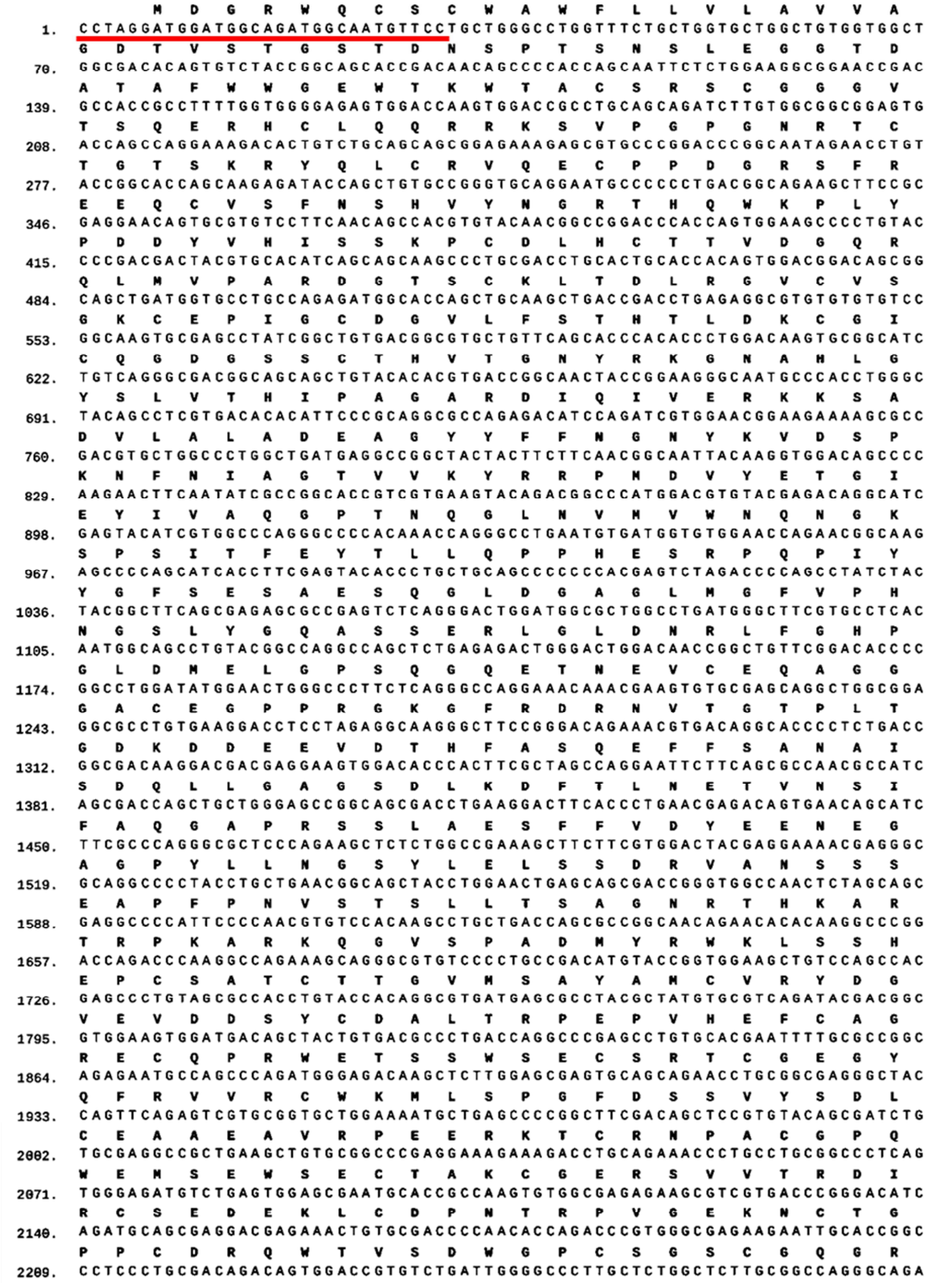

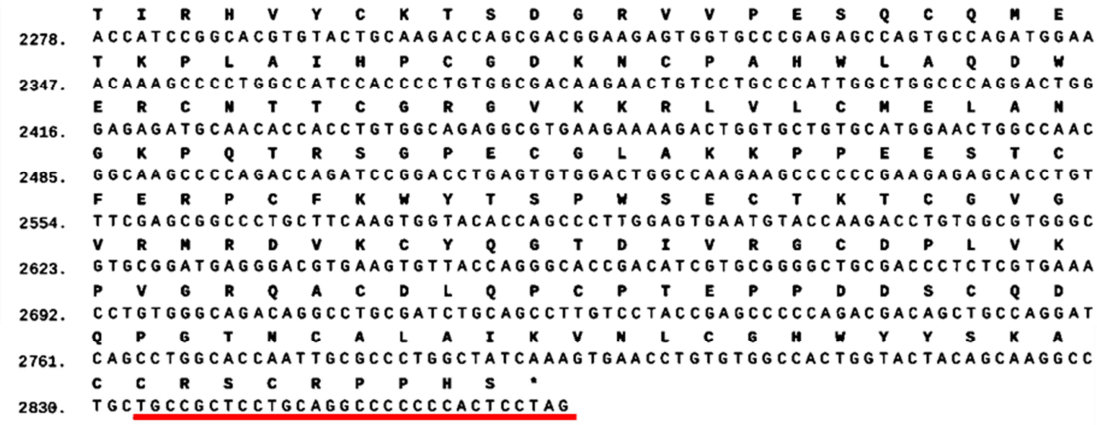


**Figure A1 Gene string sequence encoding ADAMTS-L2**

Gene sequence encoding human ADAMTS-L2 was obtained from GenBank (www.ncbi.nlm.nih.gov/genbank) Accession number: NM_014694.3. Sequence was submitted to generate a gene string sourced from GeneArt Gene Synthesis Service Thermo Fisher Scientific (*Paisley, UK*). Underlined sequences (red) were protected from codon optimisation to ensure complimentary overlap with primers and cloning vector. First 6 bp represent the kozak consensus sequence for ADAMTS-L2.

## 6.2 Appendix – Figure A2

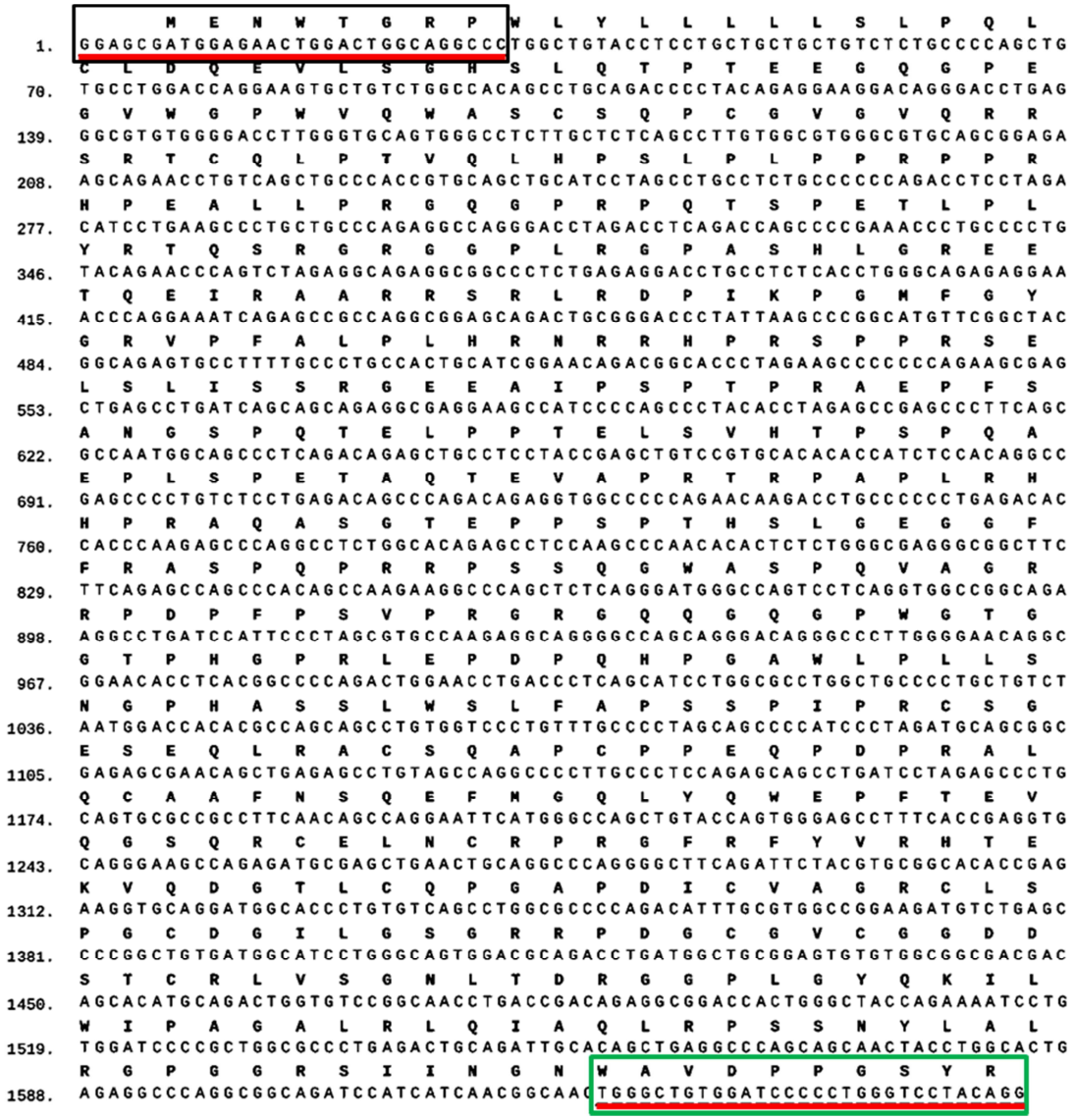


**Figure A2 Gene string sequence encoding ADAMTS-L4 – 'Start'**

Gene sequence encoding human ADAMTS-L4 was obtained from GenBank (www.ncbi.nlm.nih.gov/genbank) Accession number: NM_019032. Sequence was submitted to generate a gene string sourced from GeneArt Gene Synthesis Service Thermo Fisher Scientific (*Paisley, UK*). Underlined sequences (red) were protected from codon optimisation to ensure complimentary overlap with primers, cloning vector (black box) and second half of sequence (green box). First 6 bp represent the kozak consensus sequence for ADAMTS-L4.

## 6.3 Appendix – Figure A3

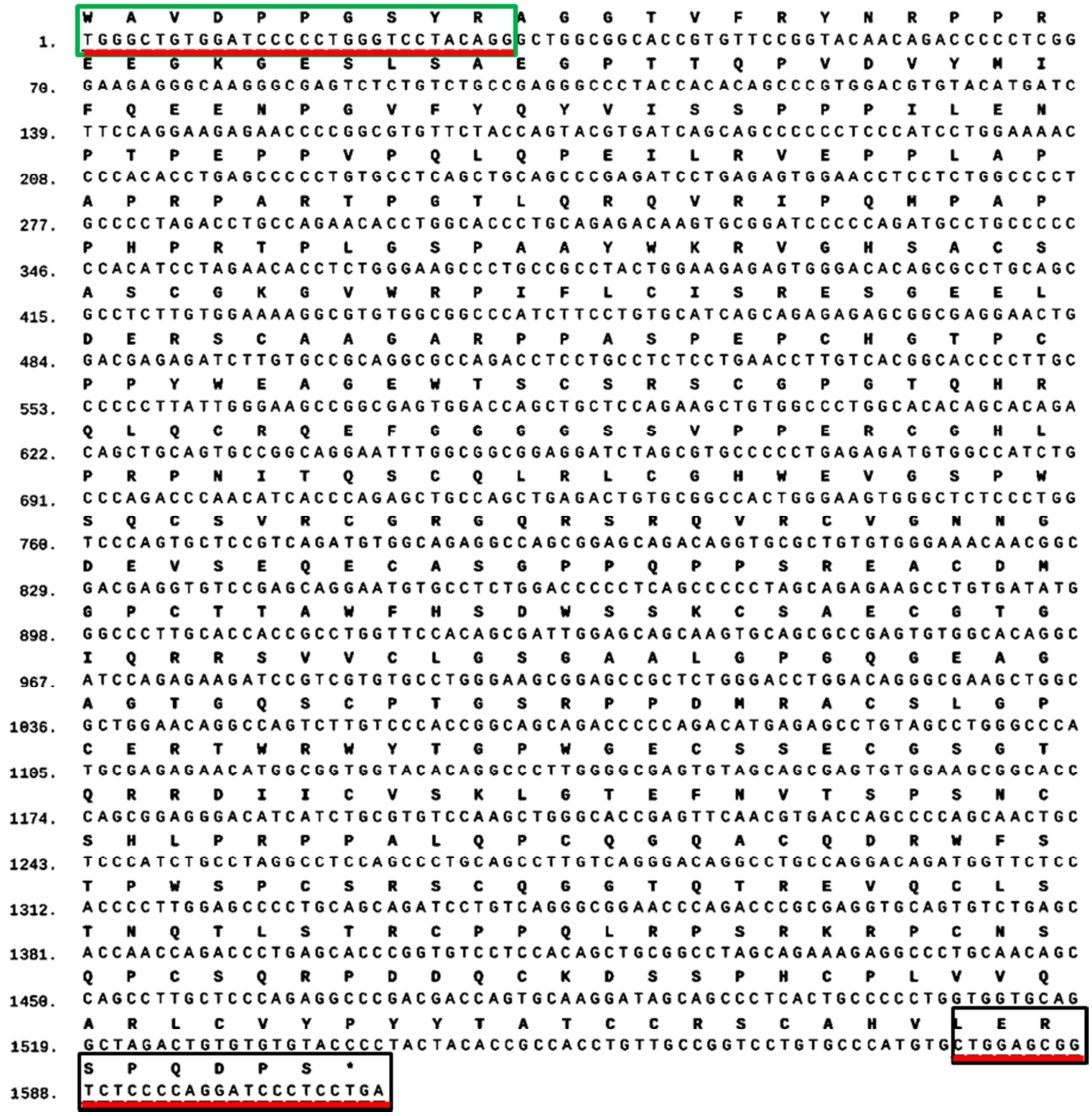


**Figure A3 Gene string sequence encoding ADAMTS-L4 – 'End'**

Gene sequence encoding human ADAMTS-L4 was obtained from GenBank (www.ncbi.nlm.nih.gov/genbank) Accession number: NM_019032. Sequence was submitted to generate a gene string sourced from GeneArt Gene Synthesis Service Thermo Fisher Scientific (*Paisley, UK*). Underlined sequences (red) were protected from codon optimisation to ensure complimentary overlap with primers, cloning vector (black box) and first half of sequence (green box). First 6 bp represent the kozak consensus sequence for ADAMTS-L4.

## 6.4 Appendix Figure – A4

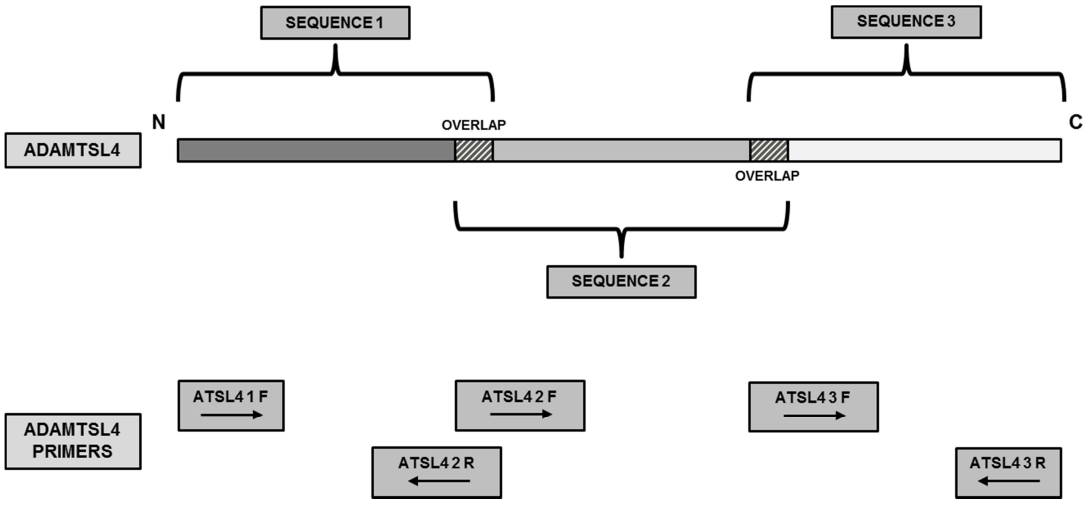


**Figure A4 Schematic representing division of ADAMTS-L4 gene sequence**
Schematic depicting the overlapping divisions of ADAMTS-L4 sequence. Overlaps depicted with hatched areas. Position of overlapping primer pairs is also shown.

## 6.5 Appendix Figure – A5

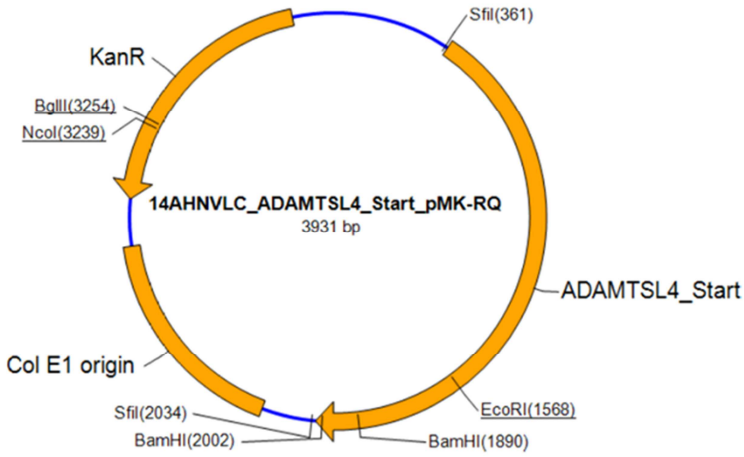


**Figure A5 Gene synthesis vector map of N-terminal region 'Start' of ADAMTS-L4**

Vector map of pMK-RQ cloning vector engineered by GeneArt Gene Synthesis Service Thermo Fisher Scientific (*Paisley, UK*) for the cloning of N-terminal region 'Start' of ADAMTS-L4. The construct contains 2 SfiI restriction sites either side of the insert and exhibits kanamycin antibiotic resistance (KanR).

## 6.6 Appendix Figure – A6

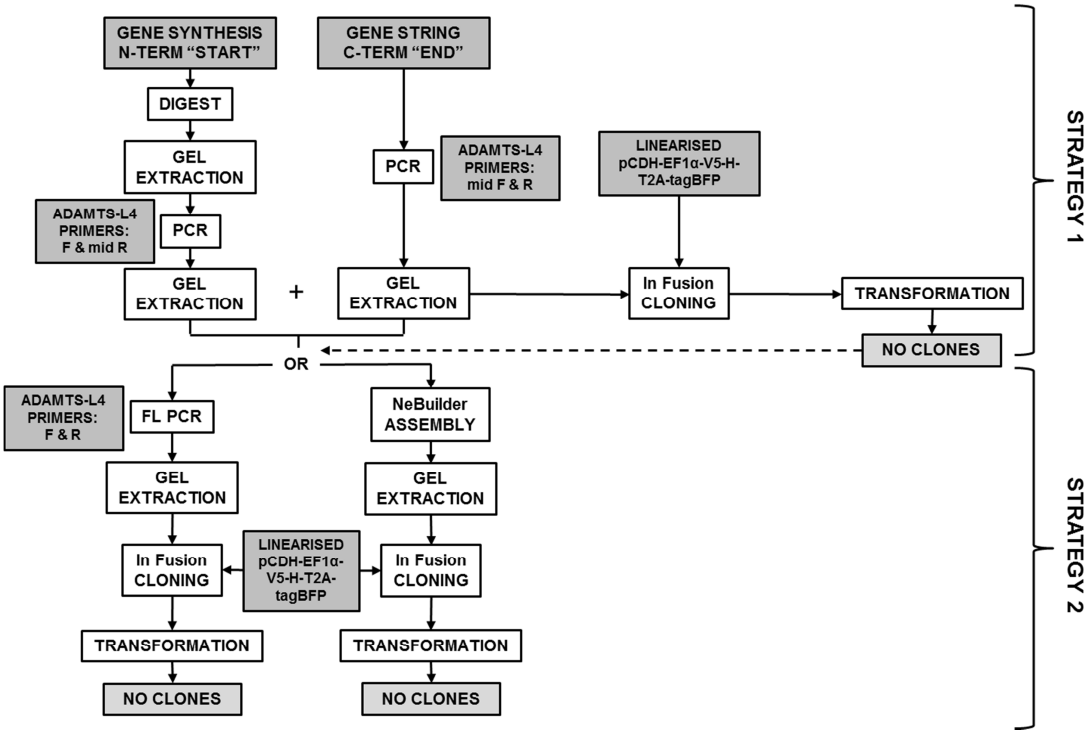


**Figure A6 Molecular cloning of recombinant ADAMTS-L4 Start and End fragments into a lentiviral expression system**

Strategies employed to clone Start and End fragments encoding ADAMTS-L4 into the pCDH lentiviral vector with a blue fluorescent tag (tagBFP). White boxes represent methods employed in the cloning process; light grey boxes denote outcomes; dark grey boxes denote cells, oligomers or DNA fragments used. Solid arrows depict the methodology followed to achieve results and dashed arrows represent changes in strategy. Two strategies were employed to clone Start and End fragment of ADAMT-L4 in to the pCDH vector. Strategy 1 involved digestion of the Start fragment from the gene synthesis cloning vector followed by amplification using the indicated primers. Amplification of gene string encoding End fragment performed using the primers indicated. Both PCR products were In Fusion cloned into the linearised pCDH-tagBFP vector and transformed. Transformations were unsuccessful, therefore Strategy 2 was applied. Strategy 2 involved overlapping and 'stitching' the Start and End PCR fragments together employing 2 different approaches. Approach 1: Amplification of FL ADAMTS-L4 with indicated primers. Approach 2: Assembling Start and End fragments with NEBuilder. Products from both approaches were cloned into the linearised pCDH-tagBFP vector using In Fusion and transformed. Both approaches were unsuccessful. The pCDH-tagBFP vector was linearised with NheI and BamHI.

## 6.7 Appendix Figure – A7

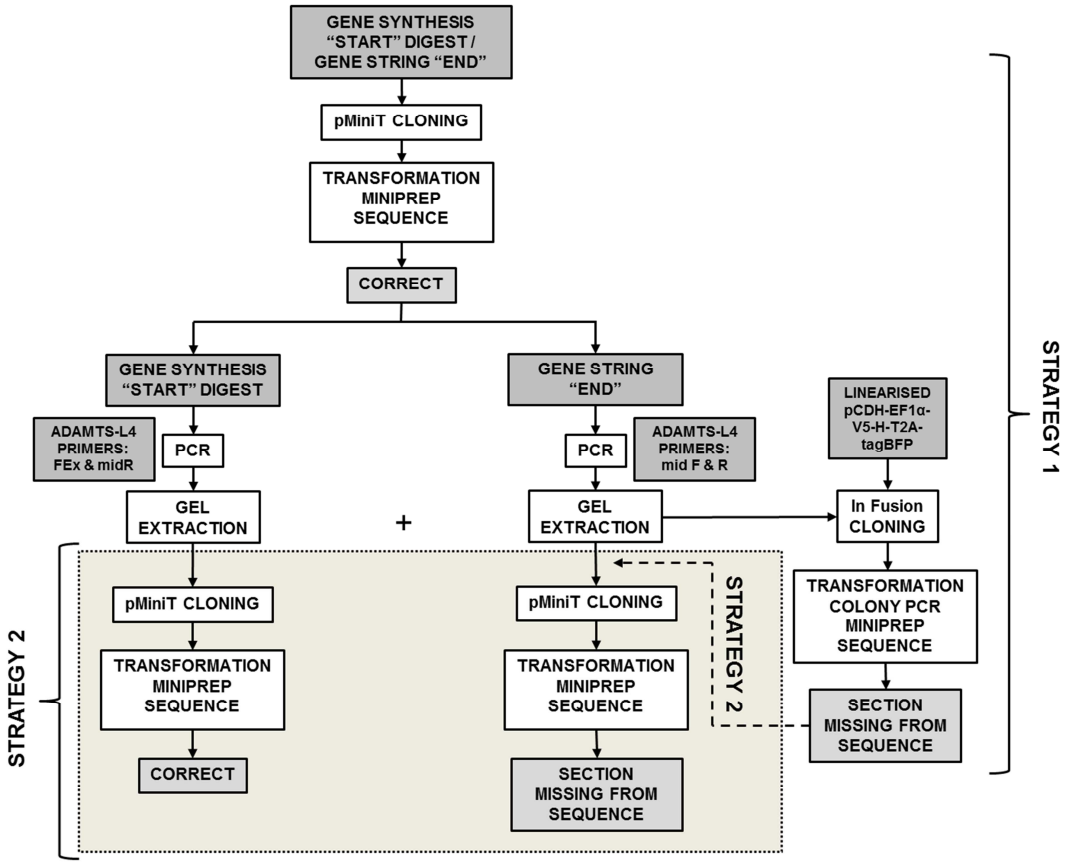


**Figure A7 Sequence verification of recombinant ADAMTS-L4 Start and End fragments using pMiniT cloning**

Strategies employed to verify the sequences of Start and End fragments encoding ADAMTS-L4 using pMiniT cloning. White boxes represent methods employed in the cloning process; light grey boxes denote outcomes; dark grey boxes denote cells, oligomers or DNA fragments used. Solid arrows depict the methodology followed to achieve results and dashed arrows represent changes in strategy. Two strategies were employed to sequence Start and End ADAMT-L4 fragments. Strategy 1 involved digestion of the Start fragment from the gene synthesis cloning vector and inserting into pMiniT cloning vector. Gene string encoding End fragment was also cloned into the pMiniT system. Sequencing of both fragments was correct. Attempted cloning of both fragments into the linearised pCDH-tagBFP vector was unsuccessful. Strategy 2 (grey box with dashed outline) involved cloning and sequencing PCR products of the Start and End fragments using pMiniT cloning. Sequence of Start PCR fragment was correct; however End fragment sequencing was incomplete. The pCDH-tagBFP vector was linearised with NheI and BamHI.

## 6.8 Appendix Figure – A8

| Domain | Sequence | Homology Model |
|---|---|---|
| TSR 1 | AFWWGEWTKWTACSRSCGGGVTSQERHCLQQRRKSVP GPGNRTCTGTSKRYQLCRVQECP |  |
| C-S-N | PDGRSFREEQCVSFNSHVYNGRTHQWKPLYPDDYVHISS PCDLHCTTVDGQRQLMVPARDGTSCKLTDLRGVCVSGKC EPIGCDGVLFSTHTLDKCGICQGDGSSCTHVTGNYRKGNA HLGYSLVTHIPAGARDIQIVERKKSADVLALADEAGYYFFNG NYKVDSPKNFNIAGTVVKYRRPMDVYETGIEYIVAQGPTNQ GLNVMVWNQNGKSPSITFEYTLLQPPHESRPQPIYYGFSE SAESQGLDGAGLMGFVPHNGSLYGQASSERLGLDNRLFG HPGLDMELGPSQGQETNEVCEQAGGGACEGPPRGKGFR DRNVTGTPLTGDKDDEEVDTHFASQEFFSANAISDQLLGA GSDLKDFTLNETVNSIFAQGAPRSSLAESFFVDYEENEGAG PYLLNGSYLELSSDRVANSSSEAPFPNVSTSLLTSAGNRTH KARTRPKARKQGVSPA | 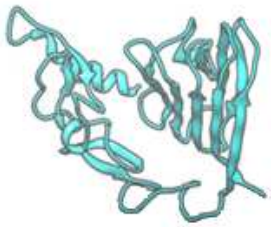 |

| | | |
|---|---|---|
| TSR 2 | DMYRWKLSSHEPCSATCTTGVMSAYAMCVRYDGVEVDD SYCDALTRPEPVHEFCAG |  |
| TSR 3 | CQPRWETSSWSECSRTCGEGYQFRVVRCWKMLSPGFDS SVYSDLCEAAEAVRPEERKTCRNPACG |  |
| TSR 4 | QWEMSEWSECTAKCGERSVVTRDIRCSEDEKLCDPNTRP VGEKNCTGPP |  |

| | | |
|---|---|---|
| TSR 5 | CDRQWTVSDWGPCSGSCGQGRTIRHVYCKTSDGRVVPE<br>SQCQMETKPLAIHPCGDKNCP |  |
| TSR 6 | HWLAQDWERCNTTCGRGVKKRLVLCMELANGKPQTRSG<br>PECGLAKKPPEESTCFE |  |
| TSR 7 | PCFKWYTSPWSECTKTCGVGVRMRDVKCYQGTDIVRGCD<br>PLVKPVGRQACDLQPCP |  |
| PLAC | PDDSCQDQPGTNCALAIKVNLCGHWYYSKACCRSCRPPH |  |

**Figure A8 Modelling of homology domains of ADAMTS-L2**

Individual homology models of ADAMTS-L2 domains were generated from protein sequences of each domain and modelled in SWISS MODEL to generate PDB files. All TSR domains and the PLA C domain were modelled individually, where as a combined model of the cysteine –rich, spacer and N-glycan rich (C-S-N) domains were created.

## 6.9 Appendix Figure – A9

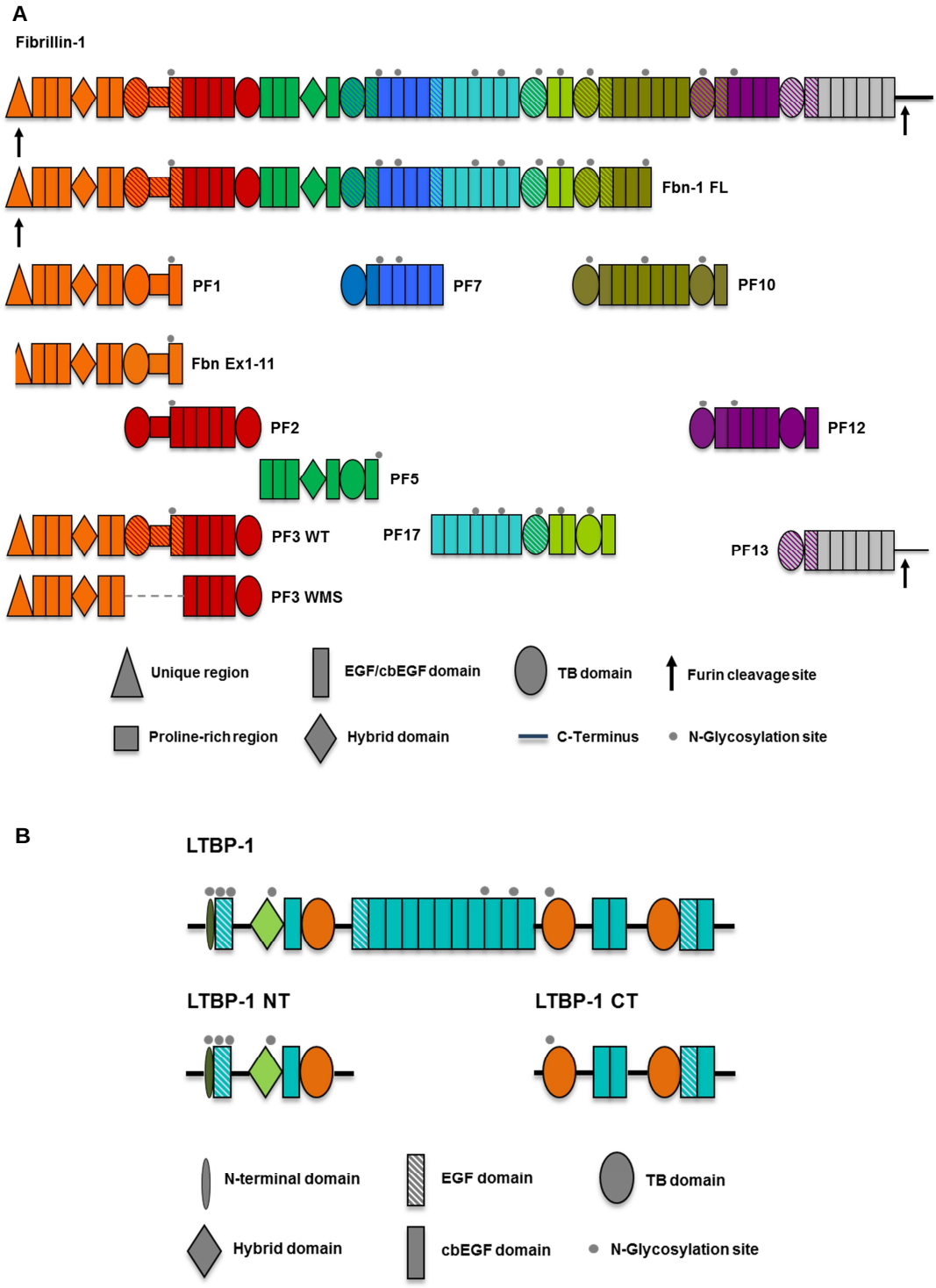


**Figure A9 Fibrillin-1 and LTBP-1 fragments used in SPR**

Schematic of Fibrillin-1 fragments (**A**) and LTBP-1 fragments (**B**) used for interaction studies with ADAMTS-L2 using SPR.